Stony Brook University

The functional morphology of subchondral and trabecular bone in the hominoid tibiotalar joint

A Dissertation Presented

by

Anne Su

to

The Graduate School

in Partial Fulfillment of the

Requirements

for the Degree of

Doctor of Philosophy

in

Anthropology

Stony Brook University

August 2011

Stony Brook University

The Graduate School

Anne Su

We, the dissertation committee for the above candidate for the
Doctor of Philosophy degree, hereby recommend
acceptance of this dissertation.

Brigitte A. Demes - Dissertation Advisor
Professor, Anatomical Sciences

Randall L. Susman - Chair of Defense
Professor, Anatomical Sciences

William L. Jungers
Professor, Anatomical Sciences

Biren A. Patel
Instructor, Anatomical Sciences

Kristian J. Carlson
Senior Researcher, Institute for Human Evolution,
University of the Witwatersrand

This dissertation is accepted by the Graduate School

Lawrence Martin
Dean of the Graduate School

Abstract of the Dissertation

The functional morphology of subchondral and trabecular bone in the hominoid tibiotalar joint

by

Anne Su

Doctor of Philosophy

in

Anthropology

Stony Brook University

2011

This dissertation investigated whether the internal bone morphology of the distal tibia and talus may help to further clarify the controversial mosaics of external morphological traits previously found in fossil hominin ankle bones that have suggested varying levels of obligate bipedal and arboreal abilities. The morphology of both subchondral bone and trabecular bone has independently been hypothesized to reflect habitual loads incurred during life. This dissertation examined these properties concurrently in a single joint to test if these properties were consistent with each other and consistent in reflecting known and assumed habitual joint loads. Using micro-CT scans from humans, chimpanzees, gorillas, orangutans, and baboons, this study quantified and compared the radiodensity and thickness of subchondral bone and the architecture and orientation of trabecular bone in nine regions across each joint to determine which morphological variables can discriminate among these taxa and may be indicators of different modes of locomotion.

The distributions of subchondral bone properties and of the underlying trabecular bone were only weakly correlated in both the distal tibia and talus. Based on morphological, kinetic, and kinematic evidence in the human tibiotalar joint, the distribution of subchondral bone properties is suggested to reflect areas of habitual joint loads common to the opposing joint surfaces while the distribution and orientation of trabecular morphology reflects attenuation of loads through the bone. The distribution of subchondral bone properties, but not trabecular bone properties, was mirrored in the opposing surfaces of the distal tibia and talus. Species were found to have distinct patterns of subchondral bone and trabecular bone morphology across the tibiotalar joint that can be understood in light of differences in observed habitual locomotor behavior, which lends support for the use of these properties in the analysis and interpretation of fossil bones. Application of this analysis to a 1.6 Ma fossil hominid talus reveals an internal morphology that is largely consistent with that of modern humans but also has features shared with other hominoids, in particular those with relatively greater locomotor variability.

Table of Contents

List of Figures

List of Tables

Acknowledgements

I am deeply indebted to my primary advisor Brigitte Demes and secondary advisor Bill Jungers, firstly for taking me on as a student with little background in anthropology, but more importantly for their guidance as I navigated into the field. I would also like to thank them for their tremendous encouragement and patience as I completed this dissertation from afar.

Many thanks are extended to my committee members, Randy Susman, Kris Carlson, and Biren Patel for their insightful comments on my dissertation and supportive discussion on how to expand in this research. Thanks especially to Biren, for being there to cheer me on every step of the way, first at Stony Brook then at Ohio University.

I'd like to thank the faculty, staff, and students in Biomedical Sciences at Ohio University for supporting me as I collected and analyzed much of my dissertation data there, and for giving me the opportunity to simultaneously gain valuable teaching experience. Larry Witmer and Ryan Ridgely generously offered use of and technical support with the Ohio University micro-CT system. Special thanks to Patrick O'Connor, Nancy Stevens, Susan Williams, and Audrone Biknevicious for being surrogate advisors and for pulling me away from my desk every so often for some fun.

I would like to thank the many individuals and institutions that enabled me to perform this dissertation research. The funding for this research was awarded by the National Science Foundation, the Wenner Gren Foundation, and the Leakey Foundation. Thank you to the following people for facilitating the loan of skeletal specimens: Lyman Jellema and Yohannes Haile-Selassie at the Cleveland Museum of Natural History (Cleveland, OH), Linda Gordon and James Mead at the National Museum of Natural History (Smithsonian Institution, Washington, D.C.), Darrin Lunde at the American Museum of Natural History (New York, NY), and Brett Nachman and John Kappelman at the University of Texas Department of Anthropology (Austin, TX). Lastly, I am indebted to Ian Wallace and Masato Nakatsukasa for allowing me to use the images they collected of fossils at the Kenya National Museum in Nairobi.

Thank you to Richard Rozic and Amit Vasanji at the Musculoskeletal Imaging Processing and Analysis Center of the Cleveland Clinic Foundation who were instrumental in guiding the technical aspects of micro-CT data collection and analysis. Timothy Ryan and Rich Ketcham were also always ready with helpful advice on the data analysis.

Words cannot adequately express the thanks I have to my parents who have always encouraged me to study, explore, and find my own path through life. It may have taken me a while, but Mom and Dad, I think I'm headed in the right direction now.

Finally to my long-time best friend and newly-minted husband Robert, thank you for being understanding in my decision to not only pursue another degree but to do so more than 500 miles away. Through the help of all the above people, I have made it full circle back to Cleveland and am ready to build a life and career with you by my side.

Dissertation Introduction

The external (cortical bone) morphology of hominoid ankle bones (distal tibia and talus) has been well studied in the effort to understand the unique morphologies of critical fossil hominin specimens such as OH 8 (Grausz et al.; Leakey et al. 1964; Susman and Stern 1982; Wood 1974), AL 288-1 (Johanson et al. 1982), and Stw 573 (Clarke 2002; Clarke and Tobias 1995) (see review by Harcourt-Smith and Aiello 2004). Indeed, interest has intensified in light of the unique foot and ankle morphologies of the newly discovered LB 1 (Jungers et al. 2008) and ARA-VP-6/500 (Lovejoy et al. 2009). Multivariate analyses of these fossil bones most often conclude that they have a "mosaic" of ape-like and human-like features, likely reflecting degrees of adaptation between arboreal climbing and obligate bipedalism (Gebo and Schwartz 2006; Harcourt-Smith 2002; Kidd and Oxnard 2005; Lisowski et al. 1974, 1976). The internal bone morphology, however, is relatively unstudied and holds the potential to help further characterize the nature of this mosaicism as well as aiding in the understanding of the relationship between internal bone morphology and habitual locomotor behavior. Thus, this dissertation seeks to answer the question: Does the internal morphology of hominid ankle bones hold a diagnostic locomotor signal?

The increasing accessibility and application of non-destructive micro-computed tomography (μCT) to anthropological studies has opened the field to the analysis of internal bony morphology. Much of this pioneering work has focused on the proximal femur, quantifying and comparing trabecular (cancellous) bone structure among extant and fossil non-hominoid primates (e.g., Fajardo 2004; Fajardo and Müller 2001; MacLatchy and Müller 2002; Ryan 2001; Ryan and Ketcham 2002, 2005; Ryan and van Rietbergen 2005; Saparin et al. 2009) to test the hypothesis that differences in habitual locomotor behavior (broadly defined at the species level) in life may be reflected in differences in trabecular architecture. Although this hypothesis has been supported by empirical evidence using experimental manipulation of applied external load on animal models (e.g., Biewener et al. 1996; Pontzer et al. 2006), cross-sectional comparative studies have yielded limited distinguishing trabecular bone characteristics between locomotor groups. The lack of a clear locomotor signal was often partially attributed to the difficulty in identifying homologously-loaded regions of bone among species with differing skeletal sizes and shapes. Also, unlike in laboratory experiments, the magnitude and direction of load that was transmitted through the joint are uncontrolled and unmeasured. Therefore, it was not clear that a difference (or lack thereof) in trabecular architecture reflected differences in habitual load.

Another aspect of internal bone morphology that has been hypothesized to reflect patterns of habitual applied joint load is the radiodensity (apparent density estimated by radiographic imaging techniques) and thickness of the subchondral bone (the plate of cortical bone situated between the joint articular cartilage and the supporting trabecular bone) (Ahluwalia 2000; Carlson and Patel 2006; Müller-Gerbl et al. 1989; Nowak et al. 2010; Patel and Carlson 2006, 2007; Polk et al. 2008; Polk et al. 2010). For example, Carlson and Patel (2006) found that quadrupedal primates had relatively larger and more concentrated areas of high subchondral apparent density in the distal radius than suspensory and bipedal primates. Although these studies could only infer that regions of high apparent density indicate regions of high load and were the regions loaded in life during habitual locomotor activities, recent empirical evidence from the knees of treadmill-exercised sheep has lent support to this hypothesis (Polk et al. 2008). Similarly, the relative thickness of subchondral bone may also reflect areas of differential load across a joint. Murray et al. (2001) found that juvenile horses run at high treadmill speeds had significantly thicker subchondral bone in the middle carpal joint than did those that walked, but only in the dorsal aspect of the joint, demonstrating that subchondral bone thickness is also site-specific within a joint, and that thicker regions may reflect regions of high habitual compressive load.

While promising, before either trabecular bone structure or subchondral bone apparent density may be accepted as morphological tools with which to infer locomotor behavior, they should be subject to a rigorous validation. Unfortunately, a direct validation is problematic because joint loads cannot easily be measured *in vivo* without invasive procedures that may compromise joint function. However, an indirect validation that subchondral bone apparent density reflects habitual compressive load may be performed in humans by comparison with data from human biomechanics studies that have quantified contact area and articular pressure in cadaver joints loaded and manipulated to simulate bipedal gait. Furthermore, because both of these approaches, trabecular bone architecture analysis and subchondral bone apparent density analysis, are attempting to find diagnostic morphology that reflects bone strength due to habitual compressive joint loads, it follows that a combination of the two methods in an investigation of a single joint region may serve as a mutual validation. Thus this study assesses the consistency of three lines of evidence in indicating differential regions of compressive load across the tibiotalar joint in hominoids: 1. trabecular bone architecture and orientation, 2. subchondral cortical bone radiodensity and thickness, and 3. articular contact area and pressure.

The hominoid ankle is well-suited for this investigation. It is likely subjected to relatively high compressive forces and its distally located position has allowed estimates of joint load through biomechanical measures, at least in humans. Also, there have been numerous hypotheses developed regarding the differences in habitual foot and ankle posture between hominid species. In this dissertation, these current hypotheses of the differences in habitual compressive joint load among species are assessed as to their consistency with differences in subchondral and trabecular bone structure.

Specifically, in this dissertation, Chapter 1 examines whether the subchondral bone thickness and radiodensity and the trabecular bone architecture and orientation in the human tibiotalar joint, as quantified from micro-computed tomography (μCT) images, agrees with joint kinematics and the patterns of articular joint contact area and pressure that have been demonstrated for simulated human gait.

Chapter 2 quantifies the patterns of subchondral bone thickness and radiodensity and trabecular bone architecture and orientation in the hominoid tibiotalar joint to test the hypothesis that indicators of bone strength as estimated from 3D μCT images of isolated bones can distinguish among species with different habitual locomotor behaviors and is consistent with current hypotheses of habitual locomotor load.

Chapter 3 uses the findings of the previous chapters to examine and interpret the trabecular bone architecture and orientation in a fossil talus, KNM-ER 1464, from Ileret, Koobi Fora, Kenya (Leakey 1973) dated to 1.56-1.60 Ma (Wood and Constantino 2007) with the hypothesis that it belonged to a hominid with a modern human-like foot.

1. Chapter 1: Regional variation of subchondral and trabecular bone properties in the human tibiotalar joint

1.1 Introduction

Bone strength is determined largely by its structural morphology and it is highest in compression (Kabel et al. 1999; Odgaard et al. 1997), supporting the commonly held view that regions of greater bone strength indicate those regions that can and do withstand the greatest amount (in frequency and/or magnitude) of compressive load. Actual bone strength is most properly measured using a material mechanical testing system. However, it has been shown that there is a direct relationship between bone strength and histologically-quantified bone tissue properties (Ding et al. 2002a). In particular, volumetric bone density and architectural anisotropy (fabric) are the best predictors (explaining more than 90% of the variance) of the mechanical strength of normal trabecular bone (Ding et al. 2002a; Odgaard et al. 1997; Ulrich et al. 1999). Other related indicators of bone strength are the thickness of individual trabecular struts, the number of struts per volume, and the shape of trabecular struts. Physically nondestructive imaging technologies such as micro-computed tomography (μCT) have been demonstrated to accurately represent histological features and thus have further extended the ability to estimate bone strength of specimens for which destructive histology is not feasible (e.g., *in vivo* animal models and fossil specimens).

1.1.1 Trabecular bone morphology

The structure of trabecular bone (also known as cancellous or spongy bone) has been widely examined using μCT imaging in the field of bone biomechanics, driven by clinical research on osteoporosis. Historically, the alignment of trabeculae has been interpreted as reflecting the trajectories of principal stresses in the bone caused by habitual applied load (Wolff 1892). Although the strict alignment of trabeculae with orthogonal principal stress trajectories has been disproven (reviewed by Cowin 2001; Roesler 1981; Roesler 1987), it nonetheless has been frequently demonstrated that trabecular bone responds epigenetically (i.e., is environmentally plastic) in human clinical case studies (e.g., Pauwels 1980) and in experimental studies where animals were exposed to varying habitual loads in controlled laboratory settings (e.g., Biewener et al. 1996; Pontzer et al. 2006). This evidence of trabecular bone response leads to the inverse hypothesis that trabecular structure and orientation within a bone should indicate the magnitude and direction of the habitual loads encountered in life. Since trabecular bone is often preserved in fossil specimens and can be relatively non-destructively imaged using μCT, the ability to interpret its structure would be highly informative in inferring habitual locomotor behavior from an isolated fossil bone.

However, unlike in controlled laboratory experiments, the actual differences in load magnitude or direction on the bones are uncontrolled and impossible to know for most skeletal specimens. Thus, the functional interpretation of differences in trabecular bone structure between specimens is difficult. For example, previous comparative studies of the morphology of trabecular bone microstructure, focusing on the proximal femur of strepsirrhine primates (Fajardo and Müller 2001; MacLatchy and Müller 2002; e.g., Ryan and Ketcham 2002), have yielded limited distinguishing characteristics between locomotor groups, partially attributed to the difficulty in identifying homologously-loaded regions of bone among species with proximal femora of differing size and shape.

1.1.2 Subchondral bone morphology

Another aspect of internal bone morphology that has been hypothesized to reflect patterns of habitual applied load is the apparent mineral density of the subchondral bone of joints, as estimated from conventional CT scans (Ahluwalia 2000; Carlson and Patel 2006; Müller-Gerbl et al. 1989; Nowak et al. 2010; Patel and Carlson 2007, 2008; Polk et al. 2008; Polk et al. 2010).

In a comparative study, Carlson and Patel (2006) found that quadrupedal primates have relatively larger and more concentrated areas of high subchondral apparent density in the distal radius than do suspensory and bipedal primates. They were able to further distinguish apparent density patterns among quadrupedal primates, with digitigrade and palmigrade monkeys displaying high density areas restricted to the dorsal region of the distal radial surface and knuckle-walking apes displaying high density areas in the volar region (Patel and Carlson 2007). These studies thus demonstrate that the distribution patterns of high radiodensity areas across the subchondral bone plate may reflect the distribution of habitual compressive joint load across the joint surface.

Changes in subchondral bone morphology is of interest in the human clinical literature as related to the progression of osteoarthritis. Large-scale, prospective studies of the location of subchondral bone lesions and incident osteoarthritis in the human knee joint suggest that subchondral bone may remodel in response to local increased contact loads within the joint (Hernandez-Molina et al. 2008; Neogi et al. 2010; Roemer et al. 2010; Segal et al. 2009). This remodeling results in a flattening of the articular surface (termed "subchondral bone attrition"), decrease in subchondral bone porosity, and an increase in subchondral bone stiffness (Radin et al. 1984). Thus, the use of imaging modalities to detect early changes in joint structure are in need of further study as potential tools for intercepting the progression of osteoarthritis (Menetrey et al. 2010).

Müller-Gerbl (2001) qualitatively reported two regular distribution patterns of subchondral mineralization in the human talocrural joint. A bicentric pattern was most commonly found, with maximum radiodensities on both the medial and lateral trochlear margins. Also occurring, though rare, was a monocentric pattern, with the maximum density located in the anteromedial region of the trochlea. In either case, whether bicentric or monocentric, a

corresponding pattern was found on the distal tibia. In this groups' work in the hip joint, they demonstrated that the presence of a bicentric radiodensity pattern versus a monocentric pattern may be related to age, with the joint becoming more congruous as the articular cartilage in the joint becomes worn (Müller-Gerbl et al. 1993). Similarly, a more congruous articulation may occur with greater body mass.

The relative physical thickness of the subchondral plate may also reflect adaptation to the relative amount of load that was transmitted through it in life. For example, it has been shown that the subchondral bone of the middle carpal joint is significantly thicker in juvenile horses run at high speeds on a treadmill than in horses that walked, but only on the dorsal aspect of the joint (Murray et al. 2001). This study thus demonstrated that subchondral bone thickness is also site-specific within a joint, and that thicker regions may reflect regions of high habitual load.

While it is well accepted that trabecular bone is sensitive to loads, and there is growing evidence that subchondral bone is as well, these two tissue types may be responding to joint loads in different ways (Frost 1999; Rafferty and Ruff 1994). For instance, Rubin et al. (2002) found significant increases in trabecular bone tissue apparent density of the proximal femur in sheep exposed to low intensity, high frequency strains while there were no significant differences found in the overlying cortical bone. Decoupled responses to loading may be advantageous from a functional perspective, because they allow joints to respond to their mechanical environment without altering articular morphology and compromising the demands of mobility (Lieberman et al. 2001). The work of Rafferty and Ruff (1994) on trabecular density in the femoral head of catarrhine primates supports this view, suggesting that the external articular surface area is mainly driven by the mobility demands of the joint and that the underlying internal trabecular morphology is independent from those demands and largely determined by the magnitude and orientation of the loads passing through the joint.

The goals of this study were to quantify the variation of subchondral bone radiodensity and trabecular bone structure and orientation in the human tibiotalar joint, and to characterize the relationship among variables to address the hypotheses that (1) the properties of subchondral bone and trabecular bone in a single bone are coupled, (2) the properties of the opposing distal tibia and talus are coupled, and (3) regional variation in properties reflect adaptations to regional load during habitual locomotor activity.

The subchondral and trabecular bone in the human ankle are well-suited for an investigation into whether their morphologies are consistent within a population, and whether they indeed reflect habitual joint load. *In vivo* joint loads are not directly measurable without invasive procedures and subsequent loss of joint integrity. Though there have been no reported direct studies of joint load (for instance using instrumented ankle prostheses), kinematic and kinetic studies have estimated net internal joint forces and torques at the ankle. Researchers have also estimated the contact area and articular pressure in the talocrural and subtalar joints in human cadavers loaded and manipulated to simulate gait. Most commonly, this has been done *in vitro* using thin pressure-sensitive film that is inserted between the articulating bones (e.g., Calhoun et al. 1994; Wang et al. 1995). More recently, this *in vitro* method has been improved

by dynamic stress sensors that record real-time, high-resolution pressure maps across the articular surface (Anderson et al. 2007; Tochigi et al. 2006). Studies of the intrinsic kinematics of foot bones have also been recently described (de Asla et al. 2006; Leardini et al. 2007). Thus, based on these studies of ankle joint biomechanics, specific predictions can be made of the subchondral and trabecular bone morphology to test the hypothesis that they are functionally adapted to habitual human locomotion.

1.1.3 Specific predictions

If the properties of subchondral bone and trabecular bone are coupled, then it is predicted that there will be significant correlations among the subchondral bone and trabecular bone properties within each bone. Similarly, if the properties of the opposing distal tibia and talus are coupled, it is predicted that there will be correlations among tibial properties and talar properties. Because the force within a joint should be applied equally and oppositely to both joint surfaces, it is predicted that there is a relationship between the bone morphology of opposing joint regions. For example, it is predicted that the region of the distal tibia with the greatest trabecular bone volume would be that which directly opposes the region of the talus with the greatest trabecular bone volume. Lastly, if regional variation in properties reflects adaptations to regional load during habitual locomotor activity, then the distribution of properties is predicted to be consistent across individuals and the distribution of properties should be consistent with published studies of ankle joint articular contact stresses, kinematics, kinetics, and myology during normal human posture and locomotion.

Bone morphology adapts to local stresses over time. During childhood, trabecular bone remodels from a non-distinct, isotropic, high-bone-volume mesh to one which is best suited to withstand local loads (Ryan and Krovitz 2006; Tanck et al. 2001). In the young adult population examined in this study, it is predicted that trabecular bone volume decreases, and trabecular anisotropy increases with age, as the bone remodels to habitual loads. It is also predicted that individuals of greater body mass would exhibit greater trabecular bone volume in order to provide greater compressive strength.

Humans engage in many locomotor activities which load the ankle joint in various ways. However, in this study it is assumed that walking is the "habitual" locomotor mode of humans to which subchondral and trabecular bone is functionally adapted. During normal walking, the rearfoot begins in an inverted position relative to the tibia as load is borne laterally at heel strike but is quickly subjected to an eversion torque (from 0% to 20% of gait) as the load moves medially, placing the joint into an everted position throughout the dynamic weightbearing phase. Finally, the rearfoot returns to an inverted position just after to toe-off (Hunt et al. 2001; Lundgren et al. 2008). Thus it appears from joint kinematics that along a mediolateral axis, the medial region of the ankle seems to bear the most load during a normal walking stride. Mechanical osteopenetration tests have confirmed that the medial regions of the talus demonstrate the greatest bone strength (Hvid et al. 1985). As well, during normal standing, the

weight of the body falls through the foot near the region of the talonavicular joint, distributing load anteriorly and posteriorly throughout the medial longitudinal arch (Neumann 2010). Thus in this study, it was predicted that relative to the lateral and central regions, the medial regions of the distal tibia and talus would have greater subchondral bone radiodensity and thickness, greater trabecular bone volume, thickness, and/or number, and greater trabecular anisotropy with the primary trabecular orientation consistently aligned with the presumed axis of compressive load.

Along an anteroposterior axis, it is predicted that the posterior regions of the ankle joint would exhibit stronger bone properties. Two peaks of ground reaction force (GRF) magnitude occur during normal walking, one peak immediately following heel strike and a second peak related to push off. The external force vector at the first peak passes just posterior to the ankle joint, thus placing high load in the posterior regions. The second GRF peak coincides with contraction of the ankle plantarflexor muscles (gastrocnemius and soleus) (Anderson and Pandy 2003), which would also result in a high magnitude compressive load in the posterior region of the joint. Histological studies of trabecular bone in the distal tibia have found higher trabecular bone volume, thickness, and number in the posterior regions versus the anterior (Lai et al. 2005). The posterior regions of the tibial plafond have also been demonstrated to have relatively greater bone strength by mechanical osteopenetration tests (Hvid et al. 1985).

It is predicted that the quantitative approach of measuring trabecular bone architecture and orientation from micro-CT scans would correspond to qualitative patterns of trabeculae described by other authors. Qualitative studies describe the trabeculae in the tibia as simply directed from the articular surface superiorly to the tibial cortex such that the trabeculae in the anterior regions are directed towards the anterior cortex and those in the posterior regions towards the posterior cortex (Takechi et al. 1982). Previous qualitative studies of the trabecular bone architecture in the talus note that the trabeculae in the anterior aspect are directed from the trochlear surface towards the talar head while those in the posterior aspect are oriented posteriorly towards the posterior calcaneal facet (Athavale et al. 2008; Pal and Routal 1998; Takechi et al. 1982). Pal and Routal (1998) also noted that the trabeculae in the talar body were mostly plate-shaped and oriented in the parasagittal plane.

1.2 Methods

1.2.1 Study sample

Articulating sets of distal tibiae and tali from 18 adult female human individuals were chosen for study from the Hamann-Todd osteological collection at the Cleveland Museum of Natural History. The skeletal materials in this collection were assembled between 1912 and 1938 by the Western Reserve University Department of Anatomy from City Hospital, Lakeside Hospital, and Warrensville Hospital (Lovejoy et al. 1985). The collection is composed of individuals born throughout the United States and in 27 foreign countries (Meindl et al. 1990). Records of sex, ethnicity, age at death, weight at death, and cause of death were examined to select females 20-35 years of age, eliminating those whose cause of death may have affected

bone morphology. Female humans were chosen for study in order to be comparable to female great apes in the larger study, which were chosen in an attempt to limit potential effects of body size differences. The majority of individuals eliminated had cause of death listed as pulmonary tuberculosis, which is a bacterial infection that often leads to extreme weight loss. Specimens were excluded from the study if records showed an extreme body mass index (BMI < 16.5 or > 30 kg/m^2) at death. Because the number of black females far exceeded the number of white females in the collection, only black females were selected in an effort to reduce potential genetic and socioeconomic effects on bone morphology (Bryant et al. 2003).

Specimens were further examined and rejected for analysis if there was any evidence of traumatic injury to the limbs, systemic abnormalities such as osteoporosis, or if they were excessively greasy, since grease may alter radiodensity values (Ruff and Leo 1986). Adult status of all individuals was confirmed by epiphyseal fusion on all long bones of each skeleton. Finally, individuals were chosen to represent a continuous range of body sizes (mean = 53.8 kg, range = 44.0-68.0) and ages (mean = 27, range 20-35) in order to assess any systematic effect of these factors on bone morphology.

1.2.2 Data collection

Each bone was scanned individually using a commercial μCT system (eXplore Locus SP, GE Healthcare Pre-Clinical Imaging, London, ON, Canada) housed within the Department of Biomedical Engineering at the Cleveland Clinic Foundation. This system is designed to image small laboratory animals *in vivo*, but was advantageous to this study because unlike many other commercial μCT systems it has a long specimen bed to accommodate the full length of the tibia. The GE eXplore Locus uses volumetric conebeam CT technology which allows the entire sample to be imaged in one rotation. The system was calibrated regularly using known density phantoms to convert the CT values to standard Hounsfield units. Beam-hardening artifacts were minimized using the system-equipped correction algorithm.

Care was taken to position and secure each bone in a standard, consistent position on the scanner bed. The long axis of the tibia was oriented parallel to the scanner bed, thus orienting the distal articular surface perpendicular to the bed. The talus was oriented in the standard basal talar plane (Lisowski et al. 1974) where the posterior and lateral tubercles and the most inferior point of the head rested naturally on the horizontal bed; the anterior edge of the trochlea was oriented perpendicular to the long axis of the scanner.

Specimens were scanned at a resolution setting of 45 μm, which has been found to be small enough to produce morphometric results similar to histologic methods (Müller et al. 1996). The source energy voltage was set to the maximum 80 kVp, which is suitable for imaging of the high-density bone. The x-ray current was set to 450 μA, which was the intensity of the x-ray beam that was recommended by the manufacturer to provide a good signal-to-noise ratio (GE Healthcare 2006). The pixel matrix size was 1024x1024, yielding a field of view of 47.1 mm

and an isometric voxel size of 0.0448 mm. Each image was reconstructed from 720 views with an exposure time of 400 ms.

Using GE Microview software (GE Healthcare, http://microview.sourceforge.net), the 3D volumes were digitally reoriented to reproducible, standardized positions that are functionally intuitive based on the horizontal supratalar plane of the ankle joint (Latimer et al. 1987). The distal tibia was oriented "square" to the articular surface; i.e., in the sagittal plane, the anterior and posterior rims of the articular surface were level and in the coronal and transverse planes, the mediolateral axis was level (Figure 1.1a). The talus was oriented relative to the trochlear surface such that in sagittal plane view, the base of the neck and the most posterior point of the trochlear surface were in the same horizontal plane, and in the coronal and transverse planes, the superiormost points of the medial and lateral trochlear rims were level (Figure 1.1b). The reoriented volumes were then exported as a stack of 16-bit DICOM format image files. The DICOM image stack of each specimen was imported into *Amira Visualization Software* (Visage Imaging, San Diego CA) for further analysis.

1.2.3 Analysis of subchondral cortical bone

1.2.3.1 Segmentation into slab

The subchondral plate of bone was semi-manually isolated from each joint surface using the brush segmentation tool (Figure 1.1). In approximately every tenth image (0.45 mm) in the volume series, the boundary between air and bone was visually determined and outlined using the brush tool. Care was taken to include only subchondral articular bone but not the surrounding non-articular cortical bone. The manually-selected air-bone boundary was then interpolated between the slices, with subsequent visual verification of accuracy. The thickness of this rough-cut, selected mask was standardized to 18 voxels (~0.81 mm), which was visually approximated to be thick enough to fully encompass the cortical plate while minimizing the inclusion of underlying trabeculae. The set of voxels within the segmented area was isolated from the rest of the specimen volume (i.e., the trabecular bone and non-articular cortical bone) using the *Amira* arithmetic tool, and saved as a separate volume. Although the thickness of the mask was user-selected and constant for each species, the actual computed thickness of the subchondral bone plate was determined automatically by a software algorithm as described below. The minimum and maximum voxel intensity values (in Hounsfield units) within this isolated subchondral volume were recorded for use in subsequent histogram analyses.

1.2.3.2 Division into anatomical regions

The subchondral bone volume was segmented into a 3x3 grid of nine anatomically-aligned regions (Figure 1.1). The maximum linear mediolateral and anteroposterior dimensions of the isolated subchondral plate were digitally measured and divided into thirds using the *Amira* measurement tool. Each region was thus defined with dimensions of 1/3 of the maximum

mediolateral length and 1/3 of the maximum anteroposterior length. The curved trochlear surface required a different, angular approach, whereby the arc between the posteriormost and anteriormost points of the articular surface was measured in degrees and then divided into thirds. The set of voxels within each region was isolated using the *Amira* arithmetic tool, saved as a separate volume, and exported as a stack of 16-bit TIFF format image files.

1.2.3.3 Quantification of radiodensity

The distribution of voxel radiodensity within each of the nine regions of the articular surfaces was quantified in the following way. An 8-bin histogram of the Hounsfield radiodensity values within each region was constructed, using the minimum and maximum values previously recorded for the entire articular surface as lower and upper bounds. Relative radiodensity intensity (Sc.%HighDens) was quantified for each region as the combined number of voxels in the highest two bins (i.e., highest 25%) as a percentage of the total number of voxels in the region. The mean voxel intensity value (in Hounsfield units) within the region was computed by *Amira* and recorded as Sc.MeanHouns. Both of these properties are proxies of the amount of high-density mineral in the bone, and together may be referred to as "subchondral bone radiodensity".

1.2.3.4 Quantification of thickness

The thickness of the subchondral cortical shell of each articular surface was quantified using *Quant3D* software (Ketcham 2005; Ketcham and Ryan 2004) as follows. *Quant3D* was developed for the purpose of quantifying the structure of 3D fabrics and was used primarily in this study to quantify trabecular bone. However, its algorithms were also used here as a subjective method of calculating subchondral thickness by in essence treating the thin subchondral plate of bone as if it were an isolated trabecular plate.

Because *Quant3D* required images to be imported in an 8-bit format, the 16-bit *Amira* TIFF image stack of each isolated region of the subchondral plate was converted to 8-bit TIFF images using *ImageJ* software (Rasband 1997-2007). The rough-cut volume containing the thin plate was binarized into bone/non-bone using an adaptive, iterative threshold technique (Ridler and Calvard 1978; Ryan and Ketcham 2002), and the structure analyzed using the star volume distribution (SVD) algorithm (Cruz-Orive et al. 1992; Ketcham and Ryan 2004). In this algorithm, for a given point within the bone structure, intercept lengths (straight-line lengths between bone-air boundaries) are calculated for a series of random angular orientations (513 orientations were used here as recommended by Ketcham and Ryan (2004)). The thickness of bone at a given point is defined as the shortest intercept length. Using 2000 random points within each bone volume, calculations were thus made of the mean thickness of the subchondral bone plate (Sc.Th) within each of the 9 regions.

1.2.4 Analysis of trabecular bone

1.2.4.1 Segmentation into anatomical regions

The trabecular bone volume of each specimen was segmented into nine roughly cubic regions directly corresponding to the overlying subchondral bone regions defined above (Figure 1.1). The set of voxels within each region was isolated using the *Amira* arithmetic tool, saved as a separate volume, and exported as a stack of 16-bit TIFF format image files.

1.2.4.2 Thresholding/Quant3D options

The 16-bit TIFF image stack of each trabecular bone region was smoothed from noise using a Gaussian filter and converted to 8-bit TIFF images using *ImageJ* software. The images were then imported into *Quant3D* for quantification of the structure and orientation of the trabecular bone within each region. Anatomical orientation axes were applied, denoting anterior, medial, and superior directions. For each of the nine regions of trabecular bone, a volume of interest (VOI) was defined as being the largest centered sphere that fit completely within each region, without including unwanted cortical bone. Because a cuboidal VOI introduces a bias in the results if a prominent feature is oriented near 45 degrees, a spherical volume of interest was chosen (Ketcham and Ryan 2004). Because of natural irregularities in bone shape, the nine VOIs within a given specimen were not exactly the same size. For example, the posterior dimension of the talar trochlea is narrower than the anterior dimension, resulting in posterior VOIs that were consistently smaller than anterior VOIs (Figure 1.1).

The trabecular bone in the VOI was binarized into bone/non-bone using an adaptive, iterative threshold technique (Ridler and Calvard 1978; Ryan and Ketcham 2002), and the structure analyzed using the star volume distribution (SVD) algorithm (Cruz-Orive et al. 1992; Ketcham and Ryan 2004).

1.2.4.3 Quantification of trabecular volume, thickness, and number

The output variables computed by *Quant3D* and used in this analysis are:

- *Relative bone volume (BV/TV)*: Also known as "bone volume fraction", it is the dimensionless ratio of the number of bone voxels present in the VOI to the total number of voxels in the VOI (Goulet et al. 1994).
- *Trabecular strut thickness (Tb.Th)*: The average trabecular strut thickness (mm) in the VOI, based on the intersections between a superimposed grid of lines and bone voxels (Hildebrand and Ruegsegger 1997).
- *Trabecular number (Tb.N)*: The estimated number of trabecular struts in the VOI, based on the number of intersections between a superimposed grid of lines and bone voxels (Hildebrand and Ruegsegger 1997).

1.2.4.4 Quantification of trabecular shape and primary orientation

A fabric tensor describing the orientation of trabeculae within each VOI was calculated using the star volume distribution (SVD) method of *Quant3D* (Ryan and Ketcham 2002). The SVD method of quantifying architectural anisotropy (fabric) has been shown to be the best predictor of mechanical anisotropy (Odgaard et al. 1997). The SVD method is based on the measured length of the longest uninterrupted line from a point lying within trabecular bone to the boundary between bone and air, repeated for a series of uniformly distributed orientations and multiple random points (Cruz-Orive et al. 1992). From these data, a fabric tensor is derived which describes how the moment of inertia of bone varies with orientation (Ketcham 2005). Three eigenvectors, μ_1, μ_2, μ_3, and three eigenvalues, τ_1, τ_2, τ_3, describing the distribution of bone are derived from the fabric tensor (Benn 1994; Ryan and Ketcham 2002). The eigenvectors represent the orientation in 3D space of the primary, secondary, and tertiary material axes. The corresponding eigenvalues, defined such that $(\tau_1 + \tau_2 + \tau_3) = 1$ and $\tau_1 > \tau_2 > \tau_3$, represent the relative magnitudes of each of the three material axes. The first eigenvector is defined to be parallel to the axis of maximum clustering in the data. The specimen is *orthotropic* if the three eigenvalues are distinct in value, *transversely isotropic* if there are two similarly-valued eigenvalues, and *isotropic* if all eigenvalues are approximately equal (a sphere). The degree of anisotropy (DA), defined as the ratio of the highest eigenvalue to the lowest eigenvalue (τ_1/τ_3), is the commonly used ratio to summarize the relative magnitudes. However this value is often difficult to evaluate and compare because there is no upper bound. Other ratios between the eigenvalues also give an indication of the shape of the trabeculae – whether plate-like or rod-like. If the first eigenvalue is high and the second and third are equally low, then the data indicates a rod-like shape; if the first two eigenvalues are equally high and the third is low, then the data indicates a plate-like shape (Benn 1994). Ding et al. (2002a) demonstrated that plate-like trabeculae are indicative of a high-stress environment while rod-like trabeculae indicate regions of low stress.

The output variables computed by *Quant3D* and used in this analysis are:

- *Trabecular degree of anisotropy (Tb.DA)*: (τ_1/τ_3). The primary eigenvalue divided by the tertiary eigenvalue. Values closer to 1 denote perfect isotropy; increasingly greater values indicate trabecular struts which are increasingly narrowed onto a single plane (Harrigan and Mann 1984).
- *Trabecular isotropy index (Tb.I)*: (τ_3/τ_1). The inverse of Tb.DA, this property is more intuitive to evaluate trabecular shape because values are bounded between 0 and 1. Values closer to 0 denote trabecular struts that are confined to a single plane (either plate-shaped or rod-shaped); a value of 1 denotes perfect isotropy (sphere-shaped) (Benn 1994).
- *Trabecular elongation index (Tb.E)*: $1-(\tau_2/\tau_1)$. Distinguishes between rod-shaped and plate-shaped trabeculae by indicating the extent of preferred orientation of trabeculae in the major plane defined by eigenvectors 1 and 2. If Tb.I is close to 0, concurrent values of Tb.E closer to 0 denote more plate-shaped trabecular struts; values of Tb.E closer to 1 denote more rod-shaped struts. (Benn 1994).

- *Direction of eigenvectors*: Orientation of the primary and secondary eigenvectors as defined by angle-angle coordinates relative to the center of the VOI.

Thus, the two indices Tb.I and Tb.E used together uniquely define the architecture of the trabecular bone mesh. A trabecular fabric composed of elongated rod-shaped trabeculae will have Tb.I closer to 0 and Tb.E closer to 1. A fabric of flat disc-shaped trabeculae will have both Tb.I and Tb.E closer to 0. A completely isotropic fabric with no preferred trabecular orientation will have Tb.I closer to 1 and Tb.E closer to 0.

1.2.5 Statistical analyses of morphological variables

Descriptive statistics were calculated for all variables to investigate their variation across individuals and across regions within the ankle joint. The distribution of data was checked for normality and log-transformed if necessary.

One-way analysis of variance with post-hoc pairwise comparison tests (Games-Howell) was performed among regions to characterize the distribution of bone properties across the talocrural joint surface.

Bivariate correlation analyses were performed for all variables to assess relationships, particularly between subchondral and trabecular bone variables within each bone. Bivariate correlation analyses were also performed between the values quantified for the tibia and the variables quantified for the talus to investigate the presence of a morphological relationship between the two articulating bones.

Kendall's coefficient of concordance (W), a normalization of the Friedman test statistic, was computed for each variable to assess the consistency of ranked values across each articular surface. In each specimen, for each variable, the 9 regions were assigned ranks based on values of that variable, with the region with the highest value ranked 9, and the region with lowest value ranked 1. The level of agreement among those sets of ranked data was assessed using Kendall's coefficient of concordance (W). A W=1 would indicate that all specimens had identical rank order of regions from highest to lowest value. A W=0 would indicate that the ranking of regions was random.

All analyses were performed using SPSS 16.0 software. The significance level of all tests was set at $p < 0.05$.

1.2.6 Statistical analysis of orientation vector data

The distribution of trabecular shape indices was visualized using ternary plots of Tb.I and Tb.E (Graham and Midgley 2000), where data points towards the top apex indicate more isotropic trabeculae and data points towards the bottom indicate more anisotropic trabeculae. Data points towards the bottom left apex indicate more plate-shaped trabeculae and data points towards the bottom right apex indicate more rod-shaped trabeculae.

The mean primary eigenvector and spherical variance was computed using GEOrient software (www.holcombe.net.au/software/rodh_software_georient.htm). The mean primary eigenvector is the resultant of all the primary eigenvectors (μ_1) from each specimen (Mardia 1972), presented in terms of two values, trend (T_m) and incline (I_m). The trend of a vector is the direction of its projection on a transverse plane, with 0/360 degrees directed anteriorly, 90 degrees directed medially, and 270 degrees directed laterally. The incline of a vector is its superiorly-directed angle from the transverse plane. The spherical variance (s) is a measure (0-1) of the variability of the data as reflected by the resultant (Mardia 1972). A low variance indicates strong vector clustering, while a high variance indicates greater vector dispersion.

1.3 Results

Table 1.1 summarizes the predictions set forth in this study and the results in the distal tibia and talus. Tables 1.2 and 1.3 list the mean values, standard deviations and coefficients of variation for each bone property by ROI for the distal tibia and talus, respectively. Tables 1.4 and 1.5 list the correlation coefficients among bone properties within each of the nine regions of interest.

1.3.1 Age relationship

In the distal tibia, Sc.Th was found to decrease with increasing age in the anterolateral regions (A1, A2, B1, and B2) (Table 1.4). Tb.BV/TV and Tb.N were also found to decrease with increasing age, but significantly only in the centrolateral (B1) region. Tb.DA and Tb.E increased with age, but only significant in the centromedial (B3) and posteromedial (C3) regions.

In the talus, Tb.DA increased with age, but reaching significance only in the anterolateral (A1) and posterolateral (C1) regions (Table 1.5).

1.3.2 Body mass relationship

In the tibia, Sc.Th and Tb.Th decreased with increasing body mass; however significance was attained only in the centrolateral (B1) and posterocentral (C2) regions (Table 1.4).

In the talus, Sc.Th, Sc.MeanHouns, and Tb.BV/TV decreased with body mass, but only along the lateral talar rim (Table 1.5). A negative relationship was found between mass and Sc.Th in the anterolateral (A1), anterocentral (A2), and centrolateral (B1) regions, and mass and Sc.MeanHouns in the centrolateral (B1) and posterolateral (C1) regions. A negative relationship was found between mass and Tb.BV/TV only in the posterolateral (C1) region.

1.3.3 Tibia

1.3.3.1 Bivariate correlations among variables

Bivariate correlations revealed significant relationships among variables, but the effect was dependent on region (Table 1.4).

Among subchondral bone variables, a strong positive relationship was found between Sc.MeanHouns and Sc.Th in all regions, as predicted if these two measures are indicators of subchondral bone strength.

Among trabecular bone variables, expected geometric relationships were found in almost all regions, such as moderate positive relationships between Tb.BV/TV and Tb.Th and Tb.N, and a strong positive relationship between Tb.DA and Tb.E. VOIs with thicker and more numerous trabeculae will inherently have greater bone volume, and trabeculae that are more elongated and rod-shaped are by nature highly anisotropic. Tb.BV/TV decreased with increasing Tb.DA and Tb.E in the anterolateral regions (A1, B1, and B2) and in the posteromedial (C3) region. Tb.N

decreased with increasing Tb.E in the anterolateral (A1), posterolateral (C1) and posteromedial (C3) regions. These results indicate that variations in bone volume in the lateral and posteromedial regions are related to variations in the shape of trabeculae.

1.3.3.2 Regional variation of scalar variables

Division of the distal tibia into thirds along the anteroposterior axis showed indicators of greater bone strength in the posterior third as predicted (Table 1.6). The posterior third (Row C) had greater Tb.BV/TV than the anterior third, with lower Tb.Th but greater Tb.N. The posterior row also tended to have greater Sc.Th than the other regions although significance was not met. Contrary to predictions however, the central third (Row B) was found to have higher Tb.E and Tb.DA, but lower Tb.I and Sc.%HighDensity than either the anterior or posterior row.

Division of the distal tibia into thirds along the mediolateral axis also revealed significant differences in variables (Table 1.7), although not as predicted. Against predictions, the central third (Column 2) had greater Tb.BV/TV and Tb.Th than the other regions, and the lateral third had greater Tb.BV/TV and Tb.Th than the medial third. The medial third (Column 3) which was predicted to have stronger bone properties, indeed showed greater Sc.Th, but had lower Tb.BV/TV, Tb.Th, and Tb.N. The trabecular bone of the medial third also had greater Tb.DA than the central and lateral thirds. The lateral third was found to have the greatest Tb.E.

Further division of the distal tibia into 9 regions more specifically highlighted regional differences (Table 1.10, Figures 1.2 and 1.3). The highest Tb.BV/TV was located in the anterocentral (A2) and posterocentral (C2) regions, while the lowest was in the medial regions (A3 and B3). The highest Tb.DA occurred in the centrolateral (B1) and centromedial (B3) regions. The anterocentral (A2) region had the highest Tb.Th. The anteromedial (A3) and centromedial (B3) regions had the lowest Tb.N. Sc.%HighDens was lowest in the central (B2) region, and highest in the anteromedial (A3) and posterolateral (C1) regions. The medial regions (A3, B3, and C3) had the highest Sc.Th.

In summary, the medial regions of the distal tibia showed subchondral bone properties indicative of stronger bone, but the mid-sagittal regions of the distal tibia exhibited trabecular bone properties that are associated with increased bone strength.

1.3.3.3 Regional variation of degree of anisotropy, trabecular shape, and primary orientation

Figure 1.6 graphically depicts the variation in trabecular shape indices Tb.I and Tb.E. Table 1.14 lists the mean primary, secondary and tertiary eigenvalues and the direction (trend and inclination) and variance of the primary eigenvector for each species by ROI. Figure 1.8 depicts the direction of the primary eigenvector for all study specimens.

The shape and orientation of trabeculae in the distal tibia were generally as predicted, particularly in the mid-coronal third (Row B). Examination of the eigenvalues on ternary plots (Figure 1.6) shows that the trabeculae in the mid-coronal third (Row B) (which had higher Tb.E

and Tb.DA,) were more consistently rod-like in shape than the anterior or posterior thirds. These elongated, rod-like trabeculae were consistently oriented as qualitatively described by other authors, almost perpendicular to the articular surface with the trabeculae in the centrolateral (B1) region directed slightly laterally and those in the centromedial (B2) region directed slightly medially towards the diaphyseal cortex (Figure 1.8). There was very little inter-individual variation in the direction of the primary eigenvectors in these regions (Table 1.14). The trabeculae in the anterocentral and anteromedial region were oriented more variably, with many principal directions oriented transversely. This seemed to be a reflection of greater bone isotropy in these regions, as well as prominent trabeculae that can be seen extending superolaterally away from the medial malleolus (Figure A1).

Division of the distal tibia into thirds along the mediolateral axis did not reveal stronger, more isotropic along the medial aspect as predicted, but rather in the mid-sagittal third (Column 2) in comparison to the lateral and medial thirds (Table 1.7). The lateral third was found to have greater Tb.E than the central third. These effects were primarily driven by the increased isotropy and decreased elongation in the anterocentral (A2) and posterocentral (C2) regions. Examination of the eigenvalues on ternary plots (Figure 1.6) confirms that the trabeculae in these areas were relatively more isotropic and plate-like in shape than those in other regions. The directions of the primary eigenvectors were as expected -- perpendicular to the articular surface, with a slight inclination towards the diaphyseal cortices (Figure 1.8). The trabeculae in the anterocentral (A2) region were the most isotropic, such that there was a bimodal pattern of the computed primary eigenvector orientations: some directed superiorly and some laterally. This bimodality is reflected in the relatively high variance computed for the primary eigenvector in this region (Table 1.14).

In summary, the most elongated rod-shaped trabeculae, thought to be indicative of relatively weaker bone, were found along a mid-coronal plane (in the centrolateral, central, and centromedial regions), while relatively more isotropic trabeculae, thought to be indicative of relatively stronger bone, were found in the mid-sagittal plane particularly in the anterocentral and posterocentral regions.

1.3.4 Talus

1.3.4.1 Bivariate correlations among variables

Bivariate correlations revealed fewer significant relationships among variables in the talus than there were in the distal tibia (Table 1.5). There was a strong negative correlation between Tb.Th and Tb.N in all regions. Moderate positive correlations were also found between Tb.BV/TV and Tb.N, and among all three of the subchondral variables.

1.3.4.2 Regional variation of scalar variables

Significant regional differences were found within the talus for each variable (Tables 1.8 and 1.9).

Although the posterior region was predicted to have stronger bone, the posterior third of the talus (Row C) was actually found to have the lowest Tb.BV/TV and Tb.Th. The mid-coronal third (Row B) instead had the greatest Tb.BV/TV and Sc.Th.

Along the mediolateral axis, the medial third showed properties related to greater bone strength as predicted, with the greatest Tb.BV/TV, Sc.%HighDensity, Sc.MeanHouns, and Sc.Th. The mid-sagittal third (Column 2) had the lowest Tb.BV/TV and Sc.%HighDensity and the highest Tb.DA. The lateral third (Column 1) had the highest Tb.E.

Examination of the 9 regions (Table 1.11, Figures 1.4 and 1.5) revealed the greatest Tb.BV/TV and relative subchondral radiodensity in the centrolateral (B1) and centromedial (B3) regions. The anteromedial region (A3) had the lowest Tb.DA but the highest Tb.Th. The centromedial (B3) region also had the highest Sc.MeanHouns and Sc.Th. The highest Tb.DA and lowest Tb.N occurred in the anterocentral (A2) region. The lowest subchondral radiodensity occurred in the central regions (A2, B2, and C2). The posterolateral (C1) region had the lowest Sc.Th and Tb.BV/TV, but the highest Tb.E.

In summary, the medial regions of the talus, like that of the distal tibia, showed subchondral bone properties indicative of stronger bone as predicted. The trabecular bone properties did not fully meet predictions. The medial regions had greater Tb.BV/TV, but the centrolateral region did as well, implying that greatest bone strength is shared between the medial and lateral talar margins.

1.3.4.3 Regional variation of degree of anisotropy, trabecular shape, and primary orientation

Figure 1.7 graphically depicts the variation in trabecular shape indices Tb.I and Tb.E. Table 1.15 lists the mean primary, secondary and tertiary eigenvalues and the direction (trend and inclination) and variance of the primary eigenvector for each species by ROI. Figure 1.9 depicts the direction of the primary eigenvector for all study specimens.

The shape and orientation of trabeculae in the talus were found to be generally as predicted from other qualitative descriptions. The mid-sagittal regions along the anteroposterior axis of the talar dome had the greatest degree of anisotropy, particularly the anterocentral (A2) region (Figure 1.4, Table 1.9). Examination of the ternary plots (Figure 1.7) reveals that the trabeculae in the mid-sagittal regions were also highly anisotropic, but more plate-like in shape as described by Athavale et al. (2008). The stereoplot of the primary eigenvectors in these regions demonstrates this as variability in primary orientation direction restricted to a single plane. The plane of the plate-like trabeculae was oriented in a slight anteromedial-to-posterolateral direction (Figure 1.9).

The trabeculae in the lateral and anteromedial regions were more elongated and rod-like in shape. The elongated trabeculae in the lateral regions were consistently oriented in the superoanteromedial direction, with very little interindividual variation (Figure 1.9, Table 1.15). The trabeculae in the anteromedial (A3) region were found to be somewhat elongated, but also relatively thick (Figure 1.4, Table 1.11). The primary eigenvectors in this region were oriented superoposterolaterally (Figure 1.9), indicating that these trabeculae are transitioning to become more parallel to the neck of the talus such as to direct load from the articular surface to the talar head.

The trabeculae in the posteromedial (C3) region were found to be the least anisotropic and the most variable in shape and primary orientation direction (Table 1.11, Figure 1.9).

In summary, the most elongated rod-shaped trabeculae, thought to be indicative of relatively weaker bone, were found along the lateral talar margin, while relatively more isotropic trabeculae, thought to be indicative of relatively stronger bone, were found in the mid-sagittal plane.

1.3.5 Relationship between distal tibia morphology and talar morphology

Table 1.16 lists the bivariate correlation coefficients between variables computed for regions of the distal tibia and those of the corresponding region of the talus. The strongest relationships found involved Tb.Th and Tb.N. Both the regional Tb.Th ($r=0.434$, $p<0.001$) and the Tb.N ($r=0.606$, $p<0.001$) in the distal tibia were positively correlated with their counterpart in the talus. Furthermore, because of the strong negative relationship between Tb.Th and Tb.N, the Tb.N in the distal tibia was negatively correlated with the Tb.Th in the talus ($r=-0.626$, $p<0.001$), and vice versa, the Tb.Th in the distal tibia was negatively correlated with the Tb.N in the talus ($r=-0.311$, $p<0.001$).

All three of the subchondral bone radiodensity variables showed positive reciprocal relationships. Regions with high Sc.%HighDens ($r=0.335$, $p<0.001$), Sc.MeanHouns ($r=0.295$, $p=0.001$), and Sc.Th ($r=0.415$, $p<0.001$) in the tibia corresponded to those in the talus.

1.4 Discussion

In this study, the subchondral and trabecular bone morphology in the human tibiotalar joint was characterized to test the overall hypothesis that the morphology of these bone tissues as quantified from micro-CT images reflect habitual functional load. The results show that there were significant relationships among the subchondral bone properties and among the trabecular bone properties in each bone. However, strong correlations between subchondral bone and trabecular bone properties were not found as predicted, suggesting that these tissue types may not reflect habitual load in the same way. The subchondral bone properties showed the strongest correspondence between opposing regions of the distal tibia and talus, while the trabecular bone properties largely did not. Regional differences in architecture in the talus, but not the distal

tibia, were found to be generally in agreement with predictions based on joint kinetics and kinematics during walking.

1.4.1 Correlations among variables

In the distal tibia, the strong positive relationship between trabecular bone volume and trabecular number, and the strong negative relationship between these variables and trabecular anisotropy and elongation, reflects the qualitatively thin rod-shaped morphology of the trabeculae (Table 1.4). Thin, elongated trabeculae suggest a loading regime that is low in magnitude (Ding et al. 2002a), but these trabeculae seem to be consistently aligned from the articular surface to the tibial cortex which suggests that the loads may also be highly predictable in direction.

In the talus, different relationships were found (Table 1.5). The strong inverse relationship between trabecular thickness and number is intuitive from structural mechanics, in that these properties can covary within a given volume of bone to provide the same strength characteristics. Bone tissue properties have been demonstrated to co-adapt in this way to withstand daily loads at the whole bone level (Tommasini et al. 2005). Here, it was found that trabecular number had a stronger correlation with bone volume than trabecular thickness, which has also been demonstrated in the hominoid thoracic vertebrae (Cotter et al. 2009). There results indirectly support the hypothesis that trabecular thickness may be relatively constrained (Swartz et al. 1998).

Along these lines, the correlations found here among trabecular bone volume and structural measures of isotropy and elongation have been noted in the past (Mittra et al. 2005), suggesting that there is a relationship between the volume of bone and the shape it assumes. For instance, within a given volume of interest, isotropic trabeculae that fill the volume would inherently have greater bone volume than a single anisotropic rod-shaped trabecula. Which attribute is the limiting factor is unknown. The volume of bone may act as a limiting factor in order to minimize weight, especially important in this distal ankle region to minimize the cost of locomotion (Huiskes 2000; Witte et al. 1991). But the shape of bone, e.g., thickness of a rod, may be limited by the physiological processes of bone tissue maintenance (Doube et al. 2011; Swartz et al. 1998).

Against predictions, relationships between subchondral bone properties and properties of the underlying trabecular bone were largely not found. Only subchondral bone thickness and trabecular bone volume were significantly positively correlated, but only in the lateral regions of the tibia and the posterolateral region of the talus. The uncoupling of trabecular bone morphological properties from that of the articular surface has been noted before (Rafferty and Ruff 1994). The varying functional demands and limitations of each tissue type may be the primary influence on morphology rather than purely to withstand mechanical load. For example, subchondral bone is considered to have two main functions: stress absorption and maintenance of joint shape (Kawcak et al. 2001). Trabecular bone is considered to also function structurally

to dissipate joint stress, but also as a physiological reservoir for calcium. Indeed, trabecular bone volume and thickness may be more plastic in reacting to changes in both systemic physiology and load conditions than is cortical bone (Rubin et al. 2002; Ward et al. 2004).

1.4.2 Relationships with age and body mass

Despite the narrow age range of the sample in this study, some significant relationships were found among bone properties, age, and body mass, but only in particular regions. The results indicate a decrease of subchondral bone thickness and trabecular bone volume and an increase in trabecular anisotropy and elongation with increasing age and with increasing body mass, but only in the centrolateral and centromedial aspects of the distal tibia and the lateral regions of the talus. Decreased bone volume and increased anisotropy with age has been shown in numerous previous studies (e.g., Ding et al. 2002b; Grote et al. 1995), in the context of osteoporotic bone loss. Interestingly, Grote et al. (1995) found that lumbar vertebral bodies showed greater age-related changes of trabecular microarchitecture than cervical vertebral bodies, suggesting that these relative differences may be linked to relatively greater habitual load. Sode et al. (2010) found that in the distal tibia, older women had decreased trabecular bone volume, thickness, and number compared to younger women, finding that those differences were more prominent in the anterior regions of the distal tibia than the posterior regions. Thus, there may be site-specific differences in how subchondral bone and trabecular bone change with age, and these may be linked to relative differences in habitual load, but a much more detailed study is necessary to examine this hypothesis.

A limitation to the interpretation of these results is that there was a significant positive correlation between age and body mass ($r = 0.383$, $p < 0.001$). Thus there may be an interaction effect between age and body mass. Additionally, any potential differences in the tibial cortical diaphysis were not measured in this study, so there is a possibility that simultaneous increase in diaphyseal strength could explain the decrease in trabecular bone strength with age and body mass.

1.4.3 Regional variation of bone properties.

In agreement with previous studies of subchondral density (Muhlhofer et al. 2009; Müller-Gerbl 2001; Müller-Gerbl and Putz 1995) in the ankle bones, and predictions based on joint kinematics, the medial regions of the tibial plafond and talar trochlea displayed relatively thicker and more radiodense subchondral bone. The trabecular bone properties in the talus also implied greater bone strength medially, with greater bone volume and trabecular isotropy. However, the trabecular bone volume distribution in the tibia did not agree with this pattern, showing relatively greater trabecular bone volume on the lateral aspect of the distal tibia. This result was primarily driven by the very low bone volume in the antero- and centromedial regions compared to the rest of the regions, rather than particularly high bone volume laterally. Thus overall, the distribution of both subchondral and trabecular bone properties were as predicted,

supporting the hypothesis that these properties reflect mediolateral differences in habitual load in the ankle.

Along the anteroposterior axis, predictions of greater bone strength being found posteriorly were somewhat met. Greater values of subchondral bone radiodensity were found in the three posterior regions, but also in the three anterior regions of the distal tibia. Significance was not reached with subchondral thickness, but the posterior regions of the distal tibia tended to be thicker. In the talus, greater values of subchondral bone thickness were found in the central regions rather than the predicted posterior regions, however this result was driven by the greater thickness in the centromedial region. Overall, these results show little difference in subchondral bone properties and inferred strength along an anteroposterior axis.

The trabecular bone distribution along the anteroposterior axis was consistent with greater bone strength posteriorly in the tibia as predicted, having greater trabecular bone volume and trabecular number. However, in the talus stronger trabecular properties were found in the anterior regions. These results primarily reflect the conversely significant differences in the antero- and centromedial regions of both bones. In the distal tibia these regions displayed decreased trabecular bone volume, thickness, and number, while in the talus these regions had increased trabecular bone volume and thickness.

The trabeculae in the distal tibia were mostly elongated and rod-like in shape, with the direction of the primary eigenvector fairly consistently directed superoposteriorly, which would be as expected to transfer force from the tibial plafond to the tibial cortex. But the trabeculae in the posterior regions of the tibia were considerably more isotropic and plate-shaped than in most other regions. This result was as predicted from the high impact heel-strike event of gait and is in agreement with Lai et al. (2005) who found higher trabecular bone volume, thickness, and number in the posterior distal tibia versus the anterior. Isotropic and plate-shaped trabeculae are generally thought to be indicators of bone that withstands higher magnitude habitual loads (Ding et al. 2002a), and indeed the posterior regions of the tibial plafond have also been demonstrated to have relatively greater bone strength by mechanical osteopenetration tests (Hvid et al. 1985).

Relatively thick trabecular bone was consistently found in the anterocentral region of the distal tibia, along with low trabecular elongation and thin subchondral bone. This was not predicted, but the anterior regions of the ankle joint have been found to be under high stress when the ankle is maximally dorsiflexed in its close-packed position during the push-off phase of gait (Haraguchi et al. 2009). The primary eigenvectors here formed two clusters -- one directed superoanteriorly that serve to transmit load to the cortex above as expected, and another directed more laterally. The two equally-prominent orientations explains the high degree of variability in direction of the primary eigenvector in this region. The laterally-directed struts are extensions from the anteromedial region where they are the predominant feature. In maximum dorsiflexion, the relatively wider anterior aspect of the talus is wedged between the medial and lateral malleoli, presumably creating a horizontally-directed load from the articulation with the medial malleolus.

A variable that was found to have significantly higher values in the lateral regions of the tibia was trabecular anisotropy. However, high values of anisotropy were also found in the medial regions so it cannot be concluded that a high level of anisotropy may be an indicator of greater joint contact stress. Greater trabecular anisotropy and elongation in the centrolateral and centromedial regions suggest that these regions were habitually exposed to highly predictable, but relatively low mechanical stress (Ding et al. 2002a). This agrees with the stereotype of human gait as generating forces and moments primarily in the sagittal plane, with relatively small abduction/adduction moments in the talocrural joint.

The shape and orientation of trabeculae in the talus is in agreement with previous qualitative studies. In their serial sections of dry tali, Pal and Routal (1998) describe "anteroposterior" plates occupying a "major part of the body of the talus", and "extending vertically from the trochlear surface to the posterior calcaneal facet". They suggest that the arrangement of the trabeculae into plates enables the load to be transmitted evenly throughout the arc of the movement of the tibia over the talus during gait. Trabecular plates have also been found to account for the majority of total trabecular bone volume in the femoral neck, proximal tibia, and L4/L5 lumbar vertebral bodies, and contribute to the compressive strength of bone samples to a much greater degree than do rods (Liu et al. 2009; Liu et al. 2008; Liu et al. 2006). Moreover, these studies find that the majority of trabecular plates are also axially oriented along the principal direction of loading, thus playing an essential role in attenuating axial compressive forces (Liu et al. 2008; Smit et al. 1997).

1.4.4 Relationships between tibia morphology and talar morphology

The positive relationship between regional subchondral bone properties in the tibia and the talus was as predicted. Regardless of the source or the location of the net load within the talocrural joint, that load seems to be applied in common to both opposing articular surfaces. In particular, it can be seen from the data that the medial regions of the joint showed the greatest subchondral radiodensity in both tibia and talus, while the central region in both bones displayed the least (Figures 1.3 and 1.6).

The trabecular bone thickness and number also was as predicted in that the regions with thick trabeculae in the tibia corresponded to those in the talus. In particular, the anterior regions were found to have the thickest trabeculae and the posterior regions the thinnest trabeculae in both bones (Figures 1.2 and 1.4).

The other trabecular bone properties were not found to be strongly correlated between bones, suggesting that they may be affected by strains or physiological processes other than compressive joint load. For example, the elongated shape of trabeculae in the distal tibia was very different from the plate-shaped trabeculae in the talus presumably due to the demands of transferring load through the very differently-shaped bones. More studies are needed of the morphology of matched articulating sets of bones in other joints and in other species to confirm these results.

Interestingly, increased trabecular bone volume, thickness, number, and isotropy were found in the anterior and posterior edges of the distal tibia and the lateral and medial edges of the talus. These bone edges form slightly incongruent saddle-shaped joint surfaces such that when they are opposed during weight-bearing, the rims of each joint surface may be spread apart ("wishboned") under tension. Characteristics of such tensile forces include trabeculae that are oriented more tangentially to the joint surface (Eckstein et al. 1999), such as was found in the anteromedial region of the distal tibia. This effect may be especially the case in the closepacked position of the joint during the pushoff phase of walking as the talus is wedged in the mortise formed by the anteromedial region of the distal tibia and the distal fibula.

1.5 Conclusion

The subchondral bone and trabecular bone properties in the human distal tibia and talus varied across the joint in ways that largely support the hypothesis that the site-specific morphology of these tissues reflect local stresses during habitual activity. The medial regions of the distal tibia and talus express high subchondral bone radiodensity and thickness that is consistent with the medially-borne joint loads during most of the weight-bearing phase of walking and standing. The anterior and posterior edges of the distal tibia and the lateral and medial edges of the talus showed increased trabecular bone volume, thickness, number, and isotropy that agree with previous studies of bone strength.

The morphology of subchondral bone and that of the underlying trabecular bone in each bone were not found to be strongly correlated, suggesting that while these tissues may be adapted to habitual loads, they may be attuned to different aspects of those loads.

Strongest correlations between the distal tibia and talus were in the subchondral bone properties and trabecular thickness and number, implying these properties may best reflect the shared load within the joint.

Tables

Table 1. 1: Summary of predictions and outcomes.

Variable	Prediction	Met in Ti	Met in Ta
Age	↑ age: ↓ Tb.BV/TV, ↑ Tb.DA	✓	✓
Body mass	↑ BM: ↑ Tb.BV/TV	×	×
All Sc	Correlations among subchondral bone variables	✓	✓
All Tb	Correlations among trabecular bone variables	many	few
All Sc and Tb	Correlations between Sc and Tb bone variables	few	few
Sc.Th, Sc.%HighDensity, Sc. MeanHouns	Medial > Lateral; Posterior > Anterior	✓ ✓(ns)	✓ × (C>A=P)
Tb.BV/TV, Tb.Th, Tb.N	Medial > Lateral Posterior > Anterior	× (L=C>M) ✓	✓ × (C=A>P)
Tb.DA, Tb.E	Lateral > Medial Anterior > Posterior	× (M=L>C) × (C>P=A)	✓ ✓(ns)
Tb.I	Medial > Lateral Posterior > Anterior	× (C>L=M) × (A=P>C)	✓ ✓(ns)
Tb orientation	Primary orientation consistent among individuals, and consistent with qualitative descriptions	✓	✓

Table 1. 2: Means and variation of all variables in the distal tibia by region.
Row A= anterior, Row C = posterior, Column 1 = lateral, Column 3 = medial.

Tibia	Lateral				ML-Central				Medial			
	A1				A2				A3			
		Mean	SD	CV		Mean	SD	CV		Mean	SD	CV
	Tb.BV/TV	0.31	0.05	0.15	Tb.BV/TV	0.34	0.05	0.14	Tb.BV/TV	0.25	0.05	0.20
	Tb.DA	4.23	1.79	0.42	Tb.DA	3.32	1.22	0.37	Tb.DA	5.43	2.96	0.54
	Tb.I	0.28	0.13	0.45	Tb.I	0.34	0.13	0.38	Tb.I	0.23	0.10	0.44
	Tb.E	0.61	0.14	0.22	Tb.E	0.39	0.16	0.40	Tb.E	0.52	0.12	0.23
Anterior	Tb.Th	0.19	0.03	0.16	Tb.Th	0.22	0.03	0.15	Tb.Th	0.18	0.04	0.22
	Tb.N	1.61	0.24	0.15	Tb.N	1.57	0.27	0.17	Tb.N	1.27	0.27	0.21
	Sc.%HighDensity	0.46	0.56	1.23	Sc.%HighDensity	0.46	0.67	1.46	Sc.%HighDensity	0.97	1.44	1.49
	Sc.Mean Houns	1233	496	0.40	Sc.Mean Houns	1187	416	0.35	Sc.Mean Houns	1332	413	0.31
	Sc.Th	0.25	0.07	0.27	Sc.Th	0.25	0.06	0.23	Sc.Th	0.33	0.05	0.15
	B1				B2				B3			
		Mean	SD	CV		Mean	SD	CV		Mean	SD	CV
	Tb.BV/TV	0.33	0.05	0.15	Tb.BV/TV	0.32	0.04	0.13	Tb.BV/TV	0.28	0.05	0.19
	Tb.DA	8.67	3.76	0.43	Tb.DA	5.81	2.72	0.47	Tb.DA	8.02	5.26	0.66
	Tb.I	0.15	0.11	0.74	Tb.I	0.22	0.11	0.51	Tb.I	0.20	0.17	0.82
	Tb.E	0.66	0.17	0.26	Tb.E	0.69	0.14	0.20	Tb.E	0.70	0.20	0.28
AP-Central	Tb.Th	0.20	0.03	0.15	Tb.Th	0.20	0.03	0.13	Tb.Th	0.18	0.03	0.15
	Tb.N	1.53	0.23	0.15	Tb.N	1.53	0.27	0.18	Tb.N	1.39	0.29	0.21
	Sc.%HighDensity	0.15	0.23	1.51	Sc.%HighDensity	0.01	0.02	3.37	Sc.%HighDensity	0.33	0.48	1.43
	Sc.Mean Houns	1216	582	0.48	Sc.Mean Houns	1049	420	0.40	Sc.Mean Houns	1241	426	0.34
	Sc.Th	0.26	0.05	0.18	Sc.Th	0.27	0.05	0.20	Sc.Th	0.31	0.06	0.20
	C1				C2				C3			
		Mean	SD	CV		Mean	SD	CV		Mean	SD	CV
	Tb.BV/TV	0.30	0.04	0.13	Tb.BV/TV	0.34	0.04	0.13	Tb.BV/TV	0.33	0.05	0.14
	Tb.DA	4.16	1.89	0.45	Tb.DA	3.60	1.69	0.47	Tb.DA	5.73	3.27	0.57
	Tb.I	0.29	0.12	0.43	Tb.I	0.34	0.15	0.45	Tb.I	0.22	0.10	0.43
	Tb.E	0.56	0.14	0.25	Tb.E	0.47	0.20	0.43	Tb.E	0.47	0.20	0.43
Posterior	Tb.Th	0.18	0.02	0.12	Tb.Th	0.19	0.02	0.11	Tb.Th	0.17	0.02	0.12
	Tb.N	1.66	0.24	0.14	Tb.N	1.72	0.25	0.15	Tb.N	1.86	0.32	0.17
	Sc.%HighDensity	0.72	0.95	1.31	Sc.%HighDensity	0.99	2.33	2.35	Sc.%HighDensity	0.58	1.18	2.04
	Sc.Mean Houns	1229	461	0.37	Sc.Mean Houns	1219	438	0.36	Sc.Mean Houns	1261	413	0.33
	Sc.Th	0.27	0.07	0.28	Sc.Th	0.31	0.10	0.34	Sc.Th	0.33	0.08	0.25

		Mean	SD	CV
	Tb.BV/TV	0.31	0.05	0.17
	Tb.DA	5.44	3.40	0.63
	Tb.I	0.25	0.14	0.54
Overall	Tb.E	0.56	0.19	0.34
	Tb.Th	0.19	0.03	0.16
	Tb.N	1.57	0.31	0.20
	Sc.%HighDensity	0.48	0.86	1.80
	Sc.MeanHouns	1219	449	0.37
	Sc.Th	0.29	0.07	0.26

Table 1. 3: Means and variation of all variables in the talus by region.
Row A= anterior, Row C = posterior, Column 1 = lateral, Column 3 = medial.

Talus	Lateral				ML-Central				Medial			
	A1				A2				A3			
		Mean	SD	CV		Mean	SD	CV		Mean	SD	CV
	Tb.BV/TV	0.39	0.04	0.11	Tb.BV/TV	0.35	0.04	0.12	Tb.BV/TV	0.40	0.05	0.12
	Tb.DA	9.12	2.87	0.31	Tb.DA	13.60	5.79	0.43	Tb.DA	3.36	0.98	0.29
	Tb.I	0.12	0.04	0.32	Tb.I	0.09	0.04	0.44	Tb.I	0.32	0.08	0.27
	Tb.E	0.62	0.13	0.21	Tb.E	0.38	0.11	0.28	Tb.E	0.50	0.11	0.22
Anterior	Tb.Th	0.20	0.03	0.15	Tb.Th	0.20	0.03	0.14	Tb.Th	0.21	0.03	0.14
	Tb.N	1.88	0.32	0.17	Tb.N	1.57	0.32	0.20	Tb.N	1.74	0.25	0.14
	Sc.%High Density	0.63	0.53	0.84	Sc.%High Density	0.01	0.02	2.33	Sc.%High Density	3.92	3.33	0.85
	Sc.Mean Houns	1487	670	0.45	Sc.Mean Houns	1337	557	0.42	Sc.Mean Houns	1726	470	0.27
	Sc.Th	0.27	0.07	0.26	Sc.Th	0.31	0.08	0.25	Sc.Th	0.36	0.08	0.23
	B1				B2				B3			
		Mean	SD	CV		Mean	SD	CV		Mean	SD	CV
	Tb.BV/TV	0.41	0.03	0.07	Tb.BV/TV	0.36	0.04	0.12	Tb.BV/TV	0.40	0.06	0.14
	Tb.DA	8.58	2.55	0.30	Tb.DA	9.34	5.47	0.59	Tb.DA	6.61	3.43	0.52
	Tb.I	0.13	0.04	0.29	Tb.I	0.15	0.08	0.56	Tb.I	0.19	0.09	0.48
	Tb.E	0.59	0.12	0.20	Tb.E	0.38	0.12	0.31	Tb.E	0.35	0.13	0.37
AP-Central	Tb.Th	0.19	0.02	0.12	Tb.Th	0.19	0.03	0.15	Tb.Th	0.20	0.03	0.15
	Tb.N	2.00	0.32	0.16	Tb.N	1.82	0.40	0.22	Tb.N	1.89	0.37	0.19
	Sc.%High Density	0.93	0.86	0.92	Sc.%High Density	0.01	0.03	3.91	Sc.%High Density	4.49	3.57	0.80
	Sc.Mean Houns	1599	745	0.47	Sc.Mean Houns	1373	642	0.47	Sc.Mean Houns	1917	625	0.33
	Sc.Th	0.32	0.09	0.30	Sc.Th	0.34	0.08	0.25	Sc.Th	0.42	0.09	0.22
	C1				C2				C3			
		Mean	SD	CV		Mean	SD	CV		Mean	SD	CV
	Tb.BV/TV	0.34	0.03	0.10	Tb.BV/TV	0.34	0.05	0.13	Tb.BV/TV	0.36	0.04	0.11
	Tb.DA	5.48	1.68	0.31	Tb.DA	9.74	5.89	0.61	Tb.DA	5.89	5.32	0.90
	Tb.I	0.20	0.05	0.24	Tb.I	0.15	0.09	0.64	Tb.I	0.27	0.14	0.50
	Tb.E	0.66	0.07	0.11	Tb.E	0.41	0.11	0.27	Tb.E	0.27	0.09	0.33
Posterior	Tb.Th	0.18	0.02	0.12	Tb.Th	0.18	0.03	0.16	Tb.Th	0.18	0.02	0.13
	Tb.N	1.80	0.32	0.18	Tb.N	1.80	0.41	0.23	Tb.N	1.86	0.28	0.15
	Sc.%High Density	1.07	0.84	0.78	Sc.%High Density	0.05	0.11	2.37	Sc.%High Density	2.22	3.53	1.59
	Sc.Mean Houns	1498	602	0.40	Sc.Mean Houns	1447	601	0.42	Sc.Mean Houns	1793	601	0.34
	Sc.Th	0.24	0.07	0.29	Sc.Th	0.29	0.07	0.25	Sc.Th	0.32	0.09	0.27

	Mean	SD	CV
Tb.BV/TV	0.37	0.05	0.13
Tb.DA	7.97	4.96	0.62
Tb.I	0.18	0.10	0.59
Tb.E	0.46	0.17	0.36
Tb.Th	0.19	0.03	0.15
Tb.N	1.82	0.35	0.19
Sc.%HighDensity	1.48	2.57	1.73
Sc.MeanHouns	1575	629	0.40
Sc.Th	0.32	0.09	0.29

Overall

Table 1. 4: Correlation coefficients (Pearson's r) among variables measured in the (a) lateral, (b) central, and (c) medial regions of the distal tibia.

a.

Lateral

	A1		Tb.BV/TV	Tb.DA	Tb.I	Tb.E	Tb.Th	Tb.N	Sc.%High Density	Sc.Mean Houns	Sc.Th	Age	Mass
Anterior	Tb.BV/TV	rho	-										
		p											
	Tb.DA	rho	-0.686 **	-									
		p	0.002										
	Tb.I	rho	0.686 **	-1.000	-								
		p	0.002	*inf*									
	Tb.E	rho	-0.664 **	0.886 ***	-0.886 ***	-							
		p	0.003	0.000	0.000								
	Tb.Th	rho	0.534 *	-0.364	0.364	-0.209	-						
		p	0.023	0.137	0.137	0.404							
	Tb.N	rho	0.593 **	-0.531 *	0.531 *	-0.672 **	-0.307	-					
		p	0.009	0.023	0.023	0.002	0.216						
	Sc.%High Density	rho	-0.121	-0.232	0.232	-0.253	-0.088	-0.034	-				
		p	0.633	0.354	0.354	0.311	0.729	0.893					
	Sc.Mean Houns	rho	0.346	-0.028	0.028	-0.011	0.544 *	-0.181	-0.046	-			
		p	0.160	0.913	0.913	0.964	0.020	0.473	0.855				
	Sc.Th	rho	0.467 *	-0.323	0.323	-0.358	0.269	0.292	0.236	0.546 *	-		
		p	0.050	0.191	0.191	0.145	0.280	0.240	0.345	0.019			
	Age	rho	-0.124	0.226	-0.226	0.214	-0.037	-0.148	-0.584 *	-0.053	-0.319	-	
		p	0.623	0.368	0.368	0.393	0.883	0.558	0.011	0.840	0.197		
	Mass	rho	-0.265	0.223	-0.223	0.345	-0.351	-0.002	-0.404	-0.053	-0.211	0.369	-
		p	0.287	0.373	0.373	0.161	0.153	0.994	0.096	0.841	0.401	0.132	

	B1		Tb.BV/TV	Tb.DA	Tb.I	Tb.E	Tb.Th	Tb.N	Sc.%High Density	Sc.Mean Houns	Sc.Th	Age	Mass
AP-Central	Tb.BV/TV	rho	-										
		p											
	Tb.DA	rho	-0.428	-									
		p	0.076										
	Tb.I	rho	0.428	-1.000	-								
		p	0.076	*inf*									
	Tb.E	rho	-0.583 *	0.309	-0.309	-							
		p	0.011	0.213	0.213								
	Tb.Th	rho	0.717 **	-0.360	0.360	-0.498 *	-						
		p	0.001	0.142	0.142	0.035							
	Tb.N	rho	0.437	-0.437	0.437	-0.106	-0.117	-					
		p	0.070	0.070	0.070	0.675	0.645						
	Sc.%High Density	rho	0.420	0.163	-0.163	-0.187	0.153	0.289	-				
		p	0.082	0.518	0.518	0.458	0.545	0.245					
	Sc.Mean Houns	rho	0.377	0.022	-0.022	-0.150	0.331	0.214	0.668 **	-			
		p	0.123	0.932	0.932	0.553	0.179	0.395	0.002				
	Sc.Th	rho	0.728 **	-0.063	0.063	-0.207	0.472 *	0.385	0.500 *	0.542 *	-		
		p	0.001	0.804	0.804	0.409	0.048	0.115	0.035	0.020			
	Age	rho	-0.705 **	0.394	-0.394	0.280	-0.358	-0.424	-0.506 *	-0.330	-0.336	-	
		p	0.001	0.105	0.105	0.261	0.144	0.079	0.032	0.211	0.172		
	Mass	rho	-0.495 *	0.054	-0.054	-0.188	-0.210	-0.466	-0.528 *	-0.021	-0.326	0.369	-
		p	0.037	0.832	0.832	0.455	0.404	0.051	0.024	0.940	0.186	0.132	

	C1		Tb.BV/TV	Tb.DA	Tb.I	Tb.E	Tb.Th	Tb.N	Sc.%High Density	Sc.Mean Houns	Sc.Th	Age	Mass
Posterior	Tb.BV/TV	rho	-										
		p											
	Tb.DA	rho	-0.459	-									
		p	0.055										
	Tb.I	rho	0.459	-1.000	-								
		p	0.055	*inf*									
	Tb.E	rho	-0.370	0.926 **	-0.926 **	-							
		p	0.130	0.000	0.000								
	Tb.Th	rho	0.465	0.007	-0.007	0.018	-						
		p	0.052	0.977	0.977	0.945							
	Tb.N	rho	0.585 *	-0.451	0.451	-0.432	-0.329	-					
		p	0.011	0.060	0.060	0.073	0.182						
	Sc.%High Density	rho	0.307	-0.236	0.236	-0.137	-0.001	0.063	-				
		p	0.216	0.345	0.345	0.587	0.997	0.804					
	Sc.Mean Houns	rho	0.319	-0.051	0.051	0.036	0.350	-0.082	0.269	-			
		p	0.197	0.842	0.842	0.887	0.155	0.748	0.280				
	Sc.Th	rho	0.523 *	-0.005	0.005	0.092	0.548	-0.069	0.207	0.874 **	-		
		p	0.026	0.984	0.984	0.717	0.019	0.785	0.409	0.000			
	Age	rho	-0.372	-0.060	0.060	-0.135	-0.190	-0.304	-0.408	0.130	-0.285	-	
		p	0.129	0.813	0.813	0.594	0.449	0.219	0.093	0.618	0.252		
	Mass	rho	-0.337	0.151	-0.151	-0.011	-0.250	-0.060	-0.332	0.194	-0.038	0.369	-
		p	0.172	0.550	0.550	0.964	0.317	0.813	0.179	0.456	0.880	0.132	

Table 1.4: Correlation coefficients (Pearson's r) among variables measured in the (a) lateral, (b) central, and (c) medial regions of the distal tibia.

b.

ML-Central

	A2		Tb.BV/TV	Tb.DA	Tb.I	Tb.E	Tb.Th	Tb.N	Sc.%High	Sc.Mean	Sc.Th	Age	Mass
Anterior	Tb.BV/TV	rho	-										
		p											
	Tb.DA	rho	-0.519 *	-									
		p	0.027										
	Tb.I	rho	0.519 *	-1.000	-								
		p	0.027	*inf*									
	Tb.E	rho	0.086	0.282	-0.282	-							
		p	0.735	0.257	0.257								
	Tb.Th	rho	0.461	-0.259	0.259	0.218	-						
		p	0.054	0.299	0.299	0.385							
	Tb.N	rho	0.628 **	-0.284	0.284	0.053	-0.290	-					
		p	0.005	0.254	0.254	0.836	0.243						
	Sc.%High	rho	-0.104	-0.270	0.270	-0.309	-0.338	0.262	-				
	Density	*p*	0.680	0.279	0.279	0.212	0.170	0.294					
	Sc.Mean	rho	-0.148	0.020	-0.020	-0.379	0.086	-0.362	-0.071	-			
	Houns	*p*	0.559	0.938	0.938	0.121	0.735	0.140	0.778				
	Sc.Th	rho	-0.125	0.102	-0.102	-0.228	0.015	-0.189	-0.150	0.686 **	-		
		p	0.622	0.687	0.687	0.363	0.951	0.453	0.553	0.002			
	Age	rho	-0.022	0.237	-0.237	0.519 *	-0.025	-0.012	-0.672 **	-0.267	-0.301	-	
		p	0.932	0.344	0.344	0.027	0.922	0.961	0.002	0.336	0.224		
	Mass	rho	-0.032	0.372	-0.372	0.192	-0.398	0.288	-0.327	-0.155	-0.293	0.369	-
		p	0.900	0.129	0.129	0.445	0.102	0.246	0.185	0.580	0.237	0.132	

	B2		Tb.BV/TV	Tb.DA	Tb.I	Tb.E	Tb.Th	Tb.N	Sc.%High	Sc.Mean	Sc.Th	Age	Mass
AP-Central	Tb.BV/TV	rho	-										
		p											
	Tb.DA	rho	-0.678 **	-									
		p	0.002										
	Tb.I	rho	0.678 **	-1.000	-								
		p	0.002	*inf*									
	Tb.E	rho	-0.686 **	0.860 ***	-0.860 ***	-							
		p	0.002	0.000	0.000								
	Tb.Th	rho	0.399	-0.377	0.377	-0.416	-						
		p	0.101	0.123	0.123	0.086							
	Tb.N	rho	0.624 **	-0.501 *	0.501 *	-0.404	-0.309	-					
		p	0.006	0.034	0.034	0.097	0.213						
	Sc.%High	rho	-0.194	0.177	-0.177	0.112	-0.464	-0.060	-				
	Density	*p*	0.441	0.482	0.482	0.660	0.053	0.813					
	Sc.Mean	rho	0.212	-0.009	0.009	-0.150	-0.090	0.049	0.330	-			
	Houns	*p*	0.399	0.971	0.971	0.553	0.723	0.848	0.181				
	Sc.Th	rho	0.160	-0.038	0.038	-0.276	-0.007	-0.003	0.330	0.862 ***	-		
		p	0.526	0.880	0.880	0.268	0.977	0.990	0.181	0.000			
	Age	rho	-0.491 *	0.084	-0.084	0.212	-0.109	-0.325	-0.528 *	-0.393	-0.413	-	
		p	0.039	0.741	0.741	0.398	0.668	0.188	0.024	0.383	0.088		
	Mass	rho	-0.192	0.138	-0.138	0.265	-0.375	0.094	-0.342	-0.286	-0.299	0.369	-
		p	0.445	0.584	0.584	0.287	0.125	0.711	0.165	0.535	0.229	0.132	

	C2		Tb.BV/TV	Tb.DA	Tb.I	Tb.E	Tb.Th	Tb.N	Sc.%High	Sc.Mean	Sc.Th	Age	Mass
Posterior	Tb.BV/TV	rho	-										
		p											
	Tb.DA	rho	-0.348	-									
		p	0.157										
	Tb.I	rho	0.348	-1.000	-								
		p	0.157	*inf*									
	Tb.E	rho	-0.209	0.822 ***	-0.822 ***	-							
		p	0.404	0.000	0.000								
	Tb.Th	rho	0.362	-0.304	0.304	-0.143	-						
		p	0.140	0.219	0.219	0.570							
	Tb.N	rho	0.744 ***	-0.265	0.265	-0.220	-0.226	-					
		p	0.000	0.287	0.287	0.381	0.367						
	Sc.%High	rho	0.140	-0.165	0.165	-0.100	-0.353	0.252	-				
	Density	*p*	0.580	0.513	0.513	0.693	0.151	0.313					
	Sc.Mean	rho	0.383	0.092	-0.092	0.325	0.075	0.325	0.193	-			
	Houns	*p*	0.117	0.717	0.717	0.188	0.766	0.188	0.442				
	Sc.Th	rho	0.216	0.127	-0.127	0.360	0.352	-0.022	-0.399	0.674 **	-		
		p	0.390	0.616	0.616	0.142	0.152	0.932	0.101	0.002			
	Age	rho	-0.390	0.215	-0.215	-0.071	-0.342	-0.180	-0.210	-0.175	-0.525 *	-	
		p	0.109	0.391	0.391	0.778	0.165	0.474	0.403	0.585	0.025		
	Mass	rho	-0.188	0.283	-0.283	0.249	-0.505 *	0.182	-0.294	-0.431	-0.080	0.369	-
		p	0.455	0.255	0.255	0.319	0.032	0.470	0.236	0.162	0.754	0.132	

Table 1.4: Correlation coefficients (Pearson's r) among variables measured in the (a) lateral, (b) central, and (c) medial regions of the distal tibia.

c.

Medial

	A3		Tb.BV/TV	Tb.DA	Tb.I	Tb.E	Tb.Th	Tb.N	Sc.%High	Sc.Mean	Sc.Th	Age	Mass
Anterior	Tb.BV/TV	rho	-										
		p											
	Tb.DA	rho	-0.573 *	-									
		p	0.013										
	Tb.I	rho	0.573 *	-1.000	-								
		p	0.013	*inf*									
	Tb.E	rho	-0.236	0.730 **	-0.730 **	-							
		p	0.345	0.001	0.001								
	Tb.Th	rho	0.540 *	-0.529 *	0.529 *	-0.127	-						
		p	0.021	0.024	0.024	0.616							
	Tb.N	rho	0.461	-0.046	0.046	-0.102	-0.309	-					
		p	0.054	0.855	0.855	0.687	0.213						
	Sc.%High	rho	-0.082	0.094	-0.094	0.022	-0.307	-0.022	-				
	Density	*p*	0.748	0.711	0.711	0.932	0.216	0.932					
	Sc.Mean	rho	-0.069	0.323	-0.323	0.540 *	0.189	-0.216	-0.296	-			
	Houns	*p*	0.785	0.191	0.191	0.021	0.453	0.390	0.233				
	Sc.Th	rho	0.317	-0.009	0.009	0.385	0.321	-0.065	-0.214	0.703 **	-		
		p	0.200	0.971	0.971	0.115	0.194	0.798	0.395	0.001			
	Age	rho	-0.257	0.177	-0.177	0.028	-0.220	-0.112	-0.068	0.124	-0.131	-	
		p	0.304	0.482	0.482	0.912	0.379	0.659	0.788	0.623	0.603		
	Mass	rho	0.123	-0.022	0.022	-0.057	-0.255	0.357	0.101	0.009	-0.146	0.369	-
		p	0.627	0.932	0.932	0.823	0.307	0.145	0.689	0.971	0.564	0.132	

	B3		Tb.BV/TV	Tb.DA	Tb.I	Tb.E	Tb.Th	Tb.N	Sc.%High	Sc.Mean	Sc.Th	Age	Mass
AP-Central	Tb.BV/TV	rho	-										
		p											
	Tb.DA	rho	-0.327	-									
		p	0.185										
	Tb.I	rho	0.327	-1.000	-								
		p	0.185	*inf*									
	Tb.E	rho	-0.397	0.822 ***	-0.822 ***	-							
		p	0.103	0.000	0.000								
	Tb.Th	rho	0.437	-0.399	0.399	-0.422	-						
		p	0.070	0.101	0.101	0.081							
	Tb.N	rho	0.723 **	-0.205	0.205	-0.141	-0.214	-					
		p	0.001	0.414	0.414	0.576	0.395						
	Sc.%High	rho	0.088	0.224	-0.224	0.360	0.055	-0.024	-				
	Density	*p*	0.729	0.372	0.372	0.142	0.829	0.926					
	Sc.Mean	rho	-0.013	0.538 *	-0.538 *	0.645 **	-0.162	-0.009	0.271	-			
	Houns	*p*	0.958	0.021	0.021	0.004	0.521	0.971	0.276				
	Sc.Th	rho	-0.158	0.490 *	-0.490 *	0.692 **	-0.212	0.009	0.251	0.688 **	-		
		p	0.531	0.039	0.039	0.001	0.399	0.971	0.316	0.002			
	Age	rho	-0.564 *	0.414	-0.414	0.247	-0.411	-0.278	0.135	-0.268	-0.289	-	
		p	0.015	0.088	0.088	0.322	0.090	0.263	0.594	0.282	0.245		
	Mass	rho	-0.048	-0.006	0.006	-0.069	-0.498 *	0.269	0.021	-0.296	0.039	0.369	-
		p	0.851	0.981	0.981	0.785	0.035	0.281	0.935	0.232	0.877	0.132	

	C3		Tb.BV/TV	Tb.DA	Tb.I	Tb.E	Tb.Th	Tb.N	Sc.%High	Sc.Mean	Sc.Th	Age	Mass
Posterior	Tb.BV/TV	rho	-										
		p											
	Tb.DA	rho	-0.571 *	-									
		p	0.013										
	Tb.I	rho	0.571 *	-1.000	-								
		p	0.013	*inf*									
	Tb.E	rho	-0.509 *	0.897	-0.897	-							
		p	0.031	0.000	0.000								
	Tb.Th	rho	0.179	-0.364	0.364	-0.176	-						
		p	0.478	0.137	0.137	0.484							
	Tb.N	rho	0.721 **	-0.447	0.447	-0.564 *	-0.321	-					
		p	0.001	0.063	0.063	0.015	0.194						
	Sc.%High	rho	-0.034	-0.179	0.179	-0.176	-0.261	0.278	-				
	Density	*p*	0.893	0.478	0.478	0.484	0.295	0.265					
	Sc.Mean	rho	0.455	-0.207	0.207	-0.129	-0.013	0.311	0.317	-			
	Houns	*p*	0.058	0.409	0.409	0.610	0.958	0.210	0.200				
	Sc.Th	rho	0.263	0.049	-0.049	0.164	0.236	-0.156	-0.127	0.775 ***	-		
		p	0.291	0.848	0.848	0.515	0.345	0.537	0.616	0.000			
	Age	rho	-0.416	0.790 ***	-0.790 ***	0.709 **	-0.388	-0.244	-0.117	-0.330	-0.393	-	
		p	0.086	0.000	0.000	0.001	0.111	0.329	0.644	0.181	0.106		
	Mass	rho	0.068	0.029	-0.029	0.165	-0.125	0.198	-0.126	-0.110	-0.027	0.369	-
		p	0.788	0.909	0.909	0.512	0.621	0.430	0.618	0.665	0.916	0.132	

Table 1. 5: Correlation coefficients (Pearson's r) among variables measured in the (a) lateral, (b) central, and (c) medial regions of the talus.

a.

Lateral

	A1		Tb.BV/TV	Tb.DA	Tb.I	Tb.E	Tb.Th	Tb.N	Sc.%High Density	Sc.Mean Houns	Sc.Th	Age	Mass
Anterior	Tb.BV/TV	rho	-										
		p											
	Tb.DA	rho	0.039	-									
		p	0.881										
	Tb.I	rho	-0.039	-1.000	-								
		p	0.881	*inf*									
	Tb.E	rho	0.159	-0.255	0.255	-							
		p	0.541	0.323	0.323								
	Tb.Th	rho	0.208	0.304	-0.304	0.051	-						
		p	0.422	0.236	0.236	0.844							
	Tb.N	rho	0.375	-0.390	0.390	0.074	-0.755 ***	-					
		p	0.138	0.122	0.122	0.779	0.000						
	Sc.%High Density	rho	0.074	0.289	-0.289	-0.284	-0.255	0.213	-				
		p	0.779	0.260	0.260	0.269	0.323	0.411					
	Sc.Mean Houns	rho	0.201	0.061	-0.061	-0.176	0.248	-0.049	0.517 *	-			
		p	0.439	0.815	0.815	0.498	0.338	0.852	0.034				
	Sc.Th	rho	0.216	0.049	-0.049	-0.321	0.358	-0.091	0.449	0.841 ***	-		
		p	0.406	0.852	0.852	0.209	0.158	0.729	0.071	0.000			
	Age	rho	-0.033	0.597 *	-0.597	-0.300	0.087	-0.050	0.122	-0.068	-0.127	-	
		p	0.899	0.011	0.011	0.242	0.739	0.848	0.642	0.797	0.628		
	Mass	rho	-0.280	0.054	-0.054	0.153	-0.308	0.056	-0.242	-0.503 *	-0.644 **	0.426	-
		p	0.277	0.837	0.837	0.557	0.229	0.830	0.350	0.040	0.005	0.088	

	B1		Tb.BV/TV	Tb.DA	Tb.I	Tb.E	Tb.Th	Tb.N	Sc.%High Density	Sc.Mean Houns	Sc.Th	Age	Mass
AP-Central	Tb.BV/TV	rho	-										
		p											
	Tb.DA	rho	-0.230	-									
		p	0.374										
	Tb.E	rho	0.230	-1.000	-								
		p	0.230	*inf*									
	Tb.I	rho	-0.598 *	0.020	-0.020	-							
		p	0.011	0.940	0.940								
	Tb.Th	rho	-0.130	0.069	-0.069	0.012	-						
		p	0.619	0.794	0.794	0.963							
	Tb.N	rho	0.498 *	-0.150	0.150	-0.211	-0.880 ***	-					
		p	0.042	0.567	0.567	0.417	0.000						
	Sc.%High Density	rho	0.468	0.154	-0.154	-0.181	-0.059	0.294	-				
		p	0.058	0.554	0.554	0.486	0.823	0.252					
	Sc.Mean Houns	rho	0.414	0.015	-0.015	-0.316	0.304	-0.032	0.451	-			
		p	0.098	0.955	0.955	0.216	0.236	0.903	0.069				
	Sc.Th	rho	0.532 *	-0.184	0.184	-0.343	0.225	0.069	0.395	0.909 ***	-		
		p	0.028	0.480	0.480	0.178	0.384	0.794	0.117	0.000			
	Age	rho	0.077	0.063	-0.063	-0.165	0.028	-0.022	-0.026	-0.207	-0.184	-	
		p	0.768	0.811	0.811	0.528	0.914	0.933	0.922	0.426	0.479		
	Mass	rho	-0.407	-0.022	0.022	0.099	-0.137	-0.076	-0.321	-0.605 *	-0.599 *	0.426	-
		p	0.105	0.933	0.933	0.704	0.599	0.772	0.208	0.010	0.011	0.088	

	C1		Tb.BV/TV	Tb.DA	Tb.I	Tb.E	Tb.Th	Tb.N	Sc.%High Density	Sc.Mean Houns	Sc.Th	Age	Mass
Posterior	Tb.BV/TV	rho	-										
		p											
	Tb.DA	rho	0.020	-									
		p	0.940										
	Tb.I	rho	-0.020	-1.000	-								
		p	0.940	*inf*									
	Tb.E	rho	0.091	0.255	-0.255	-							
		p	0.729	0.323	0.323								
	Tb.Th	rho	-0.083	-0.037	0.037	0.130	-						
		p	0.751	0.889	0.889	0.619							
	Tb.N	rho	0.520 *	0.034	-0.034	-0.017	-0.858 ***	-					
		p	0.033	0.896	0.896	0.948	0.000						
	Sc.%High Density	rho	0.456	-0.054	0.054	0.321	0.252	0.022	-				
		p	0.066	0.837	0.837	0.209	0.328	0.933					
	Sc.Mean Houns	rho	0.762 ***	-0.012	0.012	0.105	0.358	0.127	0.642 **	-			
		p	0.000	0.963	0.963	0.687	0.158	0.626	0.005				
	Sc.Th	rho	0.809 ***	-0.228	0.228	0.110	0.314	0.152	0.650 **	0.929 ***	-		
		p	0.000	0.379	0.379	0.673	0.220	0.560	0.005	0.000			
	Age	rho	-0.023	0.574 *	-0.574 *	0.068	0.057	-0.209	-0.195	-0.230	-0.189	-	
		p	0.929	0.016	0.016	0.797	0.829	0.421	0.452	0.375	0.467		
	Mass	rho	-0.439	-0.077	0.077	-0.481	-0.213	-0.128	-0.459	-0.567 *	-0.475	0.426	-
		p	0.078	0.768	0.768	0.051	0.411	0.626	0.064	0.018	0.054	0.088	

Table 1.5: Correlation coefficients (Pearson's r) among variables measured in the (a) lateral, (b) central, and (c) medial regions of the talus.

b.

ML-Central

	A2		Tb.BV/TV	Tb.DA	Tb.I	Tb.E	Tb.Th	Tb.N	Sc.%High	Sc.Mean	Sc.Th	Age	Mass
Anterior	Tb.BV/TV	rho	-										
		p											
	Tb.DA	rho	-0.498 *	-									
		p	0.042										
	Tb.I	rho	0.498 *	-1.000	-								
		p	0.042	*inf*									
	Tb.E	rho	-0.387	0.074	-0.074	-							
		p	0.125	0.779	0.779								
	Tb.Th	rho	0.083	0.358	-0.358	-0.272	-						
		p	0.751	0.158	0.158	0.291							
	Tb.N	rho	0.522 *	-0.566 *	0.566 *	-0.051	-0.775 **	-					
		p	0.032	0.018	0.018	0.844	0.000						
	Sc.%High	rho	0.254	0.200	-0.200	0.242	-0.031	0.063	-				
	Density	*p*	0.325	0.441	0.441	0.350	0.905	0.811					
	Sc.Mean	rho	0.176	0.086	-0.086	0.162	0.034	-0.064	0.585 *	-			
	Houns	*p*	0.498	0.743	0.743	0.535	0.896	0.808	0.014				
	Sc.Th	rho	0.306	-0.093	0.093	0.029	0.228	-0.115	0.626 **	0.779 ***	-		
		p	0.232	0.722	0.722	0.911	0.379	0.660	0.007	0.000			
	Age	rho	0.197	-0.109	0.109	-0.086	0.220	-0.170	0.032	0.005	-0.049	-	
		p	0.449	0.676	0.676	0.743	0.396	0.515	0.903	0.985	0.851		
	Mass	rho	-0.121	-0.270	0.270	0.031	-0.207	0.088	-0.359	-0.510 *	-0.534 *	0.426	-
		p	0.642	0.295	0.295	0.907	0.425	0.736	0.157	0.036	0.027	0.088	

	B2		Tb.BV/TV	Tb.DA	Tb.I	Tb.E	Tb.Th	Tb.N	Sc.%High	Sc.Mean	Sc.Th	Age	Mass
AP-Central	Tb.BV/TV	rho	-										
		p											
	Tb.DA	rho	-0.164	-									
		p	0.529										
	Tb.E	rho	0.164	-1.000	-								
		p	0.529	*inf*									
	Tb.I	rho	0.137	-0.074	0.074	-							
		p	0.599	0.779	0.779								
	Tb.Th	rho	-0.154	0.338	-0.338	-0.397	-						
		p	0.554	0.184	0.184	0.115							
	Tb.N	rho	0.583 *	-0.409	0.409	0.449	-0.853 ***	-					
		p	0.014	0.103	0.103	0.071	0.000						
	Sc.%High	rho	0.271	0.137	-0.137	-0.192	0.303	-0.105	-				
	Density	*p*	0.293	0.600	0.600	0.461	0.238	0.689					
	Sc.Mean	rho	-0.115	-0.360	0.360	-0.314	0.137	-0.152	0.411	-			
	Houns	*p*	0.660	0.155	0.155	0.220	0.599	0.560	0.102				
	Sc.Th	rho	0.022	-0.385	0.385	-0.336	0.238	-0.088	0.442	0.728 **	-		
		p	0.933	0.127	0.127	0.188	0.358	0.736	0.075	0.001			
	Age	rho	0.009	0.150	-0.150	-0.350	0.101	-0.108	0.166	-0.182	-0.350	-	
		p	0.974	0.566	0.566	0.168	0.700	0.679	0.524	0.485	0.168		
	Mass	rho	-0.292	0.077	-0.077	0.172	-0.187	0.063	-0.241	-0.525 *	-0.517 *	0.426	-
		p	0.255	0.768	0.768	0.510	0.474	0.811	0.352	0.030	0.034	0.088	

	C2		Tb.BV/TV	Tb.DA	Tb.I	Tb.E	Tb.Th	Tb.N	Sc.%High	Sc.Mean	Sc.Th	Age	Mass
Posterior	Tb.BV/TV	rho	-										
		p											
	Tb.DA	rho	-0.022	-									
		p	0.933										
	Tb.I	rho	0.022	-1.000	-								
		p	0.933	*inf*									
	Tb.E	rho	0.365	0.147	-0.147	-							
		p	0.149	0.573	0.573								
	Tb.Th	rho	-0.088	0.255	-0.255	-0.495 *	-						
		p	0.736	0.323	0.323	0.043							
	Tb.N	rho	0.591 *	-0.137	0.137	0.630 **	-0.816 ***	-					
		p	0.013	0.599	0.599	0.007	0.000						
	Sc.%High	rho	0.179	-0.110	0.110	0.145	0.216	-0.110	-				
	Density	*p*	0.492	0.673	0.673	0.580	0.406	0.673					
	Sc.Mean	rho	0.233	0.078	-0.078	0.081	0.270	-0.110	0.377	-			
	Houns	*p*	0.368	0.765	0.765	0.758	0.295	0.673	0.135				
	Sc.Th	rho	0.331	0.243	-0.243	0.066	0.248	-0.098	0.275	0.809 ***	-		
		p	0.195	0.348	0.348	0.801	0.338	0.708	0.286	0.000			
	Age	rho	0.061	0.034	-0.034 *	-0.018	0.043	-0.039	0.027	-0.183	-0.264	-	
		p	0.815	0.896	0.896	0.944	0.870	0.881	0.918	0.482	0.305		
	Mass	rho	0.102	0.070	-0.070	0.236	-0.096	0.110	-0.228	-0.481	-0.345	0.426	-
		p	0.697	0.790	0.790	0.363	0.715	0.673	0.378	0.051	0.175	0.088	

Table 1.5: Correlation coefficients (Pearson's r) among variables measured in the (a) lateral, (b) central, and (c) medial regions of the talus.

c.

Medial

	A3		Tb.BV/TV	Tb.DA	Tb.l	Tb.E	Tb.Th	Tb.N	Sc.%High	Sc.Mean	Sc.Th	Age	Mass
Anterior	Tb.BV/TV	rho	-										
		p											
	Tb.DA	rho	0.299	-									
		p	0.244										
	Tb.l	rho	-0.299	-1.000	-								
		p	0.244	*inf*									
	Tb.E	rho	0.137	0.615 **	-0.615 **	-							
		p	0.599	0.009	0.009								
	Tb.Th	rho	0.505 *	-0.091	0.091	0.123	-						
		p	0.039	0.729	0.729	0.639							
	Tb.N	rho	0.108	0.159	-0.159	-0.093	-0.672 **	-					
		p	0.680	0.541	0.541	0.722	0.003						
	Sc.%High	rho	-0.181	-0.328	0.328	-0.221	0.257	-0.505 *	-				
	Density	*p*	0.486	0.198	0.198	0.395	0.319	0.039					
	Sc.Mean	rho	-0.140	-0.061	0.061	0.424	0.301	-0.549 *	0.360	-			
	Houns	*p*	0.593	0.815	0.815	0.090	0.240	0.022	0.155				
	Sc.Th	rho	0.235	-0.027	0.027	-0.093	0.150	-0.397	0.157	0.297	-		
		p	0.363	0.918	0.918	0.722	0.567	0.115	0.548	0.248			
	Age	rho	0.296	0.286	-0.286	0.328	0.306	-0.070	0.100	-0.022	-0.159	-	
		p	0.248	0.265	0.265	0.198	0.232	0.789	0.704	0.933	0.543		
	Mass	rho	0.234	0.071	-0.071	-0.158	0.150	0.184	0.029	-0.449	-0.562 *	0.426	-
		p	0.365	0.786	0.786	0.544	0.566	0.479	0.911	0.071	0.019	0.088	

	B3		Tb.BV/TV	Tb.DA	Tb.l	Tb.E	Tb.Th	Tb.N	Sc.%High	Sc.Mean	Sc.Th	Age	Mass
AP-Central	Tb.BV/TV	rho	-										
		p											
	Tb.DA	rho	-0.260	-									
		p	0.314										
	Tb.E	rho	0.260	-1.000	-								
		p	0.314	*inf*									
	Tb.l	rho	0.213	-0.096	0.096	-							
		p	0.411	0.715	0.715								
	Tb.Th	rho	0.324	-0.044	0.044	-0.422	-						
		p	0.205	0.866	0.866	0.092							
	Tb.N	rho	0.404	-0.262	0.262	0.672 **	-0.686 **	-					
		p	0.107	0.309	0.309	0.003	0.002						
	Sc.%High	rho	-0.098	0.297	-0.297	-0.093	0.346	-0.461	-				
	Density	*p*	0.708	0.248	0.248	0.722	0.174	0.063					
	Sc.Mean	rho	-0.147	-0.294	0.294	-0.125	0.316	-0.387	0.500 *	-			
	Houns	*p*	0.573	0.252	0.252	0.633	0.216	0.125	0.041				
	Sc.Th	rho	0.397	-0.203	0.203	0.154	0.488 *	-0.120	0.377	0.544 *	-		
		p	0.115	0.434	0.434	0.554	0.047	0.646	0.135	0.024			
	Age	rho	-0.032	0.009	-0.009	-0.311	-0.017	-0.082	0.043	-0.047	-0.100	-	
		p	0.903	0.974	0.974	0.224	0.948	0.753	0.870	0.859	0.704		
	Mass	rho	-0.025	0.248	-0.248	0.002	-0.097	0.102	-0.074	-0.533 *	-0.378	0.426	-
		p	0.926	0.337	0.337	0.993	0.711	0.697	0.779	0.028	0.135	0.088	

	C3		Tb.BV/TV	Tb.DA	Tb.l	Tb.E	Tb.Th	Tb.N	Sc.%High	Sc.Mean	Sc.Th	Age	Mass
Posterior	Tb.BV/TV	rho	-										
		p											
	Tb.DA	rho	0.020	-									
		p	0.939										
	Tb.l	rho	-0.020	-1.000	-								
		p	0.939	*inf*									
	Tb.E	rho	-0.036	0.019	-0.019	-							
		p	0.892	0.944	0.944								
	Tb.Th	rho	0.195	-0.370	0.370	-0.489 *	-						
		p	0.453	0.144	0.144	0.046							
	Tb.N	rho	0.601 *	0.353	-0.353	0.326	-0.622 **	-					
		p	0.011	0.165	0.165	0.201	0.008						
	Sc.%High	rho	0.109	-0.143	0.143	0.107	-0.238	0.297	-				
	Density	*p*	0.677	0.585	0.585	0.681	0.359	0.247					
	Sc.Mean	rho	-0.016	-0.051	0.051	-0.399	0.121	-0.136	0.101	-			
	Houns	*p*	0.950	0.846	0.846	0.112	0.643	0.603	0.699				
	Sc.Th	rho	0.154	0.100	-0.100	-0.347	-0.071	0.118	0.543 *	0.665 **	-		
		p	0.556	0.702	0.702	0.172	0.788	0.653	0.024	0.004			
	Age	rho	0.259	0.159	-0.159	-0.056	0.299	0.035	-0.314	0.025	-0.270	-	
		p	0.316	0.542	0.542	0.830	0.243	0.894	0.220	0.924	0.295		
	Mass	rho	0.385	0.012	-0.012	-0.093	0.221	0.167	-0.201	-0.425	-0.238	0.383	-
		p	0.127	0.963	0.963	0.721	0.393	0.521	0.438	0.089	0.358	0.129	

Table 1. 6: Pairwise comparisons among regions along the anteroposterior dimension in the distal tibia.

Dependent Variable	(I) APIndex	(J) APIndex	Difference (I-J)	Std. Error	Sig.
Tb.BV/TV	Anterior	APCentral	-0.013	0.011	0.458
	Anterior	Posterior	-0.026	0.010	0.029 *
	APCentral	Posterior	-0.014	0.009	0.303
Tb.DA	Anterior	APCentral	-3.177	0.644	0.000 ***
	Anterior	Posterior	-0.172	0.459	0.926
	APCentral	Posterior	3.005	0.661	0.000 ***
Tb.I	Anterior	APCentral	0.094	0.025	0.001 **
	Anterior	Posterior	0.003	0.025	0.993
	APCentral	Posterior	-0.091	0.026	0.002 **
Tb.E	Anterior	APCentral	-0.176	0.032	0.000 ***
	Anterior	Posterior	0.006	0.034	0.985
	APCentral	Posterior	0.181	0.034	0.000 ***
Tb.Th	Anterior	APCentral	0.000	0.006	0.997
	Anterior	Posterior	0.016	0.006	0.023 *
	APCentral	Posterior	0.016	0.005	0.003 **
Tb.N	Anterior	APCentral	-0.002	0.054	0.999
	Anterior	Posterior	-0.266	0.056	0.000 ***
	APCentral	Posterior	-0.264	0.053	0.000 ***
Sc.%High Density	Anterior	APCentral	0.431	0.118	0.001 **
	Anterior	Posterior	-0.077	0.192	0.914
	APCentral	Posterior	-0.508	0.164	0.008 **
Sc.Mean Houns	Anterior	APCentral	82.221	88.543	0.623
	Anterior	Posterior	14.376	83.617	0.984
	APCentral	Posterior	-67.845	87.720	0.720
Sc.Th	Anterior	APCentral	-0.005	0.012	0.929
	Anterior	Posterior	-0.027	0.016	0.206
	APCentral	Posterior	-0.022	0.015	0.287

Table 1. 7: Pairwise comparisons among regions along the mediolateral dimension in the distal tibia.

Dependent Variable	(I) MLIndex	(J) MLIndex	Difference (I-J)	Std. Error	Sig.	
Tb.BV/TV	Lateral	MLCentral	-0.020	0.009	0.057	
	Lateral	Medial	0.025	0.010	0.038	*
	MLCentral	Medial	0.045	0.010	0.000	***
Tb.DA	Lateral	MLCentral	1.446	0.549	0.027	*
	Lateral	Medial	-0.709	0.717	0.585	
	MLCentral	Medial	-2.155	0.631	0.003	**
Tb.I	Lateral	MLCentral	-0.057	0.027	0.090	
	Lateral	Medial	0.023	0.025	0.624	
	MLCentral	Medial	0.080	0.026	0.007	**
Tb.E	Lateral	MLCentral	0.092	0.035	0.028	*
	Lateral	Medial	0.046	0.034	0.374	
	MLCentral	Medial	-0.046	0.039	0.470	
Tb.Th	Lateral	MLCentral	-0.012	0.006	0.077	
	Lateral	Medial	0.014	0.006	0.047	*
	MLCentral	Medial	0.026	0.006	0.000	***
Tb.N	Lateral	MLCentral	-0.004	0.049	0.997	
	Lateral	Medial	0.094	0.062	0.289	
	MLCentral	Medial	0.097	0.064	0.289	
Sc.%High Density	Lateral	MLCentral	0.050	0.166	0.951	
	Lateral	Medial	-0.148	0.166	0.644	
	MLCentral	Medial	-0.198	0.166	0.458	
Sc.Mean Houns	Lateral	MLCentral	74.252	86.350	0.666	
	Lateral	Medial	-51.839	86.350	0.820	
	MLCentral	Medial	-126.091	86.350	0.313	
Sc.Th	Lateral	MLCentral	-0.017	0.014	0.417	
	Lateral	Medial	-0.069	0.012	0.000	***
	MLCentral	Medial	-0.052	0.014	0.001	**

Table 1. 8: Pairwise comparisons among regions along the anteroposterior dimension in the talus.

Dependent Variable	(I) MLIndex	(J) MLIndex	Difference (I-J)	Std. Error	Sig.	
Tb.BV/TV	Anterior	APCentral	-0.009	0.010	0.627	
	Anterior	Posterior	0.033	0.009	0.001	**
	APCentral	Posterior	0.042	0.009	0.000	***
Tb.DA	Anterior	APCentral	0.721	1.059	0.775	
	Anterior	Posterior	1.862	1.131	0.232	
	APCentral	Posterior	1.141	0.903	0.419	
Tb.I	Anterior	APCentral	0.021	0.021	0.577	
	Anterior	Posterior	-0.028	0.021	0.361	
	APCentral	Posterior	-0.049	0.021	0.050	*
Tb.E	Anterior	APCentral	0.060	0.031	0.128	
	Anterior	Posterior	0.054	0.033	0.251	
	APCentral	Posterior	-0.007	0.034	0.979	
Tb.Th	Anterior	APCentral	0.011	0.006	0.114	
	Anterior	Posterior	0.027	0.005	0.000	***
	APCentral	Posterior	0.016	0.005	0.007	**
Tb.N	Anterior	APCentral	-0.172	0.068	0.035	
	Anterior	Posterior	-0.091	0.065	0.342	
	APCentral	Posterior	0.080	0.070	0.484	
Sc.%High Density	Anterior	APCentral	-0.291	0.538	0.851	
	Anterior	Posterior	0.406	0.478	0.674	
	APCentral	Posterior	0.697	0.507	0.359	
Sc.Mean Houns	Anterior	APCentral	-113.170	127.190	0.648	
	Anterior	Posterior	-62.465	118.045	0.857	
	APCentral	Posterior	50.705	129.548	0.919	
Sc.Th	Anterior	APCentral	-0.044	0.018	0.047	*
	Anterior	Posterior	0.032	0.017	0.129	
	APCentral	Posterior	0.076	0.018	0.000	***

Table 1. 9: Pairwise comparisons among regions along the mediolateral dimension in the talus.

Dependent Variable	(I) MLIndex	(J) MLIndex	Difference (I-J)	Std. Error	Sig.
Tb.BV/TV	Lateral	MLCental	0.030	0.009	0.003 **
	Lateral	Medial	-0.010	0.010	0.543
	MLCental	Medial	-0.040	0.009	0.000 ***
Tb.DA	Lateral	MLCentral	-3.374	1.004	0.004 **
	Lateral	Medial	2.437	0.677	0.001 **
	MLCentral	Medial	5.811	1.069	0.000 ***
Tb.I	Lateral	MLCental	0.021	0.013	0.274
	Lateral	Medial	-0.113	0.018	0.000 ***
	MLCental	Medial	-0.134	0.020	0.000 ***
Tb.E	Lateral	MLCentral	0.230	0.022	0.000 ***
	Lateral	Medial	0.247	0.026	0.000 ***
	MLCentral	Medial	0.017	0.026	0.787
Tb.Th	Lateral	MLCental	-0.001	0.005	0.967
	Lateral	Medial	-0.006	0.006	0.504
	MLCental	Medial	-0.005	0.006	0.678
Tb.N	Lateral	MLCentral	0.162	0.071	0.064
	Lateral	Medial	0.063	0.062	0.575
	MLCentral	Medial	-0.099	0.069	0.331
Sc.%High Density	Lateral	MLCental	0.856	0.107	0.000 ***
	Lateral	Medial	-2.663	0.508	0.000 ***
	MLCental	Medial	-3.519	0.496	0.000 ***
Sc.Mean Houns	Lateral	MLCentral	142.584	124.340	0.488
	Lateral	Medial	-283.919	121.868	0.056
	MLCentral	Medial	-426.503	114.316	0.001 **
Sc.Th	Lateral	MLCental	-0.038	0.016	0.058
	Lateral	Medial	-0.092	0.018	0.000 ***
	MLCental	Medial	-0.054	0.017	0.006 **

Table 1. 10: Pairwise regional comparisons of bone properties in the distal tibia. Only significant ($p<0.05$) comparisons are shown.

Tb.BV/TV		
A1> A3 ($p=0.004$)	**A2>** A3 ($p<0.001$) B3 ($p=0.017$)	**A3**
B1> A3 ($p<0.001$)	**B2>** A3 ($p<0.001$)	**B3**
C1> A3 ($p=0.014$)	**C2>** A3 ($p<0.001$) B3 ($p=0.012$)	**C3>** A3 ($p<0.001$)

Tb.Th		
A1	**A2>** A3 ($p=0.002$) B3 ($p=0.010$) C1 ($p=0.002$) C3 ($p<0.001$)	**A3**
B1> C3 ($p=0.008$)	**B2>** C3 ($p=0.032$)	**B3**
C1	**C2**	**C3**

Tb.N		
A1> A3 ($p=0.005$)	**A2>** A3 ($p=0.024$) C3 ($p=0.030$)	**A3**
B1	**B2**	**B3**
C1> A3 ($p<0.001$)	**C2>** A3 ($p<0.001$) B3 ($p=0.010$)	**C3>** A2 ($p=0.030$) A3 ($p<0.001$) B1 ($p=0.007$) B2 ($p=0.007$) B3 ($p<0.001$)

Tb.DA		
A1	**A2**	**A3**
B1> A1 ($p<0.001$) A2 ($p<0.001$) A3 ($p=0.035$) C1 ($p<0.001$) C2 ($p<0.001$)	**B2**	**B3>** A1 ($p=0.006$) A2 ($p<0.001$) C1 ($p=0.005$) C2 ($p=0.001$)
C1	**C2**	**C3**

Tb.I		
A1	**A2>** B1 ($p=0.001$) B3 ($p=0.032$)	**A3**
B1	**B2**	**B3**
C1	**C2>** B1 ($p=0.001$) B3 ($p=0.047$)	**C3**

Tb.E		
A1> A2 ($p=0.004$)	**A2**	**A3**
B1> A2 ($p<0.001$) C2 ($p=0.023$) C3 ($p=0.018$)	**B2>** A2 ($p<0.001$) C2 ($p=0.004$) C3 ($p=0.003$)	**B3>** A2 ($p<0.001$) C2 ($p=0.003$) C3 ($p=0.002$)
C1	**C2**	**C3**

Sc.%HighDensity		
A1 -	**A2** -	**A3** -
B1 -	**B2** -	**B3** -
C1 -	**C2** -	**C3** -

Sc.MeanHouns		
A1 -	**A2** -	**A3** -
B1 -	**B2** -	**B3** -
C1 -	**C2** -	**C3** -

Sc.Th		
A1	**A2**	**A3>** A1 (p=0.006) A2 (p=0.005) B1 (p=0.030)
B1	**B2**	**B3**
C1	**C2**	**C3>** A1 (p=0.006) A2 (p=0.005) B1 (p=0.030)

Table 1. 11: Pairwise regional comparisons of bone properties in the talus. In each region, only significant positive ($p<0.05$) comparisons are shown.

Tb.BV/TV		
A1> C1 (p=0.010) C2 (p=0.012)	**A2**	**A3>** A2 (p=0.018) C1 (p=0.002) C2 (p=0.002)
B1> A2 (p=0.006) C1 (p<0.001) C2 (p=0.001)	**B2**	**B3>** A2 (p=0.008) C1 (p=0.001) C2 (p=0.001)
C1	**C2**	**C3**

Tb.Th		
A1	**A2**	**A3>** C1 (p=0.003) C2 (p=0.012) C3 (p=0.001)
B1	**B2**	**B3**
C1	**C2**	**C3**

Tb.N		
A1	**A2**	**A3**
B1> A2 (p=0.009)	**B2**	**B3**
C1	**C2**	**C3**

Tb.DA		
A1> A3 (p=0.007)	**A2>** A1 (p=0.029) A3 (p<0.001) B1 (p=0.009) B2 (p=0.044) B3 (p<0.001) C1 (p<0.001) C3 (p<0.001)	**A3**
B1> A3 (p=0.023)	**B2>** A3 (p=0.004)	**B3**
C1	**C2>** A3 (p=0.002)	**C3**

Tb.I		
A1	**A2**	**A3>** A1 (p<0.001) A2 (p<0.001) B1 (p<0.001) B2 (p<0.001) B3 (p<0.001) C1 (p<0.001) C2 (p<0.001)
B1	**B2**	**B3>** A2 (p=0.005)
C1> A2 (p=0.003)	**C2**	**C3>** A1 (p<0.001) A2 (p<0.001) B1 (p<0.001) B2 (p<0.001) C2 (p<0.001)

Tb.E		
A1> A2 (p<0.001) B2 (p<0.001) B3 (p<0.001) C2 (p<0.001) C3 (p<0.001)	**A2**	**A3>** A2 (p=0.043) B3 (p=0.004) C3 (p<0.001)
B1> A2 (p<0.001) B2 (p<0.001) B3 (p<0.001) C2 (p<0.001) C3 (p<0.001)	**B2**	**B3**
C1> A2 (p<0.001) A3 (p=0.002) B2 (p<0.001) B3 (p<0.001) C2 (p<0.001) C3 (p<0.001)	**C2>** C3 (p=0.010)	**C3**

Sc.%HighDensity		
A1	**A2**	**A3>** A1 (p=0.002) A2 (p<0.001) B1 (p=0.007) B2 (p<0.001) C1 (p=0.013) C2 (p<0.001)
B1	**B2**	**B3>** A1 (p<0.001) A2 (p<0.001) B1 (p=0.001) B2 (p<0.001) C1 (p=0.001) C2 (p<0.001)
C1	**C2**	**C3**

Sc.MeanHouns		
A1 -	**A2** -	**A3** -
B1 -	**B2** -	**B3** -
C1 -	**C2** -	**C3** -

Sc.Th		
A1	**A2**	**A3>** A1 (p=0.035) C1 (p<0.001)
B1	**B2>** C1 (p=0.009)	**B3>** A1 (p<0.001) A2 (p=0.007) B1 (p=0.018) C1 (p<0.001) C2 (p<0.001) C3 (p=0.026)
C1	**C2**	**C3**

Table 1. 12: Consistency of ranked values in the distal tibia.

The value in each cell is the mean rank of the bone property in that region across specimens. Values closer to 9 or 1 indicate regions that were consistently the highest and lowest ranked regions, respectively, of that variable across specimens. Kendall's W measures the overall consistency of ranks, with values closer to 1 indicating the most consistent pattern.

Tb.BV/TV

4.6	6.5	1.9
5.7	5.9	3.4
4.2	6.4	6.4

Kendall's W .338

Tb.Th

4.9	7.7	3.6
6.6	6.3	4.5
3.8	4.9	2.7

Kendall's W .341

Tb.N

5.4	4.6	2.2
4.5	4.5	2.6
5.9	6.9	8.4

Kendall's W .508

Tb.DA

4.2	3.2	5.6
7.4	5.5	6.5
4.2	3.3	5.1

Kendall's W .265

Tb.I

5.8	6.8	4.4
2.6	4.5	3.5
5.8	6.7	4.9

Kendall's W .265

Tb.E

5.7	2.6	4.2
6.6	6.9	7.1
4.5	3.9	3.4

Kendall's W .357

Legend

A1	A2	A3
B1	B2	B3
C1	C2	C3

Sc.%HighDensity

5.6	4.7	7.2
3.9	1.5	5.0
6.4	4.9	5.8

Kendall's W .361

Sc.MeanHound

5.3	4.4	7.2
4.7	2.1	5.4
5.4	4.8	5.7

Kendall's W .247

Sc.Th

2.7	2.8	7.1
3.9	4.3	6.4
4.3	5.9	7.5

Kendall's W .433

Table 1. 13: Consistency of ranked values in the talus.

The value in each cell is the mean rank of the bone property in that region across specimens. Values closer to 9 or 1 indicate regions that were consistently the highest and lowest ranked regions, respectively, of that variable across specimens. Kendall's W measures the overall consistency of ranks, with values closer to 1 indicating the most consistent pattern.

Tb.BV/TV

6.1	3.3	6.3
7.2	4.0	6.8
3.2	3.2	4.8

Kendall's W .360

Tb.Th

6.0	6.4	8.1
5.0	4.3	5.9
2.9	3.5	2.8

Kendall's W .425

Tb.N

5.8	1.8	3.8
7.6	4.9	6.1
4.4	5.1	5.5

Kendall's W .350

Tb.DA

6.2	7.6	1.9
6.5	5.5	4.4
3.9	5.8	3.2

Kendall's W .427

Tb.I

3.8	2.4	8.1
3.5	4.5	5.6
6.1	4.2	6.8

Kendall's W .427

Tb.E

7.3	3.8	5.8
6.7	3.7	3.2
8.1	4.4	1.9

Kendall's W .576

Legend

A1	A2	A3
B1	B2	B3
C1	C2	C3

Sc.%HighDensity

4.9	2.0	7.6
5.9	1.3	8.4
5.9	2.6	6.1

Kendall's W .828

Sc.MeanHouns

3.7	2.4	7.1
5.5	2.5	8.4
4.4	3.6	7.3

Kendall's W .644

Sc.Th

3.2	4.8	6.6
5.4	5.8	8.4
1.6	3.9	5.5

Kendall's W .514

Table 1. 14: Mean eigenvalues and orientation of the primary eigenvector in each region of the distal tibia.

Tibia	Lateral						MLCentral						Medial					
	Eigenvalue			Primary Eigenvector			Eigenvalue			Primary Eigenvector			Eigenvalue			Primary Eigenvector		
	1	2	3	Trend	Incline	Variance	1	2	3	Trend	Incline	Variance	1	2	3	Trend	Incline	Variance
Anterior	0.609	0.229	0.162	349	70	0.06	0.519	0.309	0.172	290	47	0.24	0.594	0.276	0.130	295	44	0.09
APCentral	0.687	0.217	0.097	316	85	0.01	0.669	0.197	0.135	156	85	0.05	0.692	0.187	0.121	101	84	0.00
Posterior	0.591	0.249	0.160	169	69	0.02	0.554	0.273	0.173	166	81	0.08	0.586	0.292	0.122	112	81	0.09

Table 1. 15: Mean eigenvalues and orientation of the primary eigenvector in each region of the talus.

Talus	Lateral						MLCentral						Medial					
	Eigenvalue			Primary Eigenvector			Eigenvalue			Primary Eigenvector			Eigenvalue			Primary Eigenvector		
	1	2	3	Trend	Incline	Variance	1	2	3	Trend	Incline	Variance	1	2	3	Trend	Incline	Variance
Anterior	0.671	0.249	0.081	32	55	0.02	0.589	0.361	0.050	209	68	0.09	0.555	0.271	0.174	171	47	0.04
APCentral	0.653	0.265	0.082	51	59	0.01	0.570	0.347	0.082	113	85	0.05	0.547	0.350	0.103	211	62	0.07
Posterior	0.650	0.218	0.132	27	73	0.01	0.581	0.337	0.082	54	70	0.04	0.503	0.366	0.131	45	86	0.30

Table 1. 16: Bivariate correlation between distal tibia morphology and talus morphology.

N=135		Tibia Tb.BVTV	Tibia Tb.DA	Tibia Tb.I	Tibia Tb.E	Tibia Tb.Th	Tibia Tb.N	Tibia Sc.%High Dens	Tibia Sc.Mean Houns	Tibia Sc.Th
Talus Tb.BVTV	r	0.133	**0.177**	-0.100	0.086	0.061	0.054	-0.022	0.128	0.146
	p	0.124	**0.040**	0.251	0.319	0.483	0.531	0.801	0.139	0.091
Talus Tb.DA	r	0.152	-0.008	0.004	0.010	0.142	0.065	-0.119	-0.031	**-0.180**
	p	0.078	0.925	0.968	0.910	0.099	0.455	0.170	0.724	**0.036**
Talus Tb.I	r	**-0.188**	-0.056	0.026	**-0.176**	-0.113	-0.124	0.085	0.042	**0.252**
	p	**0.029**	0.521	0.762	**0.041**	0.192	0.151	0.326	0.625	**0.003**
TalusTb.E	r	-0.066	0.032	-0.089	**0.202**	-0.089	0.056	0.047	0.130	-0.144
	p	0.444	0.710	0.304	**0.019**	0.303	0.519	0.592	0.132	0.095
Talus Tb.Th	r	**-0.252**	0.070	-0.053	0.103	**0.434**	**-0.626**	**-0.211**	**0.177**	0.134
	p	**0.003**	0.423	0.539	0.236	**0.000**	**0.000**	**0.014**	**0.040**	0.120
Talus Tb.N	r	**0.322**	0.031	0.014	-0.046	**-0.311**	**0.606**	0.124	-0.121	-0.056
	p	**0.000**	0.724	0.870	0.599	**0.000**	**0.000**	0.152	0.160	0.519
Talus	r	**-0.352**	**0.209**	-0.121	0.071	**-0.207**	**-0.213**	**0.335**	0.146	**0.186**
Sc.%HighDens	*p*	**0.000**	**0.015**	0.160	0.414	**0.016**	**0.013**	**0.000**	0.092	**0.031**
Talus	r	**-0.264**	0.136	-0.067	0.135	0.057	**-0.266**	-0.045	**0.295**	**0.256**
Sc.MeanHouns	*p*	**0.002**	0.117	0.439	0.118	0.509	**0.002**	0.605	**0.001**	**0.003**
Talus Sc.Th	r	-0.096	**0.195**	-0.099	0.145	0.153	**-0.319**	0.131	**0.361**	**0.415**
	p	0.268	**0.024**	0.251	0.094	0.076	**0.000**	0.130	**0.000**	**0.000**

Figures

(a) Distal tibia

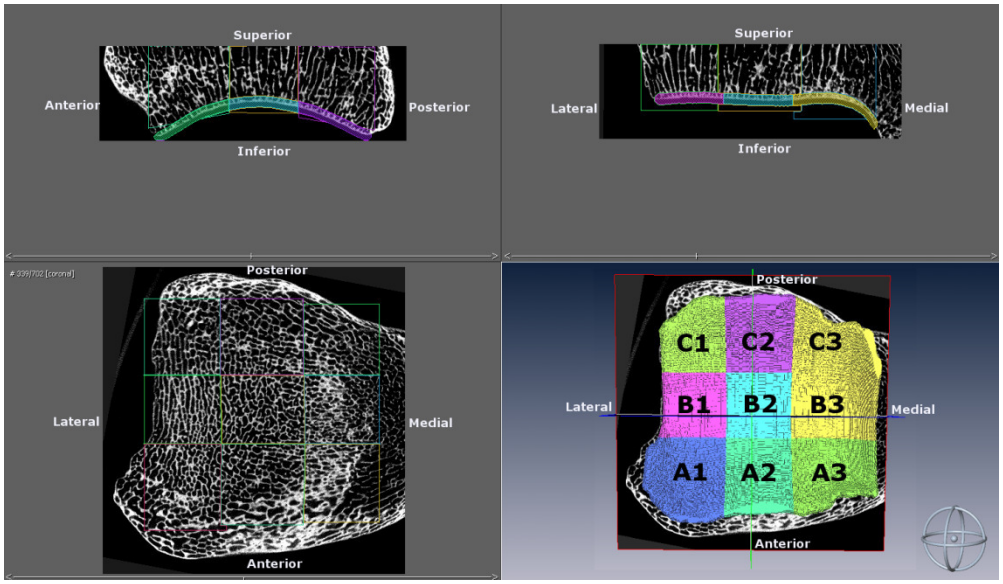

(b) Talus

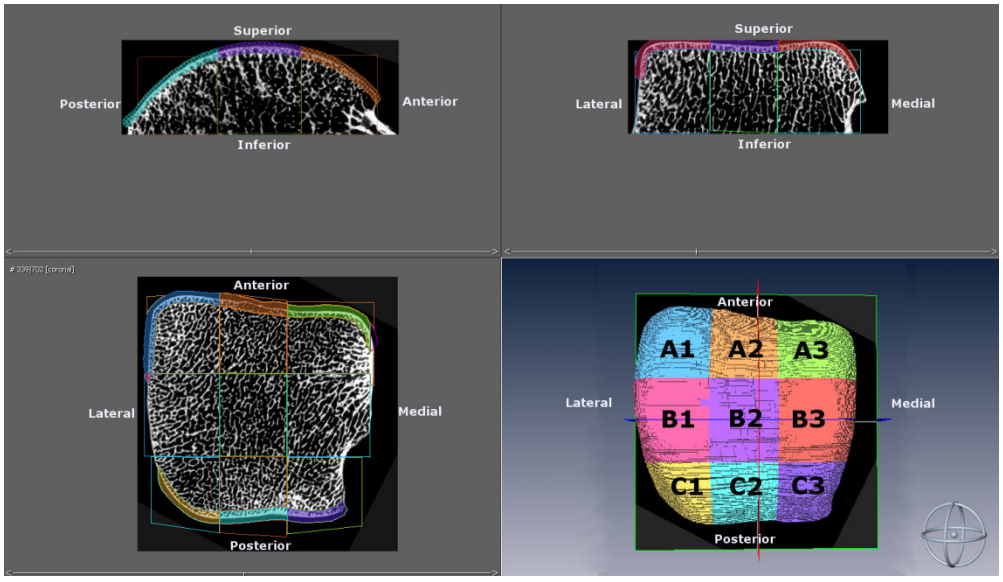

Figure 1. 1: Orientation of (a) distal tibia and (b) talus, and segmentation of the subchondral bone plate and underlying trabecular bone volume into nine regions of interest.
The subchondral bone plate extended slightly onto the malleolar articular surface of the distal tibia and onto both medial and lateral articular facets of the talus.

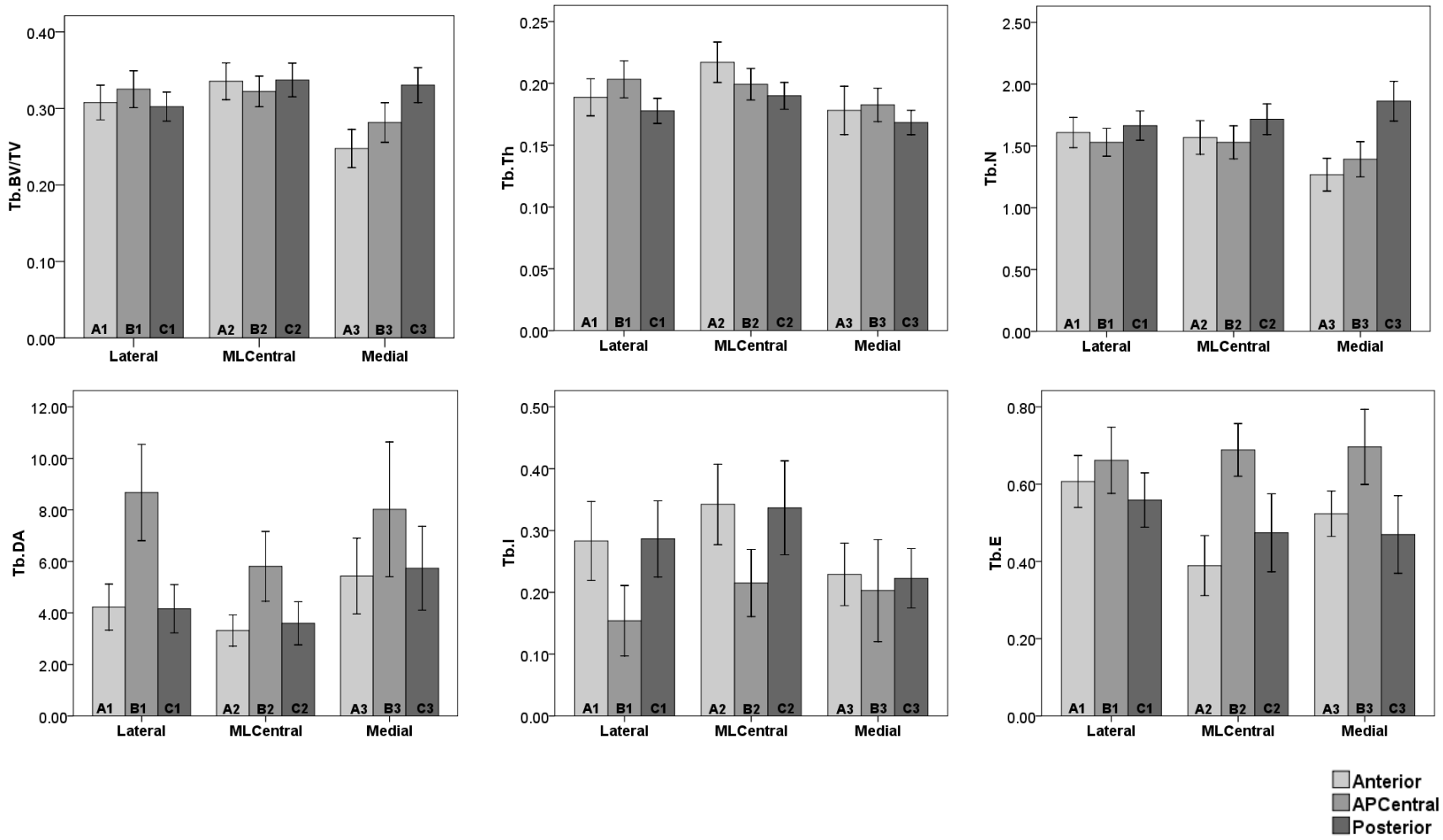

Figure 1. 2: Regional comparison of trabecular bone architecture in the distal tibia.
Trabecular bone volume fraction (Tb.BV/TV), mean thickness (Tb.Th), mean number (Tb.N), degree of anisotropy (Tb.DA), isotropy index (Tb.I), and elongation index (Tb.E). Error bars represent 95% confidence interval.

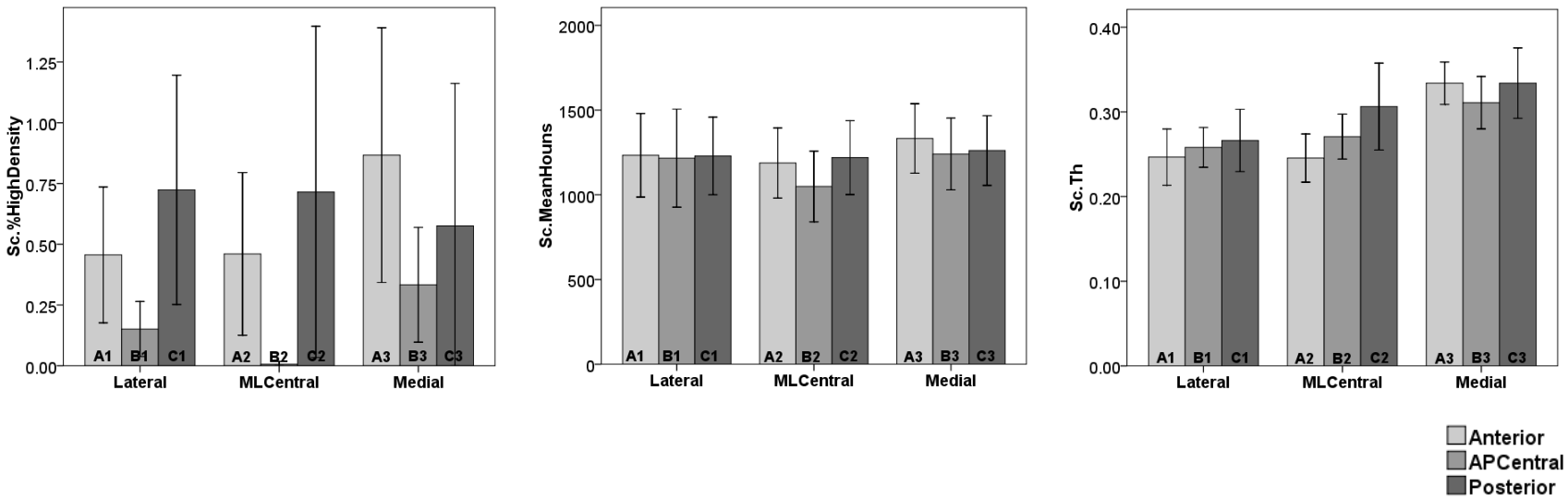

Figure 1. 3: Regional comparison of subchondral bone variables in the distal tibia.
Relative radiodensity (Sc.%HighDensity), mean radiodensity (Sc.MeanHouns), and thickness (Sc.Th). Error bars represent 95% confidence interval.

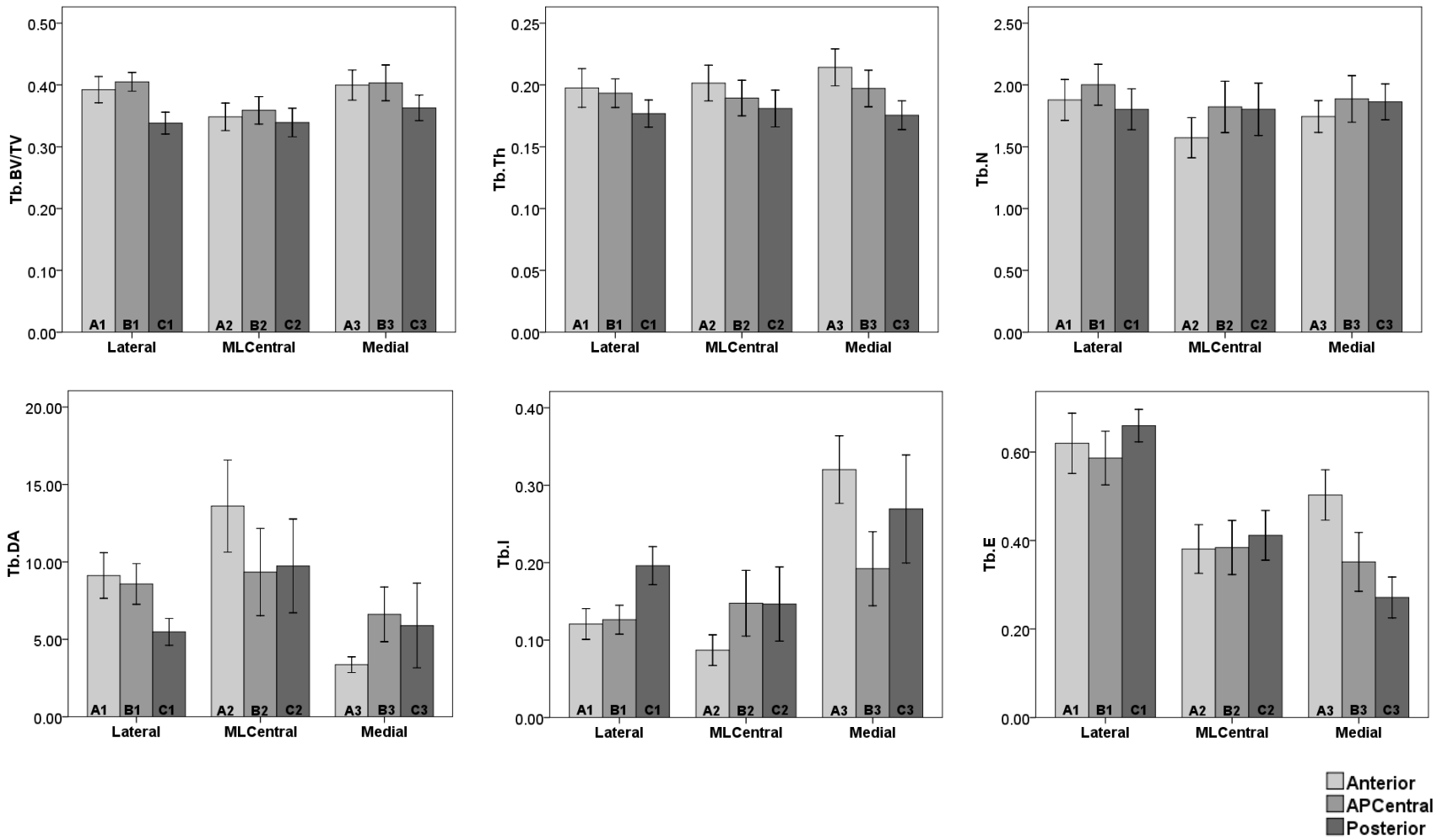

Figure 1. 4: Regional comparison of trabecular bone architecture in the talar trochlea.
Trabecular bone volume fraction (Tb.BV/TV), mean thickness (Tb.Th), mean number (Tb.N), degree of anisotropy (Tb.DA), isotropy index (Tb.I), and elongation index (Tb.E). Error bars represent 95% confidence interval.

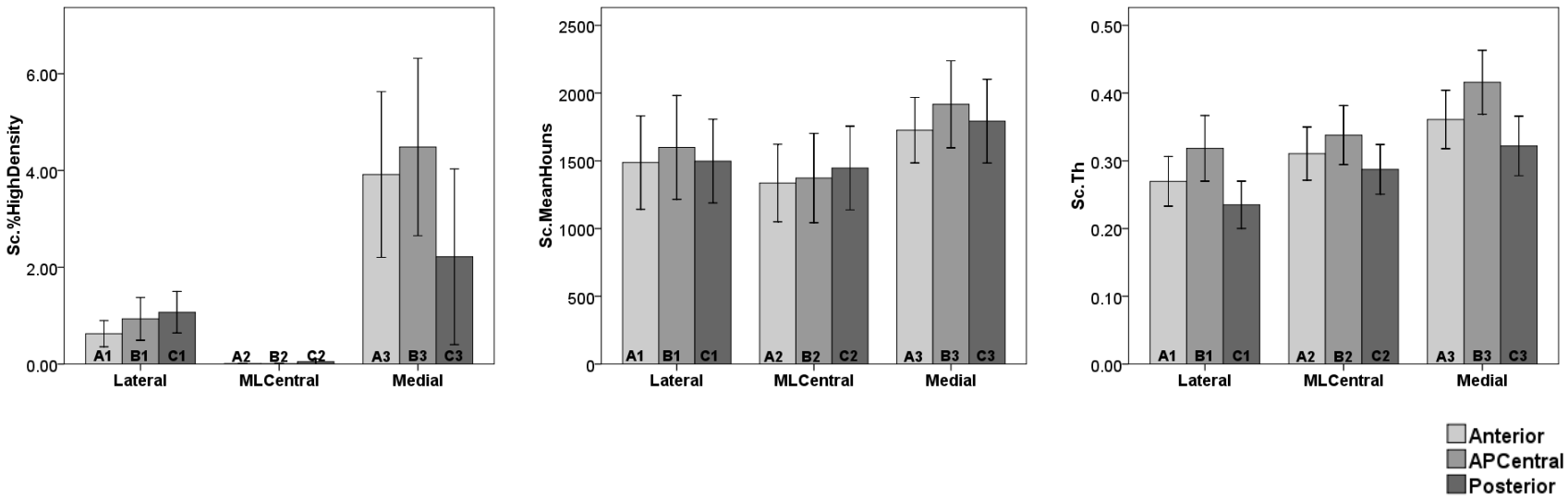

Figure 1. 5: Regional comparison of subchondral bone variables in the talar trochlea.
Relative radiodensity (a), mean radiodensity (b), and thickness (c). Error bars represent 95% confidence interval.

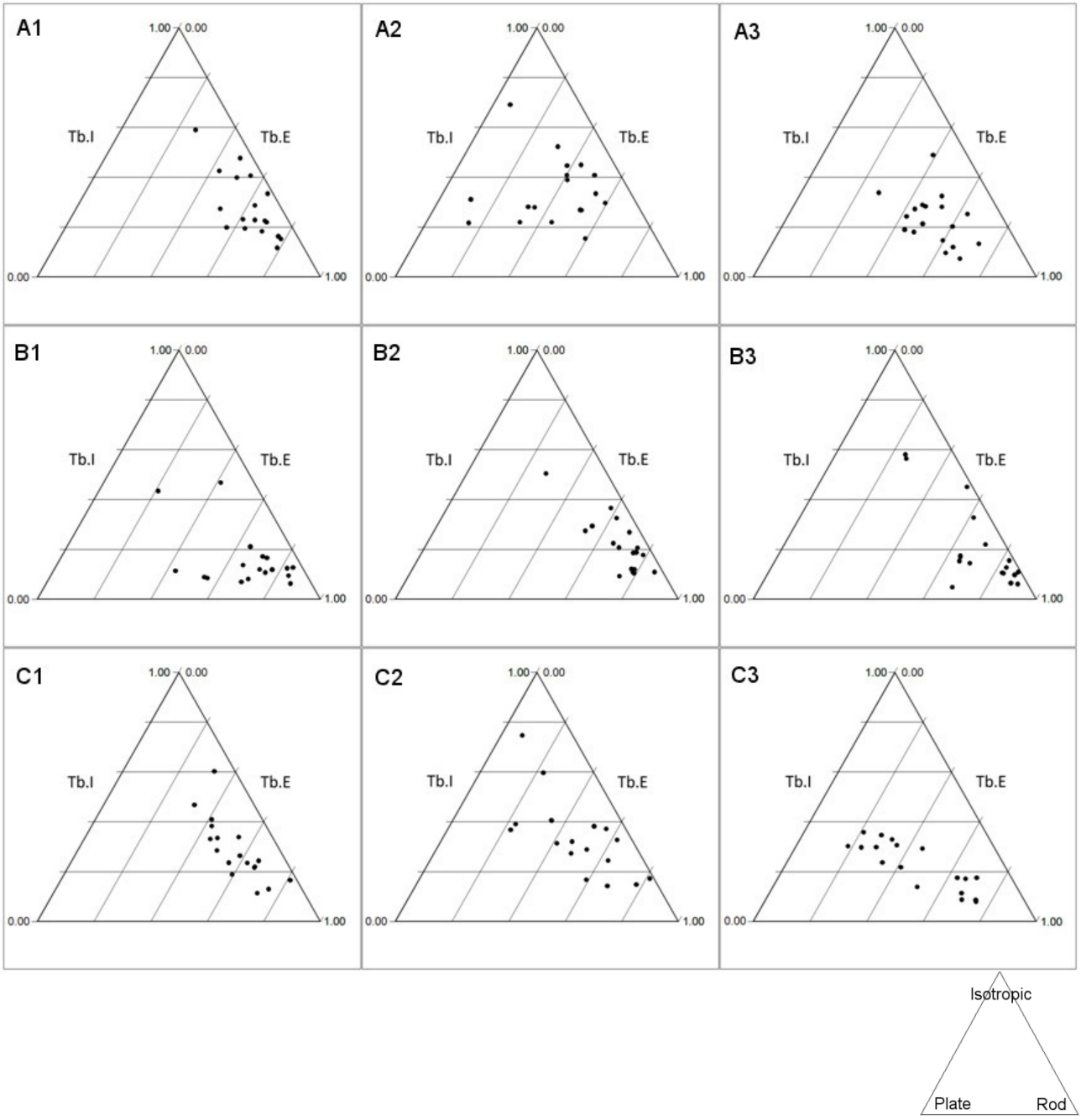

Figure 1. 6: Distribution of trabecular shape indices in the distal tibia.
Within each region, each point plots the Tb.I (τ_3/τ_1) and Tb.E ($1-(\tau_2/\tau_1)$) value; lines were drawn to enclose the distribution of each species for comparative visualization. Points towards the top apex indicate more isotropic trabeculae; points towards the bottom indicate more anisotropic trabeculae. Points towards the bottom left apex indicate more plate-shaped trabeculae; points towards the bottom right apex indicate more rod-shaped trabeculae.

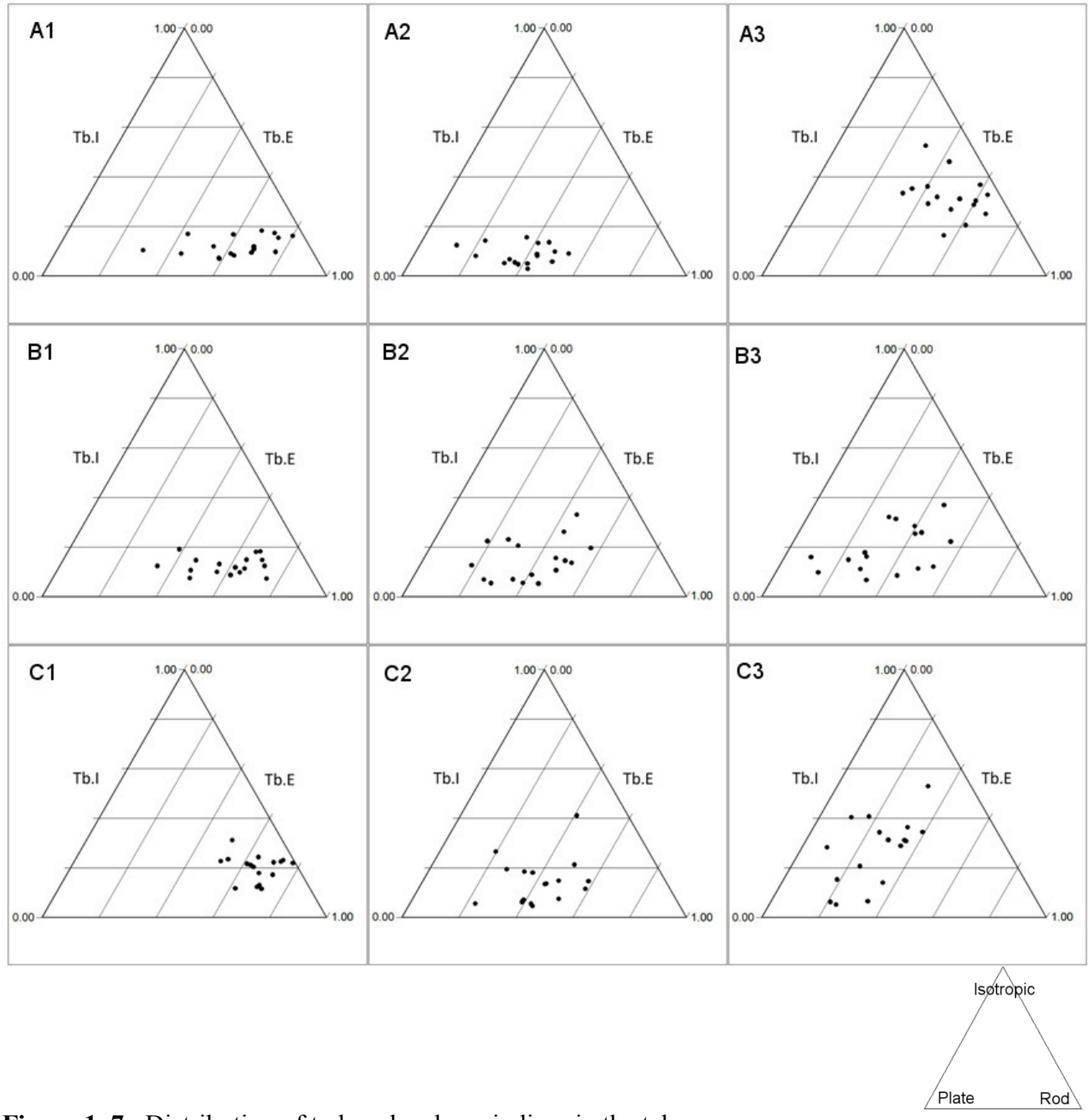

Figure 1. 7: Distribution of trabecular shape indices in the talus.
Within each region, each point plots the Tb.I (τ_3/τ_1) and Tb.E ($1-(\tau_2/\tau_1)$) value; lines were drawn to enclose the distribution of each species for comparative visualization. Points towards the top apex indicate more isotropic trabeculae; points towards the bottom indicate more anisotropic trabeculae. Points towards the bottom left apex indicate more plate-shaped trabeculae; points towards the bottom right apex indicate more rod-shaped trabeculae.

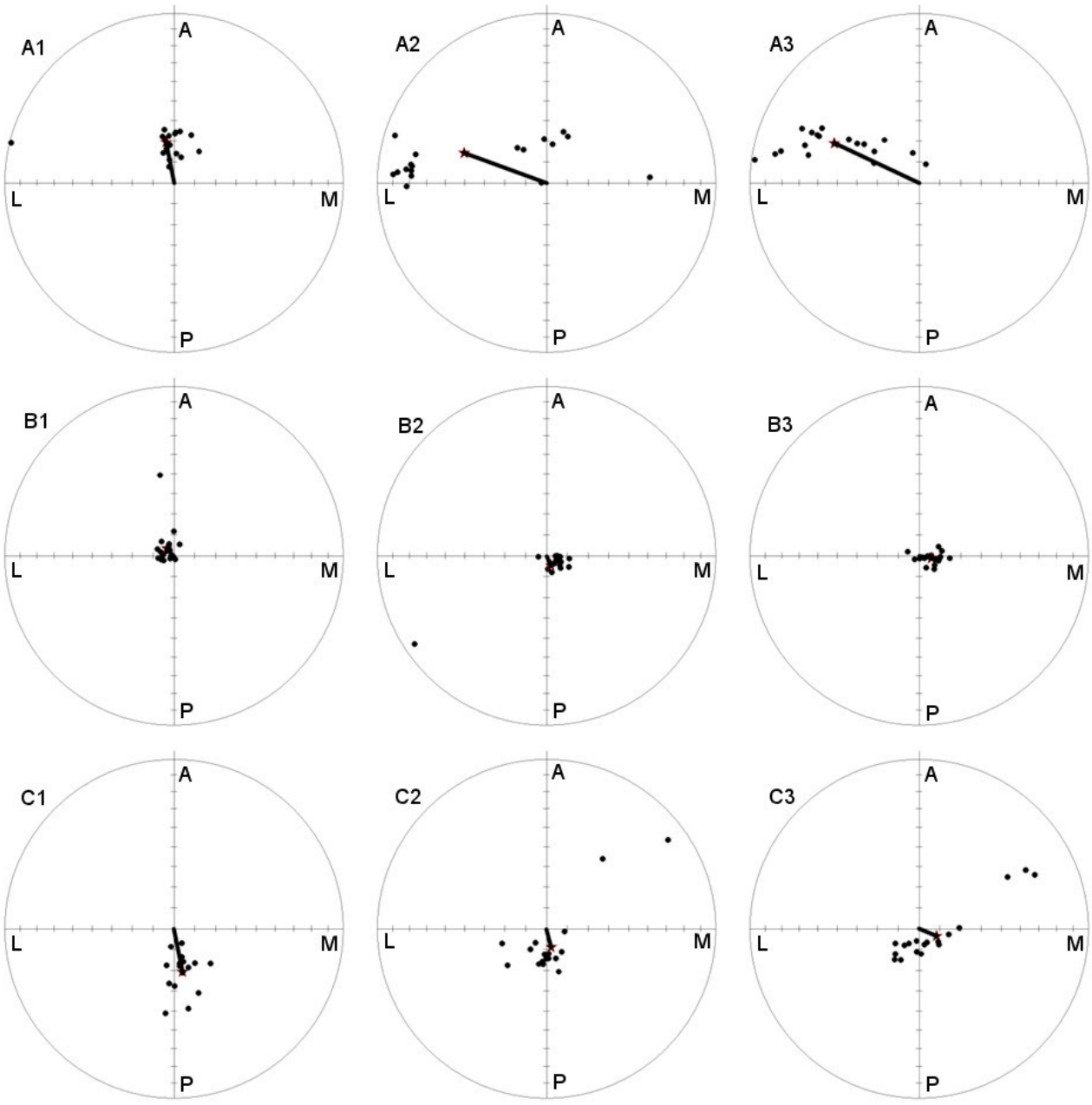

Figure 1. 8: Distribution of the primary trabecular eigenvector direction in each region of the distal tibia.
Each region is represented by a top-down view of a sphere, with each eigenvector depicted with its origin at the center of the sphere and tip on the outer surface of the sphere. Each small point represents one individual. Each large point and line from the center represents the species mean trabecular orientation. Points located towards the center of the circle represent more vertically-oriented trabeculae; points located towards the periphery represent more transversely-oriented trabeculae.

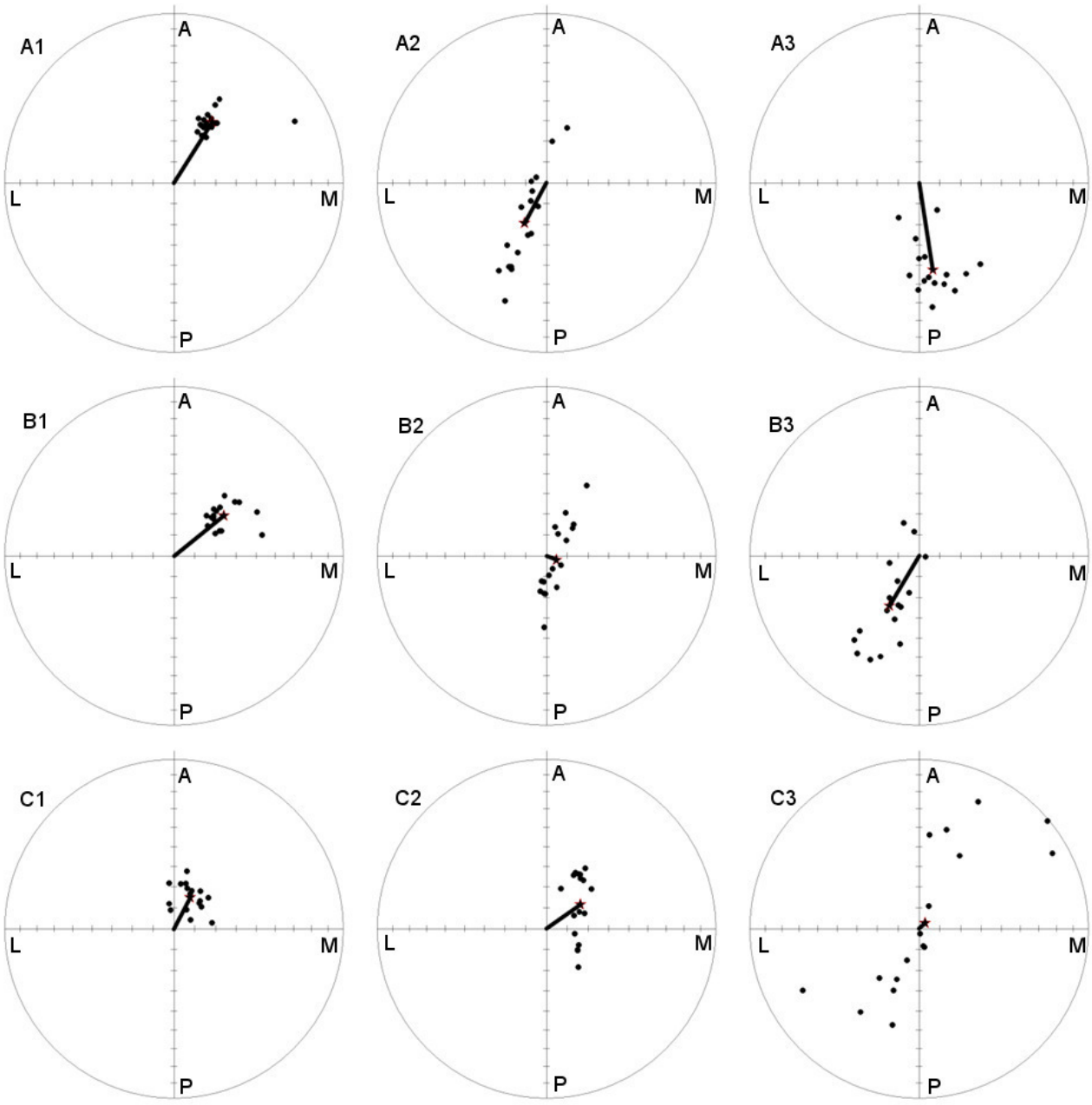

Figure 1. 9: Distribution of the primary trabecular eigenvector direction in each region of the talus. Each region is represented by a top-down view of a sphere, with each eigenvector depicted with its origin at the center of the sphere and tip on the outer surface of the sphere. Each small point represents one individual. Each large point and line from the center represents the species mean trabecular orientation. Points located towards the center of the circle represent more vertically-oriented trabeculae; points located towards the periphery represent more transversely-oriented trabeculae.

2 Chapter 2: Comparative analysis of subchondral bone and trabecular bone morphology among hominoids

2.1 Introduction

Much study and debate has been devoted to examining the differences in primate foot and ankle morphology, especially of the hominoids, as they relate to locomotor function (reviewed by Harcourt-Smith and Aiello 2004). Studies of the external morphology of the foot and ankle bones, particularly the talus, has yielded surprisingly few characteristics that are able to distinguish among the hominoid species despite very different habitual postures and locomotor modes. Distinguishing differences that have been found include (1) the trochlear surface of the talus is inclined more medially in apes than in humans, (2) the torsion of the talar head medially and the angle of inclination of the talar neck plantarly is greater in humans than in apes, (3) the mediolateral width of the anterior aspect, and the anteroposterior width of the medial aspect of the distal tibia is greater in apes than in humans. (4) the distal tibial articular surface (plafond) is posteriorly-directed in apes but usually anteriorly-directed in humans (DeSilva 2009; DeSilva and Throckmorton 2010; Gebo and Schwartz 2006; Kanamoto et al. 2011; Kidd and Oxnard 2002; Latimer et al. 1987; Lisowski et al. 1974; Morton 1922). These features are thus inferred to be indicators of the differences in habitual posture and locomotion among hominids. However, the use of these characters in morphometric studies of some important fossil talus bones reveal unique mosaics of ape-like and human-like external features that complicate locomotor reconstruction of these extinct hominins.

Perhaps more informative than external bone morphology, which may be limited by numerous genetic as well as functional constraints, is the analysis of epigenetically sensitive traits that are modified by an individual's activity pattern (Ward 2002). The internal structure of bone, both cortical and trabecular, has been shown to be one such epigenetically sensitive trait (e.g., Biewener et al. 1996; McKay et al. 2011; Polk et al. 2008; Pontzer et al. 2006). Whereas external morphologies may be limited in morphological plasticity, the internal morphology of mammalian bone is highly dynamic, constantly remodeling its inner architecture to changing biomechanical environments (Mazurier et al. 2006). The goal of this study was to investigate whether the internal morphology of the ankle bones hold a diagnostic locomotor signal that may help to further characterize the mosaicism found among fossil hominid tali.

The increasing accessibility and application of non-destructive micro-computed tomography (μCT) to anthropological studies has allowed for the analysis of internal bony morphology. Recent studies have compared trabecular structure among primates with the hypothesis that habitual locomotor differences (broadly defined at the species level) are reflected in trabecular architecture (Fajardo and Müller 2001; MacLatchy and Müller 2002; Maga et al. 2006; Ryan and Ketcham 2002, 2005; Ryan and van Rietbergen 2005; Saparin et al. 2009; Scherf and Hublin 2010; Scherf et al. 2009). Although this hypothesis has been supported by empirical evidence using experimental manipulation of applied external load on animal models (Biewener et al. 1996; Pontzer et al. 2006)

(but see Carlson et al. (2008) who did not find support), these comparative studies often found significant within-species variation in trabecular structure but few significant differences among species, with the most confident conclusion being that there are interspecific differences in degree of anisotropy (DA), an indicator of general alignment of trabeculae. For example, Ryan and Ketcham (2002) found relatively anisotropic ("aligned") trabeculae in the femoral head of leaping strepsirhine primates versus relatively isotropic ("random") trabeculae in that of nonleaping strepsirhines. The lack of a clear signal was partially attributed to the difficulty in identifying homologously-loaded regions of bone among species. Also, unlike in laboratory experiments, the magnitude and direction of load that was transmitted through the joint are uncontrolled and unknown. Therefore, it was not clear that a difference (or lack thereof) in trabecular architecture reflected differences in habitual load.

Data on trabecular bone structure in the hominid hindfoot is mostly limited to the human calcaneus, with a clinical focus on bone loss. Trabecular studies of the human talus are rarer and only descriptive, with authors noting that the trabeculae seem to be aligning with the principal stresses in the bone during bipedal standing or walking (Pal and Routal 1998; Takechi et al. 1982). Maga et al. (2006) preliminarily examined the trabecular structure in the calcaneus of hominids with samples of 1-2 specimens per group. They found no apparent differences in trabecular structure in the posterior calcaneus among humans, chimpanzees, gorillas, and orangutans, except that the DA is twice as high in humans.

The relative apparent mineral density (estimated from radiodensity values of CT scans) of the subchondral bone of joints has also been hypothesized to reflect patterns of habitual applied load (Ahluwalia 2000; Carlson and Patel 2006; Müller-Gerbl et al. 1989; Nowak et al. 2010; Patel and Carlson 2006, 2007; Polk et al. 2008). For example, Carlson and Patel (2006) found that quadrupedal primates had relatively larger and more concentrated areas of high radiodensity in the distal radius than suspensory and bipedal primates. Similarly, the relative thickness of subchondral bone may also reflect areas of differential load across a joint. Murray et al. (2001) found that juvenile horses run at high treadmill speeds had significantly thicker subchondral bone in the middle carpal joint than did those that walked, but only on the dorsal aspect of the joint, demonstrating that subchondral bone thickness is also site-specific within a joint, and that thicker regions may reflect regions of high habitual compressive load. Although most of these studies could only infer that regions of high apparent density indicated regions of high load and were the regions loaded in life during habitual locomotor activities, recent empirical evidence from the knees of treadmill-exercised sheep has lent support to this hypothesis (Polk et al. 2008).

While both subchondral bone and trabecular bone morphology may be indicative of joint load, they may be so in different ways (Frost 1999; Rafferty and Ruff 1994). For instance, Rubin et al. (2002) found significant increases in trabecular bone tissue apparent density of the proximal ¼ of the femur in sheep exposed to low intensity, high frequency strains while there were no significant differences found in the overlying cortical bone envelope, which included the femoral head subchondral bone. Decoupled responses to loading may be advantageous from a functional perspective, because they allow joints to respond to their mechanical environment without altering

articular morphology and compromising the demands of mobility (Lieberman et al. 2001). The work of Rafferty and Ruff (1994) on trabecular density in the femoral head of catarrhine primates supports this view, suggesting that the external articular surface area is mainly driven by the mobility demands of the joint and that the underlying internal trabecular morphology is independent from those demands and largely determined by the magnitude and orientation of the loads passing through the joint.

If either trabecular bone structure or subchondral bone apparent density is to be accepted as a morphological tool with which to infer locomotor behavior, they should be subject to a rigorous validation. Unfortunately, a direct validation is problematic because joint loads cannot easily be measured *in vivo* without invasive procedures that may compromise joint function. However, because both of these approaches, trabecular bone architecture analysis and subchondral bone apparent density analysis, are attempting to find diagnostic morphology that reflects bone strength due to habitual compressive joint loads, it follows that a combination of the two methods in an investigation of a specific region of bone may serve as a mutual validation. Similarly, analysis of trabecular and subchondral bone morphology in the two opposing surfaces of a joint may provide further corroborative evidence of being indicative of habitual load.

The bones of the hominoid ankle joint are well-suited for this investigation. They are likely subjected to relatively high compressive forces and as distal elements may be more sensitive to phenotypic plasticity than more proximal elements (Gebo 1986; Lieberman et al. 2001; Stock 2006). Also, there have been numerous hypotheses developed regarding the differences in habitual ankle posture between hominid species. In this study, these hypotheses are assessed as to their consistency with differences in subchondral and trabecular bone structure.

If subchondral bone and trabecular bone properties within the tibiotalar joint reflect habitual compressive load and are useful in distinguishing among species with different locomotor repertoires, then (1) the distribution of properties should be consistent among individuals of each species, (2) the distribution of properties should be different between species with different locomotor repertoires, (3) the opposing bones should display similarities in tissue distribution and architecture, and (4) the differences among species should be consistent with differences in observed joint kinematics during habitual posture and locomotion.

The goals of this study were to characterize and quantify the variation of these bone properties in the hominoid distal tibia and talus to address the hypothesis that the morphology of these tissues are indicative of habitual stresses within the bone. If so, then it is first predicted that the subchondral bone and trabecular bone properties would exhibit coordinated or complimentary morphologies within an articular surface. Furthermore, since the load distribution within a joint is applied equally and oppositely to both articular surfaces, it is predicted that the distribution of bone properties in the talus would mirror that of the distal tibia.

2.1.1 Specific predictions of morphology

From the study in Chapter 1 of the human distal tibia and talus, correlations were found among trabecular bone properties and among the subchondral bone properties. The bone structural

properties that were found to be overall best related to the distribution of load in the ankle were subchondral bone thickness (Sc.Th), trabecular bone volume fraction (Tb.BV/TV), the shape of trabeculae, and the primary orientation of trabeculae. The same correlations are predicted to be found in non-human hominoids as well.

From observational field studies of locomotor behavior (e.g., Doran 1993; Gebo 1992; Hunt 1991; Hunt 2004; Thorpe and Crompton 2006), it is well-accepted that any given wild non-human primate individual has a more diverse habitual locomotor repertoire than that of a bipedal terrestrial human (Hunt et al. 1996; Schmitt 2003). It follows then, that the habitual loads within the joints of a non-human primate will be relatively more variable than those of a human (D'Août et al. 2004; Vereecke et al. 2003), and the bone morphology should be similarly variable. Among the great apes, orangutans have the most diverse positional and locomotor behavior (Hunt 1991; Thorpe and Crompton 2006) due to their strict arboreal nature and slow quadrumanus progression through the forest canopy. It can thus be predicted that the distribution of regions of greater bone strength in orangutans will be relatively broader or more dispersed than those of the other hominoids, or that the interindividual variability in patterns will be higher than the variability in other hominoids. The highly terrestrial hamadryas baboon displays a more stereotypical locomotor repertoire than the apes (Hunt 1991). It is thus predicted that the pattern of high subchondral radiodensity in the baboons' joints will be narrower or less dispersed than those of the non-human hominoids, or that the interindividual variability in patterns will be lower than the variability in the non-human hominoids.

It is predicted that humans will display greater bone strength properties in the posterior regions in comparison to the African apes. Humans bear more weight on their calcaneus during heelstrike than do African apes, as demonstrated by plantar pressure measurements (Vereecke et al. 2003; Wunderlich 1999) and the presence of an enlarged calcaneal tuberosity (Latimer and Lovejoy 1989). Also, in humans at heelstrike the ground reaction force passes slightly posterior to the talocrural joint as the foot is forced into plantarflexion. Moreover, the arboreally-adapted apes spend more time vertical climbing with their ankle in a highly dorsiflexed position, therefore the complimentary prediction is made that they will display greater bone strength in the anterior regions of the joint.

It is predicted that the non-human hominoids would exhibit indicators of relatively stronger bone in more lateral regions in comparison to humans and baboons. The distal articular surface of the tibia has been noted to be inclined superolaterally in African apes while it is oriented essentially perpendicular to the long axis of the tibia in humans, features that are interpreted to be associated with the varus versus valgus position of the knee joint, respectively (DeSilva 2009; Latimer et al. 1987). Compared to humans, chimpanzees and gorillas place greater stress on the lateral aspects of the talocrural joint, loading their fibulae with a greater percentage of body weight (DeSilva 2009; Kanamoto et al. 2011; Latimer et al. 1987; Marchi 2007). The inclined orientation in the non-human apes serves to better position the foot in an inverted posture against a vertical substrate during climbing. The African apes however also spend a significant portion of time on the ground. During the support phase of terrestrial quadrupedalism, the chimpanzee calcaneus is believed to be in an inverted (laterally rotated) position relative to the ground while the talus (along with the forefoot) is

in an everted position Gebo (1992). Thus, from the hindfoot posture during terrestrial quadrupedalism, it may be predicted that, among the great apes, the regions of high radiodensity of chimpanzees and gorillas will be more laterally located on the tibial plafond.

Both humans and baboons engage in relatively more terrestrial locomotion and have anatomical features that support the stereotype of locomotion that is performed essentially in the sagittal plane (Aiello and Dean 2002; Harrison 1989; Rose 1977). As such, it is predicted that the load in both the human and baboon talocrural joint would be more centrally or medially located relative to the arboreal apes.

2.1.2 Specific predictions of trabecular shape and orientation

The intraspecific regional variation of trabecular shape and orientation may be an indicator of habitual load type. From the assumption that the habitual loads within the joints of a wild non-human primate are relatively more variable than those of an urban-dwelling human (D'Aout et al. 2004; Vereecke et al. 2003), it is predicted that the non-human groups would have more isotropic trabeculae than humans. Also, individuals within each primate group may be more likely to differ in habitual loads from one another, so it is predicted that the variability in trabecular orientation would be greater in the non-human groups than in the humans. Similarly, the three-dimensional nature of orangutan locomotion through the forest canopy (Hunt 1991; Thorpe and Crompton 2006) is assumed to engender more variable loading stresses in the ankle joint both inter- and intraindividually, so it is predicted that the trabecular isotropy and variability in trabecular orientation would be greatest in orangutans compared to all other species.

The posterior regions of the human tibia are predicted to have more plate-shaped trabeculae than other regions in agreement with Lai et al. (2006) and consistent with reports that the posterior tibia is stronger in osteopenetration tests (Hvid et al. 1985).

It is predicted that the primary orientation of trabeculae in the tibia would be directed more laterally and anteriorly in the African apes versus more vertically-directed in humans, based on the differences in orientation of the distal articular surface of the tibia as described above (DeSilva 2009; Latimer et al. 1987).

Baboons differ from humans and great apes in having a semi-digitigrade foot that may be advantageous for their more high-speed terrestrial locomotion (Biewener 1983; Polk 2002), but see (Patel 2009, 2010). The locomotion of the more terrestrial cercopithecines is thought to be less variable than that of more arboreal primates (Meldrum 1989, 1991), so it is predicted that baboons would display more anisotropic trabeculae than the great apes. Based on the semi-digitigrade posture, it is also predicted that the primary orientation of trabeculae in the talus is more strongly posteriorly directed in baboons than it is in the great apes (Meldrum 1991).

2.2 Methods

2.2.1 Study Sample

The taxa used in this study were modern human (*Homo sapiens sapiens*), gorilla (*Gorilla gorilla gorilla*), chimpanzee (*Pan troglodytes troglodytes*), orangutan (*Pongo pygmaeus*), and baboon (*Papio hamadryas sp.*) (Table 2.1).

Adult females of each hominoid species were selected for study in an effort to minimize the potential effects of body size on both locomotor behavior and bone morphology. Baboons were included in the study as a non-hominoid outgroup and also as a representative of terrestrial digitigrade quadrupedalism. To minimize effects of body size male baboons were selected, although it was acknowledged that sex-related differences of bone morphology such as hormonally-induced bone loss in females may affect the interpretation of results. Museum records of the female human specimens' mass at death ranged from 44.0-68.0 kg (mean 53.9 kg), which represent a range that is similar to the body mass of female chimpanzees (~ 45 kg) and female gorillas (~71 kg) (Smith and Jungers 1997). Adult status was assessed by epiphyseal fusion on all long bones of each skeleton. Specimens were rejected for analysis if there was evidence of traumatic injury to the limbs, systemic abnormalities such as osteoporosis, or if they were excessively greasy since grease may alter radiodensity values (Ruff and Leo 1986).

2.2.2 Data collection

Each bone was scanned individually using a commercial μCT system (eXplore Locus SP, GE Healthcare Pre-Clinical Imaging, London, ON, Canada) housed within the Department of Biomedical Engineering at the Cleveland Clinic Foundation. This system is designed to image small laboratory animals *in vivo*, but was advantageous to this study because unlike many other commercial μCT systems it has a long specimen bed to accommodate the full length of the tibia. The GE eXplore Locus uses volumetric conebeam CT technology which allows the entire sample to be imaged in one rotation. The system was calibrated regularly using known density phantoms to convert the CT values to standard Hounsfield units. Beam-hardening artifacts were minimized using a system-equipped algorithm.

Care was taken to position and secure each bone in a standard, consistent position on the scanner bed. The long axis of the tibia was oriented parallel to the scanner bed, thus orienting the distal articular surface perpendicular to the bed. The talus was oriented in the standard basal talar plane (Lisowski et al. 1974) where the posterior and lateral tubercles and the most inferior point of the head rested naturally on the horizontal bed; the anterior edge of the trochlea was oriented perpendicular to the long axis of the scanner.

Specimens were scanned at a resolution setting of 45 μm, which has been found to be small enough to produce morphometric results similar to histologic methods (Müller et al. 1996). The source energy voltage was set to the maximum 80 kVp, which is suitable for imaging of the high-density bone. The x-ray current was set to 450 μA, which was the intensity of the x-ray beam that provided a good signal-to-noise ratio. The pixel matrix size was 1024x1024, yielding a field of view

of 47.1 mm and an isometric voxel size of 0.0448 mm. Each image was reconstructed from 720 views with an exposure time of 400 ms.

Using GE Microview software (GE Healthcare, http://microview.sourceforge.net), the 3D volumes were digitally reoriented to reproducible, standardized positions that are functionally intuitive based on the horizontal supratalar plane of the ankle joint (Latimer et al. 1987). The distal tibia was oriented "square" to the articular surface; i.e., in the sagittal plane, the anterior and posterior rims of the articular surface were level and in the coronal and transverse planes, the medial-lateral axis was level (Figure 2.1a). The talus was oriented relative to the trochlear surface such that in sagittal plane view, the base of the neck and the most posterior point of the trochlear surface were in the same horizontal plane, and in the coronal and transverse planes, the superiormost points of the medial and lateral trochlear rims were level (Figure 2.1b). The reoriented volumes were then exported as a stack of 16-bit DICOM format image files. The DICOM image stack of each specimen was imported into *Amira Visualization Software* (Visage Imaging, San Diego CA) for further analysis.

2.2.3 Analysis of subchondral bone

2.2.3.1 Segmentation into slab

The subchondral plate of bone was semi-manually isolated from each joint surface (Figure 2.1) using the brush segmentation tool. In approximately every tenth image (0.45 mm) in the volume series, the boundary between air and the articular surface of bone was visually determined and outlined using the brush tool. Care was taken to include only subchondral articular bone but not the surrounding non-articular cortical bone. The manually-selected air-bone boundary was then interpolated between the slices, with subsequent visual verification of accuracy. The thickness of this rough-cut, selected mask was visually-approximated to be thick enough to fully encompass the cortical plate while minimizing the inclusion of underlying trabeculae and was held constant for each species (ranged from 16-21 voxels thick). The set of voxels within the mask was isolated from the rest of the specimen volume (i.e., the trabecular bone and non-articular cortical bone) using the *Amira* arithmetic tool, and saved as a separate volume. The minimum and maximum voxel intensity values (in Hounsfield units) within this isolated subchondral volume were recorded for use in subsequent histogram analyses. Although the thickness of the mask was user-selected and constant for each species, the actual computed thickness of the subchondral bone plate was determined automatically by a software algorithm as described below.

2.2.3.2 Division into anatomical regions

The subchondral bone volume was segmented into a 3x3 grid of nine anatomically-aligned regions (Figures 2.1 and 2.2). The maximum linear mediolateral and anteroposterior dimensions of the isolated subchondral plate were digitally measured and divided into thirds using the *Amira* measurement tool. Each region was thus defined with dimensions of 1/3 of the maximum mediolateral length and 1/3 of the maximum anteroposterior length. The curved trochlear surface

required a different, angular approach, whereby the arc between the posteriormost and anteriormost points of the articular surface was measured in degrees and then divided into thirds. The set of voxels within each region was isolated using the *Amira* arithmetic tool, saved as a separate volume, and exported as a stack of 16-bit TIFF format image files.

2.2.3.3 Quantification of radiodensity

The distribution of voxel radiodensity within each of the nine regions of the articular surfaces was quantified in the following way. An 8-bin histogram of the radiodensity values within each region was constructed, using the minimum and maximum values previously recorded for the entire articular surface as lower and upper bounds. Relative radiodensity intensity (Sc.%HighDensity) was quantified for each region as the combined number of voxels in the highest two bins (i.e., highest 25%) as a percentage of the total number of voxels in the region. The mean voxel intensity value within the region was computed by *Amira* and recorded as Sc.MeanHouns. Both of these properties together may be referred to as "subchondral radiodensity".

2.2.3.4 Quantification of thickness

The thickness of the subchondral cortical shell of each articular surface was quantified using *Quant3D* software (Ketcham 2005; Ketcham and Ryan 2004). *Quant3D* was developed for the purpose of quantifying the structure of 3D fabrics and was used primarily in this study to quantify trabecular bone. However, its algorithms were also used here as a subjective method of calculating subchondral thickness by in essence treating the thin subchondral plate of bone as if it were an isolated trabecular plate.

Because *Quant3D* required images to be imported in an 8-bit format, the 16-bit *Amira* TIFF image stack of each isolated region of the subchondral plate was converted to 8-bit TIFF images using *ImageJ* software (Rasband 1997-2007). The rough-cut volume containing the thin plate was binarized into bone/non-bone using an adaptive, iterative threshold technique (Ridler and Calvard 1978; Ryan and Ketcham 2002), and the structure analyzed using the star volume distribution (SVD) algorithm (Cruz-Orive et al. 1992; Ketcham and Ryan 2004). In this algorithm, for a given point within the bone structure, intercept lengths (straight-line lengths between bone-air boundaries) are calculated for 513 random angular orientations. The thickness of bone at a given point is defined as the shortest intercept length. Using 2000 random points within the bone volume, calculations were made of the mean thickness of the subchondral bone plate (Sc.Th) within each of the 9 regions.

2.2.4 Analysis of trabecular bone

2.2.4.1 Segmentation into anatomical regions

The trabecular bone volume of each specimen was segmented into nine roughly cubic regions directly corresponding to the overlying subchondral bone regions defined above (Figure

2.1). The set of voxels within each region was isolated using the *Amira* arithmetic tool, saved as a separate volume, and exported as a stack of 16-bit TIFF format image files.

2.2.4.2 Thresholding/Quant3D options

The structure and orientation of the trabecular bone within each region was quantified using *Quant3D*. The 16-bit TIFF image stack of each trabecular region was smoothed from noise using a Gaussian filter and converted to 8-bit TIFF images using *ImageJ* software, then imported into *Quant3D*. Anatomical orientation axes were applied, denoting anterior, medial, and superior directions. For each of the nine regions of trabecular bone, a volume of interest (VOI) was defined as being the largest centered sphere that fit completely within each region, without including unwanted cortical bone. Because a cuboidal VOI introduces a bias in the results if a prominent feature is oriented near 45 degrees, a spherical volume of interest was chosen (Ketcham and Ryan 2004). Because of natural irregularities in bone shape, the nine VOIs within a given specimen were not exactly the same size. For example, the posterior dimension of the distal tibia was often narrower than the anterior dimension, resulting in posterior VOIs that were consistently smaller than anterior VOIs (Figure 2.1).

The trabecular bone in the VOI was binarized into bone/non-bone using an adaptive, iterative threshold technique (Ridler and Calvard 1978; Ryan and Ketcham 2002), and the structure analyzed using the star volume distribution (SVD) algorithm (Cruz-Orive et al. 1992; Ketcham and Ryan 2004).

2.2.4.3 Quantification of trabecular volume

The output variables computed by *Quant3D* and used in this analysis are:

- *Relative bone volume (Tb.BV/TV)*: Also known as "bone volume fraction", it is the dimensionless ratio of the number of bone voxels present in the VOI to the total number of voxels in the VOI (Goulet et al. 1994).
- *Trabecular strut thickness (Tb.Th)*: The average trabecular strut thickness (mm) in the VOI, based on the intersections between a superimposed grid of lines and bone voxels (Hildebrand and Ruegsegger 1997).
- *Trabecular number (Tb.N)*: The estimated number of trabecular struts in the VOI, based on the number of intersections between a superimposed grid of lines and bone voxels (Hildebrand and Ruegsegger 1997).

2.2.4.4 Quantification of trabecular shape and primary orientation

A fabric tensor describing the orientation of trabeculae within each VOI was calculated using the star volume distribution (SVD) method of *Quant3D* (Ryan and Ketcham 2002). The SVD method of quantifying architectural anisotropy (fabric) has been shown to be the best predictor of mechanical anisotropy (Odgaard et al. 1997). The SVD method is based on the measured length of the longest uninterrupted line from a point lying within trabecular bone to the boundary between

bone and air, repeated for a series of uniformly distributed orientations and multiple random points (Cruz-Orive et al. 1992). From these data, a fabric tensor is derived which describes how the moment of inertia of bone varies with orientation (Ketcham 2005). Three eigenvectors, μ_1, μ_2, μ_3, and three eigenvalues, τ_1, τ_2, τ_3, describing the distribution of bone are derived from the fabric tensor (Benn 1994; Ryan and Ketcham 2002). The eigenvectors represent the orientation in 3D space of the primary, secondary, and tertiary material axes. The corresponding eigenvalues, defined such that $(\tau_1 + \tau_2 + \tau_3) = 1$ and $\tau_1 > \tau_2 > \tau_3$, represent the relative magnitudes of each of the three material axes. The first eigenvector is defined to be parallel to the axis of maximum clustering in the data. The specimen is *orthotropic* if the three eigenvalues are distinct in value, *transversely isotropic* if there are two similarly-valued eigenvalues, and *isotropic* if all eigenvalues are approximately equal (a sphere). The degree of anisotropy (DA), defined as the ratio of the highest eigenvalue to the lowest eigenvalue (τ_1/τ_3), is the commonly used ratio to summarize the relative magnitudes. However this value is often difficult to evaluate and compare because there is no upper bound. The Tb.DA is thus not presented in the results. The inverse metric, the isotropy index Tb.I (τ_3/τ_1), is more intuitive to evaluate trabecular shape because values are bounded between 0 and 1. Other ratios between the eigenvalues also give an indication of the shape of the trabeculae – whether plate-like or rod-like. If the first eigenvalue is high and the second and third are equally low, then the data indicates a rod-like shape; if the first two eigenvalues are equally high and the third is low, then the data indicates a plate-like shape (Benn 1994). Ding et al. (2002a) demonstrated that plate-like trabeculae are indicative of a high-stress environment while rod-like trabeculae indicate regions of low stress.

The output variables computed by *Quant3D* and used in this analysis are:

- *Trabecular degree of anisotropy (Tb.DA)*: (τ_1/τ_3). The primary eigenvalue divided by the tertiary eigenvalue. Values closer to 1 denote perfect isotropy; increasingly greater values indicate trabecular struts which are increasingly narrowed onto a single plane (Harrigan and Mann 1984).
- *Trabecular isotropy index (Tb.I)*: (τ_3/τ_1). The tertiary eigenvalue divided by the primary eigenvalue. Values closer to 0 denote trabecular struts that are confined to a single plane (either plate-shaped or rod-shaped); a value of 1 denotes perfect isotropy (sphere-shaped) (Benn 1994).
- *Trabecular elongation index (Tb.E)*: $1-(\tau_2/\tau_1)$. Distinguishes between rod-shaped and plate-shaped trabeculae by indicating the extent of preferred orientation of trabeculae in the major plane defined by eigenvectors 1 and 2. If Tb.I is close to 0, concurrent values of Tb.E closer to 0 denote more plate-shaped trabecular struts; values of Tb.E closer to 1 denote more rod-shaped struts. (Benn 1994).
- *Direction of eigenvectors*: Orientation of the primary and secondary eigenvectors as defined by angle-angle coordinates relative to the center of the VOI.

Thus, the two indices Tb.I and Tb.E used together uniquely define the architecture of the trabecular bone mesh. A trabecular fabric composed of elongated rod-shaped trabeculae will have low Tb.I and high Tb.E. A fabric of flat disc-shaped trabeculae will have low Tb.I and low Tb.E. A

completely isotropic fabric with no preferred trabecular orientation will have high Tb.I and low Tb.E.

2.2.5 Statistical analyses of morphological variables

All comparative analyses were performed using data that was uncorrected for body size. Though certainly the individual animals varied in body size, this variation was deemed to be an important parameter to include because it likely has an effect on morphology both biomechanically and behaviorally (Biewener 2005).

Bivariate correlation analyses were performed for all variables to assess relationships, particularly between subchondral and trabecular bone variables within each bone. Bivariate correlation analyses were also performed between the values quantified for the tibia and the variables quantified for the talus to investigate the presence of a morphological relationship between the two articulating bones.

Descriptive statistics were calculated for all variables to investigate their variation across individuals and across regions within the ankle joint. To test whether there were significant differences in subchondral bone and trabecular bone architecture among regions, in each species a multivariate analysis of variance with post-hoc pairwise comparisons tests (Games-Howell) was performed among regions to characterize the distribution of bone properties across the talocrural joint surface.

Two methods were used to measure the consistency of patterns within each species. First, the coefficients of variation were compared for each variable in each region. Second, Kendall's coefficient of concordance (W), a normalization of the Friedman test statistic, was computed for each variable to assess the consistency of ranked values across each articular surface. In each specimen, for each variable, the 9 regions were assigned ranks based on values of that variable, with the region with the highest value ranked 9, and the region with lowest value ranked 1. The level of agreement among those sets of ranked data was assessed using Kendall's coefficient of concordance (W). A W=1 would indicate that all specimens had identical rank order of regions from highest to lowest value. A W=0 would indicate that the ranking of regions was random.

Two methods were used to assess differences in trabecular bone pattern among species. First, a multivariate analysis of variance was used to compare the means of each variable, first overall, and then within each region among groups. Second, the pattern of mean ranks was examined for differences among species in relative distribution of bone properties across the joint.

All statistical analyses were performed using SPSS 16.0 software (SPSS, Inc., Chicago, IL). Significance levels for all analyses were $p < 0.05$.

2.2.6 Statistical analysis of trabecular shape and orientation

The distribution of trabecular shape indices was visualized using ternary plots of Tb.I and Tb.E (Graham and Midgley 2000), where data points towards the top apex indicate more isotropic trabeculae and data points towards the bottom indicate more anisotropic trabeculae. Data points

towards the bottom left apex indicate more plate-shaped trabeculae and data points towards the bottom right apex indicate more rod-shaped trabeculae.

The mean primary eigenvector and spherical variance was computed using GEOrient software (www.holcombe.net.au/software/rodh_software_georient.htm). The mean primary eigenvector is the resultant of all the primary eigenvectors (μ_1) from each specimen (Mardia 1972), presented in terms of two values, trend (T_m) and incline (I_m). The trend of a vector is the direction of its projection on a transverse plane, with 0/360 degrees directed anteriorly, 90 degrees directed medially, and 270 degrees directed laterally. The incline of a vector is its superiorly-directed angle from the transverse plane. The spherical variance (s) is a measure (0-1) of the variability of the data as reflected by the resultant (Mardia 1972). A low variance indicates strong vector clustering, while a high variance indicates greater vector dispersion.

2.3 Results

Table 2.2 summarizes the predictions set forth in this study and the results in the distal tibia and talus. Significant differences were found in overall bone properties among the species and in patterns of distribution of properties across each bone, however not always in agreement with predictions based on observed kinematic behavior. These results are described in further detail below.

2.3.1 Bivariate correlations among variables

Tables 2.3 and 2.4 list the bivariate correlation coefficients (Pearson's r) among measured variables first omnibus including all species, followed by correlations within each species group for the distal tibia and talus, respectively. Figures 2.2 and 2.3 depict the relationship among bone variables in each region of the distal tibia and talus.

As predicted, in both tibia and talus with all species combined, moderate positive correlations were found among the trabecular bone variables Tb.BV/TV, Tb.I, Tb.Th, and Tb.N while negative correlations were found between these variables and Tb.DA and Tb.E (Tables 2.4 and 2.5). A moderate negative correlation was also found between Tb.Th and Tb.N. In the subchondral bone, Sc.MeanHouns was positively correlated with both Sc.%HighDensity and Sc.Th. Moderately positive correlations were found between the subchondral bone variables and the Tb.BV/TV of the underlying trabecular bone in both the tibia and talus. Weaker positive correlations were also found between the subchondral bone variables and Tb.Th and Tb.N. With all species combined, weak negative correlations were found between the subchondral bone variables and Tb.DA and Tb.E.

In the distal tibia, considering each species separately, the correlations among trabecular bone variables remained, and the correlations among subchondral bone variables remained, but those between subchondral bone variables and the underlying trabecular bone weakened relative to when all species were combined (Table 2.3). Positive relationships were still found between Sc.Th and Tb.BV/TV and between Sc.Th and Tb.Th in all species except *Homo*. In *Gorilla,* a moderate

negative relationship was found between Sc.Th and Tb.N. but in *Papio*, a moderate positive correlation was found between these two variables.

In the talus, taking each species separately, many of the correlations among trabecular bone variables were weakened or lost, but the correlations among subchondral bone variables remained (Table 2.4). Positive correlations were also mostly maintained between subchondral bone radiodensity and Sc.Th on the one hand and Tb.BV/TV and Tb.Th on the other hand. No relationship was found between Tb.N and the overlying subchondral bone properties in *Homo* and *Pan*, but in *Gorilla*, *Pongo*, and *Papio*, a moderate negative correlation was maintained between Sc.Th and Tb.N.

In summary, in general Tb.Th and Tb.N were found to be highly correlated with each other and with Tb.BV/TV. Sc.%HighDensity and Sc.MeanHouns were highly correlated with Sc.Th.

2.3.2 Overall species means and variability

Tables 2.5 and 2.6 list the species mean values, standard deviations and coefficients of variation for each bone property for the distal tibia and talus, respectively. Significant pairwise interspecific differences were found for each bone structural property at the overall whole-bone level (Tables 2.9 and 2.10).

In both the distal tibia and talus *Homo* displayed bone properties indicative of less robust, more anisotropic, bone relative to the other species. *Homo* had the lowest Sc.Th ($p<0.001$), and Tb.BV/TV ($p<0.001$) compared to other species, and was found to have a greater overall Tb.DA ($p<0.05$) and Tb.E ($p<0.001$). In both the distal tibia and talus, *Homo* displayed the greatest degree of variability in Sc.Th across the articular surface (Tables 2.5 and 2.6).

In both the distal tibia and talus *Papio* displayed bone properties indicative of relatively stronger bone. *Papio* had the greatest overall Tb.BV/TV ($p<0.001$) and Sc.%HighDensity ($p<0.001$ in distal tibia, $p<0.05$ in talus) compared to other species. In the distal tibia, *Papio* had the highest Sc.MeanHouns ($p<0.01$), greatest Tb.I ($p<0.001$) except vs. *Homo*, and least Tb.E ($p<0.01$). In both the distal tibia and talus, *Papio* displayed the least variability in subchondral bone properties across the articular surface.

The bone properties of *Pan* and *Gorilla* generally fell in between those of *Homo* and *Papio*, but there were exceptions. In the distal tibia, *Pan* had the lowest Tb.Th ($p<0.001$) but greatest Tb.N ($p<0.001$) among groups. In the talus, *Pan* and *Gorilla* together had the greatest Sc.Th. In the tibia, *Pan* and *Gorilla* were least variable in Tb.BV/TV.

In the distal tibia, *Pongo* had the greatest overall Sc.Th, although significantly so only versus *Homo* ($p<0.001$) and *Pan* ($p=0.011$). In the talus, *Pongo* had the least Tb.I and Tb.E, although significantly so only against *Homo* ($p<0.001$) and *Gorilla* ($p<0.05$). In both the distal tibia and talus, *Pongo* displayed the greatest degree of intraspecific variability in Tb.BV/TV. *Pongo* was not found to have overall more isotropic trabeculae than the African apes in the tibia, but did overall tend to have the most isotropic and least elongated trabeculae in the talus ($p<0.001$).

In summary, *Papio* displayed bone properties indicative of relatively stronger bone while those in *Homo* were relatively weaker. *Pongo* displayed the greatest degree of variability in trabecular bone volume, but not in other properties.

2.3.3 Comparisons among species within each region

The data in each of the nine regions was examined to further clarify which regions were most important in distinguishing the differences among species. Tables 2.7 and 2.8 list the mean values, standard deviations and coefficients of variation for each bone property in each of the nine regions of the distal tibia and talus, respectively. Figures 2.2 and 2.3 illustrate the mean values and the 95% confidence interval for the distal tibia and talus, respectively. Separate analyses of variance in each region show that subchondral bone and trabecular bone properties could differentiate among species, although certain regions were more diagnostic than others. Tables 2.11 and 2.12 list the polarity of pairwise comparisons between each species for each variable for each of the nine regions of the distal tibia and talus, respectively.

Homo was distinguished from the other taxa in having significantly lower Sc.Th in almost all regions in both the distal tibia and talus. Although *Homo* had overall significantly lower Tb.BV/TV in both the distal tibia and talus, *Homo* did not differ significantly from the other hominoids (but did from *Papio*) in the mid-coronal (B1, B2, and B3) regions of the distal tibia or the medial (A3, B3) and posterocentral (C2) regions of the talus, suggesting that these regions may be particularly load-bearing in *Homo*. *Homo* also displayed overall greater Tb.E than all groups, but significantly so in the anterolateral (A1) and central (B2) regions of the distal tibia and lateral (A1, B1, C1) regions of the talus, suggesting that these regions may be relatively weaker than others.

Papio was distinguished from the apes in having the greatest Sc.%HighDensity in the anterior (A1, A2) and posterior (C1, C2) regions of the distal tibia and the posterior (C1, C2) regions of the talus. *Papio* was also distinguished from the apes in having significantly greater Tb.BV/TV in almost all regions of the distal tibia and talus. *Papio* exhibited the least Tb.DA and least Tb.E in all regions, but generally not significantly so.

Pongo was distinguished from the other taxa particularly in the anterolateral region of the distal tibia, by greater Tb.BV/TV and subchondral bone properties. In the distal tibia, *Pan* was distinguished from all other taxa in having significantly higher Tb.N in all regions.

Gorilla was not consistently significantly distinguished from other taxa in any trabecular variable. *Pan* and *Gorilla* were not different in most factors, except that *Pan* was distinguished from *Gorilla* in having significantly greater Tb.N in the distal tibia and greater Tb.BV/TV in the posterior (C1, C2, C3) regions of the talus.

2.3.4 Comparisons among regions within each species

The prediction that the distribution of bone properties across the distal tibia and talus would differ among species was met. Separate analyses of variance in each species showed that the regional patterns of some subchondral bone and trabecular bone properties across the distal tibia and

talar joint surfaces varied among species. Tables 2.13 to 2.26 list the polarity of pairwise comparisons, first among divisions into thirds along the anteroposterior axis and the mediolateral axis, and then among divisions into 9 regions to more accurately assess regional differences. Figures 2.4 and 2.5 illustrate the pattern of distribution of each variable in each species.

2.3.4.1 Tb.BV/TV

The prediction that the more arboreal great apes would have greater Tb.BV/TV in the lateral vs. medial regions was met in both the distal tibia and talus, driven primarily by the anterolateral (A1) and centrolateral (B1) regions (Table 2.13 and 2.14). In *Homo* however, predictions that Tb.BV/TV would be greater in the medial regions were not met. In the *Homo* distal tibia, the mid-sagittal region (MLCentral) displayed the greatest Tb.BV/TV, and in the *Homo* talus, no difference was found between the medial and lateral talar rims. In all species, the medial regions of the tibia and the mid-sagittal regions of the talus had significantly the least Tb.BV/TV, suggesting these are features characteristic of all hominoid tibiae.

The prediction that the more arboreal great apes would have greater Tb.BV/TV in the anterior vs. posterior regions was not statistically met in either the distal tibia or talus, although came close in the talus (Table 2.13 and 2.14). The prediction that *Homo* would have greater Tb.BV/TV in the posterior regions was met in the tibia but not the talus. In the talus, the greatest Tb.BV/TV was instead found in the mid-coronal and anterior regions, along the lateral and medial talar rims.

2.3.4.2 Tb. I

Because trabecular bone that is more isotropic in shape is thought to be mechanically stronger, it was hypothesized that greater Tb.I would be found in the lateral and anterior regions of the great ape bones, the medial and posterior regions of the human, and the central regions in baboons. Only the talus of humans and both the distal tibia and talus of baboons met these predictions (Tables 2.15 and 2.16). In general, in the more arboreal great apes there was little difference in Tb.I among regions, while in the two highly terrestrial species there were distinct zones of increased isotropy.

2.3.4.3 Tb.E

Conversely, trabecular bone that is more elongated in shape is thought to be mechanically weaker in compression. The predicted distribution along a mediolateral axis was met only in the human talus, where greater elongation was found in the lateral regions (Tables 2.17 and 2.18). Greatest elongation was found in the mid-coronal regions of the *Homo*, *Pan* and *Gorilla* tibia, driven primarily by the centrolateral (B1) and centromedial (B3) regions. Increased elongation was evenly distributed along both lateral and medial aspects of the *Papio* tibia and just in the central region of the *Papio* talus.

2.3.4.4 Tb.Th

Along a mediolateral axis, the thickest trabeculae in the distal tibia were found in the mid-sagittal regions in almost all species, except for *Gorilla* (Tables 2.19 and 2.20). This met only the prediction set for *Papio*. Along an anteroposterior axis, the thickest trabeculae were in the anterior regions of all species, meeting the predictions for the great apes but not for *Homo* and *Papio*.

2.3.4.5 Tb.N

The number of trabeculae was greatest along the lateral aspect of the talus in the great apes, and central/lateral regions in both tibia and talus in *Papio* as predicted (Tables 2.21 and 2.22). Also as predicted, the posterior regions in the *Homo* distal tibia had the greatest Tb.N, although all other species also tended to have greater Tb.N posteriorly as well.

2.3.4.6 Sc.MeanHouns

In general in the distal tibia, the greatest subchondral bone radiodensity was found medially in great apes contra predictions (Tables 2.23 and 2.24). In *Papio,* greater Sc.MeanHouns was found centrally in the tibia and laterally in the talus as predicted. *Homo* had greatest Sc.MeanHouns in the medial regions of the distal tibia and talus as predicted, although not significantly in the tibia. Only *Pongo* met predictions in having high Sc.MeanHouns in the anterior regions of the tibia.

2.3.4.7 Sc.Th

As predicted, the greatest subchondral bone thickness was found in the medial regions of both bones in *Homo* (Tables 2.25 and 2.26). However, the *Pan* tibia and *Gorilla* talus also showed greater Sc.Th medially, against predictions. *Pongo* met predictions with greatest Sc.Th anteriorly in both distal tibia and talus, but the other great apes did not. *Papio* also met predictions with increased Sc.Th posteriorly in the distal tibia and centrally in the talus.

In summary, the patterns of distribution of bone properties across the talocrural joint are largely similar among species despite different locomotor behaviors and assumed differences in joint habitual load. However, the small differences that were found make sense in light of observed behavior.

2.3.5 Intraspecific consistency of regional patterns of distribution

The prediction that the distribution of bone properties across the distal tibia and talus would be consistent within each species was tested by ranking the values of each region. Tables 2.27 and 2.28 show the mean ranks for each variable within each region of the distal tibia and talus, respectively, and the value of Kendall's coefficient of concordance (W). Kendall's W expresses the level of consistency in the pattern of ranks among specimens. W=0 denotes no consistency (random), W=1 denotes that all specimens had identical patterns of ranked data. Each species

displayed moderately consistent patterns of distribution of bone variables, but these patterns were different among species.

In the distal tibia, the prediction that *Homo* would be more consistent and *Pongo* would be less consistent in bone distribution than all other groups was not met. In fact, the opposite pattern was found. The distribution of bone properties was in general the least consistent within *Homo* compared to the other species. In *Homo*, the most consistent variable was Tb.N (W=0.508), driven by the consistently greater Tb.N in the posteromedial (C3) region. Conversely, *Pongo* had in general the most consistent distribution of bone properties in the distal tibia. In particular, the pattern of Tb.BV/TV was highly consistent (W=0.803) in showing the greatest value in the anterolateral (A1) region and the least value invariably in the centromedial (B3) region. The pattern of Sc.%HighDensity was also consistent (W=0.679), with the greatest values usually in the anterolateral (A1) and anteromedial (A3) regions. In *Pan* and *Gorilla*, Tb.BV/TV was also the most consistent variable (W=0.720 and 0.693, respectively), with the greatest value in the posterocentral (C2) region and the least in the centromedial (B3) region. In *Papio*, the most consistent variable was Sc.MeanHouns (W=0.756), with the greatest value in the posterocentral (C2) region and the least in the centrolateral (B1) region. In general, the patterns of trabecular shape variables (Tb.DA, Tb.I, and Tb.E) in the distal tibia were inconsistent in all species.

In the talus, *Homo* and *Papio* in general showed greater consistency in subchondral bone properties, while the great apes were in general more consistent in trabecular bone properties. In *Homo*, Sc.%HighDensity showed the most consistent pattern (W=0.828), with the greatest value in the centromedial (B3) region and the lowest value in the central (B2) region. In *Papio*, Sc. MeanHouns was the most consistent (W=0.820), with the greatest value in the posterolateral (C1) region and the lowest value in the anterocentral (A2) region. In *Pan* and *Gorilla*, Tb.BV/TV and Tb.Th were most consistent, with the greatest Tb.BV/TV distributed between the anterolateral (A1) and centrolateral (B1) regions, and the greatest Tb.Th in the anterolateral (A1) and anteromedial (A3) regions. In *Pongo*, Tb.BV/TV was most consistent (W=0.746), with the greatest value invariably in the anterolateral (A1) region. In general, the patterns of trabecular shape variables (Tb.DA, Tb.I, and Tb.E) were very inconsistent in the non-human species, although moderately consistent in *Homo*.

2.3.6 Regional distribution of trabecular shape

Figures 2.6 and 2.7 depict the variation in mean shape of the trabecular struts in each region of the distal tibia and talus, respectively. Within each region, Tb.I and Tb.E are plotted in a ternary diagram, where data points towards the top apex indicate more isotropic trabeculae and data points towards the bottom indicate more anisotropic trabeculae. Data points towards the bottom left apex indicate more plate-shaped trabeculae and data points towards the bottom right apex indicate more rod-shaped trabeculae. Although the trabeculae in the distal tibia of all species groups was generally elongated and rod-like in shape, each species showed relative regional differences in trabecular anisotropy and shape.

In the *Homo* distal tibia the most elongated rod-shaped trabeculae was found along a mid-coronal plane in the centrolateral (B1), central (B2), and centromedial (B3) regions, while relatively more isotropic trabeculae was found in the anterocentral (A2) and posterocentral (C2) regions. However, in the *Homo* talus, the lateral regions (A1, B1, C1) showed the most elongated, rod-shaped trabeculae compared to the other regions ($p<0.001$). The trabeculae then shift towards being more plate-shaped in the central and medial thirds of the talus.

In *Pan* and *Gorilla,* in the distal tibia the most elongated trabeculae were found in the centrolateral (B1) and centromedial (B3) regions, but in the talus were found in the central (B2) and posterocentral (C2) regions. More isotropic trabeculae were found in the anterocentral (A2) and posterocentral (C2) regions of the distal tibia but in the anterolateral (A1) and anterocentral (A2) regions of the talus.

In *Pongo,* in the distal tibia the most isotropic trabeculae were found in the central regions. The *Pongo* talus overall tended to have the most isotropic and least elongated trabeculae among species, but no significant differences were found in trabecular shape intraspecifically among regions of the *Pongo* talus.

In *Papio*, the trabeculae along both the lateral and medial aspects of the distal tibia were significantly more elongated than those in the center region of the bone. Within the *Papio* talus, the central (B2) and centrolateral (B1) regions were characterized by more elongated rod-shaped trabeculae while the centromedial (B3) region had more plate-shaped trabeculae.

2.3.7 Intraspecific consistency of trabecular primary orientation

Tables 2.29 and 2.30 list the mean primary, secondary and tertiary eigenvalues and the direction (trend and incline) and variance of the primary eigenvector for each species by ROI. Figures 2.8 and 2.10 compare the degree of spherical variance in the direction of the primary eigenvector among species and among regions of the distal tibia and talus, respectively.

2.3.7.1 Distal tibia

In the distal tibia, the spherical variance in primary eigenvector direction within the centrolateral, centromedial, and posterolateral regions of all species was generally very low (0.01-0.04), indicating very consistently-oriented trabeculae among individuals (Figure 2.8). In *Homo*, *Pan*, and *Gorilla*, the anterocentral and posterocentral regions of the tibia, which had the greatest trabecular bone volume, displayed the greatest variation in primary eigenvector direction. This result is due to the trabeculae in this region being more plate-like in shape. The regions with the least variation in trabecular direction had the highest elongation (centrolateral, centromedial, posterolateral) but lower bone volume. *Papio* as well had both the greatest bone volume and the greatest variance in eigenvector direction located in the mid-sagittal regions (anterocentral, central, and posterocentral), while the least variance in direction (centrolateral, centromedial, posterolateral) corresponded to the highest elongation and lower bone volume.

The prediction that *Pongo* would have more variation in the orientation of trabeculae than all other groups was not met. The least variance in direction was in the posterolateral and posterocentral regions but orangutans were no more variable than the other groups. The greatest variance in direction was in the anterolateral (also greatest bone volume) and central (also lowest bone volume) regions, but again this magnitude of variation was not more than the level of variation found in other groups.

2.3.7.2 Talus

In the talus, spherical variances in primary eigenvector direction within each region ranged from 0.01 in the lateral regions of *Homo* indicating strong directional consistency, to 0.42 in the anterolateral region of *Pongo* indicating greater variation in primary trabecular orientation. Indeed as predicted, the overall direction of trabecular orientation was less variable in *Homo* (median s = 0.04) than in all other groups. Also as predicted, the overall trabecular orientation was more variable in *Pongo* (median s = 0.19) than in all other groups.

However, the variance in primary eigenvector direction was not homogenous across the regions of the talus (Figure 2.10). In each species group, some regions displayed more variance than other regions. Furthermore, the regions that displayed the greatest variance, and conversely the greatest consistency, in primary eigenvector direction differed across species groups. In *Homo*, the most variance in orientation was in the posteromedial region (s = 0.30), in *Pan* was in the posterolateral region (s = 0.40), *Gorilla* in the anterocentral region (s = 0.26), in *Pongo* in the anterolateral region (s = 0.42), and in *Papio* was in the anteromedial region (s = 0.28). It must be noted however that in the non-human groups the three eigenvalues were relatively similar in magnitude, indicating a more isotropic trabecular structure. Thus the interpretation of the variation in direction of the "primary" eigenvector is difficult in the non-human groups since there is less differentiation between the primary and the secondary eigenvector.

The regions with the most consistent trabecular orientation were the centrolateral and posterolateral regions in *Homo* (s = 0.01), the central and posterocentral regions in *Pan* and *Gorilla* (s = 0.02-0.04), and the centrolateral region in *Pongo* (s = 0.05) and *Papio* (s = 0.02). With the exception of the centrolateral region in *Homo* and *Pongo*, the prediction that trabecular orientation would be more consistent in regions with greater bone volume was not met. Indeed, the opposite was found – the regions with more consistent trabecular orientation were often the regions with decreased bone volume.

2.3.8 Primary orientation of trabeculae

Figures 2.9 and 2.11 depict stereoplots of the principal eigenvector for each specimen by region, including the mean eigenvector direction for each species. Note that for species groups with low variation in trabecular primary orientation, the mean vector is a useful summary; however, for groups with relatively high variation in orientation, the mean vector is less meaningful.

2.3.8.1 Distal tibia

In the central regions along the lateral-medial axis, the primary trabecular orientation in all species was essentially vertically-directed, normal to the articular surface. However, in the non-human species, the primary orientation diverged slightly posterolaterally particularly in the centrolateral and centromedial regions.

In the posterior regions, there was more variation in the direction of trabecular orientation among species. The trabeculae in most non-human species groups were oriented consistently in the posterolateral direction in all non-human groups, due to the oblique orientation of the tibia. The trabeculae in the posterior regions of the *Homo* tibiae by contrast were oriented more directly posteriorly, if not slightly posteromedially. In the *Pan* and *Papio* tibia, the trabeculae in the posterocentral and posteromedial regions displayed more scattered, horizontally-oriented principal directions, indicative of plate-shaped trabeculae. The scatter of the principal eigenvectors however continue to indicate planes that are oriented posterolaterally.

In the anterolateral and anteromedial regions, *Pongo* was distinguished from the other groups in having clearly more posteriorly-oriented trabeculae. This is a result of the more convexly rounded anterior aspect of the tibial plafond and thus reflects the greater degree of dorsiflexion that is allowed in this joint.

In the anterior regions in all species, the trabeculae were generally more horizontally oriented. In the anteromedial region, all species had elongated trabeculae oriented somewhat laterally. But *Homo* and *Papio* displayed trabeculae that were much more strongly laterally directed while the orientation in *Pongo* was more vertical with only a slight lateral component. In the anterolateral and anterocentral regions the primary orientations become more scattered, indicating more isotropic trabeculae. The *Pan* sample in particular had strongly horizontally-oriented trabeculae in the anterocentral region.

2.3.8.2 Talus

The results show differences in trabecular primary orientation among species groups, with some regions displaying more distinctive differences than others. In the regions displaying the greatest degree of anisotropy, the lateral regions, all groups seem to have similarly oriented primary directions in the anterolateral and centrolateral regions, roughly corresponding to a radial pattern that approximates a direction normal to the articular surface. That is, in the anterolateral region, most vectors are directed superoanteriorly and in the central region, most vectors are directed more superomedially. But in the posterolateral region, while most non-human specimens have the trabeculae directed superoposteriorly somewhat normal to the articular surface, the primary direction in *Homo* differs in being directed superoanteriorly. On inspection, these trabeculae are directed from superoanteriorly on the talar trochlea to inferoposteriorly towards the posterior calcaneal facet.

Homo also differed from the other groups in the anteromedial region. The relatively more anisotropic *Homo* trabeculae are directed from posterosuperiorly to anteroinferiorly towards the talar neck and head, while those of the great apes and *Papio* (though more scattered) are mostly oriented

from anterosuperiorly to posteroinferiorly. Thus the trabecular orientation in the non-human groups is consistent with a surface normal alignment while that of *Homo* is not.

The trabeculae in the anterocentral region of the African apes however was not oriented normal to the articular surface but rather was more transversely oriented from superolaterally to inferomedially. This trajectory appears to direct stress from the talar dome to the talar neck and anterior calcaneal facet.

2.4 Discussion

This study tested the hypothesis that subchondral bone and trabecular bone properties reflect habitual compressive load by assessing predicted differences in the distal tibia and talus among species with presumably different joint loads. The results showed some differences in internal bone morphology among species in support of the hypothesis, but often not in the direction predicted by behavioral and postural observations.

2.4.1 Relationships among subchondral and trabecular bone variables

Bivariate correlation analysis revealed that there were significant relationships among trabecular bone properties on the one hand, and between subchondral bone radiodensity and subchondral bone thickness on the other hand in both the tibia and talus. Intuitively and mathematically, this was expected of the trabecular bone properties because they are computed by *Quant3D* software from algorithms that rely on the same linear and volumetric geometric measurements. This result is consistent with studies in bone biomechanics that emphasize Tb.BV/TV as a property that encompasses all other morphological variables and has been shown to have the strongest correlation to bone mechanical strength (Thomsen et al. 2002; Vesterby et al. 1991). The relationship between subchondral bone thickness and subchondral bone radiodensity as quantified from micro-CT Hounsfield values has not been demonstrated before. In separate studies of the proximal tibial plateau, Milz and Putz (1994) quantified the distribution of subchondral bone thickness and Johnston et al. (Johnston et al. 2010; 2009) examined the distribution of subchondral radiodensity taken from 0.5 mm voxel resolution quantitative CT system. Both studies found thicker/more radiodense bone in the central regions and thinner bone around the periphery of the joint surface. Thus, these results imply that future comparative studies may be simplified to focus on Tb.BV/TV and Sc.Th as basic morphological correlates of bone strength.

However, the morphology of the two bone tissue types was not found to be tightly coupled as hypothesized. Regions exhibiting greater subchondral bone radiodensity and/or thickness were not always coincident with those exhibiting greater trabecular bone volume. For example, in the *Pan* and *Gorilla* distal tibia the greatest subchondral bone strength was focused on the medial region while the greatest bone volume was found across the anterior and posterior margins. Thus, if the two bone types are responding to the same stimulus, they are doing so in different ways. Alternatively, each tissue may be responding to different aspects of habitual joint load. In the

analysis of the distribution of properties in the human ankle joint (Chapter 1), the subchondral bone properties were found to be more consistent with shared joint loads presumed during walking, while it was suggested that the trabecular bone morphology may reflects other internal strains that are dependent on bone shape and the transfer of load through the bone. This could be true of non-human primates as well.

Subchondral bone radiodensity (determined by mineralization and the settings of the x-ray beam) was found to correlate well with subchondral bone thickness (physically measured from the image), in agreement with previous research (Madry et al. 2010; Milz et al. 1997). Whether these two measured properties are inherently dependent upon each other as a function of the micro-CT imaging process, or whether they are independent and correlated due to common adaptation to load, is unknown. Nevertheless, the relationship shown will support the use of subchondral thickness as a character to help infer habitual stress differentials across a joint surface, such as in a fossilized bone.

2.4.2 Overall Species means

A few species-level differences were found in internal bone morphology of both the distal tibia and the talus that may be used to distinguish among species. In general, these results separated the more terrestrial humans and baboons from the more arboreal great apes.

Humans were distinguished from the other groups in having overall absolutely thinner subchondral bone in both the distal tibia and the talus. Overall thinner subchondral bone may be an epigenetic response to humans loading their joints with low magnitude habitual loads relative to the apes and baboons, or it could be a genetic difference. One way to investigate this question would be to examine an ontogenetic series to see when during locomotor development humans and apes show these subchondral bone differences (Adam et al. 1998; Ryan and Krovitz 2006). In this study, females of each species were chosen expressly to limit the effects of body size differences, but it is unknown if subchondral bone thickness scales with body size. It is also unclear how trabecular thickness varies with body size. In two broad comparative studies of trabecular bone in the femoral head, one study found that trabecular thickness scaled with negative allometry (Swartz et al. 1998), while another found that thickness scaled with positive allometry (Doube et al. 2011).

Humans were also distinguished from other groups in having lower trabecular bone volume and more anisotropic, elongated trabeculae in both the distal tibia and the talus. This interspecific result has also been shown for the trabeculae in the hominoid proximal calcaneus (Maga et al. 2006) and the T8 thoracic vertebral body (Cotter et al. 2009). Thus it seems that humans systemically have less bone volume than other hominoids, even in regions where mechanical stress would be expected to be relatively greater in humans (i.e., proximal calcaneus). This result is consistent with the general gracile body form of modern humans (Pearson 2000; Ruff 2006; Ruff et al. 1993; Trinkaus 1997), and in particular having less bone mass in the distal most region of the hindlimb reduces the energy necessary during walking for accelerating and decelerating the limb (Witte et al. 1991). However, it cannot be ruled out that the lower overall bone volume seen here may be a specific characteristic of the urban-dwelling female humans in this sample. An analysis of males, and of individuals from an archeological population, would further inform if this lower bone volume might

be sex-related, related to daily activity levels, or even related to the use of modern footwear (Trinkaus 2005).

Additionally, as predicted, the degree of anisotropy was found to be greater in humans than the other groups suggesting that despite decreased bone volume, bone strength may derive from the alignment of trabeculae with habitual, predictable stresses. Results from the hominoid proximal calcaneus (Maga et al. 2006) concur with this finding, although no interspecific differences were found in degree of anisotropy in the hominoid T8 thoracic vertebra (Cotter et al. 2009). As a corollary, this suggests that the greater-volume, less-anisotropic arrangement of trabeculae in non-human hominoids may be better suited to withstand more habitually variable joint loads as would be encountered in daily activity.

Baboons overall displayed the greatest trabecular bone volume, and greatest trabecular thickness than the other species in both the distal tibia and talus. This suggests that perhaps the talocrural joint in baboons is habitually subjected to relatively greater duration, greater magnitude, or more variable stresses than the great apes. This is plausible because the baboons are documented to spend more time in active standing activities, thus loading their tibia more often, than apes (Hunt 1991; Hunt 2004). Furthermore, the joint loads that result from the relatively high-speed, longer sustained, terrestrial locomotion of baboons may involve greater strain rates than those generated from arboreal locomotion and thus may be relatively more osteogenic (Turner 1998).

2.4.3 Comparison of trabecular and subchondral bone morphology among species

Significant differences in subchondral and trabecular bone properties were found among regions of the distal tibia and talus in all groups.

2.4.3.1 Subchondral bone

The human distal tibia and talus did not show significant differences in subchondral radiodensity across the joint as predicted. Two interpretations of this result are: (1) that habitual stresses in the human ankle were consistent among individuals and were relatively homogenous across the distal tibia, or that (2) the subchondral bone radiodensity reflects habitual stresses that were variable among the sample individuals. The results of the analysis of rank consistency support the latter interpretation. Humans were found to have relatively low interindividual consistency in subchondral bone properties compared with the other species. The anteromedial region was the region with consistently greater radiodensity and the centrocentral region was the region with least radiodensity, but otherwise the other regions did not show consistent rankings among individuals. Previous studies of subchondral bone radiodensity have also found inconsistent patterns among individuals, although those differences were attributed to age (Müller-Gerbl et al. 1993; von Eisenhart et al. 1999). These studies found that younger individuals tended to display maximum radiodensity along the margins of a concave joint surface while older individuals displayed peak radiodensity towards the center of the joint surface. Joint contact area during static loading of

cadaver ankles is also reported to have high interindividual variability, attributed to incongruities in the human ankle joint (Matricali et al. 2009).

In the non-human groups, significant differences were found in subchondral bone radiodensity across the distal tibia and talus. Moreover they were much more consistent in pattern, supporting the hypothesis that subchondral bone radiodensity may be reflecting intraspecific similarities in joint stresses. Among the non-human groups, baboons displayed the greatest consistency in subchondral bone pattern, perhaps supporting the stereotype that the locomotion of more terrestrial primates is less variable than that of more arboreal primates. However, the consistency of subchondral bone properties among the apes was not as predicted; highly-arboreal orangutans were not more variable than the relatively more terrestrial African apes.

For humans and baboons, the patterns of subchondral bone radiodensity distribution in the talus was relatively more consistent than in the tibia. Furthermore, the patterns in the talus in these more terrestrial species were relatively more consistent than those in the more arboreal great apes. This is in line with the hypothesis that the great apes are more variable, or unpredictable, in their movement behavior and thus joint load, in the three-dimensional arboreal environment than more terrestrial animals whose joint movements are stereotypical and more predictable across the ground. The interpretation of the corollary result that the patterns in the tibia of more terrestrial species are less consistent than those in more arboreal species is less clear.

The regions that were significantly more radiodense in the African apes were found mostly medially in both the tibia and talus. This result however does not agree with predictions that greater bone strength would be found laterally based on the oblique posture of the ankle joint (DeSilva 2009; Kanamoto et al. 2011; Latimer et al. 1987) and more load-bearing laterally by the fibula (Marchi 2007). Rather, the results agree with these studies in interpreting the oblique posture of the ankle joint as facilitating an inverted foot for vertical climbing. During vertical climbing, it is intuitive that the greatest load would be borne on the medial aspect of the ankle joint. Thus, these results suggest that the subchondral bone radiodensity pattern in African apes may reflect bone strength related to the loads during habitual climbing activities. Alternatively, the finding that all hominoid species displayed greater subchondral bone radiodensity in the medial regions points to the possibility that this property is a consequence simply of the angle that the medial malleolus makes with the tibia plafond.

In the talus, the African apes also displayed high radiodensity in the centrolateral region of the talus. This lateral region of the talus is likely not related to the articulation with the distal tibia but rather to the fibula which has an important load-bearing function in these animals (Stern and Susman 1983). The morphology of the distal fibula was not investigated here, but it is likely that the thicker, denser subchondral bone on the centrolateral region of the talus corresponds to the loading region with the fibula.

Orangutans also showed regional differences, but unlike the African apes showed high radiodensity in the anterolateral regions of both the tibia and talus as well as the medial regions, suggesting that these differences may be related to the differences in habitual joint load between the semi-arboreal chimpanzee and gorilla and the fully-arboreal orangutan. The presence of an area of

high subchondral radiodensity to the anterolateral as well as the anteromedial region of the joint agrees with that predicted from highly dorsiflexed postures. The orangutan is stereotyped to assume highly variable quadrumanus hanging postures, and these results suggest that either a dorsiflexed posture may be dominant or perhaps that the fibularis muscles that cross the joint laterally are habitually imposing a joint load, for instance in lateral grasping or bridging postures.

Baboons had the greatest subchondral bone radiodensity and thickness in the posterocentral region in the tibia and the posterolateral region in the talus. Baboons also had less radiodense subchondral bone in the anteromedial region of the talus. In all other groups, the anteromedial region showed (often significantly) greater subchondral bone density and thickness, so the relatively decreased subchondral bone radiodensity there in baboons is distinctive. Baboons are distinguished from the apes by spending more time in a quadrupedal standing posture, moreover in a semi-digitigrade posture (Hunt 1991; Meldrum 1991; Schmitt and Larson 1995), which was predicted to place greater load on the posterior aspect of the joint. These results thus further support the hypothesis that subchondral bone morphology may be an indicator of habitual postural joint load. Medially to laterally, the subchondral bone properties were more evenly distributed in the baboon tibia, in agreement with the stereotype that the terrestrial baboon posture is largely held within the sagittal plane, with less abduction/adduction bias at the ankle than is found in the more arboreal great apes.

In summary, these results confirm those of previous researchers in showing variation in subchondral radiodensity and thickness across a joint surface (e.g., Carlson and Patel 2006; Eckstein et al. 2009; Eckstein et al. 1995; Noble and Alexander 1985; Nowak et al. 2010; Patel and Carlson 2006, 2007; Simkin et al. 1991). Additionally, these results support the hypothesis that subchondral bone properties are distinctive at the species level and are in part consistent with differences in observed habitual postures. Whether the radiodensity patterns are genetically-determined or an epigenetic result of habitual locomotor behavior cannot be addressed here. However, experimental studies have shown that subchondral bone radiodensity patterns differ among individuals of the same species exposed to different locomotor environments (Polk et al. 2008; Polk et al. 2010).

2.4.3.2 Trabecular bone

2.4.3.2.1 Trabecular bone quantity

The distribution of bone tissue quantity (BV/TV, Tb.Th and Tb.N) within the tibia and talus was much more consistent in the non-human species than in the humans. This result echoes that of the subchondral bone radiodensity variability in the tibia, and supports the conclusion that humans are relatively inconsistent in the regional distribution of bone tissue in the distal tibia. This result is opposite to the prediction that humans would be relatively more consistent than wild primates. However, the variation of values within each region was not unusually high, implying that the joint load may have been more evenly distributed across the human tibiotalar joint.

In the great ape distal tibia, greater trabecular bone volume was located generally along the anterior and posterior regions and lesser volume was found in the mid-coronal regions. This

somewhat agreed with predictions of increased bone strength anteriorly as an adaptation to a highly dorsiflexed posture during habitual locomotion. Peak magnitude loads occur in the joint while it is in a highly dorsiflexed posture during the propulsive phase of both terrestrial quadrupedalism and vertical climbing. But increased bone volume was also found posteriorly, which may also be related to posteriorly placed peak magnitude loads perhaps during terrestrial locomotion, or may be simply related to the shape of the bone. As discussed in Chapter 1, the saddle-like shape of the distal tibia may subject the projecting anterior and posterior rims to tensile "wishboning" forces as the slightly-incongruent joint is compressed under body weight.

By contrast, in baboons the trabecular bone volume resembled that of humans in that it was more evenly distributed into the mid-coronal regions of the tibia. If greater volume of trabecular bone serves to attenuate peak stresses, then this pattern implies that the center of the baboon distal tibia may experience the greatest impact loads during habitual locomotion. Baboons are one of the more terrestrially-adapted primates, with relatively extended limb morphology (Hunt 1991; Meldrum 1991; Polk 2002, 2004). A study of the subchondral bone distribution in other terrestrial quadrupeds like dogs would reveal if this is a functional trait related to terrestrial locomotion.

2.4.3.2.2 Trabecular shape

The degree of anisotropy and shape of trabeculae within regions of the hominoid distal tibia and talus were overall less consistent than measures of trabecular bone volume, thickness and number and subchondral bone radiodensity and thickness in all species.

Humans, with a stereotypically predictable, sagittal-plane locomotion, showed relatively greater trabecular anisotropy and displayed more elongated trabeculae overall than the non-human hominoids, particularly in the centrolateral and centromedial regions. Regions of greater trabecular anisotropy have been hypothesized to indicate regions that were subjected to relatively low-magnitude but more predictable stresses (Fajardo and Muller 2001; MacLatchy and Muller 2002; Maga et al. 2006; Ryan and Ketcham 2002, 2005; Ryan and van Rietbergen 2005). This is understandable in terms of the stereotype of human locomotion being primarily in the sagittal plane, without much abduction/adduction of the ankle. However baboons, which are also stereotyped as having relatively predictable, sagittal-plane locomotion, were found to have somewhat less trabecular anisotropy in the distal tibia than the other species although it was predicted that they would display more anisotropy. Thus, although there were species-level differences in overall mean trabecular shape in the distal tibia, it does not seem that they provide much resolution in inferring behavioral differences. The overall greater anisotropy and decreased bone volume of trabeculae in the human ankle may be attributed to a systemic gracilization of bone morphology in the species rather than a function solely of mechanical loads.

More anisotropic rod-shaped trabeculae were found in the lateral regions of the human talus, a pattern that was different from that of the other species. This pattern implies that the trabecular bone in the lateral region of the talus may be structurally weaker than the other regions. The lateral region of the human ankle joint bears relatively less load during human walking than the medial region, consistent with the process that bone remodels to remove volume where it is not needed. To

pursue this hypothesis, it would be interesting to compare an ontogenetic series of human tali to assess the development of trabecular architecture at successive stages of locomotor development.

The central region of the talus displayed the most elongated trabeculae in the African apes and baboons, implying that the trabecular bone in this region is structurally weaker than other regions. The most isotropic plate-like trabeculae was found in the anteromedial region of the African apes and in the centromedial region of baboons, implying that the trabecular bone in these regions was structurally stronger than that in other regions. By analogy to humans, this implies that the peak load borne by the talus in chimpanzees and gorillas may be in the anteromedial region, while that in the baboons is slightly more posterior in the centromedial region. An emphasis on the anteromedial region in the African apes is consistent with the highly dorsiflexed and inverted posture of the ankle joint observed at the time of peak load bearing during vertical climbing (DeSilva 2009).

Consistent with predictions, orangutans had overall more isotropic, less elongated trabeculae in the talus than the other groups, and there were no significant differences found in trabecular shape among regions, both results suggesting that habitual loads are more evenly distributed throughout the bone.

Overall, the results of this study demonstrate regional differences in trabecular shape within the talus, and these differences are consistent with those predicted based on observed locomotor behavior.

2.4.3.2.3 Trabecular orientation

The orientation of trabeculae in the distal tibia was relatively similar among species, all strongly directed from the articular surface superiorly to the diaphyseal cortex. This similarity in morphology implies similarity in function of the distal tibia, to attenuate and transfer largely vertically-directed loads. The slight differences that were found between humans and the other species mostly reflected the geometric differences of the angle of the tibial shaft to the plafond that has been noted from external measurements (Latimer et al. 1987; Marchi 2007; Stern and Susman 1983).

The more horizontally-oriented trabeculae in the anteromedial region of the distal tibiae, particularly in humans and baboons was unexpected. In humans, it has been noted that during maximum dorsiflexion, in the close-packed position of the ankle, the relatively greater width of the anterior talus is tightly wedged between the medial and lateral malleoli, creating a “wishbone” effect on the ankle mortise. This increased pressure from the talus may explain the presence of these plate-like trabeculae.

In the talus, the trabeculae just deep to the subchondral plate in the non-human species tended to be arranged in a radial pattern across the talar trochlea, with the orientation of the primary eigenvectors directed approximately normal to the articular surface. Other studies of trabeculae in convex joint surfaces find similar orientations (Polk et al. 2008; Pontzer et al. 2006). This pattern suggests habitual loads that vary throughout the range of motion of the joint and that are primarily

directed normal to the joint surface, in agreement with the observation that non-human hominoids load their joint more variably than do humans.

However, the orientation of trabeculae in the human talus differed significantly from that of the other species in the posterolateral and anteromedial regions. In these two regions, the orientation of the primary eigenvector was directed from the talar dome towards the inferior and anterior articular surfaces, consistent with the trajectory of load from the tibia to the calcaneus and navicular of the forefoot. The presence of this morphology implies the direction of habitual loads in humans may have been very narrowly confined compared to that in non-human hominoids.

Another hypothesis that has been proposed to explain the orientation of bony trabeculae is that these trabecular trajectories are genetically determined, formed during development prior to active locomotor weightbearing (Abel and Macho 2011; Cunningham and Black 2009a, 2009b; Lovejoy et al. 2003; Lovejoy et al. 2002; Ryan and Krovitz 2006). However, the orientation of trabeculae found here in the talus was not entirely consistent with this hypothesis. In 3 month old human infants, the talus is approximately 55% ossified, with the ossification center located in the talar neck and lateral aspect of the cartilaginous anlage (Howard and Benson 1992; Hubbard et al. 1993). Ossification then proceeds distally, proximally, and medially, with the proximal part of the talus ossifying last at approximately age 8 years. It would thus be expected that the trabeculae in the talus radiate from the neck. The orientation of trabeculae in the anteromedial region was indeed consistent with this trajectory, but that in the posterolateral region was not. These results echo the view that there is a basic structural model formed by the developing bone tissue that can be then modified by external mechanical stimuli later in life. (Abel and Macho 2011; Turner 1998). A study of the location and progression of ossification centers in the other hominoid species would further inform the degree to which the trabecular orientation in the ape talus is reflective of developmental processes or remodeling processes.

2.5 Conclusion

2.5.1 Bivariate correlations

Overall, the hypothesis that there is a relationship between subchondral bone and trabecular bone strength is supported, although the properties are not as strongly coupled as predicted. Moderate to weak positive relationships were found between subchondral bone radiodensity and thickness and trabecular bone volume and thickness in all groups in both the distal tibia and talus. A weak negative relationship was also found between subchondral thickness and underlying trabecular number in some groups in the talus. However, the distribution of trabecular bone anisotropy in the distal tibia did not display a strong relationship with overlying subchondral bone properties. Subchondral bone radiodensity as quantified by Hounsfield units is correlated to subchondral thickness, thus maybe used as a proxy when radiodensity cannot be accurately measured, for instance in fossilized bone.

2.5.2 Subchondral bone

In both the distal tibia and talus, species could be distinguished from each other in overall differences in subchondral bone properties that may reflect habitual differences in postural or locomotor loads in the ankle joint. Humans had overall thinner subchondral bone, and baboons had overall more radiodense subchondral bone, than the great apes.

Regional differences were found in the distribution of subchondral thickness and radiodensity in each species that may be related to the regional distribution of habitual stress in the joint. The distribution of subchondral radiodensity was found to differ among species, in ways consistent with differences in observed postural behavior.

The hypothesis that the regional differences in subchondral bone properties are coincident within opposing surfaces of an articulation is supported. In all species, the regions found to be significantly different in the distal tibia largely matched the regions that were significantly different in the talus.

2.5.3 Trabecular bone

Overall trabecular bone architecture in both the distal tibia and talus differs among species – humans have lower bone volume and greater anisotropy and baboons have greater bone volume and trabecular thickness, but fewer trabecular number and lower anisotropy than the other groups. Chimpanzees had greater trabecular number and lower trabecular thickness than all other groups.

Within the distal tibia, the hypothesis that there are regional differences in trabecular architecture was somewhat supported. In all species groups, significant differences were found in some measures of trabecular structure, particularly bone volume and thickness, but differences were less often found in degree of anisotropy and trabecular number. Overall, humans were distinguished from other species in having much lower bone volume fraction and thinner trabeculae, while baboons were distinguished in having much higher bone volume fraction and thicker trabeculae. Chimpanzees were distinguished from other species in having more trabeculae per millimeter, and orangutans were distinguished in having greater bone volume fraction and subchondral radiodensity in the anterolateral region. The regional pattern of distribution of trabecular architecture was generally similar among the hominoids, displaying increased bone properties in the anterior and posterior margins. Baboons had a different pattern of distribution that emphasized the center of the distal tibia. The results imply that the distal tibia is subjected to similar habitual loads in all hominoids, but the loads differ in the baboon.

All species had moderately to strongly consistent patterns of trabecular bone volume and thickness in the distal tibia; humans were the least consistent. All species except chimpanzees also had moderately consistent patterns of trabecular number, with humans and baboons showing the greatest consistency. All species also showed moderately consistent patterns of trabecular anisotropy and elongation except for gorillas.

Within the talus, the hypothesis that there are regional differences in trabecular architecture was supported. In all species groups, significant differences were found in some measures of trabecular structure, particularly bone volume, thickness, and number but differences were less often found in degree of anisotropy.

The hypothesis that the regional differences in trabecular bone properties are coincident within two articulating bones is not supported. While some trabecular variables were found to be significantly different in the corresponding anterior regions of both articular surfaces, most often the regions that were significantly different within the tibia did not match the regions that were significantly different in the talus.

2.5.4 Trabecular shape and orientation

A diagnostic locomotor signal was not found in the trabecular shape or primary orientation of trabeculae in the distal tibia that would be of help in interpreting locomotor behavior beyond features measureable in the external morphology. Trabecular shape indices quantified in the distal tibia do not distinguish among hominoid species with different locomotor behaviors. Humans, chimpanzees, and gorillas all show more plate-shaped trabeculae in the anterocentral and posterocentral regions which imply these regions withstood greater habitual loads in life. Both orangutans and baboons display more plate-shaped trabeculae in the central region, implying a different distribution of habitual load. The primary orientation of trabeculae in the distal tibia also was largely similar among species, although there were slight differences that agree with postural differences predicted by external morphology.

However, distinct differences among species in trabecular orientation in the talus may help in the interpretation of habitual locomotor behaviors from an isolated talar bone. Humans showed the greatest overall consistency in trabecular orientation throughout the talus, supporting the stereotype that humans are much less variable in the direction of habitual joint load within the ankle. Orangutans showed the greatest overall variance in trabecular orientation, supporting the stereotype that the joint loads in orangutan locomotion are more variable. The primary orientation of trabeculae in the talus differs among species in ways that were predicted from behavioral observations. Humans differed from the non-human groups in that the orientation of trabeculae in the posterolateral and anteromedial regions were directed toward the posterior calcaneal facet and talar head, respectively, while that of other groups tended to be normal to the trochlear surface.

Tables

Table 2. 1: Comparative study sample.

	Sex	N Tibia	N Talus	Collections	Locomotor behavior
Homo sapiens	F	18	18	CMNH	Terrestrial plantigrade bipedalism
Pan troglodytes	F	20	20	CMNH, AMNH, NMNH	Semi-arboreal plantigrade quadrupedalism
Gorilla gorilla	F	17	15	CMNH, AMNH, NMNH	
Pongo pygmaeus	F	14	13	NMNH	Arboreal, quadrumanous
Papio hamadryas	M	17	18	Bramblett (UT Austin)	Terrestrial semi-digitigrade quadrupedalism

AMNH = American Museum of Natural History, CMNH = Cleveland Museum of Natural History, NMNH = Smithsonian National Museum of Natural History.

Table 2. 2: Summary of predictions and the outcomes of the study.

(a) Predictions of relative variability among species. Ti = distal tibia, Ta = talus, *H= Homo, Pn = Pan, G= Gorilla, Po=Pongo, Pp=Papio*

(b) Predictions of regional distribution of bone properties based on behavioral kinematics and the outcomes of the study. If the prediction was not met (×), the polarity of significant comparisons ($p<0.05$) is noted. ✓(ns) indicates the predicted polarity was found, but did not reach significance. ×(ns) indicates the predicted polarity was not found, and no significant differences were found among regions. A=anterior, P=posterior, L=lateral, M=medial, C=central.

(a)

Variability in:	Prediction	Result in Ti	Result in Ta
Sc radiodensity	*Po* >(*Pn*, *G*)>*Pp* >*H*	*H* >*Pn* >*Po* >*G* >*Pp*	*H* >*Po* >*G* >*Pn* >*Pp*
Sc thickness	*Po* >(*Pn*, *G*)>*Pp* >*H*	*H* >*Pn* >*Po* >*G* >*Pp*	*H* >*G* >*Po* >*Pn* >*Pp*
Tb volume	*Po* >(*Pn*, *G*)>*Pp* >*H*	*Po* >(*H*, *Pp*)>(*Pn*, *G*)	*Po* >*Pp* >*G* >*Pn* >*H*
Tb isotropy	*Po* >(*Pn*, *G*)>*Pp* >*H*	*H* >*Po* >*G* >*Pn* >*Pp*	*H* >*G* >(*Pn*, *Po*)>*Pp*
Tb orientation	*Po* >(Pan, *G*)>*Pp* >*H*	*Pp* >*Pn* >(*H*, *Po*)>*G*	*Po* >*Pp* >*Pn* >*G* >*H*

(b)

Tb.BV/TV		Prediction	Species	Met in Ti	Met in Ta
	ML axis	Medial > Lateral	*Homo*	× (C>L>M)	× (M=L>C)
		Lateral > Medial	*Pan*	✓	✓
			Gorilla	✓	✓
			Pongo	✓	✓
		Central>(Lateral, Medial)	*Papio*	✓	× (M=L>C)
	AP axis	Posterior > Anterior	*Homo*	✓	× (C=A>P)
			Papio	× (A>C=P)	✓ (ns)
		Anterior>Posterior	*Pan*	✓ (ns)	✓
			Gorilla	✓ (ns)	✓ (ns)
			Pongo	× (A=P>C)	✓ (ns)
Tb.I					
	ML axis	Medial > Lateral	*Homo*	× (C>M=L))	✓
		Lateral > Medial	*Pan*	× (C>M=L)	× (ns)
			Gorilla	× (ns)	× (ns)
			Pongo	✓ (ns)	× (ns)
		Central>(Lateral, Medial)	*Papio*	✓	× (L=C>M)
	AP axis	Posterior > Anterior	*Homo*	× (A=P>C)	✓ (ns)
			Papio	× (A=C>P)	× (P=A>C)
		Anterior>Posterior	*Pan*	× (A=P>C)	× (ns)
			Gorilla	× (ns)	× (ns)
			Pongo	× (ns)	× (ns)

Tb.E					
	ML axis	Lateral > Medial	*Homo*	✓ (ns)	✓
		Medial > Lateral	*Pan*	× (L>C=M)	✓ (ns)
			Gorilla	× (ns)	× (ns)
			Pongo	× (L=M>C)	× (ns)
			Papio	✓ (ns)	× (C>M=L)
	AP axis	Anterior > Posterior	*Homo*	× (C>A=P)	✓ (ns)
		Posterior > Anterior	*Pan*	× (C>A=P)	✓
			Gorilla	✓ (ns)	✓
			Pongo	✓	× (ns)
			Papio	✓ (ns)	✓ (ns)
Tb.Th					
	ML axis	Medial > Lateral	*Homo*	× (C=L>M)	✓ (ns)
		Lateral > Medial	*Pan*	✓	✓ (ns)
			Gorilla	✓ (ns)	× (ns)
			Pongo	✓ (ns)	× (ns)
		Central>(Lateral, Medial)	*Papio*	✓	× (ns)
	AP axis	Posterior > Anterior	*Homo*	× (A=C>P)	× (A=C>P)
			Papio	× (A>P=C)	× (A=C>P)
		Anterior>Posterior	*Pan*	✓ (A>C=P)	✓
			Gorilla	✓	✓
			Pongo	✓ (ns)	✓ (ns)
Tb.N					
	ML axis	Medial > Lateral	*Homo*	× (ns)	×(ns)
		Lateral > Medial	*Pan*	✓ (ns)	✓
			Gorilla	× (C>M=L)	✓
			Pongo	✓ (ns)	✓
		Central>(Lateral, Medial)	*Papio*	× (L>C=M)	✓
	AP axis	Posterior > Anterior	*Homo*	✓	✓ (ns)
			Papio	✓	✓
		Anterior>Posterior	*Pan*	× (P>A=C)	× (P>C>A)
			Gorilla	× (ns)	× (P=C>A)
			Pongo	× (P>C=A)	× (C>A=P)
Sc.MeanHouns					
	ML axis	Medial > Lateral	*Homo*	✓ (ns)	✓
		Lateral > Medial	*Pan*	× (M>C=L)	× (L=M>C)
			Gorilla	× (M>L=C)	× (M>L>C)
			Pongo	× (ns)	× (L=M>C)
		Central>(Lateral, Medial)	*Papio*	✓	× (L>M>C)
	AP axis	Posterior > Anterior	*Homo*	× (ns)	y (ns)
			Papio	✓ (ns)	✓
		Anterior>Posterior	*Pan*	× (A=P>C)	× (ns)

			Gorilla	× (P=A>C)	✓ (ns)
			Pongo	✓	× (P>C=A)
Sc.Th					
	ML axis	Medial > Lateral	*Homo*	✓	✓
		Lateral > Medial	*Pan*	× (M>C=L)	× (M>C=L)
			Gorilla	× (ns)	× (M>L=C)
			Pongo	✓ (ns)	× (M>C=L)
		Central>(Lateral, Medial)	*Papio*	✓	× (M>C=L)
	AP axis	Posterior > Anterior	*Homo*	✓ (ns)	× (C>A=P)
			Papio	✓	✓ (ns)
		Anterior>Posterior	*Pan*	× (P>C=A)	?? (ns)
			Gorilla	× (P>C=A)	✓
			Pongo	✓ (ns)	✓

Table 2. 3: Correlation coefficients (Pearson's r) among variables measured in the distal tibia.

All Species

	Tb.BV/TV	Tb.DA	Tb.I	Tb.E	Tb.Th	Tb.N	Sc.%High Density	Sc.Mean Houns	Sc.Th
Tb.BV/TV	-								
Tb.DA	-0.504 ***	-							
Tb.I	0.504 ***	-1.000 ***	-						
Tb.E	-0.519 ***	0.780 ***	-0.780 ***	-					
Tb.Th	0.489 ***	-0.418 ***	0.418 ***	-0.429 ***	-				
Tb.N	0.397 ***	-0.115 **	0.115 **	-0.087 *	-0.430 ***	-			
Sc.%HighDensity	0.267 ***	-0.150 ***	0.150 ***	-0.251 ***	0.103 **	0.023	-		
Sc.MeanHouns	0.406 ***	-0.122 **	0.122 **	-0.221 ***	0.191 ***	0.058	0.579 ***	-	
Sc.Th	0.506 ***	-0.176 ***	0.176 ***	-0.206 ***	0.207 ***	0.138 ***	0.292 ***	0.526 ***	-

Homo

	Tb.BV/TV	Tb.DA	Tb.I	Tb.E	Tb.Th	Tb.N	Sc.%High Density	Sc.Mean Houns	Sc.Th
Tb.BV/TV	-								
Tb.DA	**-0.391** ***	-							
Tb.I	**0.417** ***	**-0.804** ***	-						
Tb.E	**-0.366** ***	**0.659** ***	**-0.773** ***	-					
Tb.Th	**0.488** ***	**-0.284** ***	**0.307** ***	**-0.196** *	-				
Tb.N	**0.656** ***	**-0.298** ***	**0.284** ***	**-0.306** ***	**-0.268** **	-			
Sc.%HighDensity	0.028	-0.108	**0.216** *	**-0.211** **	**-0.172** *	**0.160** *	-		
Sc.MeanHouns	**0.200** *	-0.011	-0.003	0.000	0.106	0.074	0.041	-	
Sc.Th	0.120	0.062	-0.035	0.038	-0.019	0.042	-0.027	**0.542** ***	-

Pan

	Tb.BV/TV	Tb.DA	Tb.I	Tb.E	Tb.Th	Tb.N	Sc.%High Density	Sc.Mean Houns	Sc.Th
Tb.BV/TV	-								
Tb.DA	**-0.535** ***	-							
Tb.I	**0.616** ***	**-0.873** ***	-						
Tb.E	**-0.622** ***	**0.728** ***	**-0.790** ***	-					
Tb.Th	**0.700** ***	**-0.467** ***	**0.531** ***	**-0.494** ***	-				
Tb.N	**0.303** ***	**-0.152** *	**0.157** *	**-0.150** *	**-0.276** ***	-			
Sc.%HighDensity	-0.021	-0.058	-0.006	-0.060	0.003	-0.081	-		
Sc.MeanHouns	**0.251** ***	**-0.166** *	**0.152** *	**-0.226** **	0.137	0.022	**0.625** ***	-	
Sc.Th	**0.308** ***	-0.110	0.125	**-0.164** *	**0.166** *	-0.019	**0.379** ***	**0.563** ***	-

Gorilla

	Tb.BV/TV	Tb.DA	Tb.I	Tb.E	Tb.Th	Tb.N	Sc.%High Density	Sc.Mean Houns	Sc.Th
Tb.BV/TV	-								
Tb.DA	**-0.247** **	-							
Tb.I	**0.246** **	**-0.863** ***	-						
Tb.E	**-0.357** ***	**0.710** ***	**-0.755** ***	-					
Tb.Th	**0.660** ***	**-0.311** ***	**0.391** ***	**-0.394** ***	-				
Tb.N	**0.346** ***	-0.027	-0.062	-0.054	**-0.379** ***	-			
Sc.%HighDensity	-0.068	-0.143	0.061	-0.096	0.020	-0.156	-		
Sc.MeanHouns	0.128	0.093	**-0.166** *	0.022	0.120	-0.126	**0.475** ***	-	
Sc.Th	**0.232** **	0.110	-0.064	0.040	**0.434** ***	**-0.366** ***	**0.176** *	**0.535** ***	-

Pongo

	Tb.BV/TV	Tb.DA	Tb.I	Tb.E	Tb.Th	Tb.N	Sc.%High Density	Sc.Mean Houns	Sc.Th
Tb.BV/TV	-								
Tb.DA	**-0.393** ***	-							
Tb.I	**0.337** ***	**-0.680** ***	-						
Tb.E	**-0.437** ***	**0.526** ***	**-0.707** ***	-					
Tb.Th	**0.729** ***	**-0.308** ***	**0.385** ***	**-0.507** ***	-				
Tb.N	**0.240** **	**-0.205** *	0.003	0.014	**-0.325** ***	-			
Sc.%HighDensity	0.165	-0.092	0.007	-0.066	0.113	-0.076	-		
Sc.MeanHouns	**0.344** ***	0.008	-0.163	-0.054	0.159	0.151	**0.552** ***	-	
Sc.Th	**0.683** ***	-0.158	0.161	**-0.218** *	**0.614** ***	0.006	**0.299** **	**0.416** ***	-

Papio

	Tb.BV/TV	Tb.DA	Tb.I	Tb.E	Tb.Th	Tb.N	Sc.%High Density	Sc.Mean Houns	Sc.Th
Tb.BV/TV	-								
Tb.DA	**-0.346** ***	-							
Tb.I	**0.359** ***	**-0.858** ***	-						
Tb.E	**-0.269** **	**0.575** ***	**-0.724** ***	-					
Tb.Th	**0.397** ***	**-0.422** ***	**0.439** ***	**-0.369** ***	-				
Tb.N	**0.172** *	**0.196** *	-0.143	0.087	**-0.669** ***	-			
Sc.%HighDensity	**0.336** ***	-0.082	0.070	**-0.187** *	**0.229** **	**-0.166** *	-		
Sc.MeanHouns	**0.335** ***	-0.148	0.093	**-0.232** **	0.067	0.141	**0.540** ***	-	
Sc.Th	**0.469** ***	-0.124	0.099	-0.022	-0.100	**0.448** ***	-0.011	**0.356** ***	-

***p<0.001, **p<0.01, *p<0.05

Table 2. 4: Correlation coefficients (Pearson's r) among variables measured in the talus.

All Species

	Tb.BV/TV	Tb.DA	Tb.I	Tb.E	Tb.Th	Tb.N	Sc.%High Density	Sc.Mean Houns	Sc.Th
Tb.BV/TV	-								
Tb.DA	-0.456 ***	-							
Tb.I	0.456 ***	-1.000 ***	-						
Tb.E	-0.392 ***	0.511 ***	-0.511 ***	-					
Tb.Th	0.697 ***	-0.296 ***	0.296 ***	-0.354 ***	-				
Tb.N	-0.222 ***	0.104 **	-0.104 **	0.250 ***	-0.711 ***	-			
Sc.%HighDensity	0.457 ***	-0.183 ***	0.183 ***	-0.191 ***	0.248 ***	-0.028	-		
Sc.MeanHouns	0.376 ***	-0.090 *	0.090 *	-0.178 ***	0.247 ***	-0.077 *	0.621 ***	-	
Sc.Th	0.340 ***	-0.135 ***	0.135 ***	-0.225 ***	0.369 ***	-0.157 ***	0.255 ***	0.518 ***	-

Homo

	Tb.BV/TV	Tb.DA	Tb.I	Tb.E	Tb.Th	Tb.N	Sc.%High Density	Sc.Mean Houns	Sc.Th
Tb.BV/TV	-								
Tb.DA	**-0.222** **	-							
Tb.I	0.139	**-0.821** ***	-						
Tb.E	0.101	-0.062	-0.129	-					
Tb.Th	**0.242** **	0.064	0.019	-0.071	-				
Tb.N	**0.509** ***	**-0.212** **	0.080	**0.179** *	**-0.679** ***	-			
Sc.%HighDensity	**0.211** **	**-0.258** **	**0.303** ***	-0.114	**0.189** *	-0.045	-		
Sc.MeanHouns	**0.173** *	-0.140	0.132	-0.089	**0.249** **	-0.082	**0.304** ***	-	
Sc.Th	**0.400** ***	-0.133	0.121	**-0.312** ***	**0.353** ***	-0.058	**0.437** ***	**0.592** ***	-

Pan

	Tb.BV/TV	Tb.DA	Tb.I	Tb.E	Tb.Th	Tb.N	Sc.%High Density	Sc.Mean Houns	Sc.Th
Tb.BV/TV	-								
Tb.DA	-0.142	-							
Tb.I	0.123	**-0.879** ***	-						
Tb.E	**-0.234** **	0.142	**-0.269** ***	-					
Tb.Th	**0.535** ***	0.019	-0.014	**-0.342** ***	-				
Tb.N	0.023	**-0.193** **	**0.168** *	**0.208** **	**-0.753** ***	-			
Sc.%HighDensity	**0.198** **	0.074	-0.063	-0.006	0.105	-0.024	-		
Sc.MeanHouns	**0.467** ***	-0.011	0.070	**-0.175** *	0.131	0.115	**0.506** ***	-	
Sc.Th	**0.456** ***	-0.106	0.144	**-0.174** *	**0.345** ***	-0.120	**0.319** ***	**0.643** ***	-

Gorilla

	Tb.BV/TV	Tb.DA	Tb.I	Tb.E	Tb.Th	Tb.N	Sc.%High Density	Sc.Mean Houns	Sc.Th
Tb.BV/TV	-								
Tb.DA	-0.024	-							
Tb.I	-0.027	**-0.930** ***	-						
Tb.E	**-0.289** **	**0.225** *	**-0.285** **	-					
Tb.Th	**0.671** ***	-0.109	0.049	**-0.206** *	-				
Tb.N	0.059	-0.016	0.051	0.036	**-0.647** ***	-			
Sc.%HighDensity	**0.302** **	-0.001	0.000	-0.134	**0.261** **	-0.128	-		
Sc.MeanHouns	**0.366** ***	**0.187** *	**-0.182** *	-0.101	0.170	0.010	**0.380** ***	-	
Sc.Th	**0.397** ***	0.126	-0.149	-0.045	**0.524** ***	**-0.381** ***	**0.318** ***	**0.584** ***	-

Pongo

	Tb.BV/TV	Tb.DA	Tb.I	Tb.E	Tb.Th	Tb.N	Sc.%High Density	Sc.Mean Houns	Sc.Th
Tb.BV/TV	-								
Tb.DA	**-0.484** ***	-							
Tb.I	**0.504** ***	**-0.927** ***	-						
Tb.E	**-0.303** **	**0.594** ***	**-0.636** ***	-					
Tb.Th	**0.763** ***	**-0.369** ***	**0.456** ***	**-0.328** ***	-				
Tb.N	-0.077	-0.033	-0.089	0.157	**-0.601** ***	-			
Sc.%HighDensity	0.167	-0.150	0.167	-0.094	-0.018	**0.190** *	-		
Sc.MeanHouns	**0.440** ***	**-0.287** **	**0.320** ***	**-0.282** **	**0.334** ***	-0.040	**0.562** ***	-	
Sc.Th	**0.580** ***	**-0.314** **	**0.371** ***	**-0.329** ***	**0.598** ***	**-0.399** ***	**0.240** **	**0.541** ***	-

Papio

	Tb.BV/TV	Tb.DA	Tb.I	Tb.E	Tb.Th	Tb.N	Sc.%High Density	Sc.Mean Houns	Sc.Th
Tb.BV/TV	-								
Tb.DA	-0.123	-							
Tb.I	**0.157** *	**-0.887** ***	-						
Tb.E	**-0.432** ***	**0.282** ***	**-0.392** ***	-					
Tb.Th	**0.331** ***	-0.154	**0.174** *	**-0.326** ***	-				
Tb.N	**-0.428** ***	-0.078	0.113	**0.234** **	**-0.631** ***	-			
Sc.%HighDensity	**0.327** ***	-0.105	**0.175** *	-0.115	**0.156** *	-0.007	-		
Sc.MeanHouns	**0.623** ***	-0.013	0.066	**-0.221** **	**0.254** **	-0.137	**0.722** ***	-	
Sc.Th	**0.433** ***	0.044	-0.048	**-0.157** *	**0.321** ***	**-0.221** **	0.136	**0.433** ***	-

***p<0.001, **p<0.01, *p<0.05

Table 2. 5: Species means and variation for all study variables in the distal tibia.

	Homo			*Pan*			*Gorilla*		
	Mean	Std. Dev.	CV	Mean	Std. Dev.	CV	Mean	Std. Dev.	CV
Tb.BV/TV	0.31	0.05	0.17	0.41	0.07	0.16	0.38	0.06	0.16
Tb.DA	5.44	3.40	0.63	3.73	1.79	0.48	4.15	2.01	0.49
Tb.I	0.25	0.14	0.54	0.33	0.14	0.42	0.30	0.14	0.46
Tb.E	0.56	0.19	0.34	0.48	0.19	0.41	0.48	0.19	0.39
Tb.Th	0.19	0.03	0.16	0.17	0.03	0.19	0.19	0.03	0.14
Tb.N	1.57	0.31	0.20	2.12	0.25	0.12	1.76	0.26	0.15
Sc.%High Density	0.48	0.86	1.80	1.99	3.30	1.65	1.38	2.38	1.72
Sc.Mean Houns	1219	449	0.37	1246	216	0.17	1197	159	0.13
Sc.Th	0.29	0.07	0.26	0.38	0.09	0.23	0.40	0.08	0.21

	Pongo			*Papio*			**Total**		
	Mean	Std. Dev.	CV	Mean	Std. Dev.	CV	Mean	Std. Dev.	CV
Tb.BV/TV	0.39	0.10	0.25	0.50	0.08	0.17	0.40	0.10	0.24
Tb.DA	4.47	3.88	0.87	2.93	1.58	0.54	4.12	2.74	0.66
Tb.I	0.32	0.17	0.52	0.41	0.16	0.38	0.32	0.15	0.48
Tb.E	0.42	0.18	0.42	0.35	0.17	0.50	0.46	0.20	0.43
Tb.Th	0.20	0.04	0.20	0.22	0.04	0.20	0.19	0.04	0.20
Tb.N	1.63	0.29	0.18	1.78	0.33	0.18	1.79	0.35	0.20
Sc.%High Density	2.37	3.47	1.46	4.31	6.23	1.45	2.07	3.86	1.86
Sc.Mean Houns	1318	199	0.15	1427	174	0.12	1277	276	0.22
Sc.Th	0.41	0.09	0.22	0.41	0.07	0.17	0.38	0.09	0.25

Table 2. 6: Species means and variation for all study variables in the talus.

	Homo			*Pan*			*Gorilla*		
	Mean	Std. Dev.	CV	Mean	Std. Dev.	CV	Mean	Std. Dev.	CV
Tb.BV/TV	0.37	0.05	0.13	0.48	0.07	0.15	0.44	0.07	0.16
Tb.DA	7.97	4.96	0.62	2.79	1.02	0.37	3.06	1.02	0.33
Tb.I	0.18	0.10	0.59	0.40	0.12	0.30	0.36	0.11	0.31
Tb.E	0.46	0.17	0.36	0.30	0.13	0.45	0.32	0.13	0.39
Tb.Th	0.19	0.03	0.15	0.22	0.04	0.17	0.23	0.04	0.19
Tb.N	1.82	0.35	0.19	1.76	0.27	0.16	1.68	0.26	0.16
Sc.%High Density	1.48	2.57	1.73	6.19	8.71	1.41	2.71	4.05	1.49
Sc.Mean Houns	1575	629	0.40	1490	276	0.19	1437	286	0.20
Sc.Th	0.32	0.09	0.29	0.39	0.08	0.21	0.40	0.09	0.24

	Pongo			*Papio*			Total		
	Mean	Std. Dev.	CV	Mean	Std. Dev.	CV	Mean	Std. Dev.	CV
Tb.BV/TV	0.44	0.09	0.21	0.62	0.12	0.19	0.48	0.12	0.25
Tb.DA	2.21	0.83	0.38	2.39	0.98	0.41	3.73	3.26	0.87
Tb.I	0.50	0.15	0.30	0.47	0.14	0.29	0.38	0.17	0.45
Tb.E	0.26	0.14	0.54	0.27	0.13	0.49	0.32	0.16	0.49
Tb.Th	0.20	0.04	0.21	0.27	0.04	0.17	0.22	0.05	0.21
Tb.N	1.75	0.30	0.17	1.42	0.26	0.18	1.68	0.32	0.19
Sc.%High Density	3.73	6.06	1.62	8.45	9.76	1.16	4.73	7.47	1.58
Sc.Mean Houns	1450	302	0.21	1550	274	0.18	1505	384	0.25
Sc.Th	0.36	0.08	0.23	0.34	0.06	0.16	0.36	0.09	0.24

Table 2. 7: Species means and variation of all variables in the distal tibia by region. Row A= anterior, Row C = posterior, Column 1 = lateral, Column 3 = medial.

Tibia

A1

	Homo			*Pan*			*Gorilla*			*Pongo*			*Papio*		
	Mean	**SD**	**CV**	**Mean**	**SD**	**CV**	**Mean**	**SD**	**CV**	**Mean**	**SD**	**CV**	**Mean**	**SD**	**CV**
Tb.BV/TV	0.31	0.05	0.15	0.45	0.06	0.13	0.43	0.05	0.13	0.51	0.08	0.16	0.55	0.07	0.12
Tb.DA	4.23	1.79	0.42	3.18	1.21	0.38	4.50	2.66	0.59	3.35	1.86	0.56	2.25	0.98	0.44
Tb.I	0.28	0.13	0.45	0.36	0.13	0.36	0.30	0.16	0.54	0.37	0.14	0.39	0.49	0.13	0.27
Tb.E	0.61	0.14	0.22	0.40	0.19	0.48	0.46	0.19	0.42	0.37	0.13	0.35	0.21	0.16	0.74
Tb.Th	0.19	0.03	0.16	0.18	0.03	0.16	0.21	0.03	0.14	0.22	0.03	0.13	0.21	0.03	0.15
Tb.N	1.61	0.24	0.15	2.16	0.19	0.09	1.73	0.19	0.11	1.61	0.26	0.16	1.91	0.19	0.10
Sc.%High Density	0.46	0.56	1.23	1.21	1.18	0.97	1.30	1.65	1.27	5.87	5.52	0.94	7.98	5.72	0.72
Sc.Mean Houns	1233	496	0.40	1217	138	0.11	1213	145	0.12	1490	180	0.12	1453	83	0.06
Sc.Th	0.25	0.07	0.27	0.37	0.07	0.18	0.41	0.08	0.19	0.50	0.07	0.15	0.41	0.07	0.18

B1

	Homo			*Pan*			*Gorilla*			*Pongo*			*Papio*		
	Mean	**SD**	**CV**	**Mean**	**SD**	**CV**	**Mean**	**SD**	**CV**	**Mean**	**SD**	**CV**	**Mean**	**SD**	**CV**
Tb.BV/TV	0.33	0.05	0.15	0.39	0.04	0.11	0.35	0.03	0.09	0.36	0.05	0.15	0.50	0.07	0.13
Tb.DA	8.67	3.76	0.43	4.80	1.93	0.40	4.91	2.35	0.48	4.51	3.68	0.82	3.07	1.35	0.44
Tb.I	0.15	0.11	0.74	0.25	0.11	0.44	0.27	0.17	0.62	0.36	0.21	0.59	0.38	0.15	0.40
Tb.E	0.66	0.17	0.26	0.66	0.13	0.20	0.64	0.20	0.31	0.53	0.25	0.47	0.51	0.17	0.33
Tb.Th	0.20	0.03	0.15	0.16	0.02	0.11	0.19	0.02	0.11	0.18	0.03	0.14	0.18	0.03	0.16
Tb.N	1.53	0.23	0.15	2.09	0.20	0.09	1.68	0.21	0.13	1.64	0.21	0.13	1.99	0.28	0.14
Sc.%High Density	0.15	0.23	1.51	0.04	0.16	4.26	0.13	0.46	3.52	0.02	0.05	2.12	0.62	1.19	1.93
Sc.Mean Houns	1216	582	0.48	1083	109	0.10	1065	87	0.08	1148	109	0.10	1242	90	0.07
Sc.Th	0.26	0.05	0.18	0.35	0.09	0.25	0.37	0.07	0.20	0.40	0.10	0.24	0.44	0.07	0.17

C1

	Homo			*Pan*			*Gorilla*			*Pongo*			*Papio*		
	Mean	**SD**	**CV**	**Mean**	**SD**	**CV**	**Mean**	**SD**	**CV**	**Mean**	**SD**	**CV**	**Mean**	**SD**	**CV**
Tb.BV/TV	0.30	0.04	0.13	0.43	0.05	0.11	0.39	0.04	0.11	0.39	0.06	0.15	0.52	0.06	0.12
Tb.DA	4.16	1.89	0.45	4.86	2.47	0.51	4.17	1.89	0.45	4.45	1.87	0.42	4.79	2.42	0.50
Tb.I	0.29	0.12	0.43	0.26	0.12	0.47	0.29	0.12	0.42	0.27	0.12	0.44	0.26	0.11	0.44
Tb.E	0.56	0.14	0.25	0.55	0.14	0.25	0.47	0.16	0.34	0.54	0.12	0.22	0.44	0.14	0.31
Tb.Th	0.18	0.02	0.12	0.17	0.02	0.12	0.19	0.02	0.10	0.19	0.03	0.16	0.18	0.04	0.19
Tb.N	1.66	0.24	0.14	2.19	0.19	0.09	1.71	0.19	0.11	1.75	0.19	0.11	2.17	0.26	0.12
Sc.%High Density	0.72	0.95	1.31	0.68	1.13	1.67	1.24	1.61	1.30	0.51	0.88	1.73	4.36	5.25	1.21
Sc.Mean Houns	1229	461	0.37	1144	182	0.16	1199	124	0.10	1206	164	0.14	1455	91	0.06
Sc.Th	0.27	0.07	0.28	0.34	0.08	0.23	0.39	0.08	0.20	0.38	0.09	0.23	0.43	0.06	0.15

Tibia

A2

	Homo			*Pan*			*Gorilla*			*Pongo*			*Papio*		
	Mean	**SD**	**CV**	**Mean**	**SD**	**CV**	**Mean**	**SD**	**CV**	**Mean**	**SD**	**CV**	**Mean**	**SD**	**CV**
Tb.BV/TV	0.34	0.05	0.14	0.44	0.06	0.13	0.41	0.04	0.11	0.45	0.08	0.18	0.54	0.06	0.12
Tb.DA	3.32	1.22	0.37	2.84	0.84	0.30	3.99	1.74	0.44	5.36	3.83	0.72	2.05	0.36	0.17
Tb.I	0.34	0.13	0.38	0.38	0.10	0.27	0.29	0.11	0.37	0.25	0.13	0.52	0.50	0.08	0.16
Tb.E	0.39	0.16	0.40	0.41	0.12	0.30	0.45	0.20	0.45	0.31	0.14	0.47	0.21	0.09	0.44
Tb.Th	0.22	0.03	0.15	0.21	0.04	0.19	0.20	0.02	0.09	0.23	0.05	0.22	0.26	0.03	0.10
Tb.N	1.57	0.27	0.17	1.99	0.47	0.24	1.83	0.25	0.14	1.61	0.31	0.19	1.67	0.21	0.13
Sc.%High Density	0.46	0.67	1.46	1.88	2.53	1.34	0.81	0.86	1.06	2.35	2.28	0.97	7.05	6.51	0.92
Sc.Mean Houns	1187	416	0.35	1231	185	0.15	1165	104	0.09	1464	165	0.11	1518	161	0.11
Sc.Th	0.25	0.06	0.23	0.32	0.08	0.26	0.36	0.08	0.23	0.45	0.07	0.16	0.37	0.07	0.19

B2

	Homo			*Pan*			*Gorilla*			*Pongo*			*Papio*		
	Mean	**SD**	**CV**	**Mean**	**SD**	**CV**	**Mean**	**SD**	**CV**	**Mean**	**SD**	**CV**	**Mean**	**SD**	**CV**
Tb.BV/TV	0.32	0.04	0.13	0.37	0.04	0.12	0.34	0.04	0.11	0.32	0.06	0.20	0.55	0.08	0.15
Tb.DA	5.81	2.72	0.47	3.96	2.10	0.53	4.72	2.49	0.53	2.24	0.69	0.31	1.82	0.36	0.20
Tb.I	0.22	0.11	0.51	0.33	0.17	0.51	0.29	0.18	0.61	0.49	0.14	0.30	0.57	0.12	0.20
Tb.E	0.69	0.14	0.20	0.49	0.23	0.46	0.48	0.18	0.38	0.31	0.14	0.45	0.23	0.12	0.51
Tb.Th	0.20	0.03	0.13	0.16	0.02	0.12	0.18	0.03	0.14	0.19	0.04	0.21	0.27	0.04	0.14
Tb.N	1.53	0.27	0.18	2.15	0.27	0.13	1.81	0.30	0.17	1.53	0.25	0.16	1.59	0.25	0.16
Sc.%High Density	0.01	0.02	3.37	0.00	0.00	3.37	0.00	0.00	2.49	0.01	0.02	1.78	0.00	0.00	3.43
Sc.Mean Houns	1049	420	0.40	1021	134	0.13	1026	124	0.12	1108	118	0.11	1261	102	0.08
Sc.Th	0.27	0.05	0.20	0.36	0.10	0.27	0.38	0.10	0.27	0.34	0.10	0.29	0.42	0.07	0.16

C2

	Homo			*Pan*			*Gorilla*			*Pongo*			*Papio*		
	Mean	**SD**	**CV**	**Mean**	**SD**	**CV**	**Mean**	**SD**	**CV**	**Mean**	**SD**	**CV**	**Mean**	**SD**	**CV**
Tb.BV/TV	0.34	0.04	0.13	0.47	0.06	0.13	0.42	0.04	0.11	0.44	0.09	0.19	0.54	0.08	0.14
Tb.DA	3.60	1.69	0.47	2.73	1.19	0.43	3.47	2.20	0.63	4.89	3.17	0.65	2.17	0.72	0.33
Tb.I	0.34	0.15	0.45	0.43	0.16	0.37	0.35	0.13	0.37	0.30	0.18	0.60	0.50	0.15	0.29
Tb.E	0.47	0.20	0.43	0.33	0.20	0.59	0.41	0.14	0.35	0.42	0.16	0.38	0.24	0.13	0.56
Tb.Th	0.19	0.02	0.11	0.19	0.04	0.23	0.20	0.03	0.14	0.21	0.04	0.22	0.22	0.06	0.28
Tb.N	1.72	0.25	0.15	2.21	0.26	0.12	1.91	0.24	0.12	1.78	0.26	0.15	1.85	0.33	0.18
Sc.%High Density	0.99	2.33	2.35	1.94	2.35	1.21	0.46	0.81	1.78	0.97	1.10	1.13	8.38	12.10	1.44
Sc.Mean Houns	1219	438	0.36	1343	157	0.12	1224	158	0.13	1350	182	0.14	1646	141	0.09
Sc.Th	0.31	0.10	0.34	0.45	0.07	0.16	0.47	0.07	0.15	0.47	0.09	0.20	0.46	0.05	0.12

Tibia

A3

	Homo			*Pan*			*Gorilla*			*Pongo*			*Papio*		
	Mean	**SD**	**CV**	**Mean**	**SD**	**CV**	**Mean**	**SD**	**CV**	**Mean**	**SD**	**CV**	**Mean**	**SD**	**CV**
Tb.BV/TV	0.25	0.05	0.20	0.39	0.05	0.14	0.40	0.06	0.15	0.35	0.05	0.15	0.48	0.07	0.14
Tb.DA	5.43	2.96	0.54	3.53	1.26	0.36	3.62	1.38	0.38	4.18	2.18	0.52	3.01	1.06	0.35
Tb.I	0.23	0.10	0.44	0.32	0.11	0.34	0.31	0.10	0.32	0.28	0.10	0.36	0.36	0.09	0.25
Tb.E	0.52	0.12	0.23	0.46	0.13	0.29	0.35	0.18	0.52	0.46	0.15	0.34	0.43	0.11	0.25
Tb.Th	0.18	0.04	0.22	0.16	0.02	0.14	0.21	0.03	0.13	0.18	0.03	0.15	0.23	0.03	0.12
Tb.N	1.27	0.27	0.21	2.07	0.25	0.12	1.73	0.25	0.15	1.64	0.34	0.20	1.51	0.19	0.13
Sc.%High Density	0.97	1.44	1.49	5.58	5.84	1.05	1.96	2.50	1.28	6.79	4.26	0.63	5.59	3.47	0.62
Sc.Mean Houns	1332	413	0.31	1490	183	0.12	1296	137	0.11	1426	161	0.11	1514	151	0.10
Sc.Th	0.33	0.05	0.15	0.45	0.06	0.13	0.44	0.07	0.15	0.42	0.06	0.13	0.38	0.06	0.17

B3

	Homo			*Pan*			*Gorilla*			*Pongo*			*Papio*		
	Mean	**SD**	**CV**	**Mean**	**SD**	**CV**	**Mean**	**SD**	**CV**	**Mean**	**SD**	**CV**	**Mean**	**SD**	**CV**
Tb.BV/TV	0.28	0.05	0.19	0.32	0.05	0.16	0.30	0.04	0.14	0.26	0.05	0.21	0.39	0.06	0.15
Tb.DA	8.02	5.26	0.66	4.56	1.85	0.41	3.93	1.17	0.30	6.18	8.01	1.30	3.09	1.35	0.44
Tb.I	0.20	0.17	0.82	0.26	0.11	0.43	0.29	0.15	0.53	0.29	0.18	0.61	0.37	0.12	0.33
Tb.E	0.70	0.20	0.28	0.62	0.16	0.26	0.57	0.16	0.29	0.47	0.18	0.38	0.44	0.16	0.36
Tb.Th	0.18	0.03	0.15	0.15	0.01	0.08	0.17	0.03	0.16	0.17	0.03	0.19	0.20	0.03	0.13
Tb.N	1.39	0.29	0.21	1.96	0.36	0.18	1.65	0.39	0.24	1.38	0.31	0.23	1.53	0.28	0.18
Sc.%High Density	0.33	0.48	1.43	2.35	3.07	1.31	2.27	2.80	1.23	3.07	2.23	0.73	0.62	0.79	1.28
Sc.Mean Houns	1241	426	0.34	1239	180	0.15	1219	102	0.08	1297	133	0.10	1267	86	0.07
Sc.Th	0.31	0.06	0.20	0.38	0.07	0.17	0.39	0.08	0.20	0.35	0.07	0.20	0.38	0.05	0.14

C3

	Homo			*Pan*			*Gorilla*			*Pongo*			*Papio*		
	Mean	**SD**	**CV**	**Mean**	**SD**	**CV**	**Mean**	**SD**	**CV**	**Mean**	**SD**	**CV**	**Mean**	**SD**	**CV**
Tb.BV/TV	0.33	0.05	0.14	0.43	0.06	0.13	0.36	0.04	0.11	0.41	0.08	0.21	0.46	0.06	0.12
Tb.DA	5.73	3.27	0.57	3.09	1.05	0.34	4.02	1.77	0.44	5.07	4.32	0.85	4.08	1.76	0.43
Tb.I	0.22	0.10	0.43	0.36	0.13	0.37	0.28	0.10	0.37	0.29	0.16	0.55	0.29	0.12	0.43
Tb.E	0.47	0.20	0.43	0.37	0.17	0.45	0.47	0.13	0.27	0.41	0.15	0.36	0.39	0.10	0.27
Tb.Th	0.17	0.02	0.12	0.17	0.02	0.14	0.18	0.02	0.11	0.20	0.04	0.19	0.20	0.03	0.14
Tb.N	1.86	0.32	0.17	2.18	0.23	0.10	1.76	0.22	0.13	1.69	0.29	0.17	1.80	0.26	0.14
Sc.%High Density	0.58	1.18	2.04	4.27	3.76	0.88	4.25	4.20	0.99	1.74	1.44	0.82	4.19	3.90	0.93
Sc.Mean Houns	1261	413	0.33	1444	153	0.11	1368	151	0.11	1376	167	0.12	1487	118	0.08
Sc.Th	0.33	0.08	0.25	0.43	0.07	0.15	0.44	0.07	0.16	0.42	0.07	0.17	0.38	0.05	0.13

Table 2. 8: Species means and variation of all variables in the talus by region.
Row A= anterior, Row C = posterior, Column 1 = lateral, Column 3 = medial.

Talus

A1

	Homo			*Pan*			*Gorilla*			*Pongo*			*Papio*		
	Mean	SD	CV	Mean	SD	CV	Mean	SD	CV	Mean	SD	CV	Mean	SD	CV
Tb.BV/TV	0.39	0.04	0.11	0.58	0.06	0.10	0.55	0.05	0.09	0.58	0.08	0.13	0.74	0.08	0.10
Tb.DA	9.12	2.87	0.31	2.80	0.68	0.24	3.48	0.93	0.27	1.91	0.66	0.35	1.95	0.37	0.19
Tb.I	0.12	0.04	0.32	0.38	0.10	0.27	0.31	0.08	0.26	0.56	0.14	0.24	0.53	0.08	0.16
Tb.E	0.62	0.13	0.21	0.24	0.13	0.56	0.28	0.11	0.41	0.24	0.13	0.52	0.22	0.10	0.45
Tb.Th	0.20	0.03	0.15	0.25	0.04	0.15	0.26	0.04	0.16	0.23	0.04	0.18	0.28	0.04	0.13
Tb.N	1.88	0.32	0.17	1.76	0.26	0.15	1.74	0.27	0.16	1.87	0.40	0.21	1.20	0.22	0.18
Sc.%High Density	0.63	0.53	0.84	8.76	9.49	1.08	3.77	2.43	0.64	7.06	4.63	0.66	11.96	9.66	0.81
Sc.Mean Houns	1487	670	0.45	1655	201	0.12	1524	228	0.15	1729	197	0.11	1714	128	0.07
Sc.Th	0.27	0.07	0.26	0.41	0.07	0.18	0.42	0.05	0.11	0.41	0.06	0.15	0.34	0.03	0.09

B1

	Homo			*Pan*			*Gorilla*			*Pongo*			*Papio*		
	Mean	SD	CV	Mean	SD	CV	Mean	SD	CV	Mean	SD	CV	Mean	SD	CV
Tb.BV/TV	0.41	0.03	0.07	0.54	0.05	0.09	0.51	0.05	0.10	0.49	0.05	0.10	0.62	0.06	0.10
Tb.DA	8.58	2.55	0.30	3.12	1.12	0.36	3.30	1.23	0.37	2.01	0.46	0.23	2.29	0.55	0.24
Tb.I	0.13	0.04	0.29	0.36	0.11	0.32	0.35	0.13	0.38	0.52	0.13	0.25	0.46	0.10	0.22
Tb.E	0.59	0.12	0.20	0.28	0.14	0.49	0.30	0.12	0.40	0.28	0.15	0.55	0.34	0.12	0.35
Tb.Th	0.19	0.02	0.12	0.24	0.03	0.13	0.24	0.04	0.15	0.21	0.03	0.17	0.29	0.04	0.16
Tb.N	2.00	0.32	0.16	1.79	0.22	0.12	1.81	0.29	0.16	1.94	0.27	0.14	1.48	0.21	0.14
Sc.%High Density	0.93	0.86	0.92	9.68	11.25	1.16	5.21	6.39	1.23	2.74	1.94	0.71	13.86	10.88	0.79
Sc.Mean Houns	1599	745	0.47	1644	141	0.09	1562	197	0.13	1511	204	0.14	1750	144	0.08
Sc.Th	0.32	0.09	0.30	0.46	0.08	0.18	0.45	0.08	0.18	0.39	0.08	0.20	0.39	0.05	0.12

C1

	Homo			*Pan*			*Gorilla*			*Pongo*			*Papio*		
	Mean	SD	CV	Mean	SD	CV	Mean	SD	CV	Mean	SD	CV	Mean	SD	CV
Tb.BV/TV	0.34	0.03	0.10	0.47	0.06	0.13	0.41	0.04	0.09	0.44	0.03	0.08	0.60	0.07	0.11
Tb.DA	5.48	1.68	0.31	2.43	0.82	0.34	2.50	0.60	0.24	2.38	0.83	0.35	1.73	0.39	0.22
Tb.I	0.20	0.05	0.24	0.46	0.15	0.32	0.42	0.11	0.26	0.47	0.16	0.35	0.60	0.12	0.19
Tb.E	0.66	0.07	0.11	0.26	0.09	0.35	0.33	0.11	0.34	0.29	0.12	0.43	0.25	0.10	0.39
Tb.Th	0.18	0.02	0.12	0.20	0.03	0.15	0.20	0.02	0.12	0.19	0.03	0.17	0.24	0.03	0.12
Tb.N	1.80	0.32	0.18	1.96	0.21	0.11	1.79	0.22	0.12	1.93	0.24	0.12	1.73	0.20	0.12
Sc.%High Density	1.07	0.84	0.78	6.58	7.86	1.19	2.07	2.28	1.10	1.40	1.88	1.34	22.29	10.25	0.46
Sc.Mean Houns	1498	602	0.40	1470	272	0.18	1249	215	0.17	1314	228	0.17	1833	193	0.11
Sc.Th	0.24	0.07	0.29	0.33	0.08	0.25	0.28	0.07	0.23	0.28	0.05	0.17	0.31	0.04	0.11

Talus

A2

	Homo			*Pan*			*Gorilla*			*Pongo*			*Papio*		
	Mean	SD	CV	Mean	SD	CV	Mean	SD	CV	Mean	SD	CV	Mean	SD	CV
Tb.BV/TV	0.35	0.04	0.12	0.44	0.06	0.14	0.43	0.06	0.14	0.41	0.09	0.22	0.49	0.08	0.16
Tb.DA	13.60	5.79	0.43	3.40	1.30	0.38	2.87	0.92	0.32	2.60	1.01	0.39	1.94	0.31	0.16
Tb.I	0.09	0.04	0.44	0.32	0.09	0.27	0.38	0.10	0.27	0.44	0.16	0.36	0.53	0.08	0.15
Tb.E	0.38	0.11	0.28	0.27	0.12	0.44	0.24	0.13	0.54	0.29	0.16	0.55	0.27	0.12	0.43
Tb.Th	0.20	0.03	0.14	0.25	0.03	0.13	0.25	0.05	0.20	0.21	0.06	0.28	0.25	0.04	0.15
Tb.N	1.57	0.32	0.20	1.46	0.24	0.16	1.48	0.24	0.16	1.49	0.25	0.17	1.44	0.23	0.16
Sc.%High Density	0.01	0.02	2.33	0.88	2.19	2.48	0.75	1.56	2.10	2.68	3.76	1.40	0.00	0.00	2.48
Sc.Mean Houns	1337	557	0.42	1214	220	0.18	1276	365	0.29	1291	200	0.15	1090	93	0.08
Sc.Th	0.31	0.08	0.25	0.34	0.08	0.22	0.38	0.09	0.24	0.36	0.06	0.16	0.28	0.04	0.15

B2

	Homo			*Pan*			*Gorilla*			*Pongo*			*Papio*		
	Mean	SD	CV	Mean	SD	CV	Mean	SD	CV	Mean	SD	CV	Mean	SD	CV
Tb.BV/TV	0.36	0.04	0.12	0.41	0.04	0.09	0.41	0.05	0.11	0.36	0.06	0.16	0.47	0.07	0.16
Tb.DA	9.34	5.47	0.59	2.43	0.50	0.21	3.38	1.21	0.36	2.79	1.32	0.47	2.53	0.85	0.33
Tb.I	0.15	0.08	0.56	0.43	0.10	0.24	0.33	0.11	0.34	0.43	0.18	0.42	0.43	0.12	0.27
Tb.E	0.38	0.12	0.31	0.38	0.14	0.37	0.43	0.12	0.28	0.29	0.17	0.59	0.39	0.12	0.31
Tb.Th	0.19	0.03	0.15	0.20	0.02	0.08	0.22	0.02	0.11	0.19	0.04	0.20	0.23	0.04	0.16
Tb.N	1.82	0.40	0.22	1.77	0.18	0.10	1.67	0.22	0.13	1.69	0.23	0.14	1.52	0.24	0.16
Sc.%High Density	0.01	0.03	3.91	0.97	4.19	4.31	0.10	0.34	3.29	0.19	0.39	2.04	0.01	0.02	1.74
Sc.Mean Houns	1373	642	0.47	1235	192	0.16	1255	305	0.24	1184	281	0.24	1222	99	0.08
Sc.Th	0.34	0.08	0.25	0.38	0.07	0.19	0.40	0.12	0.30	0.30	0.10	0.33	0.36	0.07	0.19

C2

	Homo			*Pan*			*Gorilla*			*Pongo*			*Papio*		
	Mean	SD	CV	Mean	SD	CV	Mean	SD	CV	Mean	SD	CV	Mean	SD	CV
Tb.BV/TV	0.34	0.05	0.13	0.45	0.03	0.06	0.36	0.04	0.11	0.38	0.06	0.14	0.64	0.08	0.13
Tb.DA	9.74	5.89	0.61	2.49	0.69	0.28	3.65	1.14	0.31	2.17	0.76	0.35	1.80	0.42	0.23
Tb.I	0.15	0.09	0.64	0.43	0.11	0.25	0.30	0.08	0.28	0.51	0.16	0.32	0.58	0.12	0.20
Tb.E	0.41	0.11	0.27	0.39	0.11	0.29	0.40	0.07	0.16	0.26	0.13	0.52	0.25	0.14	0.55
Tb.Th	0.18	0.03	0.16	0.19	0.02	0.09	0.19	0.02	0.10	0.19	0.04	0.19	0.28	0.04	0.14
Tb.N	1.80	0.41	0.23	1.93	0.20	0.10	1.71	0.23	0.13	1.61	0.27	0.17	1.45	0.22	0.15
Sc.%High Density	0.05	0.11	2.37	2.38	5.97	2.50	0.24	0.35	1.45	2.33	3.00	1.29	6.35	4.79	0.75
Sc.Mean Houns	1447	601	0.42	1428	242	0.17	1246	168	0.13	1498	324	0.22	1515	170	0.11
Sc.Th	0.29	0.07	0.25	0.38	0.06	0.15	0.35	0.07	0.21	0.34	0.09	0.27	0.34	0.03	0.10

Talus

A3

	Homo			*Pan*			*Gorilla*			*Pongo*			*Papio*		
	Mean	SD	CV	Mean	SD	CV	Mean	SD	CV	Mean	SD	CV	Mean	SD	CV
Tb.BV/TV	0.40	0.05	0.12	0.47	0.06	0.12	0.47	0.07	0.14	0.43	0.11	0.24	0.63	0.09	0.15
Tb.DA	3.36	0.98	0.29	2.37	0.82	0.35	2.35	0.57	0.24	2.36	0.72	0.30	2.48	0.82	0.33
Tb.I	0.32	0.08	0.27	0.46	0.13	0.28	0.45	0.11	0.24	0.46	0.14	0.31	0.43	0.11	0.25
Tb.E	0.50	0.11	0.22	0.23	0.14	0.61	0.23	0.10	0.44	0.33	0.13	0.39	0.21	0.14	0.67
Tb.Th	0.21	0.03	0.14	0.26	0.04	0.17	0.27	0.06	0.20	0.21	0.05	0.21	0.30	0.05	0.16
Tb.N	1.74	0.25	0.14	1.47	0.22	0.15	1.45	0.22	0.15	1.55	0.22	0.14	1.27	0.17	0.14
Sc.%High Density	3.92	3.33	0.85	11.24	9.96	0.89	5.83	5.00	0.86	5.01	9.83	1.96	4.16	3.51	0.84
Sc.Mean Houns	1726	470	0.27	1581	277	0.18	1603	232	0.14	1334	234	0.18	1466	109	0.07
Sc.Th	0.36	0.08	0.23	0.45	0.06	0.14	0.48	0.06	0.12	0.41	0.04	0.10	0.32	0.04	0.11

B3

	Homo			*Pan*			*Gorilla*			*Pongo*			*Papio*		
	Mean	SD	CV	Mean	SD	CV	Mean	SD	CV	Mean	SD	CV	Mean	SD	CV
Tb.BV/TV	0.40	0.06	0.14	0.46	0.04	0.10	0.44	0.04	0.10	0.44	0.07	0.15	0.66	0.10	0.15
Tb.DA	6.61	3.43	0.52	3.25	1.57	0.48	3.19	0.79	0.25	2.04	0.49	0.24	3.73	1.60	0.43
Tb.I	0.19	0.09	0.48	0.35	0.10	0.28	0.33	0.09	0.27	0.51	0.12	0.22	0.31	0.11	0.35
Tb.E	0.35	0.13	0.37	0.30	0.11	0.36	0.38	0.10	0.27	0.15	0.06	0.38	0.21	0.10	0.47
Tb.Th	0.20	0.03	0.15	0.22	0.03	0.12	0.23	0.03	0.11	0.21	0.04	0.20	0.28	0.04	0.14
Tb.N	1.89	0.37	0.19	1.78	0.18	0.10	1.67	0.18	0.11	1.83	0.22	0.12	1.39	0.19	0.14
Sc.%High Density	4.49	3.57	0.80	5.22	5.77	1.11	3.11	2.76	0.89	1.19	1.37	1.15	6.09	5.59	0.92
Sc.Mean Houns	1917	625	0.33	1467	224	0.15	1607	236	0.15	1393	247	0.18	1636	132	0.08
Sc.Th	0.42	0.09	0.22	0.37	0.07	0.18	0.43	0.09	0.22	0.34	0.07	0.22	0.40	0.05	0.14

C3

	Homo			*Pan*			*Gorilla*			*Pongo*			*Papio*		
	Mean	SD	CV	Mean	SD	CV	Mean	SD	CV	Mean	SD	CV	Mean	SD	CV
Tb.BV/TV	0.36	0.04	0.11	0.49	0.06	0.12	0.41	0.05	0.12	0.45	0.08	0.17	0.70	0.10	0.15
Tb.DA	5.89	5.32	0.90	2.80	0.76	0.27	2.86	0.99	0.35	1.64	0.34	0.21	3.05	0.83	0.27
Tb.I	0.27	0.14	0.50	0.39	0.12	0.31	0.39	0.12	0.32	0.63	0.11	0.17	0.35	0.10	0.27
Tb.E	0.27	0.09	0.33	0.33	0.14	0.43	0.32	0.12	0.39	0.17	0.09	0.52	0.29	0.15	0.53
Tb.Th	0.18	0.02	0.13	0.20	0.02	0.11	0.20	0.02	0.09	0.20	0.04	0.20	0.23	0.02	0.09
Tb.N	1.86	0.28	0.15	1.91	0.23	0.12	1.78	0.28	0.16	1.80	0.25	0.14	1.27	0.23	0.18
Sc.%High Density	2.22	3.53	1.59	10.00	10.48	1.05	3.33	5.74	1.72	10.98	10.17	0.93	11.30	9.09	0.80
Sc.Mean Houns	1793	601	0.34	1719	204	0.12	1608	156	0.10	1791	220	0.12	1727	122	0.07
Sc.Th	0.32	0.09	0.27	0.42	0.06	0.14	0.42	0.06	0.15	0.39	0.06	0.15	0.34	0.03	0.10

Table 2. 9: Pairwise comparisons of species, overall in distal tibia

Overall

Tb.BV/TV	*Homo*	*p*	*Pan*	*p*	*Gorilla*	*p*	*Pongo*	*p*	*Papio*	*p*
Homo	-									
Pan	***Pan>Homo***	**0.000**	-							
Gorilla	***Gorilla>Homo***	**0.000**	***Pan>Gorilla***	**0.001**	-					
Pongo	***Pongo>Homo***	**0.000**	*Pan>Pongo*	0.112	*Pongo>Gorilla*	0.718	-			
Papio	***Papio>Homo***	**0.000**	***Papio>Pan***	**0.000**	***Papio>Gorilla***	**0.000**	***Papio>Pongo***	**0.000**	-	

Tb.DA	*Homo*	*p*	*Pan*	*p*	*Gorilla*	*p*	*Pongo*	*p*	*Papio*	*p*
Homo	-									
Pan	***Homo>Pan***	**0.000**	-							
Gorilla	***Homo>Gorilla***	**0.000**	*Gorilla>Pan*	0.564	-					
Pongo	***Homo>Pongo***	**0.015**	*Pongo>Pan*	0.095	*Pongo>Gorilla*	0.849	-			
Papio	***Homo>Papio***	**0.000**	***Pan>Papio***	**0.036**	***Gorilla>Papio***	**0.000**	***Pongo>Papio***	**0.000**	-	

Tb.I	*Homo*	*p*	*Pan*	*p*	*Gorilla*	*p*	*Pongo*	*p*	*Papio*	*p*
Homo	-									
Pan	***Homo>Pan***	0.000	-							
Gorilla	***Homo>Gorilla***	0.045	*Pan>Gorilla*	0.402	-					
Pongo	***Homo>Pongo***	0.001	*Pan>Pongo*	0.998	*Pongo>Gorilla*	0.711	-			
Papio	***Homo>Papio***	0.000	***Papio>Pan***	0.000	***Papio>Gorilla***	0.000	***Papio>Pongo***	0.000	-	

Tb.E	*Homo*	*p*	*Pan*	*p*	*Gorilla*	*p*	*Pongo*	*p*	*Papio*	*p*
Homo	-									
Pan	***Homo>Pan***	**0.000**	-							
Gorilla	***Homo>Gorilla***	**0.001**	*Gorilla>Pan*	1.000	-					
Pongo	***Homo>Pongo***	**0.000**	*Pan>Pongo*	0.092	*Gorilla>Pongo*	0.097	-			
Papio	***Homo>Papio***	**0.000**	***Pan>Papio***	**0.000**	***Gorilla>Papio***	**0.000**	***Pongo>Papio***	**0.004**	-	

Tb.Th	*Homo*	*p*	*Pan*	*p*	*Gorilla*	*p*	*Pongo*	*p*	*Papio*	*p*
Homo	-									
Pan	***Homo>Pan***	**0.000**	-							
Gorilla	*Gorilla>Homo*	0.948	***Gorilla>Pan***	**0.000**	-					
Pongo	*Pongo>Homo*	0.405	***Pongo>Pan***	**0.000**	*Pongo>Gorilla*	0.838	-			
Papio	***Papio>Homo***	**0.000**	***Papio>Pan***	**0.000**	***Papio>Gorilla***	**0.000**	***Papio>Pongo***	**0.000**	-	

Tb.N	*Homo*	*p*	*Pan*	*p*	*Gorilla*	*p*	*Pongo*	*p*	*Papio*	*p*
Homo	-									
Pan	***Pan>Homo***	**0.000**	-							
Gorilla	***Gorilla>Homo***	**0.000**	***Pan>Gorilla***	**0.000**	-					
Pongo	*Pongo>Homo*	0.475	***Pan>Pongo***	**0.000**	***Gorilla>Pongo***	**0.001**	-			
Papio	***Papio>Homo***	**0.000**	***Pan>Papio***	**0.000**	*Papio>Gorilla*	0.978	***Papio>Pongo***	**0.000**	-	

Sc.%HighDen	*Homo*	*p*	*Pan*	*p*	*Gorilla*	*p*	*Pongo*	*p*	*Papio*	*p*
Homo	-									
Pan	***Pan>Homo***	**0.001**	-							
Gorilla	*Gorilla>Homo*	0.184	*Pan>Gorilla*	0.523	-					
Pongo	***Pongo>Homo***	**0.000**	*Pongo>Pan*	0.895	*Pongo>Gorilla*	0.162	-			
Papio	***Papio>Homo***	**0.000**	***Papio>Pan***	**0.000**	***Papio>Gorilla***	**0.000**	***Papio>Pongo***	**0.000**	-	

Sc.MeanHoun	*Homo*	*p*	*Pan*	*p*	*Gorilla*	*p*	*Pongo*	*p*	*Papio*	*p*
Homo	-									
Pan	*Pan>Homo*	0.872	-							
Gorilla	*Homo>Gorilla*	0.952	*Pan>Gorilla*	0.433	-					
Pongo	***Pongo>Homo***	**0.014**	*Pongo>Pan*	0.115	***Pongo>Gorilla***	**0.001**	-			
Papio	***Papio>Homo***	**0.000**	***Papio>Pan***	**0.000**	***Papio>Gorilla***	**0.000**	***Papio>Pongo***	**0.006**	-	

Sc.Th	*Homo*	*p*	*Pan*	*p*	*Gorilla*	*p*	*Pongo*	*p*	*Papio*	*p*
Homo	-									
Pan	***Pan>Homo***	**0.000**	-							
Gorilla	***Gorilla>Homo***	**0.000**	*Gorilla>Pan*	0.133	-					
Pongo	***Pongo>Homo***	**0.000**	***Pongo>Pan***	**0.011**	*Pongo>Gorilla*	0.869	-			
Papio	***Papio>Homo***	**0.000**	*Papio>Pan*	0.059	*Papio>Gorilla*	0.998	*Pongo>Papio*	0.962	-	

Table 2. 10: Pairwise comparisons of species, overall in talus.

Overall

Tb.BV/TV	Homo	p	Pan	p	Gorilla	p	Pongo	p	Papio	p
Homo	-									
Pan	**Pan>Homo**	**0.000**	-							
Gorilla	**Gorilla>Homo**	**0.000**	**Pan>Gorilla**	**0.003**	-					
Pongo	**Pongo>Homo**	**0.000**	**Pan>Pongo**	**0.003**	Gorilla>Pongo	1.000	-			
Papio	**Papio>Homo**	**0.000**	**Papio>Pan**	**0.000**	**Papio>Gorilla**	**0.000**	**Papio>Pongo**	**0.000**	-	

Tb.DA	Homo	p	Pan	p	Gorilla	p	Pongo	p	Papio	p
Homo	-									
Pan	**Homo>Pan**	**0.000**	-							
Gorilla	**Homo>Gorilla**	**0.000**	Gorilla>Pan	0.863	-					
Pongo	**Homo>Pongo**	**0.000**	Pan>Pongo	0.265	**Gorilla>Pongo**	**0.049**	-			
Papio	**Homo>Papio**	**0.000**	Pan>Papio	0.549	Gorilla>Papio	0.131	Papio>Pongo	0.975	-	

Tb.I	Homo	p	Pan	p	Gorilla	p	Pongo	p	Papio	p
Homo	-									
Pan	**Homo>Pan**	**0.000**	-							
Gorilla	**Homo>Gorilla**	**0.000**	Gorilla>Pan	0.095	-					
Pongo	**Homo>Pongo**	**0.000**	**Pan>Pongo**	**0.000**	**Gorilla>Pongo**	**0.000**	-			
Papio	**Homo>Papio**	**0.000**	**Pan>Papio**	**0.000**	**Gorilla>Papio**	**0.000**	Papio>Pongo	0.131	-	

Tb.E	Homo	p	Pan	p	Gorilla	p	Pongo	p	Papio	p
Homo	-									
Pan	**Homo>Pan**	**0.000**	-							
Gorilla	**Homo>Gorilla**	**0.000**	Gorilla>Pan	0.496	-					
Pongo	**Homo>Pongo**	**0.000**	Pan>Pongo	0.127	**Gorilla>Pongo**	**0.003**	-			
Papio	**Homo>Papio**	**0.000**	Pan>Papio	0.376	**Gorilla>Papio**	**0.012**	Papio>Pongo	0.955	-	

Tb.Th	Homo	p	Pan	p	Gorilla	p	Pongo	p	Papio	p
Homo	-									
Pan	**Pan>Homo**	**0.000**	-							
Gorilla	**Gorilla>Homo**	**0.000**	Gorilla>Pan	0.814	-					
Pongo	Pongo>Homo	0.077	**Pan>Pongo**	**0.000**	**Gorilla>Pongo**	**0.000**	-			
Papio	**Papio>Homo**	**0.000**	**Papio>Pan**	**0.000**	**Papio>Gorilla**	**0.000**	**Papio>Pongo**	**0.000**	-	

Tb.N	Homo	p	Pan	p	Gorilla	p	Pongo	p	Papio	p
Homo	-									
Pan	Homo>Pan	0.333	-							
Gorilla	**Homo>Gorilla**	**0.001**	Pan>Gorilla	0.109	-					
Pongo	Homo>Pongo	0.230	Pan>Pongo	0.994	Pongo>Gorilla	0.367	-			
Papio	**Homo>Papio**	**0.000**	**Pan>Papio**	**0.000**	**Gorilla>Papio**	**0.000**	**Pongo>Papio**	**0.000**	-	

Sc.%HighDen	Homo	p	Pan	p	Gorilla	p	Pongo	p	Papio	p
Homo	-									
Pan	**Pan>Homo**	**0.000**	-							
Gorilla	Gorilla>Homo	0.591	**Pan>Gorilla**	**0.000**	-					
Pongo	Pongo>Homo	0.070	**Pan>Pongo**	**0.027**	Pongo>Gorilla	0.790	-			
Papio	**Papio>Homo**	**0.000**	**Papio>Pan**	**0.026**	**Papio>Gorilla**	**0.000**	**Papio>Pongo**	**0.000**	-	

Sc.MeanHoun	Homo	p	Pan	p	Gorilla	p	Pongo	p	Papio	p
Homo	-									
Pan	Homo>Pan	0.255	-							
Gorilla	**Homo>Gorilla**	**0.022**	Pan>Gorilla	0.745	-					
Pongo	Homo>Pongo	0.057	Pan>Pongo	0.896	Pongo>Gorilla	0.999	-			
Papio	Homo>Papio	0.979	Papio>Pan	0.592	Papio>Gorilla	0.089	Papio>Pongo	0.188	-	

Sc.Th	Homo	p	Pan	p	Gorilla	p	Pongo	p	Papio	p
Homo	-									
Pan	**Pan>Homo**	**0.000**	-							
Gorilla	**Gorilla>Homo**	**0.000**	Gorilla>Pan	0.908	-					
Pongo	**Pongo>Homo**	**0.001**	**Pan>Pongo**	**0.003**	**Gorilla>Pongo**	**0.000**	-			
Papio	**Papio>Homo**	**0.035**	**Pan>Papio**	**0.000**	**Gorilla>Papio**	**0.000**	Pongo>Papio	0.617	-	

Table 2. 11: Pairwise comparisons of species, by region of distal tibia

a. ROI A1

Tb.BV/TV	Homo	p	Pan	p	Gorilla	p	Pongo	p	Papio	p
Homo	-									
Pan	**Pan>Homo**	**0.000**	-							
Gorilla	**Gorilla>Homo**	**0.000**	Pan>Gorilla	0.887	-					
Pongo	**Pongo>Homo**	**0.000**	**Pongo>Pan**	**0.016**	**Pongo>Gorilla**	**0.002**	-			
Papio	**Papio>Homo**	**0.000**	**Papio>Pan**	**0.000**	**Papio>Gorilla**	**0.000**	Papio>Pongo	0.444	-	

Tb.DA	Homo	p	Pan	p	Gorilla	p	Pongo	p	Papio	p
Homo	-									
Pan	Homo>Pan	0.350	-							
Gorilla	Gorilla>Homo	0.991	Gorilla>Pan	0.153	-					
Pongo	Homo>Pongo	0.631	Pongo>Pan	0.999	Gorilla>Pongo	0.375	-			
Papio	**Homo>Papio**	**0.012**	Pan>Papio	0.484	**Gorilla>Papio**	**0.003**	Pongo>Papio	0.433	-	

Tb.I	Homo	p	Pan	p	Gorilla	p	Pongo	p	Papio	p
Homo	-									
Pan	Pan>Homo	0.456	-							
Gorilla	Gorilla>Homo	0.996	Pan>Gorilla	0.719	-					
Pongo	Pongo>Homo	0.453	Pongo>Pan	1.000	Pongo>Gorilla	0.688	-			
Papio	**Papio>Homo**	0.000	**Papio>Pan**	0.023	**Papio>Gorilla**	0.001	Papio>Pongo	0.086	-	

Tb.E	Homo	p	Pan	p	Gorilla	p	Pongo	p	Papio	p
Homo	-									
Pan	**Homo>Pan**	**0.002**	-							
Gorilla	Homo>Gorilla	0.088	Gorilla>Pan	0.816	-					
Pongo	**Homo>Pongo**	**0.001**	Pan>Pongo	0.969	Gorilla>Pongo	0.522	-			
Papio	**Homo>Papio**	**0.000**	**Pan>Papio**	**0.006**	**Gorilla>Papio**	**0.000**	**Pongo>Papio**	**0.086**	-	

Tb.Th	Homo	p	Pan	p	Gorilla	p	Pongo	p	Papio	p
Homo	-									
Pan	Homo>Pan	0.902	-							
Gorilla	Gorilla>Homo	0.153	**Gorilla>Pan**	**0.013**	-					
Pongo	Pongo>Homo	0.058	**Pongo>Pan**	**0.004**	Pongo>Gorilla	0.983	-			
Papio	Papio>Homo	0.080	**Papio>Pan**	**0.005**	Papio>Gorilla	0.998	Pongo>Papio	0.999	-	

Tb.N	Homo	p	Pan	p	Gorilla	p	Pongo	p	Papio	p
Homo	-									
Pan	**Pan>Homo**	**0.000**	-							
Gorilla	Gorilla>Homo	0.407	**Pan>Gorilla**	**0.000**	-					
Pongo	Pongo>Homo	1.000	**Pan>Pongo**	**0.000**	Gorilla>Pongo	0.495	-			
Papio	**Papio>Homo**	**0.001**	**Pan>Papio**	**0.004**	Papio>Gorilla	0.140	**Papio>Pongo**	**0.002**	-	

Sc.%HighDen	Homo	p	Pan	p	Gorilla	p	Pongo	p	Papio	p
Homo	-									
Pan	Pan>Homo	0.959	-							
Gorilla	Gorilla>Homo	0.951	Gorilla>Pan	1.000	-					
Pongo	**Pongo>Homo**	**0.000**	**Pongo>Pan**	**0.002**	**Pongo>Gorilla**	**0.004**	-			
Papio	**Papio>Homo**	**0.000**	**Papio>Pan**	**0.000**	**Papio>Gorilla**	**0.000**	Papio>Pongo	0.447	-	

Sc.MeanHoun	Homo	p	Pan	p	Gorilla	p	Pongo	p	Papio	p
Homo	-									
Pan	Homo>Pan	1.000	-							
Gorilla	Homo>Gorilla	0.999	Pan>Gorilla	1.000	-					
Pongo	**Pongo>Homo**	**0.048**	**Pongo>Pan**	**0.021**	**Pongo>Gorilla**	**0.029**	-			
Papio	Papio>Homo	0.093	**Papio>Pan**	**0.043**	Papio>Gorilla	0.057	Pongo>Papio	0.995	-	

Sc.Th	Homo	p	Pan	p	Gorilla	p	Pongo	p	Papio	p
Homo	-									
Pan	**Pan>Homo**	**0.000**	-							
Gorilla	**Gorilla>Homo**	**0.000**	Gorilla>Pan	0.479	-					
Pongo	**Pongo>Homo**	**0.000**	**Pongo>Pan**	**0.000**	**Pongo>Gorilla**	**0.007**	-			
Papio	**Papio>Homo**	**0.000**	Papio>Pan	0.285	Papio>Gorilla	0.998	**Pongo>Papio**	**0.018**	-	

b. ROI A2

Tb.BV/TV	Homo	p	Pan	p	Gorilla	p	Pongo	p	Papio	p
Homo	-									
Pan	**Pan>Homo**	**0.000**								
Gorilla	**Gorilla>Homo**	**0.006**	Pan>Gorilla	0.366						
Pongo	**Pongo>Homo**	**0.000**	Pongo>Pan	0.941	Pongo>Gorilla	0.139				
Papio	**Papio>Homo**	**0.000**	**Papio>Pan**	**0.000**	**Papio>Gorilla**	**0.000**	**Papio>Pongo**	**0.001**		

Tb.DA	Homo	p	Pan	p	Gorilla	p	Pongo	p	Papio	p
Homo	-									
Pan	Homo>Pan	0.922								
Gorilla	Gorilla>Homo	0.815	Gorilla>Pan	0.301						
Pongo	**Pongo>Homo**	**0.021**	**Pongo>Pan**	**0.001**	Pongo>Gorilla	0.252				
Papio	Homo>Papio	0.254	Pan>Papio	0.674	**Gorilla>Papio**	**0.023**	**Pongo>Papio**	**0.000**		

Tb.I	Homo	p	Pan	p	Gorilla	p	Pongo	p	Papio	p
Homo	-									
Pan	Pan>Homo	0.817	-							
Gorilla	Homo>Gorilla	0.601	Pan>Gorilla	0.085	-					
Pongo	Homo>Pongo	0.116	**Pan>Pongo**	0.006	Gorilla>Pongo	0.831	-			
Papio	**Papio>Homo**	0.000	**Papio>Pan**	0.009	**Papio>Gorilla**	0.000	**Papio>Pongo**	0.000	-	

Tb.E	Homo	p	Pan	p	Gorilla	p	Pongo	p	Papio	p
Homo	-									
Pan	Pan>Homo	0.983	-							
Gorilla	Gorilla>Homo	0.759	Gorilla>Pan	0.953	-					
Pongo	Homo>Pongo	0.553	Pan>Pongo	0.236	Gorilla>Pongo	0.077	-			
Papio	**Homo>Papio**	**0.005**	**Pan>Papio**	**0.000**	**Gorilla>Papio**	**0.000**	Pongo>Papio	0.345	-	

Tb.Th	Homo	p	Pan	p	Gorilla	p	Pongo	p	Papio	p
Homo	-									
Pan	Homo>Pan	0.997	-							
Gorilla	Homo>Gorilla	0.667	Pan>Gorilla	0.815	-					
Pongo	Pongo>Homo	0.658	Pongo>Pan	0.430	Pongo>Gorilla	0.081	-			
Papio	**Papio>Homo**	**0.006**	**Papio>Pan**	**0.001**	**Papio>Gorilla**	**0.000**	Papio>Pongo	0.283	-	

Tb.N	Homo	p	Pan	p	Gorilla	p	Pongo	p	Papio	p
Homo	-									
Pan	**Pan>Homo**	**0.000**	-							
Gorilla	**Gorilla>Homo**	**0.016**	**Pan>Gorilla**	**0.035**	-					
Pongo	Pongo>Homo	0.985	**Pan>Pongo**	**0.000**	Gorilla>Pongo	0.103	-			
Papio	Papio>Homo	0.750	**Pan>Papio**	**0.000**	Gorilla>Papio	0.287	Papio>Pongo	0.973	-	

Sc.%HighDen	Homo	p	Pan	p	Gorilla	p	Pongo	p	Papio	p
Homo	-									
Pan	Pan>Homo	0.655	-							
Gorilla	Gorilla>Homo	0.998	Pan>Gorilla	0.850	-					
Pongo	Pongo>Homo	0.494	Pongo>Pan	0.994	Pongo>Gorilla	0.692	-			
Papio	**Papio>Homo**	**0.000**	**Papio>Pan**	**0.000**	**Papio>Gorilla**	**0.000**	**Papio>Pongo**	**0.001**	-	

Sc.MeanHoun	Homo	p	Pan	p	Gorilla	p	Pongo	p	Papio	p
Homo	-									
Pan	Pan>Homo	0.977	-							
Gorilla	Homo>Gorilla	0.999	Pan>Gorilla	0.909	-					
Pongo	**Pongo>Homo**	**0.012**	**Pongo>Pan**	**0.038**	**Pongo>Gorilla**	**0.006**	-			
Papio	**Papio>Homo**	**0.001**	**Papio>Pan**	**0.003**	**Papio>Gorilla**	**0.000**	Papio>Pongo	0.968	-	

Sc.Th	Homo	p	Pan	p	Gorilla	p	Pongo	p	Papio	p
Homo	-									
Pan	**Pan>Homo**	**0.029**	-							
Gorilla	**Gorilla>Homo**	**0.000**	Gorilla>Pan	0.470	-					
Pongo	**Pongo>Homo**	**0.000**	**Pongo>Pan**	**0.000**	**Pongo>Gorilla**	**0.005**	-			
Papio	**Papio>Homo**	**0.000**	Papio>Pan	0.128	Papio>Gorilla	0.957	**Pongo>Papio**	**0.036**	-	

c. ROI A3

Tb.BV/TV	Homo	p	Pan	p	Gorilla	p	Pongo	p	Papio	p
Homo	-									
Pan	**Pan>Homo**	**0.000**	-							
Gorilla	**Gorilla>Homo**	**0.000**	Gorilla>Pan	0.984	-					
Pongo	**Pongo>Homo**	**0.000**	Pan>Pongo	0.205	Gorilla>Pongo	0.096	-			
Papio	**Papio>Homo**	**0.000**	**Papio>Pan**	**0.000**	**Papio>Gorilla**	**0.003**	**Papio>Pongo**	**0.000**	-	

Tb.DA	Homo	p	Pan	p	Gorilla	p	Pongo	p	Papio	p
Homo	-									
Pan	**Homo>Pan**	**0.017**	-							
Gorilla	**Homo>Gorilla**	**0.043**	Gorilla>Pan	1.000	-					
Pongo	Homo>Pongo	0.338	Pongo>Pan	0.849	Pongo>Gorilla	0.925	-			
Papio	**Homo>Papio**	**0.002**	Pan>Papio	0.915	Gorilla>Papio	0.877	Pongo>Papio	0.429	-	

Tb.I	Homo	p	Pan	p	Gorilla	p	Pongo	p	Papio	p
Homo	-									
Pan	Pan>Homo	0.0501	-							
Gorilla	Gorilla>Homo	0.1311	Pan>Gorilla	0.9991	-					
Pongo	Pongo>Homo	0.5769	Pan>Pongo	0.8326	Gorilla>Pongo	0.9393	-			
Papio	**Papio>Homo**	0.0025	Papio>Pan	0.7323	Papio>Gorilla	0.6311	Papio>Pongo	0.2321	-	

Tb.E	Homo	p	Pan	p	Gorilla	p	Pongo	p	Papio	p
Homo	-									
Pan	Homo>Pan	0.576	-							
Gorilla	**Homo>Gorilla**	**0.005**	Pan>Gorilla	0.151	-					
Pongo	Homo>Pongo	0.687	Pongo>Pan	1.000	Pongo>Gorilla	0.236	-			
Papio	Homo>Papio	0.342	Pan>Papio	0.987	Papio>Gorilla	0.433	Pongo>Papio	0.991	-	

Tb.Th	Homo	p	Pan	p	Gorilla	p	Pongo	p	Papio	p
Homo	-									
Pan	Homo>Pan	0.345	-							
Gorilla	**Gorilla>Homo**	**0.036**	**Gorilla>Pan**	**0.000**	-					
Pongo	Pongo>Homo	0.979	Pongo>Pan	0.148	Gorilla>Pongo	0.201	-			
Papio	**Papio>Homo**	**0.000**	**Papio>Pan**	**0.000**	Papio>Gorilla	0.267	**Papio>Pongo**	**0.001**	-	

Tb.N	Homo	p	Pan	p	Gorilla	p	Pongo	p	Papio	p
Homo	-									
Pan	**Pan>Homo**	**0.000**	-							
Gorilla	**Gorilla>Homo**	**0.000**	**Pan>Gorilla**	**0.001**	-					
Pongo	**Pongo>Homo**	**0.001**	**Pan>Pongo**	**0.000**	Gorilla>Pongo	0.855	-			
Papio	Papio>Homo	0.056	**Pan>Papio**	**0.000**	Gorilla>Papio	0.095	Pongo>Papio	0.629	-	

Sc.%HighDen	Homo	p	Pan	p	Gorilla	p	Pongo	p	Papio	p
Homo	-									
Pan	**Pan>Homo**	**0.002**	-							
Gorilla	Gorilla>Homo	0.921	**Pan>Gorilla**	**0.040**	-					
Pongo	**Pongo>Homo**	**0.000**	Pongo>Pan	0.894	**Pongo>Gorilla**	**0.008**	-			
Papio	**Papio>Homo**	**0.005**	Papio>Pan	1.000	Papio>Gorilla	0.061	Pongo>Papio	0.912	-	

Sc.MeanHoun	Homo	p	Pan	p	Gorilla	p	Pongo	p	Papio	p
Homo	-									
Pan	Pan>Homo	0.227	-							
Gorilla	Homo>Gorilla	0.991	Pan>Gorilla	0.090	-					
Pongo	Pongo>Homo	0.799	Pan>Pongo	0.931	Pongo>Gorilla	0.550	-			
Papio	Papio>Homo	0.162	Papio>Pan	0.998	Papio>Gorilla	0.063	Papio>Pongo	0.837	-	

Sc.Th	Homo	p	Pan	p	Gorilla	p	Pongo	p	Papio	p
Homo	-									
Pan	**Pan>Homo**	**0.000**	-							
Gorilla	**Gorilla>Homo**	**0.000**	Pan>Gorilla	0.929	-					
Pongo	**Pongo>Homo**	**0.001**	Pan>Pongo	0.470	Gorilla>Pongo	0.916	-			
Papio	Papio>Homo	0.246	**Pan>Papio**	**0.001**	**Gorilla>Papio**	**0.023**	Pongo>Papio	0.235	-	

d. ROI B1

Tb.BV/TV	Homo	p	Pan	p	Gorilla	p	Pongo	p	Papio	p
Homo	-									
Pan	**Pan>Homo**	**0.002**	-							
Gorilla	Gorilla>Homo	0.580	Pan>Gorilla	0.182	-					
Pongo	Pongo>Homo	0.423	Pan>Pongo	0.404	Pongo>Gorilla	0.998	-			
Papio	**Papio>Homo**	**0.000**	**Papio>Pan**	**0.000**	**Papio>Gorilla**	**0.000**	**Papio>Pongo**	**0.000**	-	

Tb.DA	Homo	p	Pan	p	Gorilla	p	Pongo	p	Papio	p
Homo	-									
Pan	**Homo>Pan**	**0.000**	-							
Gorilla	**Homo>Gorilla**	**0.001**	Gorilla>Pan	1.000	-					
Pongo	**Homo>Pongo**	**0.000**	Pan>Pongo	0.998	Gorilla>Pongo	0.994	-			
Papio	**Homo>Papio**	**0.000**	Pan>Papio	0.291	Gorilla>Papio	0.289	Pongo>Papio	0.589	-	

Tb.I	Homo	p	Pan	p	Gorilla	p	Pongo	p	Papio	p
Homo	-									
Pan	Pan>Homo	0.312	-							
Gorilla	Gorilla>Homo	0.147	Gorilla>Pan	0.983	-					
Pongo	**Pongo>Homo**	0.002	Pongo>Pan	0.183	Pongo>Gorilla	0.490	-			
Papio	**Papio>Homo**	0.000	Papio>Pan	0.053	Papio>Gorilla	0.234	Papio>Pongo	0.996	-	

Tb.E	Homo	p	Pan	p	Gorilla	p	Pongo	p	Papio	p
Homo	-									
Pan	Pan>Homo	1.000	-							
Gorilla	Homo>Gorilla	0.999	Pan>Gorilla	0.997	-					
Pongo	Homo>Pongo	0.263	Pan>Pongo	0.213	Gorilla>Pongo	0.418	-			
Papio	Homo>Papio	0.124	Pan>Papio	0.090	Gorilla>Papio	0.233	Pongo>Papio	0.999	-	

Tb.Th	Homo	p	Pan	p	Gorilla	p	Pongo	p	Papio	p
Homo	-									
Pan	**Homo>Pan**	**0.000**	-							
Gorilla	Homo>Gorilla	0.261	**Gorilla>Pan**	**0.038**	-					
Pongo	Homo>Pongo	0.235	Pongo>Pan	0.085	Gorilla>Pongo	1.000	-			
Papio	Homo>Papio	0.194	Papio>Pan	0.058	Gorilla>Papio	1.000	Papio>Pongo	1.000	-	

Tb.N	Homo	p	Pan	p	Gorilla	p	Pongo	p	Papio	p
Homo	-									
Pan	**Pan>Homo**	**0.000**	-							
Gorilla	Gorilla>Homo	0.256	**Pan>Gorilla**	**0.000**	-					
Pongo	Pongo>Homo	0.660	**Pan>Pongo**	**0.000**	Gorilla>Pongo	0.978	-			
Papio	**Papio>Homo**	**0.000**	Pan>Papio	0.701	**Papio>Gorilla**	**0.001**	**Papio>Pongo**	**0.000**	-	

Sc.%HighDen	Homo	p	Pan	p	Gorilla	p	Pongo	p	Papio	p
Homo	-									
Pan	Homo>Pan	0.971	-							
Gorilla	Homo>Gorilla	1.000	Gorilla>Pan	0.987	-					
Pongo	Homo>Pongo	0.971	Pan>Pongo	1.000	Gorilla>Pongo	0.986	-			
Papio	Papio>Homo	0.127	**Papio>Pan**	**0.020**	Papio>Gorilla	0.107	**Papio>Pongo**	**0.042**	-	

Sc.MeanHoun	Homo	p	Pan	p	Gorilla	p	Pongo	p	Papio	p
Homo	-									
Pan	Homo>Pan	0.558	-							
Gorilla	Homo>Gorilla	0.494	Pan>Gorilla	1.000	-					
Pongo	Homo>Pongo	0.958	Pongo>Pan	0.959	Pongo>Gorilla	0.921	-			
Papio	Papio>Homo	0.999	Papio>Pan	0.394	Papio>Gorilla	0.346	Papio>Pongo	0.881	-	

Sc.Th	Homo	p	Pan	p	Gorilla	p	Pongo	p	Papio	p
Homo	-									
Pan	**Pan>Homo**	**0.003**	-							
Gorilla	**Gorilla>Homo**	**0.000**	Gorilla>Pan	0.836	-					
Pongo	**Pongo>Homo**	**0.000**	Gorilla>Pongo	0.313	Pongo>Gorilla	0.899	-			
Papio	**Papio>Homo**	**0.000**	**Gorilla>Papio**	**0.006**	Papio>Gorilla	0.134	Papio>Pongo	0.655	-	

e. ROI B2

Tb.BV/TV	Homo	p	Pan	p	Gorilla	p	Pongo	p	Papio	p
Homo	-									
Pan	Pan>Homo	0.063								
Gorilla	Gorilla>Homo	0.852	Pan>Gorilla	0.503						
Pongo	Pongo>Homo	1.000	Pan>Pongo	0.111	Gorilla>Pongo	0.897				
Papio	**Papio>Homo**	**0.000**	**Papio>Pan**	**0.000**	**Papio>Gorilla**	**0.000**	**Papio>Pongo**	**0.000**		

Tb.DA	Homo	p	Pan	p	Gorilla	p	Pongo	p	Papio	p
Homo	-									
Pan	**Homo>Pan**	**0.035**								
Gorilla	Homo>Gorilla	0.488	Gorilla>Pan	0.761						
Pongo	**Homo>Pongo**	**0.000**	Pan>Pongo	0.091	**Gorilla>Pongo**	**0.007**				
Papio	**Homo>Papio**	**0.000**	**Pan>Papio**	**0.010**	**Gorilla>Papio**	**0.000**	Pongo>Papio	0.976		

Tb.I	Homo	p	Pan	p	Gorilla	p	Pongo	p	Papio	p
Homo	-									
Pan	Pan>Homo	0.136	-							
Gorilla	Gorilla>Homo	0.510	Pan>Gorilla	0.964	-					
Pongo	**Pongo>Homo**	0.000	**Pongo>Pan**	0.015	**Pongo>Gorilla**	0.004	-			
Papio	**Papio>Homo**	0.000	**Papio>Pan**	0.000	**Papio>Gorilla**	0.000	Papio>Pongo	0.519	-	

Tb.E	Homo	p	Pan	p	Gorilla	p	Pongo	p	Papio	p
Homo	-									
Pan	**Homo>Pan**	**0.003**								
Gorilla	**Homo>Gorilla**	**0.005**	Pan>Gorilla	1.000						
Pongo	**Homo>Pongo**	**0.000**	**Pan>Pongo**	**0.031**	Gorilla>Pongo	0.057				
Papio	**Homo>Papio**	**0.000**	**Pan>Papio**	**0.000**	**Gorilla>Papio**	**0.001**	Pongo>Papio	0.686		

Tb.Th	Homo	p	Pan	p	Gorilla	p	Pongo	p	Papio	p
Homo	-									
Pan	**Homo>Pan**	**0.000**	-							
Gorilla	Homo>Gorilla	0.280	Gorilla>Pan	0.109	-					
Pongo	Homo>Pongo	0.746	**Pongo>Pan**	**0.026**	Pongo>Gorilla	0.962	-			
Papio	**Papio>Homo**	**0.000**	**Papio>Pan**	**0.000**	**Papio>Gorilla**	**0.000**	**Papio>Pongo**	**0.000**	-	

Tb.N	Homo	p	Pan	p	Gorilla	p	Pongo	p	Papio	p
Homo	-									
Pan	**Pan>Homo**	**0.000**	-							
Gorilla	**Gorilla>Homo**	**0.025**	**Pan>Gorilla**	**0.001**	-					
Pongo	Pongo>Homo	1.000	**Pan>Pongo**	**0.000**	**Gorilla>Pongo**	**0.047**	-			
Papio	Papio>Homo	0.972	**Pan>Papio**	**0.000**	Gorilla>Papio	0.126	Papio>Pongo	0.983	-	

Sc.%HighDen	Homo	p	Pan	p	Gorilla	p	Pongo	p	Papio	p
Homo	-									
Pan	Homo>Pan	0.544	-							
Gorilla	Homo>Gorilla	0.648	Gorilla>Pan	1.000	-					
Pongo	Pongo>Homo	0.842	Pongo>Pan	0.101	Pongo>Gorilla	0.156	-			
Papio	Homo>Papio	0.658	Papio>Pan	1.000	Papio>Gorilla	1.000	Pongo>Papio	0.160	-	

Sc.MeanHoun	Homo	p	Pan	p	Gorilla	p	Pongo	p	Papio	p
Homo	-									
Pan	Homo>Pan	0.994	-							
Gorilla	Homo>Gorilla	0.998	Gorilla>Pan	1.000	-					
Pongo	Pongo>Homo	0.942	Gorilla>Pongo	0.773	Pongo>Gorilla	0.839	-			
Papio	**Papio>Homo**	**0.041**	**Gorilla>Papio**	**0.009**	**Papio>Gorilla**	**0.020**	Papio>Pongo	0.304	-	

Sc.Th	Homo	p	Pan	p	Gorilla	p	Pongo	p	Papio	p
Homo	-									
Pan	**Pan>Homo**	**0.010**	-							
Gorilla	**Gorilla>Homo**	**0.004**	Gorilla>Pan	0.981	-					
Pongo	Pongo>Homo	0.171	Pan>Pongo	0.935	Gorilla>Pongo	0.731	-			
Papio	**Papio>Homo**	**0.000**	Papio>Pan	0.298	Papio>Gorilla	0.680	Papio>Pongo	0.103	-	

f. ROI B3

Tb.BV/TV	Homo	p	Pan	p	Gorilla	p	Pongo	p	Papio	p
Homo	-									
Pan	Pan>Homo	0.089	-							
Gorilla	Gorilla>Homo	0.691	Pan>Gorilla	0.781	-					
Pongo	Homo>Pongo	0.847	**Pan>Pongo**	**0.008**	Gorilla>Pongo	0.181	-			
Papio	**Papio>Homo**	**0.000**	**Papio>Pan**	**0.002**	**Papio>Gorilla**	**0.000**	**Papio>Pongo**	**0.000**	-	

Tb.DA	Homo	p	Pan	p	Gorilla	p	Pongo	p	Papio	p
Homo	-									
Pan	Homo>Pan	0.074	-							
Gorilla	**Homo>Gorilla**	**0.036**	Pan>Gorilla	0.990	-					
Pongo	Homo>Pongo	0.723	Pongo>Pan	0.783	Pongo>Gorilla	0.566	-			
Papio	**Homo>Papio**	**0.006**	Pan>Papio	0.809	Gorilla>Papio	0.976	Pongo>Papio	0.247	-	

Tb.I	Homo	p	Pan	p	Gorilla	p	Pongo	p	Papio	p
Homo	-									
Pan	Pan>Homo	0.746	-							
Gorilla	Gorilla>Homo	0.370	Gorilla>Pan	0.953	-					
Pongo	Pongo>Homo	0.422	Pongo>Pan	0.961	Pongo>Gorilla	1.000	-			
Papio	**Papio>Homo**	0.011	Papio>Pan	0.153	Papio>Gorilla	0.565	Papio>Pongo	0.615	-	

Tb.E	Homo	p	Pan	p	Gorilla	p	Pongo	p	Papio	p
Homo	-									
Pan	Homo>Pan	0.575	-							
Gorilla	Homo>Gorilla	0.189	Pan>Gorilla	0.915	-					
Pongo	**Homo>Pongo**	**0.003**	Pan>Pongo	0.105	Gorilla>Pongo	0.507	-			
Papio	**Homo>Papio**	**0.000**	**Pan>Papio**	**0.015**	Gorilla>Papio	0.178	Pongo>Papio	0.984	-	

Tb.Th	Homo	p	Pan	p	Gorilla	p	Pongo	p	Papio	p
Homo	-									
Pan	**Homo>Pan**	**0.000**	-							
Gorilla	Homo>Gorilla	0.565	**Gorilla>Pan**	**0.025**	-					
Pongo	Homo>Pongo	0.486	Pongo>Pan	0.067	Gorilla>Pongo	1.000	-			
Papio	Papio>Homo	0.092	**Papio>Pan**	**0.000**	**Papio>Gorilla**	**0.001**	**Papio>Pongo**	**0.001**	-	

Tb.N	Homo	p	Pan	p	Gorilla	p	Pongo	p	Papio	p
Homo	-									
Pan	**Pan>Homo**	**0.000**	-							
Gorilla	Gorilla>Homo	0.156	**Pan>Gorilla**	**0.038**	-					
Pongo	Homo>Pongo	1.000	**Pan>Pongo**	**0.000**	Gorilla>Pongo	0.175	-			
Papio	Papio>Homo	0.756	**Pan>Papio**	**0.001**	Gorilla>Papio	0.811	Papio>Pongo	0.748	-	

Sc.%HighDen	Homo	p	Pan	p	Gorilla	p	Pongo	p	Papio	p
Homo	-									
Pan	**Pan>Homo**	**0.039**	-							
Gorilla	Gorilla>Homo	0.078	Pan>Gorilla	1.000	-					
Pongo	**Pongo>Homo**	**0.007**	Pongo>Pan	0.873	Pongo>Gorilla	0.853	-			
Papio	Papio>Homo	0.995	Pan>Papio	0.116	Gorilla>Papio	0.192	**Pongo>Papio**	**0.022**	-	

Sc.MeanHoun	Homo	p	Pan	p	Gorilla	p	Pongo	p	Papio	p
Homo	-									
Pan	Homo>Pan	1.000	-							
Gorilla	Homo>Gorilla	0.999	Pan>Gorilla	0.999	-					
Pongo	Pongo>Homo	0.956	Pongo>Pan	0.945	Pongo>Gorilla	0.873	-			
Papio	Papio>Homo	0.997	Papio>Pan	0.995	Papio>Gorilla	0.972	Pongo>Papio	0.996	-	

Sc.Th	Homo	p	Pan	p	Gorilla	p	Pongo	p	Papio	p
Homo	-									
Pan	**Pan>Homo**	**0.008**	-							
Gorilla	**Gorilla>Homo**	**0.006**	Gorilla>Pan	0.997	-					
Pongo	Pongo>Homo	0.361	Pan>Pongo	0.696	Gorilla>Pongo	0.554	-			
Papio	**Papio>Homo**	**0.018**	Pan>Papio	1.000	Gorilla>Papio	0.995	Papio>Pongo	0.781	-	

g. ROI C1

Tb.BV/TV	Homo	p	Pan	p	Gorilla	p	Pongo	p	Papio	p
Homo	-									
Pan	**Pan>Homo**	**0.000**	-							
Gorilla	**Gorilla>Homo**	**0.000**	Pan>Gorilla	0.158	-					
Pongo	**Pongo>Homo**	**0.000**	Pan>Pongo	0.344	Pongo>Gorilla	0.999	-			
Papio	**Papio>Homo**	**0.000**	**Papio>Pan**	**0.000**	**Papio>Gorilla**	**0.000**	**Papio>Pongo**	**0.000**	-	

Tb.DA	Homo	p	Pan	p	Gorilla	p	Pongo	p	Papio	p
Homo	-									
Pan	Pan>Homo	0.843	-							
Gorilla	Gorilla>Homo	1.000	Pan>Gorilla	0.858	-					
Pongo	Pongo>Homo	0.996	Pan>Pongo	0.980	Pongo>Gorilla	0.996	-			
Papio	Papio>Homo	0.909	Pan>Papio	1.000	Papio>Gorilla	0.919	Papio>Pongo	0.992	-	

Tb.I	Homo	p	Pan	p	Gorilla	p	Pongo	p	Papio	p
Homo	-									
Pan	Homo>Pan	0.929	-							
Gorilla	Gorilla>Homo	1.000	Gorilla>Pan	0.922	-					
Pongo	Homo>Pongo	0.989	Pongo>Pan	0.999	Gorilla>Pongo	0.987	-			
Papio	Homo>Papio	0.948	Papio>Pan	1.000	Gorilla>Papio	0.942	Pongo>Papio	1.000	-	

Tb.E	Homo	p	Pan	p	Gorilla	p	Pongo	p	Papio	p
Homo	-									
Pan	Homo>Pan	0.998	-							
Gorilla	Homo>Gorilla	0.402	Pan>Gorilla	0.533	-					
Pongo	Homo>Pongo	0.996	Pan>Pongo	1.000	Pongo>Gorilla	0.705	-			
Papio	Homo>Papio	0.096	Pan>Papio	0.141	Gorilla>Papio	0.944	Pongo>Papio	0.280	-	

Tb.Th	Homo	p	Pan	p	Gorilla	p	Pongo	p	Papio	p
Homo	-									
Pan	Homo>Pan	0.591	-							
Gorilla	Gorilla>Homo	0.307	**Gorilla>Pan**	**0.007**	-					
Pongo	Pongo>Homo	0.877	Pongo>Pan	0.141	Gorilla>Pongo	0.905	-			
Papio	Papio>Homo	0.982	Papio>Pan	0.269	Gorilla>Papio	0.651	Pongo>Papio	0.993	-	

Tb.N	Homo	p	Pan	p	Gorilla	p	Pongo	p	Papio	p
Homo	-									
Pan	**Pan>Homo**	**0.000**	-							
Gorilla	Gorilla>Homo	0.970	**Pan>Gorilla**	**0.000**	-					
Pongo	Pongo>Homo	0.795	**Pan>Pongo**	**0.000**	Pongo>Gorilla	0.985	-			
Papio	**Papio>Homo**	**0.000**	Pan>Papio	0.999	**Papio>Gorilla**	**0.000**	**Papio>Pongo**	**0.000**	-	

Sc.%HighDen	Homo	p	Pan	p	Gorilla	p	Pongo	p	Papio	p
Homo	-									
Pan	Homo>Pan	1.000	-							
Gorilla	Gorilla>Homo	0.975	Gorilla>Pan	0.960	-					
Pongo	Homo>Pongo	0.999	Pan>Pongo	1.000	Gorilla>Pongo	0.930	-			
Papio	**Papio>Homo**	**0.001**	**Papio>Pan**	**0.000**	**Papio>Gorilla**	**0.005**	**Papio>Pongo**	**0.001**	-	

Sc.MeanHoun	Homo	p	Pan	p	Gorilla	p	Pongo	p	Papio	p
Homo	-									
Pan	Homo>Pan	0.811	-							
Gorilla	Homo>Gorilla	0.996	Gorilla>Pan	0.956	-					
Pongo	Homo>Pongo	0.999	Pongo>Pan	0.947	Pongo>Gorilla	1.000	-			
Papio	Papio>Homo	0.061	**Papio>Pan**	**0.002**	**Papio>Gorilla**	**0.027**	**Papio>Pongo**	**0.048**	-	

Sc.Th	Homo	p	Pan	p	Gorilla	p	Pongo	p	Papio	p
Homo	-									
Pan	**Pan>Homo**	**0.030**	-							
Gorilla	**Gorilla>Homo**	**0.000**	Gorilla>Pan	0.177	-					
Pongo	**Pongo>Homo**	**0.000**	Pongo>Pan	0.425	Gorilla>Pongo	0.996	-			
Papio	**Papio>Homo**	**0.000**	**Papio>Pan**	**0.002**	Papio>Gorilla	0.571	Papio>Pongo	0.389	-	

h. ROI C2

Tb.BV/TV	Homo	p	Pan	p	Gorilla	p	Pongo	p	Papio	p
Homo	-									
Pan	**Pan>Homo**	**0.000**	-							
Gorilla	**Gorilla>Homo**	**0.001**	Pan>Gorilla	0.155	-					
Pongo	**Pongo>Homo**	**0.000**	Pan>Pongo	0.557	Pongo>Gorilla	0.971	-			
Papio	**Papio>Homo**	**0.000**	**Papio>Pan**	**0.004**	**Papio>Gorilla**	**0.000**	**Papio>Pongo**	**0.000**	-	

Tb.DA	Homo	p	Pan	p	Gorilla	p	Pongo	p	Papio	p
Homo	-									
Pan	Homo>Pan	0.602	-							
Gorilla	Homo>Gorilla	1.000	Gorilla>Pan	0.745	-					
Pongo	Pongo>Homo	0.309	**Pongo>Pan**	**0.010**	Pongo>Gorilla	0.233	-			
Papio	Homo>Papio	0.175	Pan>Papio	0.886	Gorilla>Papio	0.270	**Pongo>Papio**	**0.001**	-	

Tb.I	Homo	p	Pan	p	Gorilla	p	Pongo	p	Papio	p
Homo	-									
Pan	Pan>Homo	0.358	-							
Gorilla	Gorilla>Homo	0.998	Pan>Gorilla	0.576	-					
Pongo	Homo>Pongo	0.940	Pan>Pongo	0.099	Gorilla>Pongo	0.832	-			
Papio	**Papio>Homo**	0.014	Papio>Pan	0.511	**Papio>Gorilla**	0.039	**Papio>Pongo**	0.003	-	

Tb.E	Homo	p	Pan	p	Gorilla	p	Pongo	p	Papio	p
Homo	-									
Pan	Homo>Pan	0.080	-							
Gorilla	Homo>Gorilla	0.828	Gorilla>Pan	0.597	-					
Pongo	Homo>Pongo	0.902	Pongo>Pan	0.570	Pongo>Gorilla	1.000	-			
Papio	**Homo>Papio**	**0.001**	Pan>Papio	0.425	**Gorilla>Papio**	**0.029**	**Pongo>Papio**	**0.032**	-	

Tb.Th	Homo	p	Pan	p	Gorilla	p	Pongo	p	Papio	p
Homo	-									
Pan	Pan>Homo	1.000	-							
Gorilla	Gorilla>Homo	0.966	Gorilla>Pan	0.979	-					
Pongo	Pongo>Homo	0.797	Pongo>Pan	0.828	Pongo>Gorilla	0.988	-			
Papio	Papio>Homo	0.145	Papio>Pan	0.147	Papio>Gorilla	0.467	Papio>Pongo	0.816	-	

Tb.N	Homo	p	Pan	p	Gorilla	p	Pongo	p	Papio	p
Homo	-									
Pan	**Pan>Homo**	**0.000**	-							
Gorilla	Gorilla>Homo	0.199	**Pan>Gorilla**	**0.007**	-					
Pongo	Pongo>Homo	0.963	**Pan>Pongo**	**0.000**	Gorilla>Pongo	0.640	-			
Papio	Papio>Homo	0.586	**Pan>Papio**	**0.001**	Gorilla>Papio	0.956	Papio>Pongo	0.951	-	

Sc.%HighDen	Homo	p	Pan	p	Gorilla	p	Pongo	p	Papio	p
Homo	-									
Pan	Pan>Homo	0.956	-							
Gorilla	Homo>Gorilla	1.000	Pan>Gorilla	0.919	-					
Pongo	Pongo>Homo	1.000	Pan>Pongo	0.986	Pongo>Gorilla	0.999	-			
Papio	**Papio>Homo**	**0.001**	**Papio>Pan**	**0.004**	**Papio>Gorilla**	**0.001**	**Papio>Pongo**	**0.003**	-	

Sc.MeanHoun	Homo	p	Pan	p	Gorilla	p	Pongo	p	Papio	p
Homo	-									
Pan	Pan>Homo	0.508	-							
Gorilla	Gorilla>Homo	1.000	Pan>Gorilla	0.559	-					
Pongo	Pongo>Homo	0.564	Pongo>Pan	1.000	Pongo>Gorilla	0.608	-			
Papio	**Papio>Homo**	**0.000**	**Papio>Pan**	**0.002**	**Papio>Gorilla**	**0.000**	**Papio>Pongo**	**0.010**	-	

Sc.Th	Homo	p	Pan	p	Gorilla	p	Pongo	p	Papio	p
Homo	-									
Pan	**Pan>Homo**	**0.000**	-							
Gorilla	**Gorilla>Homo**	**0.000**	Gorilla>Pan	0.941	-					
Pongo	**Pongo>Homo**	**0.000**	Pongo>Pan	0.949	Pongo>Gorilla	1.000	-			
Papio	**Papio>Homo**	**0.000**	Papio>Pan	0.999	Gorilla>Papio	0.991	Pongo>Papio	0.992	-	

i. ROI C3

Tb.BV/TV	Homo	p	Pan	p	Gorilla	p	Pongo	p	Papio	p
Homo	-									
Pan	**Pan>Homo**	**0.000**	-							
Gorilla	Gorilla>Homo	0.583	**Pan>Gorilla**	**0.004**	-					
Pongo	**Pongo>Homo**	**0.003**	Pan>Pongo	0.869	Pongo>Gorilla	0.136	-			
Papio	**Papio>Homo**	**0.000**	Papio>Pan	0.359	**Papio>Gorilla**	**0.000**	Papio>Pongo	0.087	-	

Tb.DA	Homo	p	Pan	p	Gorilla	p	Pongo	p	Papio	p
Homo	-									
Pan	**Homo>Pan**	**0.015**	-							
Gorilla	Homo>Gorilla	0.289	Gorilla>Pan	0.795	-					
Pongo	Homo>Pongo	0.950	Pongo>Pan	0.170	Pongo>Gorilla	0.789	-			
Papio	Homo>Papio	0.320	Papio>Pan	0.760	Papio>Gorilla	1.000	Pongo>Papio	0.819	-	

Tb.I	Homo	p	Pan	p	Gorilla	p	Pongo	p	Papio	p
Homo	-									
Pan	**Pan>Homo**	0.005	-							
Gorilla	Gorilla>Homo	0.590	Pan>Gorilla	0.284	-					
Pongo	Pongo>Homo	0.600	Pan>Pongo	0.374	Pongo>Gorilla	1.000	-			
Papio	Papio>Homo	0.514	Pan>Papio	0.348	Papio>Gorilla	1.000	Papio>Pongo	1.000	-	

Tb.E	Homo	p	Pan	p	Gorilla	p	Pongo	p	Papio	p
Homo	-									
Pan	Homo>Pan	0.278	-							
Gorilla	Homo>Gorilla	1.000	Gorilla>Pan	0.324	-					
Pongo	Homo>Pongo	0.776	Pongo>Pan	0.966	Gorilla>Pongo	0.813	-			
Papio	Homo>Papio	0.561	Papio>Pan	0.995	Gorilla>Papio	0.611	Pongo>Papio	0.999	-	

Tb.Th	Homo	p	Pan	p	Gorilla	p	Pongo	p	Papio	p
Homo	-									
Pan	Pan>Homo	0.997	-							
Gorilla	Gorilla>Homo	0.540	Gorilla>Pan	0.705	-					
Pongo	**Pongo>Homo**	**0.004**	**Pongo>Pan**	**0.006**	Pongo>Gorilla	0.194	-			
Papio	**Papio>Homo**	**0.001**	**Papio>Pan**	**0.002**	Papio>Gorilla	0.120	Papio>Pongo	1.000	-	

Tb.N	Homo	p	Pan	p	Gorilla	p	Pongo	p	Papio	p
Homo	-									
Pan	**Pan>Homo**	**0.002**	-							
Gorilla	Homo>Gorilla	0.803	**Pan>Gorilla**	**0.000**	-					
Pongo	Homo>Pongo	0.371	**Pan>Pongo**	**0.000**	Gorilla>Pongo	0.942	-			
Papio	Homo>Papio	0.945	**Pan>Papio**	**0.000**	Papio>Gorilla	0.996	Papio>Pongo	0.808	-	

Sc.%HighDen	Homo	p	Pan	p	Gorilla	p	Pongo	p	Papio	p
Homo	-									
Pan	**Pan>Homo**	**0.005**	-							
Gorilla	**Gorilla>Homo**	**0.010**	Pan>Gorilla	1.000	-					
Pongo	Pongo>Homo	0.850	Pan>Pongo	0.162	Gorilla>Pongo	0.212	-			
Papio	**Papio>Homo**	**0.012**	Pan>Papio	1.000	Gorilla>Papio	1.000	Papio>Pongo	0.236	-	

Sc.MeanHoun	Homo	p	Pan	p	Gorilla	p	Pongo	p	Papio	p
Homo	-									
Pan	Pan>Homo	0.099	-							
Gorilla	Gorilla>Homo	0.643	Pan>Gorilla	0.844	-					
Pongo	Pongo>Homo	0.629	Pan>Pongo	0.907	Pongo>Gorilla	1.000	-			
Papio	**Papio>Homo**	**0.036**	Papio>Pan	0.978	Papio>Gorilla	0.559	Papio>Pongo	0.665	-	

Sc.Th	Homo	p	Pan	p	Gorilla	p	Pongo	p	Papio	p
Homo	-									
Pan	**Pan>Homo**	**0.000**	-							
Gorilla	**Gorilla>Homo**	**0.000**	Gorilla>Pan	1.000	-					
Pongo	**Pongo>Homo**	**0.012**	Pan>Pongo	0.931	Gorilla>Pongo	0.928	-			
Papio	Papio>Homo	0.281	Pan>Papio	0.121	Gorilla>Papio	0.146	Pongo>Papio	0.624	-	

Table 2. 12: Pairwise comparisons of species, by region of talus

a. ROI A1

Tb.BV/TV	*Homo*	*p*	*Pan*	*p*	*Gorilla*	*p*	*Pongo*	*p*	*Papio*	*p*
Homo	-									
Pan	***Pan>Homo***	**0.00**	-							
Gorilla	***Gorilla>Homo***	**0.00**	*Pan>Gorilla*	0.64	-					
Pongo	***Pongo>Homo***	**0.00**	*Pongo>Pan*	1.00	*Pongo>Gorilla*	0.61	-			
Papio	***Papio>Homo***	**0.00**	***Papio>Pan***	**0.00**	***Papio>Gorilla***	**0.00**	***Papio>Pongo***	**0.00**	-	

Tb.D	*Homo*	*p*	*Pan*	*p*	*Gorilla*	*p*	*Pongo*	*p*	*Papio*	*p*
Homo	-									
Pan	***Homo>Pan***	**0.00**	-							
Gorilla	***Homo>Gorilla***	**0.00**	*Gorilla>Pan*	0.65	-					
Pongo	***Homo>Pongo***	**0.00**	*Pan>Pongo*	0.41	***Gorilla>Pongo***	**0.04**	-			
Papio	***Homo>Papio***	**0.00**	*Pan>Papio*	0.36	***Gorilla>Papio***	**0.02**	*Papio>Pongo*	1.00	-	

Tb.	*Homo*	*p*	*Pan*	*p*	*Gorilla*	*p*	*Pongo*	*p*	*Papio*	*p*
Homo	-									
Pan	***Pan>Homo***	0.00	-							
Gorilla	***Gorilla>Homo***	0.00	*Pan>Gorilla*	0.16	-					
Pongo	***Pongo>Homo***	0.00	***Pongo>Pan***	0.00	***Pongo>Gorilla***	0.00	-			
Papio	***Papio>Homo***	0.00	***Papio>Pan***	0.00	***Papio>Gorilla***	0.00	*Pongo>Papio*	0.83	-	

Tb.	*Homo*	*p*	*Pan*	*p*	*Gorilla*	*p*	*Pongo*	*p*	*Papio*	*p*
Homo	-									
Pan	***Homo>Pan***	**0.00**	-							
Gorilla	***Homo>Gorilla***	**0.00**	*Gorilla>Pan*	0.86	-					
Pongo	***Homo>Pongo***	**0.00**	*Pongo>Pan*	1.00	*Gorilla>Pongo*	0.93	-			
Papio	***Homo>Papio***	**0.00**	*Pan>Papio*	0.99	*Gorilla>Papio*	0.67	*Pongo>Papio*	0.99	-	

Tb.T	*Homo*	*p*	*Pan*	*p*	*Gorilla*	*p*	*Pongo*	*p*	*Papio*	*p*
Homo	-									
Pan	***Pan>Homo***	**0.00**	-							
Gorilla	***Gorilla>Homo***	**0.00**	*Gorilla>Pan*	0.99	-					
Pongo	*Pongo>Homo*	0.16	*Pan>Pongo*	0.28	*Gorilla>Pongo*	0.20	-			
Papio	***Papio>Homo***	**0.00**	*Papio>Pan*	0.14	*Papio>Gorilla*	0.40	***Papio>Pongo***	**0.00**	-	

Tb.	*Homo*	*p*	*Pan*	*p*	*Gorilla*	*p*	*Pongo*	*p*	*Papio*	*p*
Homo	-									
Pan	*Homo>Pan*	0.75	-							
Gorilla	*Homo>Gorilla*	0.68	*Pan>Gorilla*	0.99	-					
Pongo	*Homo>Pongo*	1.00	*Pongo>Pan*	0.83	*Pongo>Gorilla*	0.76	-			
Papio	***Homo>Papio***	**0.00**	***Pan>Papio***	**0.00**	***Gorilla>Papio***	**0.00**	***Pongo>Papio***	**0.00**	-	

Sc.%HighDen	*Homo*	*p*	*Pan*	*p*	*Gorilla*	*p*	*Pongo*	*p*	*Papio*	*p*
Homo	-									
Pan	***Pan>Homo***	**0.00**	-							
Gorilla	*Gorilla>Homo*	0.71	*Pan>Gorilla*	0.23	-					
Pongo	*Pongo>Homo*	0.09	*Pan>Pongo*	0.95	*Pongo>Gorilla*	0.72	-			
Papio	***Papio>Homo***	**0.00**	*Papio>Pan*	0.60	***Papio>Gorilla***	**0.01**	*Papio>Pongo*	0.29	-	

Sc.MeanHoun	*Homo*	*p*	*Pan*	*p*	*Gorilla*	*p*	*Pongo*	*p*	*Papio*	*p*
Homo	-									
Pan	*Pan>Homo*	0.59	-							
Gorilla	*Gorilla>Homo*	0.99	*Pan>Gorilla*	0.81	-					
Pongo	*Pongo>Homo*	0.33	*Pongo>Pan*	0.97	*Pongo>Gorilla*	0.54	-			
Papio	*Papio>Homo*	0.31	*Papio>Pan*	0.98	*Papio>Gorilla*	0.54	*Pongo>Papio*	1.00	-	

Sc.T	*Homo*	*p*	*Pan*	*p*	*Gorilla*	*p*	*Pongo*	*p*	*Papio*	*p*
Homo	-									
Pan	***Pan>Homo***	**0.00**	-							
Gorilla	***Gorilla>Homo***	**0.00**	*Gorilla>Pan*	0.99	-					
Pongo	***Pongo>Homo***	**0.00**	*Pan>Pongo*	1.00	*Gorilla>Pongo*	0.99	-			
Papio	***Papio>Homo***	**0.00**	***Pan>Papio***	**0.00**	***Gorilla>Papio***	**0.00**	***Pongo>Papio***	**0.03**	-	

b. ROI A2

Tb.BV/TV	Homo	p	Pan	p	Gorilla	p	Pongo	p	Papio	p
Homo	-									
Pan	**Pan>Homo**	**0.001**	-							
Gorilla	**Gorilla>Homo**	**0.007**	Pan>Gorilla	0.996	-					
Pongo	Pongo>Homo	0.126	Pan>Pongo	0.617	Gorilla>Pongo	0.862	-			
Papio	**Papio>Homo**	**0.000**	Papio>Pan	0.144	Papio>Gorilla	0.104	**Papio>Pongo**	**0.007**	-	

Tb.DA	Homo	p	Pan	p	Gorilla	p	Pongo	p	Papio	p
Homo	-									
Pan	**Homo>Pan**	**0.000**	-							
Gorilla	**Homo>Gorilla**	**0.000**	Pan>Gorilla	0.982	-					
Pongo	**Homo>Pongo**	**0.000**	Pan>Pongo	0.927	Gorilla>Pongo	0.999	-			
Papio	**Homo>Papio**	**0.000**	Pan>Papio	0.490	Gorilla>Papio	0.880	Pongo>Papio	0.966	-	

Tb.I	Homo	p	Pan	p	Gorilla	p	Pongo	p	Papio	p
Homo	-									
Pan	**Pan>Homo**	0.000	-							
Gorilla	**Gorilla>Homo**	0.000	Gorilla>Pan	0.503	-					
Pongo	**Pongo>Homo**	0.000	**Pongo>Pan**	0.011	Pongo>Gorilla	0.475	-			
Papio	**Papio>Homo**	0.000	**Papio>Pan**	0.000	**Papio>Gorilla**	0.000	Papio>Pongo	0.089	-	

Tb.E	Homo	p	Pan	p	Gorilla	p	Pongo	p	Papio	p
Homo	-									
Pan	Homo>Pan	0.051	-							
Gorilla	**Homo>Gorilla**	**0.027**	Pan>Gorilla	0.987	-					
Pongo	Homo>Pongo	0.295	Pongo>Pan	0.982	Pongo>Gorilla	0.873	-			
Papio	Homo>Papio	0.068	Papio>Pan	1.000	Papio>Gorilla	0.984	Pongo>Papio	0.988	-	

Tb.Th	Homo	p	Pan	p	Gorilla	p	Pongo	p	Papio	p
Homo	-									
Pan	**Pan>Homo**	**0.016**	-							
Gorilla	**Gorilla>Homo**	**0.011**	Gorilla>Pan	0.992	-					
Pongo	Pongo>Homo	0.903	Pan>Pongo	0.250	Gorilla>Pongo	0.157	-			
Papio	**Papio>Homo**	**0.003**	Papio>Pan	0.962	Papio>Gorilla	1.000	Papio>Pongo	0.078	-	

Tb.N	Homo	p	Pan	p	Gorilla	p	Pongo	p	Papio	p
Homo	-									
Pan	Homo>Pan	0.691	-							
Gorilla	Homo>Gorilla	0.878	Gorilla>Pan	0.999	-					
Pongo	Homo>Pongo	0.899	Pongo>Pan	0.999	Pongo>Gorilla	1.000	-			
Papio	Homo>Papio	0.575	Pan>Papio	0.999	Gorilla>Papio	0.991	Pongo>Papio	0.989	-	

Sc.%HighDen	Homo	p	Pan	p	Gorilla	p	Pongo	p	Papio	p
Homo	-									
Pan	Pan>Homo	0.654	-							
Gorilla	Gorilla>Homo	0.832	Pan>Gorilla	1.000	-					
Pongo	**Pongo>Homo**	**0.003**	Pongo>Pan	0.082	Pongo>Gorilla	0.084	-			
Papio	Homo>Papio	1.000	Pan>Papio	0.635	Gorilla>Papio	0.821	**Pongo>Papio**	**0.003**	-	

Sc.MeanHoun	Homo	p	Pan	p	Gorilla	p	Pongo	p	Papio	p
Homo	-									
Pan	Homo>Pan	0.787	-							
Gorilla	Homo>Gorilla	0.986	Gorilla>Pan	0.983	-					
Pongo	Homo>Pongo	0.995	Pongo>Pan	0.965	Pongo>Gorilla	1.000	-			
Papio	Homo>Papio	0.181	Pan>Papio	0.772	Gorilla>Papio	0.509	Pongo>Papio	0.451	-	

Sc.Th	Homo	p	Pan	p	Gorilla	p	Pongo	p	Papio	p
Homo	-									
Pan	Pan>Homo	0.617	-							
Gorilla	**Gorilla>Homo**	**0.044**	Gorilla>Pan	0.503	-					
Pongo	Pongo>Homo	0.288	Pongo>Pan	0.949	Gorilla>Pongo	0.938	-			
Papio	Homo>Papio	0.790	Pan>Papio	0.077	**Gorilla>Papio**	**0.002**	**Pongo>Papio**	**0.025**	-	

c. ROI A3

Tb.BV/TV	Homo	p	Pan	p	Gorilla	p	Pongo	p	Papio	p
Homo	-									
Pan	Pan>Homo	0.055	-							
Gorilla	Gorilla>Homo	0.109	Pan>Gorilla	1.000	-					
Pongo	Pongo>Homo	0.776	Pan>Pongo	0.659	Gorilla>Pongo	0.749	-			
Papio	**Papio>Homo**	**0.000**	**Papio>Pan**	**0.000**	**Papio>Gorilla**	**0.000**	**Papio>Pongo**	**0.000**	-	

Tb.DA	Homo	p	Pan	p	Gorilla	p	Pongo	p	Papio	p
Homo	-									
Pan	**Homo>Pan**	**0.003**	-							
Gorilla	**Homo>Gorilla**	**0.007**	Pan>Gorilla	1.000	-					
Pongo	**Homo>Pongo**	**0.010**	Pan>Pongo	1.000	Pongo>Gorilla	1.000	-			
Papio	**Homo>Papio**	**0.015**	Papio>Pan	0.993	Papio>Gorilla	0.991	Papio>Pongo	0.993	-	

Tb.I	Homo	p	Pan	p	Gorilla	p	Pongo	p	Papio	p
Homo	-									
Pan	**Pan>Homo**	0.004	-							
Gorilla	**Gorilla>Homo**	0.023	Pan>Gorilla	0.998	-					
Pongo	**Pongo>Homo**	0.012	Pongo>Pan	1.000	Pongo>Gorilla	0.9984	-			
Papio	**Papio>Homo**	0.038	Pan>Papio	0.948	Gorilla>Papio	0.9963	Pongo>Papio	0.964	-	

Tb.E	Homo	p	Pan	p	Gorilla	p	Pongo	p	Papio	p
Homo	-									
Pan	**Homo>Pan**	**0.000**	-							
Gorilla	**Homo>Gorilla**	**0.000**	Pan>Gorilla	1.000	-					
Pongo	**Homo>Pongo**	**0.005**	Pongo>Pan	0.154	Pongo>Gorilla	0.179	-			
Papio	**Homo>Papio**	**0.000**	Pan>Papio	0.986	Gorilla>Papio	0.996	Pongo>Papio	0.061	-	

Tb.Th	Homo	p	Pan	p	Gorilla	p	Pongo	p	Papio	p
Homo	-									
Pan	**Pan>Homo**	**0.030**	-							
Gorilla	**Gorilla>Homo**	**0.004**	Gorilla>Pan	0.870	-					
Pongo	Homo>Pongo	0.999	**Pan>Pongo**	**0.024**	**Gorilla>Pongo**	**0.003**	-			
Papio	**Papio>Homo**	**0.000**	Papio>Pan	0.058	Papio>Gorilla	0.533	**Papio>Pongo**	**0.000**	-	

Tb.N	Homo	p	Pan	p	Gorilla	p	Pongo	p	Papio	p
Homo	-									
Pan	**Homo>Pan**	**0.003**	-							
Gorilla	**Homo>Gorilla**	**0.003**	Pan>Gorilla	0.998	-					
Pongo	Homo>Pongo	0.113	Pongo>Pan	0.870	Pongo>Gorilla	0.772	-			
Papio	**Homo>Papio**	**0.000**	**Pan>Papio**	**0.039**	Gorilla>Papio	0.142	**Pongo>Papio**	**0.006**	-	

Sc.%HighDen	Homo	p	Pan	p	Gorilla	p	Pongo	p	Papio	p
Homo	-									
Pan	**Pan>Homo**	**0.018**	-							
Gorilla	Gorilla>Homo	0.942	Pan>Gorilla	0.182	-					
Pongo	Pongo>Homo	0.993	Pan>Pongo	0.101	Gorilla>Pongo	0.998	-			
Papio	Papio>Homo	1.000	**Pan>Papio**	**0.021**	Gorilla>Papio	0.963	Pongo>Papio	0.997	-	

Sc.MeanHoun	Homo	p	Pan	p	Gorilla	p	Pongo	p	Papio	p
Homo	-									
Pan	Homo>Pan	0.560	-							
Gorilla	Homo>Gorilla	0.769	Gorilla>Pan	0.999	-					
Pongo	**Homo>Pongo**	**0.004**	Pan>Pongo	0.134	Gorilla>Pongo	0.129	-			
Papio	Homo>Papio	0.074	Pan>Papio	0.745	Gorilla>Papio	0.681	Papio>Pongo	0.728	-	

Sc.Th	Homo	p	Pan	p	Gorilla	p	Pongo	p	Papio	p
Homo	-									
Pan	**Pan>Homo**	**0.000**	-							
Gorilla	**Gorilla>Homo**	**0.000**	Gorilla>Pan	0.494	-					
Pongo	Pongo>Homo	0.117	Pan>Pongo	0.584	**Gorilla>Pongo**	**0.047**	-			
Papio	Homo>Papio	0.316	**Pan>Papio**	**0.000**	**Gorilla>Papio**	**0.000**	**Pongo>Papio**	**0.001**	-	

d. ROI B1

Tb.BV/TV	Homo	p	Pan	p	Gorilla	p	Pongo	p	Papio	p
Homo	-									
Pan	**Pan>Homo**	**0.000**	-							
Gorilla	**Gorilla>Homo**	**0.000**	Pan>Gorilla	0.565	-					
Pongo	**Pongo>Homo**	**0.000**	Pan>Pongo	0.085	Gorilla>Pongo	0.842	-			
Papio	**Papio>Homo**	**0.000**	**Papio>Pan**	**0.000**	**Papio>Gorilla**	**0.000**	**Papio>Pongo**	**0.000**	-	

Tb.DA	Homo	p	Pan	p	Gorilla	p	Pongo	p	Papio	p
Homo	-									
Pan	**Homo>Pan**	**0.000**	-							
Gorilla	**Homo>Gorilla**	**0.000**	Gorilla>Pan	0.996	-					
Pongo	**Homo>Pongo**	**0.000**	Pan>Pongo	0.196	Gorilla>Pongo	0.137	-			
Papio	**Homo>Papio**	**0.000**	Pan>Papio	0.384	Gorilla>Papio	0.275	Papio>Pongo	0.983	-	

Tb.I	Homo	p	Pan	p	Gorilla	p	Pongo	p	Papio	p
Homo	-									
Pan	**Pan>Homo**	0.000	-							
Gorilla	**Gorilla>Homo**	0.000	Pan>Gorilla	0.998	-					
Pongo	**Pongo>Homo**	0.000	**Pongo>Pan**	0.000	**Pongo>Gorilla**	0.000	-			
Papio	**Papio>Homo**	0.000	**Papio>Pan**	0.034	**Papio>Gorilla**	0.030	Pongo>Papio	0.461	-	

Tb.E	Homo	p	Pan	p	Gorilla	p	Pongo	p	Papio	p
Homo	-									
Pan	**Homo>Pan**	**0.000**	-							
Gorilla	**Homo>Gorilla**	**0.000**	Gorilla>Pan	0.999	-					
Pongo	**Homo>Pongo**	**0.000**	Pan>Pongo	1.000	Gorilla>Pongo	0.997	-			
Papio	**Homo>Papio**	**0.000**	Papio>Pan	0.612	Papio>Gorilla	0.826	Papio>Pongo	0.631	-	

Tb.Th	Homo	p	Pan	p	Gorilla	p	Pongo	p	Papio	p
Homo	-									
Pan	**Pan>Homo**	**0.001**	-							
Gorilla	**Gorilla>Homo**	**0.002**	Gorilla>Pan	1.000	-					
Pongo	Pongo>Homo	0.874	**Pan>Pongo**	**0.031**	Gorilla>Pongo	0.053	-			
Papio	**Papio>Homo**	**0.000**	**Papio>Pan**	**0.001**	**Papio>Gorilla**	**0.005**	**Papio>Pongo**	**0.000**	-	

Tb.N	Homo	p	Pan	p	Gorilla	p	Pongo	p	Papio	p
Homo	-									
Pan	Homo>Pan	0.124	-							
Gorilla	Homo>Gorilla	0.251	Gorilla>Pan	1.000	-					
Pongo	Homo>Pongo	0.959	Pongo>Pan	0.552	Pongo>Gorilla	0.712	-			
Papio	**Homo>Papio**	**0.000**	**Pan>Papio**	**0.004**	**Gorilla>Papio**	**0.006**	**Pongo>Papio**	**0.000**	-	

Sc.%HighDen	Homo	p	Pan	p	Gorilla	p	Pongo	p	Papio	p
Homo	-									
Pan	**Pan>Homo**	**0.013**	-							
Gorilla	Gorilla>Homo	0.585	Pan>Gorilla	0.509	-					
Pongo	Pongo>Homo	0.974	Pan>Pongo	0.122	Gorilla>Pongo	0.931	-			
Papio	**Papio>Homo**	**0.000**	Papio>Pan	0.505	**Papio>Gorilla**	**0.028**	**Papio>Pongo**	**0.003**	-	

Sc.MeanHoun	Homo	p	Pan	p	Gorilla	p	Pongo	p	Papio	p
Homo	-									
Pan	Pan>Homo	0.996	-							
Gorilla	Homo>Gorilla	0.999	Pan>Gorilla	0.970	-					
Pongo	Homo>Pongo	0.968	Pongo>Pan	0.855	Gorilla>Pongo	0.996	-			
Papio	Papio>Homo	0.752	Papio>Pan	0.904	Papio>Gorilla	0.619	Papio>Pongo	0.402	-	

Sc.Th	Homo	p	Pan	p	Gorilla	p	Pongo	p	Papio	p
Homo	-									
Pan	**Pan>Homo**	**0.000**	-							
Gorilla	**Gorilla>Homo**	**0.000**	Pan>Gorilla	0.993	-					
Pongo	Pongo>Homo	0.107	Pan>Pongo	0.087	Gorilla>Pongo	0.282	-			
Papio	**Papio>Homo**	**0.041**	Pan>Papio	0.074	Gorilla>Papio	0.283	Papio>Pongo	1.000	-	

e. ROI B2

Tb.BV/TV	Homo	p	Pan	p	Gorilla	p	Pongo	p	Papio	p
Homo	-									
Pan	**Pan>Homo**	**0.039**	-							
Gorilla	Gorilla>Homo	0.109	Pan>Gorilla	1.000	-					
Pongo	Pongo>Homo	1.000	Pan>Pongo	0.093	Gorilla>Pongo	0.196	-			
Papio	**Papio>Homo**	**0.000**	**Papio>Pan**	**0.009**	**Papio>Gorilla**	**0.013**	**Papio>Pongo**	**0.000**	-	

Tb.DA	Homo	p	Pan	p	Gorilla	p	Pongo	p	Papio	p
Homo	-									
Pan	**Homo>Pan**	**0.000**	-							
Gorilla	**Homo>Gorilla**	**0.000**	Gorilla>Pan	0.842	-					
Pongo	**Homo>Pongo**	**0.000**	Pongo>Pan	0.995	Gorilla>Pongo	0.978	-			
Papio	**Homo>Papio**	**0.000**	Papio>Pan	1.000	Gorilla>Papio	0.895	Pongo>Papio	0.999	-	

Tb.I	Homo	p	Pan	p	Gorilla	p	Pongo	p	Papio	p
Homo	-									
Pan	**Pan>Homo**	0.000	-							
Gorilla	**Gorilla>Homo**	0.001	Pan>Gorilla	0.124	-					
Pongo	**Pongo>Homo**	0.000	Pongo>Pan	1.000	Pongo>Gorilla	0.192	-			
Papio	**Papio>Homo**	0.000	Pan>Papio	1.000	Papio>Gorilla	0.144	Pongo>Papio	1.000	-	

Tb.E	Homo	p	Pan	p	Gorilla	p	Pongo	p	Papio	p
Homo	-									
Pan	Homo>Pan	1.000	-							
Gorilla	Gorilla>Homo	0.879	Gorilla>Pan	0.810	-					
Pongo	Homo>Pongo	0.362	Pan>Pongo	0.391	Gorilla>Pongo	0.074	-			
Papio	Papio>Homo	1.000	Papio>Pan	1.000	Gorilla>Papio	0.901	Papio>Pongo	0.314	-	

Tb.Th	Homo	p	Pan	p	Gorilla	p	Pongo	p	Papio	p
Homo	-									
Pan	Pan>Homo	0.701	-							
Gorilla	Gorilla>Homo	0.068	Gorilla>Pan	0.536	-					
Pongo	Homo>Pongo	0.998	Pan>Pongo	0.552	**Gorilla>Pongo**	**0.048**	-			
Papio	**Papio>Homo**	**0.000**	**Papio>Pan**	**0.011**	Papio>Gorilla	0.550	**Papio>Pongo**	**0.000**	-	

Tb.N	Homo	p	Pan	p	Gorilla	p	Pongo	p	Papio	p
Homo	-									
Pan	Homo>Pan	0.973	-							
Gorilla	Homo>Gorilla	0.545	Pan>Gorilla	0.849	-					
Pongo	Homo>Pongo	0.655	Pan>Pongo	0.916	Pongo>Gorilla	1.000	-			
Papio	**Homo>Papio**	**0.011**	**Pan>Papio**	**0.043**	Gorilla>Papio	0.494	Pongo>Papio	0.427	-	

Sc.%HighDen	Homo	p	Pan	p	Gorilla	p	Pongo	p	Papio	p
Homo	-									
Pan	Pan>Homo	0.631	-							
Gorilla	Gorilla>Homo	1.000	Pan>Gorilla	0.756	-					
Pongo	Pongo>Homo	0.999	Pan>Pongo	0.833	Pongo>Gorilla	1.000	-			
Papio	Papio>Homo	1.000	Pan>Papio	0.620	Gorilla>Papio	1.000	Pongo>Papio	0.999	-	

Sc.MeanHoun	Homo	p	Pan	p	Gorilla	p	Pongo	p	Papio	p
Homo	-									
Pan	Homo>Pan	0.761	-							
Gorilla	Homo>Gorilla	0.885	Gorilla>Pan	1.000	-					
Pongo	Homo>Pongo	0.595	Pan>Pongo	0.994	Gorilla>Pongo	0.985	-			
Papio	Homo>Papio	0.715	Pan>Papio	1.000	Gorilla>Papio	0.999	Papio>Pongo	0.998	-	

Sc.Th	Homo	p	Pan	p	Gorilla	p	Pongo	p	Papio	p
Homo	-									
Pan	Pan>Homo	0.683	-							
Gorilla	Gorilla>Homo	0.295	Gorilla>Pan	0.934	-					
Pongo	Homo>Pongo	0.795	Pan>Pongo	0.133	**Gorilla>Pongo**	**0.037**	-			
Papio	Papio>Homo	0.944	Pan>Papio	0.981	Gorilla>Papio	0.709	Papio>Pongo	0.363	-	

f. ROI B3

Tb.BV/TV	*Homo*	*p*	*Pan*	*p*	*Gorilla*	*p*	*Pongo*	*p*	*Papio*	*p*
Homo	-									
Pan	***Pan>Homo***	**0.048**	-							
Gorilla	*Gorilla>Homo*	0.640	*Pan>Gorilla*	0.735	-					
Pongo	*Pongo>Homo*	0.574	*Pan>Pongo*	0.824	*Pongo>Gorilla*	1.000	-			
Papio	***Papio>Homo***	**0.000**	***Papio>Pan***	**0.000**	***Papio>Gorilla***	**0.000**	***Papio>Pongo***	**0.000**	-	

Tb.DA	*Homo*	*p*	*Pan*	*p*	*Gorilla*	*p*	*Pongo*	*p*	*Papio*	*p*
Homo	-									
Pan	***Homo>Pan***		-							
Gorilla	***Homo>Gorilla***	**0.000**	*Pan>Gorilla*	1.000	-					
Pongo	***Homo>Pongo***	**0.000**	*Pan>Pongo*	0.408	*Gorilla>Pongo*	0.541	-			
Papio	***Homo>Papio***	**0.000**	*Papio>Pan*	0.941	*Papio>Gorilla*	0.934	*Papio>Pongo*	0.127	-	

Tb.I	*Homo*	*p*	*Pan*	*p*	*Gorilla*	*p*	*Pongo*	*p*	*Papio*	*p*
Homo	-									
Pan	***Pan>Homo***	0.000	-							
Gorilla	***Gorilla>Homo***	0.002	*Pan>Gorilla*	0.995	-					
Pongo	***Pongo>Homo***	0.000	***Pongo>Pan***	0.000	***Pongo>Gorilla***	0.000	-			
Papio	***Papio>Homo***	0.010	*Pan>Papio*	0.730	*Gorilla>Papio*	0.945	***Pongo>Papio***	0.000	-	

Tb.E	*Homo*	*p*	*Pan*	*p*	*Gorilla*	*p*	*Pongo*	*p*	*Papio*	*p*
Homo	-									
Pan	*Homo>Pan*	0.554	-							
Gorilla	*Gorilla>Homo*	0.963	*Gorilla>Pan*	0.220	-					
Pongo	***Homo>Pongo***	**0.000**	***Pan>Pongo***	**0.002**	***Gorilla>Pongo***	**0.000**	-			
Papio	***Homo>Papio***	**0.001**	*Pan>Papio*	0.054	***Gorilla>Papio***	**0.000**	*Papio>Pongo*	0.638	-	

Tb.Th	*Homo*	*p*	*Pan*	*p*	*Gorilla*	*p*	*Pongo*	*p*	*Papio*	*p*
Homo	-									
Pan	*Pan>Homo*	0.230	-							
Gorilla	*Gorilla>Homo*	0.099	*Gorilla>Pan*	0.973	-					
Pongo	*Pongo>Homo*	0.891	*Pan>Pongo*	0.854	*Gorilla>Pongo*	0.580	-			
Papio	***Papio>Homo***	**0.000**	***Papio>Pongo***	**0.000**	***Papio>Gorilla***	**0.000**	***Papio>Pongo***	**0.000**	-	

Tb.N	*Homo*	*p*	*Pan*	*p*	*Gorilla*	*p*	*Pongo*	*p*	*Papio*	*p*
Homo	-									
Pan	*Homo>Pan*	0.631	-							
Gorilla	*Homo>Gorilla*	0.104	*Pan>Gorilla*	0.720	-					
Pongo	*Homo>Pongo*	0.975	*Pongo>Pan*	0.961	*Pongo>Gorilla*	0.406	-			
Papio	***Homo>Papio***	**0.000**	***Pan>Papio***	**0.000**	***Gorilla>Papio***	**0.012**	***Pongo>Papio***	**0.000**	-	

Sc.%HighDen	*Homo*	*p*	*Pan*	*p*	*Gorilla*	*p*	*Pongo*	*p*	*Papio*	*p*
Homo	-									
Pan	*Pan>Homo*	0.987	-							
Gorilla	*Gorilla>Homo*	0.908	*Pan>Gorilla*	0.644	-					
Pongo	*Pongo>Homo*	0.260	*Pan>Pongo*	0.086	*Gorilla>Pongo*	0.789	-			
Papio	*Papio>Homo*	0.818	*Papio>Pan*	0.973	*Papio>Gorilla*	0.326	***Papio>Pongo***	**0.025**	-	

Sc.MeanHoun	*Homo*	*p*	*Pan*	*p*	*Gorilla*	*p*	*Pongo*	*p*	*Papio*	*p*
Homo	-									
Pan	***Homo>Pan***	**0.001**	-							
Gorilla	*Homo>Gorilla*	0.097	*Gorilla>Pan*	0.763	-					
Pongo	***Homo>Pongo***	**0.001**	*Pan>Pongo*	0.973	*Gorilla>Pongo*	0.483	-			
Papio	*Homo>Papio*	0.116	*Papio>Pan*	0.548	*Papio>Gorilla*	0.999	*Papio>Pongo*	0.296	-	

Sc.Th	*Homo*	*p*	*Pan*	*p*	*Gorilla*	*p*	*Pongo*	*p*	*Papio*	*p*
Homo	-									
Pan	*Homo>Pan*	0.406	-							
Gorilla	*Gorilla>Homo*	0.991	*Gorilla>Pan*	0.219	-					
Pongo	***Homo>Pongo***	**0.045**	*Pan>Pongo*	0.691	***Gorilla>Pongo***	**0.020**	-			
Papio	*Homo>Papio*	0.985	*Papio>Pan*	0.725	*Gorilla>Papio*	0.878	*Papio>Pongo*	0.130	-	

g. ROI C1

Tb.BV/TV	Homo	p	Pan	p	Gorilla	p	Pongo	p	Papio	p
Homo	-									
Pan	**Pan>Homo**	**0.000**	-							
Gorilla	**Gorilla>Homo**	**0.001**	**Pan>Gorilla**	**0.010**	-					
Pongo	**Pongo>Homo**	**0.000**	Pan>Pongo	0.284	Pongo>Gorilla	0.735	-			
Papio	**Papio>Homo**	**0.000**	**Papio>Pan**	**0.000**	**Papio>Gorilla**	**0.000**	**Papio>Pongo**	**0.000**	-	

Tb.DA	Homo	p	Pan	p	Gorilla	p	Pongo	p	Papio	p
Homo	-									
Pan	**Homo>Pan**	**0.000**	-							
Gorilla	**Homo>Gorilla**	**0.000**	Gorilla>Pan	1.000	-					
Pongo	**Homo>Pongo**	**0.000**	Pan>Pongo	1.000	Gorilla>Pongo	0.998	-			
Papio	**Homo>Papio**	**0.000**	Pan>Papio	0.192	Gorilla>Papio	0.187	Pongo>Papio	0.369	-	

Tb.I	Homo	p	Pan	p	Gorilla	p	Pongo	p	Papio	p
Homo	-									
Pan	**Pan>Homo**	0.000	-							
Gorilla	**Gorilla>Homo**	0.000	Pan>Gorilla	0.930	-					
Pongo	**Pongo>Homo**	0.000	Pongo>Pan	0.998	Pongo>Gorilla	0.856	-			
Papio	**Papio>Homo**	0.000	**Papio>Pan**	0.005	**Papio>Gorilla**	0.001	**Papio>Pongo**	0.035	-	

Tb.E	Homo	p	Pan	p	Gorilla	p	Pongo	p	Papio	p
Homo	-									
Pan	**Homo>Pan**	**0.000**	-							
Gorilla	**Homo>Gorilla**	**0.000**	Gorilla>Pan	0.239	-					
Pongo	**Homo>Pongo**	**0.000**	Pongo>Pan	0.860	Gorilla>Pongo	0.868	-			
Papio	**Homo>Papio**	**0.000**	Pan>Papio	0.999	Gorilla>Papio	0.174	Pongo>Papio	0.767	-	

Tb.Th	Homo	p	Pan	p	Gorilla	p	Pongo	p	Papio	p
Homo	-									
Pan	Pan>Homo		-							
Gorilla	Gorilla>Homo	0.061	Gorilla>Pan	0.995	-					
Pongo	Pongo>Homo	0.644	Pan>Pongo	0.880	Gorilla>Pongo	0.735	-			
Papio	**Papio>Homo**	**0.000**	**Papio>Pan**	**0.000**	**Papio>Gorilla**	**0.003**	**Papio>Pongo**	**0.000**	-	

Tb.N	Homo	p	Pan	p	Gorilla	p	Pongo	p	Papio	p
Homo	-									
Pan	Pan>Homo	0.298	-							
Gorilla	Homo>Gorilla	1.000	Pan>Gorilla	0.297	-					
Pongo	Pongo>Homo	0.641	Pan>Pongo	0.995	Pongo>Gorilla	0.618	-			
Papio	Homo>Papio	0.883	**Pan>Papio**	**0.033**	Gorilla>Papio	0.935	Pongo>Papio	0.167	-	

Sc.%HighDen	Homo	p	Pan	p	Gorilla	p	Pongo	p	Papio	p
Homo	-									
Pan	Pan>Homo	0.072	-							
Gorilla	Gorilla>Homo	0.992	Pan>Gorilla	0.252	-					
Pongo	Pongo>Homo	1.000	Pan>Pongo	0.155	Gorilla>Pongo	0.999	-			
Papio	**Papio>Homo**	**0.000**	**Papio>Pan**	**0.000**	**Papio>Gorilla**	**0.000**	**Papio>Pongo**	**0.000**	-	

Sc.MeanHoun	Homo	p	Pan	p	Gorilla	p	Pongo	p	Papio	p
Homo	-									
Pan	Homo>Pan	0.999	-							
Gorilla	Homo>Gorilla	0.272	Pan>Gorilla	0.355	-					
Pongo	Homo>Pongo	0.596	Pan>Pongo	0.707	Pongo>Gorilla	0.988	-			
Papio	**Papio>Homo**	**0.039**	**Papio>Pan**	**0.014**	**Papio>Gorilla**	**0.000**	**Papio>Pongo**	**0.001**	-	

Sc.Th	Homo	p	Pan	p	Gorilla	p	Pongo	p	Papio	p
Homo	-									
Pan	**Pan>Homo**	**0.000**	-							
Gorilla	Gorilla>Homo	0.212	Pan>Gorilla	0.259	-					
Pongo	Pongo>Homo	0.398	Pan>Pongo	0.146	Gorilla>Pongo	0.998	-			
Papio	**Papio>Homo**	**0.008**	Pan>Papio	0.869	Papio>Gorilla	0.801	Papio>Pongo	0.617	-	

h. ROI C2

Tb.BV/TV	Homo	p	Pan	p	Gorilla	p	Pongo	p	Papio	p
Homo	-									
Pan	**Pan>Homo**	**0.000**	-							
Gorilla	Gorilla>Homo	0.691	**Pan>Gorilla**	**0.000**	-					
Pongo	Pongo>Homo	0.212	**Pan>Pongo**	**0.009**	Pongo>Gorilla	0.920	-			
Papio	**Papio>Homo**	**0.000**	**Papio>Pan**	**0.000**	**Papio>Gorilla**	**0.000**	**Papio>Pongo**	**0.000**	-	

Tb.DA	Homo	p	Pan	p	Gorilla	p	Pongo	p	Papio	p
Homo	-									
Pan	**Homo>Pan**	**0.000**	-							
Gorilla	**Homo>Gorilla**	**0.000**	Gorilla>Pan	0.752	-					
Pongo	**Homo>Pongo**	**0.000**	Pan>Pongo	0.998	Gorilla>Pongo	0.644	-			
Papio	**Homo>Papio**	**0.000**	Pan>Papio	0.942	Gorilla>Papio	0.346	Pongo>Papio	0.996	-	

Tb.I	Homo	p	Pan	p	Gorilla	p	Pongo	p	Papio	p
Homo	-									
Pan	**Pan>Homo**	0.000	-							
Gorilla	**Gorilla>Homo**	0.004	**Pan>Gorilla**	0.009	-					
Pongo	**Pongo>Homo**	0.000	Pongo>Pan	0.294	**Pongo>Gorilla**	0.000	-			
Papio	**Papio>Homo**	0.000	**Papio>Pan**	0.001	**Papio>Gorilla**	0.000	Papio>Pongo	0.433	-	

Tb.E	Homo	p	Pan	p	Gorilla	p	Pongo	p	Papio	p
Homo	-									
Pan	Homo>Pan	0.968	-							
Gorilla	Homo>Gorilla	1.000	Gorilla>Pan	0.994	-					
Pongo	**Homo>Pongo**	**0.005**	**Pan>Pongo**	**0.019**	**Gorilla>Pongo**	**0.013**	-			
Papio	**Homo>Papio**	**0.001**	**Pan>Papio**	**0.003**	**Gorilla>Papio**	**0.002**	Pongo>Papio	0.999	-	

Tb.Th	Homo	p	Pan	p	Gorilla	p	Pongo	p	Papio	p
Homo	-									
Pan	Pan>Homo	0.611	-							
Gorilla	Gorilla>Homo	0.979	Pan>Gorilla	0.940	-					
Pongo	Pongo>Homo	0.811	Pan>Pongo	1.000	Pongo>Gorilla	0.986	-			
Papio	**Papio>Homo**	**0.000**	**Papio>Pan**	**0.000**	**Papio>Gorilla**	**0.000**	**Papio>Pongo**	**0.000**	-	

Tb.N	Homo	p	Pan	p	Gorilla	p	Pongo	p	Papio	p
Homo	-									
Pan	Pan>Homo	0.636	-							
Gorilla	Homo>Gorilla	0.863	Pan>Gorilla	0.146	-					
Pongo	Homo>Pongo	0.350	**Pan>Pongo**	**0.016**	Gorilla>Pongo	0.912	-			
Papio	**Homo>Papio**	**0.003**	**Pan>Papio**	**0.000**	Gorilla>Papio	0.079	Pongo>Papio	0.473	-	

Sc.%HighDen	Homo	p	Pan	p	Gorilla	p	Pongo	p	Papio	p
Homo	-									
Pan	Pan>Homo	0.374	-							
Gorilla	Gorilla>Homo	1.000	Pan>Gorilla	0.518	-					
Pongo	Pongo>Homo	0.510	Pan>Pongo	1.000	Pongo>Gorilla	0.636	-			
Papio	**Papio>Homo**	**0.000**	**Papio>Pan**	**0.021**	**Papio>Gorilla**	**0.000**	**Papio<Po**	**0.046**	-	

Sc.MeanHoun	Homo	p	Pan	p	Gorilla	p	Pongo	p	Papio	p
Homo	-									
Pan	Homo>Pan	1.000	-							
Gorilla	Homo>Gorilla	0.483	Pan>Gorilla	0.546	-					
Pongo	Pongo>Homo	0.994	Pongo>Pan	0.978	Pongo>Gorilla	0.316	-			
Papio	Papio>Homo	0.976	Papio>Pan	0.934	Papio>Gorilla	0.186	Papio>Pongo	1.000	-	

Sc.Th	Homo	p	Pan	p	Gorilla	p	Pongo	p	Papio	p
Homo	-									
Pan	**Pan>Homo**		**0.001**							
Gorilla	Gorilla>Homo	0.074	Pan>Gorilla	0.681	-					
Pongo	Pongo>Homo	0.193	Pan>Pongo	0.446	Gorilla>Pongo	0.996	-			
Papio	Papio>Homo	0.174	Pan>Papio	0.274	Gorilla>Papio	0.983	Pongo>Papio	1.000	-	

i. ROI C3

Tb.BV/TV	Homo	p	Pan	p	Gorilla	p	Pongo	p	Papio	p
Homo	-									
Pan	**Pan>Homo**	**0.000**	-							
Gorilla	Gorilla>Homo	0.250	**Pan>Gorilla**	**0.013**	-					
Pongo	**Pongo>Homo**	**0.006**	Pan>Pongo	0.488	Pongo>Gorilla	0.584	-			
Papio	**Papio>Homo**	**0.000**	**Papio>Pan**	**0.000**	**Papio>Gorilla**	**0.000**	**Papio>Pongo**	**0.000**	-	

Tb.DA	Homo	p	Pan	p	Gorilla	p	Pongo	p	Papio	p
Homo	-									
Pan	**Homo>Pan**	**0.003**	-							
Gorilla	**Homo>Gorilla**	**0.011**	Gorilla>Pan	1.000	-					
Pongo	**Homo>Pongo**	**0.000**	Pan>Pongo	0.701	Gorilla>Pongo	0.722	-			
Papio	**Homo>Papio**	**0.011**	Papio>Pan	0.998	Papio>Gorilla	0.999	Papio>Pongo	0.542	-	

Tb.I	Homo	p	Pan	p	Gorilla	p	Pongo	p	Papio	p
Homo	-									
Pan	**Pan>Homo**	0.024	-							
Gorilla	Gorilla>Homo	0.055	Pan>Gorilla	1.000	-					
Pongo	**Pongo>Homo**	0.000	**Pongo>Pan**	0.000	**Pongo>Gorilla**	0.000	-			
Papio	Papio>Homo	0.254	Pan>Papio	0.863	Gorilla>Papio	0.914	**Pongo>Papio**	0.000	-	

Tb.E	Homo	p	Pan	p	Gorilla	p	Pongo	p	Papio	p
Homo	-									
Pan	Pan>Homo	0.658	-							
Gorilla	Gorilla>Homo	0.807	Pan>Gorilla	1.000	-					
Pongo	Homo>Pongo	0.203	**Pan>Pongo**	**0.007**	**Gorilla>Pongo**	**0.022**	-			
Papio	Papio>Homo	0.995	Pan>Papio	0.869	Gorilla>Papio	0.946	Papio<Po	0.089	-	

Tb.Th	Homo	p	Pan	p	Gorilla	p	Pongo	p	Papio	p
Homo	-									
Pan	**Pan>Homo**	**0.041**	-							
Gorilla	Gorilla>Homo	0.076	Pan>Gorilla	1.000	-					
Pongo	**Pongo>Homo**	**0.035**	Pongo>Pan	0.996	Pongo>Gorilla	0.997	-			
Papio	**Papio>Homo**	**0.000**	**Papio>Pan**	**0.001**	**Papio>Gorilla**	**0.003**	**Papio>Pongo**	**0.012**	-	

Tb.N	Homo	p	Pan	p	Gorilla	p	Pongo	p	Papio	p
Homo	-									
Pan	Pan>Homo	0.973	-							
Gorilla	Homo>Gorilla	0.880	Pan>Gorilla	0.533	-					
Pongo	Homo>Pongo	0.969	Pan>Pongo	0.739	Pongo>Gorilla	0.999	-			
Papio	**Homo>Papio**	**0.000**	**Pan>Papio**	**0.000**	**Gorilla>Papio**	**0.000**	**Pongo>Papio**	**0.000**	-	

Sc.%HighDen	Homo	p	Pan	p	Gorilla	p	Pongo	p	Papio	p
Homo	-									
Pan	**Pan>Homo**	**0.046**	-							
Gorilla	Gorilla>Homo	0.996	Pan>Gorilla	0.158	-					
Pongo	**Pongo>Homo**	**0.043**	Pongo>Pan	0.997	Pongo>Gorilla	0.132	-			
Papio	**Papio>Homo**	**0.016**	Papio>Pan	0.989	Papio>Gorilla	0.067	Papio>Pongo	1.000	-	

Sc.MeanHoun	Homo	p	Pan	p	Gorilla	p	Pongo	p	Papio	p
Homo	-									
Pan	Homo>Pan	0.955	-							
Gorilla	Homo>Gorilla	0.495	Pan>Gorilla	0.853	-					
Pongo	Homo>Pongo	1.000	Pongo>Pan	0.969	Pongo>Gorilla	0.568	-			
Papio	Homo>Papio	0.972	Papio>Pan	1.000	Papio>Gorilla	0.832	Pongo>Papio	0.981	-	

Sc.Th	Homo	p	Pan	p	Gorilla	p	Pongo	p	Papio	p
Homo	-									
Pan	**Pan>Homo**	**0.000**	-							
Gorilla	**Gorilla>Homo**	**0.000**	Gorilla>Pan	1.000	-					
Pongo	**Pongo>Homo**	**0.019**	Pan>Pongo	0.702	Gorilla>Pongo	0.723	-			
Papio	Papio>Homo	0.858	**Pan>Papio**	**0.002**	**Gorilla>Papio**	**0.004**	Pongo>Papio	0.164	-	

Table 2. 13: Pairwise comparisons of Tb.BV/TV in regions along the mediolateral axis (left) and the anteroposterior axis (right) in the (a) distal tibia and (b) talus.

(a) Distal tibia

Tibia					
Tb.BV/TV			**0.000**		
Homo	MLCentral	**>**	Lateral	**>**	Medial
		0.057		**0.038**	
			0.001		
Pan	MLCentral	=	Lateral	**>**	Medial
		0.752		**0.002**	
			0.012		
Gorilla	MLCentral	=	Lateral	**>**	Medial
		0.993		**0.014**	
			0.000		
Pongo	Lateral	=	MLCentral	**>**	Medial
		0.726		**0.006**	
			0.000		
Papio	MLCentral	=	Lateral	**>**	Medial
		0.257		**0.000**	

Tibia					
Tb.BV/TV			**0.029**		
Homo	Posterior	=	APCentral	=	Anterior
		0.303		0.458	
			0.000		
Pan	Posterior	=	Anterior	**>**	APCentral
		0.338		**0.000**	
			0.000		
Gorilla	Anterior	=	Posterior	**>**	APCentral
		0.086		**0.000**	
			0.000		
Pongo	Anterior	=	Posterior	**>**	APCentral
		0.347		**0.000**	
			0.035		
Papio	Anterior	=	Posterior	=	APCentral
		0.593		0.212	

(b) Talus

Talus					
Tb.BV/TV			**0.000**		
Homo	Medial	=	Lateral	**>**	MLCentral
		0.543		**0.003**	
			0.000		
Pan	Lateral	**>**	Medial	**>**	MLCentral
		0.000		**0.000**	
			0.000		
Gorilla	Lateral	**>**	Medial	**>**	MLCentral
		0.002		**0.008**	
			0.000		
Pongo	Lateral	**>**	Medial	**>**	MLCentral
		0.004		**0.004**	
			0.000		
Papio	Medial	=	Lateral	**>**	MLCentral
		0.908		**0.000**	

Talus					
Tb.BV/TV			**0.000**		
Homo	APCentral	=	Anterior	**>**	Posterior
		0.627		**0.001**	
			0.142		
Pan	Anterior	=	Posterior	=	APCentral
		0.121		0.996	
			0.000		
Gorilla	Anterior	=	APCentral	**>**	Posterior
		0.098		**0.000**	
			0.060		
Pongo	Anterior	=	APCentral	=	Posterior
		0.147		0.909	
			0.003		
Papio	Posterior	=	Anterior	=	APCentral
		0.368		0.246	

Table 2. 14: Pairwise regional comparisons of trabecular bone volume (Tb.BV/TV) in the (a) distal tibia and (b) talus. Only significant ($p<0.05$) comparisons are shown.

(a) Distal tibia

***Homo* tibia Tb.BV/TV**		
A1> A3 (p=0.004)	**A2>** A3 (p<0.001) B3 (p=0.017)	**A3**
B1> A3 (p<0.001)	**B2>** A3 (p<0.001)	**B3**
C1> A3 (p=0.014)	**C2>** A3 (p<0.001) B3 (p=0.012)	**C3>** A3 (p<0.001)

***Papio* tibia Tb.BV/TV**		
A1> A3 (p=0.046) B3 (p<0.001) C3 (p=0.005)	**A2>** B3 (p<0.001) C3 (p=0.014)	**A3>** B3 (p=0.004)
B1> B3 (p<0.001)	**B2>** B3 (p<0.001) C3 (p=0.003)	**B3**
C1> B3 (p<0.001)	**C2>** B3 (p<0.001) C3 (p=0.011)	**C3>** B3 (p=0.036)

***P an* tibia Tb.BV/TV**		
A1> A3 (p=0.044) B1 (p=0.006) B2 (p<0.001) B3 (p<0.001)	**A2>** B1 (p=0.021) B2 (p=0.001) B3 (p<0.001)	**A3>** B3 (p<0.001)
B1> B3 (p=0.004)	**B2**	**B3**
C1> B2 (p=0.014)	**C2>** A3 (p<0.001) B1 (p<0.001) B2 (p<0.001) B3 (p<0.001)	**C3>** B2 (p=0.012) B3 (p<0.001)

***Gorilla* tibiaTb.BV/TV**		
A1> B1 (p=0.006) B2 (p<0.001) B3 (p<0.001) C3 (p=0.001)	**A2>** B1 (p=0.012) B2 (p=0.002) B3 (p<0.001)	**A3>** B1 (p=0.014) B2 (p=0.002) B3 (p<0.001)
B1	**B2**	**B3**
C1> B2 (p=0.049) B3 (p<0.001)	**C2>** B1 (p<0.001) B2 (p<0.001) B3 (p<0.001) C3 (p=0.001)	**C3>** B3 (p<0.013)

***Pongo* tibia Tb.BV/TV**		
A1> A3 (p<0.001) B1 (p<0.001) B2 (p<0.001) B3 (p<0.001) C1 (p=0.001) C3 (p=0.004)	**A2>** A3 (p=0.005) B1 (p=0.007) B2 (p<0.001) B3 (p<0.001)	**A3>** B3 (p=0.022)
B1> B3 (p=0.017)	**B2**	**B3**
C1> B3 (p<0.001)	**C2>** A3 (p=0.041) B2 (p=0.001) B3 (p<0.001)	**C3>** B2 (p=0.040) B3 (p<0.001)

(b) Talus

Homo talus Tb.BV/TV		
A1> C1 (p=0.010) C2 (p=0.012)	**A2**	**A3>** A2 (p=0.018) C1 (p=0.002) C2 (p=0.002)
B1> A2 (p=0.006) C1 (p<0.001) C2 (p=0.001)	**B2**	**B3>** A2 (p=0.008) C1 (p=0.001) C2 (p=0.001)
C1	**C2**	**C3**

Papio talus Tb.BV/TV		
A1> A2 (p<0.001) A3 (p=0.001) B1 (p<0.001) B2 (p<0.001) C1 (p<0.001) C2 (p=0.013)	**A2**	**A3>** A2 (p<0.001) B2 (p<0.001)
B1> A2 (p<0.001) B2 (p<0.001)	**B2**	**B3>** A2 (p<0.001) B2 (p<0.001)
C1> A2 (p=0.003) B2 (p<0.001)	**C2>** A2 (p<0.001) B2 (p<0.001)	**C3>** A2 (p<0.001) B2 (p<0.001)

Pan talus Tb.BV/TV		
A1> A2 (p<0.001) A3 (p<0.001) B2 (p<0.001) B3 (p<0.001) C1 (p=0.010) C2 (p=0.012) C3 (p<0.001)	**A2**	**A3>** B2 (p=0.011)
B1> A2 (p<0.001) A3 (p=0.001) B2 (p<0.001) B3 (p<0.001) C1 (p=0.003) C2 (p<0.001)	**B2**	**B3>** B2 (p=0.029)
C1> B2 (p=0.005)	**C2**	**C3>** B2 (p<0.001)

Gorilla talus Tb.BV/TV		
A1> A2 (p<0.001) A3 (p=0.001) B2 (p<0.001) B3 (p<0.001) C1 (p<0.001) C2 (p<0.001) C3 (p<0.001)	**A2>** C2 (p=0.011)	**A3>** B2 (p=0.045) C2 (p<0.001)
B1> A2 (p=0.002) B2 (p<0.001) B3 (p=0.003) C1 (p<0.001) C2 (p<0.001) C3 (p<0.001)	**B2**	**B3>** C2 (p=0.008)
C1	**C2**	**C3**

Pongo talus Tb.BV/TV		
A1> A2 (p<0.001) A3 (p<0.001) B1 (p=0.041) B2 (p<0.001) B3 (p<0.001) C1 (p<0.001) C2 (p<0.001) C3 (p<0.001)	**A2**	**A3**
B1> B2 (p<0.001) C2 (p=0.004)	**B2**	**B3**
C1	**C2**	**C3>** B2 (p=0.033)

Table 2. 15: Pairwise comparisons of Tb.I in regions along the mediolateral axis (left) and the anteroposterior axis (right) in the (a) distal tibia and (b) talus.

(a) Distal tibia

Tibia						
Tb.I			**0.007**			
Homo	MLCentral	=	Lateral	=	Medial	
		0.090		0.624		
			0.001			
Pan	MLCentral	>	Medial	=	Lateral	
		0.023		0.440		
			0.677			
Gorilla	MLCentral	=	Medial	=	Lateral	
		0.809		0.950		
			0.274			
Pongo	MLCentral	=	Lateral	=	Medial	
		0.951		0.404		
			0.000			
Papio	MLCentral	>	Lateral	=	Medial	
		0.000		0.340		

Tibia						
Tb.I			**0.001**			
Homo	Anterior	=	Posterior	>	APCentral	
		0.993		**0.002**		
			0.002			
Pan	Anterior	=	Posterior	>	APCentral	
		0.991		**0.014**		
			0.730			
Gorilla	Posterior	=	Anterior	=	APCentral	
		0.932		0.894		
			0.032			
Pongo	APCentral	=	Anterior	=	Posterior	
		0.068		0.870		
			0.002			
Papio	Anterior	=	APCentral	>	Posterior	
		0.912		**0.018**		

(b) Talus

Talus						
Tb.I			**0.000**			
Homo	Medial	>	Lateral	=	MLCentral	
		0.000		0.274		
			0.982			
Pan	Lateral	=	Medial	=	MLCentral	
		1.000		0.980		
			0.062			
Gorilla	Medial	=	Lateral	=	MLCentral	
		0.453		0.581		
			0.081			
Pongo	Medial	=	Lateral	=	MLCentral	
		0.887		0.206		
			0.000			
Papio	Lateral	=	MLCentral	>	Medial	
		0.698		**0.000**		

Talus						
Tb.I			**0.050**			
Homo	Posterior	=	Anterior	=	APCentral	
		0.361		0.577		
			0.086			
Pan	Posterior	=	Anterior	=	APCentral	
		0.245		0.888		
			0.218			
Gorilla	Anterior	=	Posterior	=	APCentral	
		0.936		0.401		
			0.361			
Pongo	Posterior	=	APCentral	=	Anterior	
		0.383		0.998		
			0.000			
Papio	Posterior	=	Anterior	>	APCentral	
		0.849		**0.000**		

Table 2. 16: Pairwise regional comparisons of trabecular isotropy (Tb.I) in the (a) distal tibia and (b) talus. Only significant ($p<0.05$) comparisons are shown.

(a) Distal tibia

Homo tibia Tb.I		
A1	**A2>** B1 (p=0.001) B3 (p=0.032)	**A3**
B1	**B2**	**B3**
C1	**C2>** B1 (p=0.001) B3 (p=0.047)	**C3**

Papio tibia Tb.I		
A1> A3 (p=0.035) C1 (p<0.001) C3 (p<0.001)	**A2>** A3 (p=0.021) B3 (p=0.043) C1 (p<0.001) C3 (p<0.001)	**A3**
B1	**B2>** A3 (p<0.001) B1 (p<0.001) B3 (p<0.001) C1 (p<0.001) C3 (p<0.001)	**B3**
C1	**C2>** A3 (p=0.017) B3 (p=0.036) C1 (p<0.001) C3 (p<0.001)	**C3**

P an tibia Tb.I		
A1	**A2>** B1 (p=0.019) C1 (p=0.041)	**A3**
B1	**B2**	**B3**
C1	**C2>** B1 (p<0.001) B3 (p=0.001) C1 (p=0.001)	**C3**

Gorilla tibia Tb.I		
A1 -	**A2** -	**A3** -
B1 -	**B2** -	**B3** -
C1 -	**C2** -	**C3** -

Pongo tibia Tb.I		
A1	**A2**	**A3**
B1	**B2>** A2 (p=0.002) A3 (p=0.019) B3 (p=0.033) C1 (p=0.008) C2 (p=0.037) C3 (p=0.024)	**B3**
C1	**C2**	**C3**

(b) Talus

Homo talus Tb.I		
A1	**A2**	**A3>** A1 (p<0.001) A2 (p<0.001) B1 (p<0.001) B2 (p<0.001) B3 (p<0.001) C1 (p<0.001) C2 (p<0.001)
B1	**B2**	**B3>** A2 (p=0.005)
C1> A2 (p=0.003)	**C2**	**C3>** A1 (p<0.001) A2 (p<0.001) B1 (p<0.001) B2 (p<0.001) C2 (p<0.001)

Papio talus Tb.I		
A1> B3 (p<0.001) C3 (p<0.001)	**A2>** B3 (p<0.001) C3 (p<0.001)	**A3>** B3 (p=0.010)
B1> B3 (p=0.001) C3 (p=0.048)	**B2>** B3 (p=0.014)	**B3**
C1> A3 (p<0.001) B1 (p=0.002) B2 (p<0.001) B3 (p<0.001) C3 (p<0.001)	**C2>** A3 (p=0.002) B1 (p=0.021) B2 (p=0.001) B3 (p<0.001) C3 (p<0.001)	**C3**

Pan talus Tb.I		
A1	**A2**	**A3>** A2 (p=0.006) B3 (p=0.048)
B1	**B2**	**B3**
C1> A2 (p=0.008)	**C2**	**C3**

Gorilla talus Tb.I		
A1	**A2**	**A3>** A1 (p=0.015) C2 (p=0.006)
B1	**B2**	**B3**
C1> C2 (p=0.043)	**C2**	**C3**

Pongo talus Tb.I		
A1	**A2**	**A3**
B1	**B2**	**B3**
C1	**C2**	**C3>** A2 (p=0.031) B2 (p=0.022)

Table 2. 17: Pairwise comparisons of Tb.E in regions along the mediolateral axis (left) and the anteroposterior axis (right) in the (a) distal tibia and (b) talus.

(a) Distal tibia

Tibia						
Tb.E			**0.028**			
Homo	Lateral	=	Medial	=	MLCentral	
		0.374		0.470		
			0.001			
Pan	Lateral	=	Medial	=	MLCentral	
		0.193		0.084		
			0.086			
Gorilla	Lateral	=	Medial	=	MLCentral	
		0.203		0.902		
			0.002			
Pongo	Lateral	=	Medial	**>**	MLCentral	
		0.643		**0.015**		
			0.000			
Papio	Medial	=	Lateral	**>**	MLCentral	
		0.585		**0.000**		

Tibia						
Tb.E			**0.000**			
Homo	APCentral	**>**	Anterior	=	Posterior	
		0.000		0.985		
			0.000			
Pan	APCentral	**>**	Anterior	=	Posterior	
		0.000		0.957		
			0.001			
Gorilla	APCentral	**>**	Posterior	=	Anterior	
		0.003		0.639		
			0.059			
Pongo	Posterior	=	APCentral	=	Anterior	
		0.903		0.306		
			0.006			
Papio	APCentral	=	Posterior	=	Anterior	
		0.487		0.064		

(b) Talus

Talus						
Tb.E			**0.000**			
Homo	Lateral	**>**	MLCentral	=	Medial	
		0.000		0.787		
			0.002			
Pan	MLCentral	**>**	Medial	=	Lateral	
		0.050		0.545		
			0.097			
Gorilla	MLCentral	=	Medial	=	Lateral	
		0.167		0.976		
			0.139			
Pongo	MLCentral	=	Lateral	=	Medial	
		0.959		0.184		
			0.034			
Papio	MLCentral	=	Lateral	=	Medial	
		0.492		0.258		

Talus						
Tb.E			0.128			
Homo	Anterior	=	Posterior	=	APCentral	
		0.251		0.979		
			0.003			
Pan	Posterior	=	APCentral	**>**	Anterior	
		0.989		**0.006**		
			0.000			
Gorilla	APCentral	=	Posterior	**>**	Anterior	
		0.808		**0.000**		
			0.256			
Pongo	Anterior	=	APCentral	=	Posterior	
		0.328		0.999		
			0.004			
Papio	APCentral	=	Posterior	=	Anterior	
		0.118		0.454		

Table 2. 18: Pairwise regional comparisons of trabecular elongation (Tb.E) in the (a) distal tibia and (b) talus. Only significant ($p<0.05$) comparisons are shown.

(a) Distal tibia

***Homo* tibia Tb.E**		
A1> A2 (p=0.004)	**A2**	**A3**
B1> A2 (p<0.001) C2 (p=0.023) C3 (p=0.018)	**B2>** A2 (p<0.001) C2 (p=0.004) C3 (p=0.003)	**B3>** A2 (p<0.001) C2 (p=0.003) C3 (p=0.002)
C1	**C2**	**C3**

***Papio* tibia Tb.E**		
A1	**A2**	**A3>** A1 (p<0.001) A2 (p<0.001) B2 (p<0.001) C2 (p<0.001)
B1> A1 (p<0.001) A2 (p<0.001) B2 (p<0.001) C2 (p<0.001)	**B2**	**B3>** A1 (p<0.001) A2 (p<0.001) B2 (p<0.001) C2 (p=0.001)
C1> A1 (p<0.001) A2 (p<0.001) B2 (p<0.001) C2 (p=0.001)	**C2**	**C3>** A1 (p=0.004) A2 (p=0.004) B2 (p=0.019) C2 (p=0.027)

***P an* tibia Tb.E**		
A1	**A2**	**A3**
B1> A1 (p<0.001) A2 (p<0.001) A3 (p=0.002) B2 (p=0.014) C2 (p<0.001) C3 (p<0.001)	**B2**	**B3>** A1 (p=0.001) A2 (p=0.003) A3 (p=0.046) C2 (p<0.001) C3 (p<0.001)
C1> C2 (p=0.001) C3 (p=0.018)	**C2**	**C3**

***Gorilla* tibia Tb.E**		
A1	**A2**	**A3**
B1> A2 (p=0.034) A3 (p<0.001) C2 (p=0.005)	**B2**	**B3>** A3 (p=0.012)
C1	**C2**	**C3**

***Pongo* tibia Tb.E**		
A1	**A2**	**A3**
B1> A2 (p=0.013) B2 (p=0.016)	**B2**	**B3**
C1> A2 (p=0.008) B2 (p=0.010)	**C2**	**C3**

(b) Talus

Homo talus Tb.E		
A1> A2 (p<0.001) B2 (p<0.001) B3 (p<0.001) C2 (p<0.001) C3 (p<0.001)	**A2**	**A3>** A2 (p=0.043) B3 (p=0.004) C3 (p<0.001)
B1> A2 (p<0.001) B2 (p<0.001) B3 (p<0.001) C2 (p<0.001) C3 (p<0.001)	**B2**	**B3**
C1> A2 (p<0.001) A3 (p=0.002) B2 (p<0.001) B3 (p<0.001) C2 (p<0.001) C3 (p<0.001)	**C2>** C3 (p=0.010)	**C3**

Papio talus Tb.E		
A1	**A2**	**A3**
B1> A3 (p=0.027) B3 (p=0.022)	**B2>** A1 (p=0.002) A3 (p=0.001) B3 (p<0.001) C1 (p=0.026) C2 (p=0.019)	**B3**
C1	**C2**	**C3**

Pan talus Tb.E		
A1	**A2**	**A3**
B1	**B2>** A1 (p=0.017) A3 (p=0.008)	**B3**
C1	**C2>** A1 (p=0.008) A3 (p=0.004) C1 (p=0.039)	**C3**

Gorilla talus Tb.E		
A1	**A2**	**A3**
B1	**B2>** A1 (p=0.016) A2 (p=0.001) A3 (p<0.001) B1 (p=0.048)	**B3>** A3 (p=0.014)
C1	**C2>** A2 (p=0.007) A3 (p=0.001)	**C3**

Pongo talus Tb.E		
A1	**A2**	**A3>** B3 (p=0.020)
B1	**B2**	**B3**
C1	**C2**	**C3**

Table 2. 19: Pairwise comparisons of Tb.Th in regions along the mediolateral axis (left) and the anteroposterior axis (right) in the (a) distal tibia and (b) talus.

(a) Distal tibia

Tibia						
Tb.Th			**0.000**			
Homo	MLCentral	=	Lateral	**>**	Medial	
		0.077		**0.047**		
			0.000			
Pan	MLCentral	**>**	Lateral	**>**	Medial	
		0.014		**0.024**		
			0.105			
Gorilla	Lateral	=	MLCentral	=	Medial	
		0.668		0.420		
			0.029			
Pongo	MLCentral	=	Lateral	=	Medial	
		0.335		0.264		
			0.000			
Papio	MLCentral	**>**	Medial	**>**	Lateral	
		0.000		**0.019**		

Tibia						
Tb.Th			**0.023**			
Homo	Anterior	=	APCentral	**>**	Posterior	
		0.997		**0.003**		
			0.000			
Pan	Anterior	=	Posterior	**>**	APCentral	
		0.342		**0.000**		
			0.000			
Gorilla	Anterior	**>**	Posterior	**>**	APCentral	
		0.007		**0.019**		
			0.001			
Pongo	Anterior	=	Posterior	**>**	APCentral	
		0.284		**0.048**		
			0.001			
Papio	Anterior	=	APCentral	=	Posterior	
		0.190		0.189		

(b) Talus

Talus						
Tb.Th			0.504			
Homo	Medial	=	MLCentral	=	Lateral	
		0.678		0.967		
			0.017			
Pan	Lateral	=	Medial	=	MLCentral	
		0.638		0.181		
			0.166			
Gorilla	Lateral	=	Medial	=	MLCentral	
		0.970		0.308		
			0.531			
Pongo	Lateral	=	Medial	=	MLCentral	
		0.982		0.652		
			0.100			
Papio	Medial	=	Lateral	=	MLCentral	
		0.988		0.109		

Talus						
Tb.Th			**0.000**			
Homo	Anterior	=	APCentral	**>**	Posterior	
		0.114		**0.007**		
			0.000			
Pan	Anterior	**>**	APCentral	**>**	Posterior	
		0.000		**0.000**		
			0.000			
Gorilla	Anterior	**>**	APCentral	**>**	Posterior	
		0.001		**0.000**		
			0.063			
Pongo	Anterior	=	APCentral	=	Posterior	
		0.175		0.856		
			0.001			
Papio	Anterior	=	APCentral	**>**	Posterior	
		0.462		**0.055**		

Table 2. 20: Pairwise regional comparisons of trabecular thickness (Tb.Th) in the (a) distal tibia and (b) talus. Only significant ($p<0.05$) comparisons are shown.

(a) Distal tibia

***Homo* tibia Tb.Th**		
A1	**A2>** A3 (p=0.002) B3 (p=0.010) C1 (p=0.002) C3 (p<0.001)	**A3**
B1> C3 (p=0.008)	**B2>** C3 (p=0.032)	**B3**
C1	**C2**	**C3**

***Papio* tibia Tb.Th**		
A1	**A2>** A1 (p=0.012) B1 (p<0.001) B3 (p<0.001) C1 (p<0.001) C3 (p<0.001)	**A3>** B1 (p=0.018) C1 (p=0.019)
B1	**B2>** A1 (p=0.001) A3 (p=0.021) B1 (p<0.001) B3 (p<0.001) C1 (p<0.001) C2 (p=0.006) C3 (p<0.001)	**B3**
C1	**C2>** C1 (p=0.029)	**C3**

***P an* tibia Tb.Th**		
A1> B3 (p=0.001)	**A2>** A1 (p=0.002) A3 (p<0.001) B1 (p<0.001) B2 (p<0.001) B3 (p<0.001) C1 (p<0.001) C3 (p<0.001)	**A3**
B1	**B2**	**B3**
C1	**C2>** A3 (p=0.007) B1 (p=0.018) B2 (p=0.001) B3 (p<0.001)	**C3>** B3 (p=0.048)

***Gorilla* tibiaTb.Th**		
A1> B2 (p=0.004) B3 (p<0.001) C3 (p=0.012)	**A2>** B3 (p=0.008)	**A3>** B2 (p=0.030) B3 (p=0.001)
B1	**B2**	**B3**
C1	**C2>** B3 (p=0.017)	**C3**

***Pongo* tibia Tb.Th**		
A1> B3 (p=0.013)	**A2>** A3 (p=0.012) B1 (p=0.014) B2 (p=0.021) B3 (p<0.001) C1 (p=0.020)	**A3>** B2 (p=0.030) B3 (p=0.001)
B1	**B2**	**B3**
C1	**C2**	**C3**

(b) Talus

Homo talus Tb.Th		
A1	**A2**	**A3>** C1 (p=0.003) C2 (p=0.012) C3 (p=0.001)
B1	**B2**	**B3**
C1	**C2**	**C3**

Pan talus Tb.Th		
A1> B2 (p<0.001) B3 (p=0.007) C1 (p<0.001) C2 (p<0.001) C3 (p<0.001)	**A2>** B2 (p<0.001) C1 (p<0.001) C2 (p<0.001) C3 (p<0.001)	**A3>** B2 (p<0.001) B3 (p=0.002) C1 (p<0.001) C2 (p<0.001) C3 (p<0.001)
B1> B2 (p=0.001) C1 (p<0.001) C2 (p<0.001) C3 (p<0.001)	**B2**	**B3**
C1	**C2**	**C3**

Gorilla talus Tb.Th		
A1> B2 (p=0.048) C1 (p=0.002) C2 (p<0.001) C3 (p<0.001)	**A2>** C1 (p=0.014) C2 (p<0.001) C3 (p=0.004)	**A3>** B2 (p=0.001) B3 (p=0.016) C1 (p<0.001) C2 (p<0.001) C3 (p<0.001)
B1> C2 (p=0.002) C3 (p=0.037)	**B2**	**B3**
C1	**C2**	**C3**

Papio talus Tb.Th		
A1> B2 (p=0.003) C1 (p=0.026) C3 (p=0.003)	**A2** -	**A3>** A2 (p=0.016) B2 (p<0.001) C1 (p<0.001) C3 (p<0.001)
B1> B2 (p=0.001) C1 (p=0.008) C3 (p=0.001)	**B2** -	**B3>** B2 (p=0.003) C1 (p=0.021) C3 (p=0.002)
C1 -	**C2>** C3 (p=0.027)	**C3** -

Pongo talus Tb.Th		
A1 -	**A2** -	**A3** -
B1 -	**B2** -	**B3** -
C1 -	**C2** -	**C3** -

Table 2. 21: Pairwise comparisons of Tb.N in regions along the mediolateral axis (left) and the anteroposterior axis (right) in the (a) distal tibia and (b) talus.

(a) Distal tibia

Tibia						
Tb.N			0.289			
Homo	MLCentral	=	Lateral	=	Medial	
		0.997		0.289		
			0.278			
Pan	MLCentral	=	Lateral	=	Medial	
		0.999		0.236		
			0.007			
Gorilla	MLCentral	**>**	Medial	=	Lateral	
		0.039		0.993		
			0.278			
Pongo	Lateral	=	MLCentral	=	Medial	
		0.903		0.547		
			0.000			
Papio	Lateral	**>**	MLCentral	=	Medial	
		0.000		0.232		

Tibia						
Tb.N			**0.000**			
Homo	Posterior	**>**	APCentral	=	Anterior	
		0.000		0.999		
			0.015			
Pan	Posterior	**>**	Anterior	=	APCentral	
		0.035		0.741		
			0.288			
Gorilla	Posterior	=	Anterior	=	APCentral	
		0.815		0.582		
			0.001			
Pongo	Posterior	=	Anterior	=	APCentral	
		0.121		0.222		
			0.000			
Papio	Posterior	**>**	APCentral	=	Anterior	
		0.001		0.991		

(b) Talus

Talus						
Tb.N			0.064			
Homo	Lateral	=	Medial	=	MLCentral	
		0.575		0.331		
			0.043			
Pan	Lateral	**>**	Medial	=	MLCentral	
		0.043		1.000		
			0.014			
Gorilla	Lateral	**>**	Medial	=	MLCentral	
		0.031		0.978		
			0.000			
Pongo	Lateral	**>**	Medial	=	MLCentral	
		0.015		0.070		
			0.001			
Papio	MLCentral	=	Lateral	**>**	Medial	
		0.999		**0.005**		

Talus						
Tb.N			**0.035**			
Homo	APCentral	=	Posterior	=	Anterior	
		0.484		0.342		
			0.000			
Pan	Posterior	**>**	APCentral	**>**	Anterior	
		0.000		**0.000**		
			0.002			
Gorilla	Posterior	=	APCentral	**>**	Anterior	
		0.711		**0.015**		
			0.024			
Pongo	APCentral	=	Posterior	=	Anterior	
		0.807		0.104		
			0.002			
Papio	Posterior	=	APCentral	**>**	Anterior	
		0.911		**0.001**		

Table 2. 22: Pairwise regional comparisons of trabecular number (Tb.N) in the (a) distal tibia and (b) talus. Only significant ($p<0.05$) comparisons are shown.

(a) Distal tibia

***Homo* tibia Tb.N**		
A1> A3 (p=0.005)	**A2>** A3 (p=0.024) C3 (p=0.030)	**A3**
B1	**B2**	**B3**
C1> A3 (p<0.001)	**C2>** A3 (p<0.001) B3 (p=0.010)	**C3>** A2 (p=0.030) A3 (p<0.001) B1 (p=0.007) B2 (p=0.007) B3 (p<0.001)

***Papio* tibia Tb.N**		
A1> A3 (p<0.001) B2 (p=0.010) B3 (p=0.001)	**A2** -	**A3** -
B1> A2 (p=0.008) A3 (p<0.001) B2 (p<0.001) B3 (p<0.001)	**B2** -	**B3** -
C1> A2 (p<0.001) A3 (p<0.001) B2 (p<0.001) B3 (p<0.001) C2 (p=0.009) C3 (p=0.001)	**C2>** A3 (p=0.004) B3 (p=0.008)	**C3>** A3 (p=0.032)

***P an* tibia Tb.N**		
A1 -	**A2** -	**A3** -
B1 -	**B2** -	**B3** -
C1 -	**C2** -	**C3** -

***Gorilla* tibiaTb.N**		
A1 -	**A2** -	**A3** -
B1 -	**B2** -	**B3** -
C1 -	**C2** -	**C3** -

***Pongo* tibia Tb.N**		
A1 -	**A2** -	**A3** -
B1 -	**B2** -	**B3** -
C1> B3 (p=0.014)	**C2>** B3 (p=0.006)	**C3** -

(b) Talus

Homo talus Tb.N		
A1	**A2**	**A3**
B1> A2 (p=0.009)	**B2**	**B3**
C1	**C2**	**C3**

Pan talus Tb.N		
A1> A2 (p=0.001) A3 (p=0.001)	**A2**	**A3**
B1> A2 (p<0.001) A3 (p<0.001)	**B2>** A2 (p=0.001) A3 (p=0.001)	**B3>** A2 (p<0.001) A3 (p=0.001)
C1> A2 (p<0.001) A3 (p<0.001)	**C2>** A2 (p<0.001) A3 (p<0.001)	**C3>** A2 (p<0.001) A3 (p<0.001)

Gorilla talus Tb.N		
A1	**A2**	**A3**
B1> A2 (p=0.017) A3 (p=0.005)	**B2**	**B3**
C1> A2 (p=0.027) A3 (p=0.008)	**C2**	**C3>** A2 (p=0.046) A3 (p=0.015)

Papio talus Tb.N		
A1	**A2>** A1 (p=0.027)	**A3**
B1> A1 (p=0.006)	**B2>** A1 (p=0.001) A3 (p=0.016) C3 (p=0.017)	**B3**
C1> A1 (p<0.001) A2 (p=0.004) A3 (p<0.001) B1 (p=0.018) B3 (p<0.001) C2 (p=0.005) C3 (p<0.001)	**C2>** A1 (p=0.020)	**C3**

Pongo talus Tb.N		
A1> A2 (p=0.011)	**A2**	**A3**
B1> A2 (p=0.001) A3 (p=0.010)	**B2**	**B3>** A2 (p=0.033)
C1> A2 (p=0.002) A3 (p=0.013)	**C2**	**C3**

Table 2. 23: Pairwise comparisons of Sc.MeanHouns in regions along the mediolateral axis (left) and the anteroposterior axis (right) in the (a) distal tibia and (b) talus.

(a) Distal tibia

Tibia					
Sc.Mean Houns			0.313		
Homo	Medial	=	Lateral	=	MLCentral
		0.820		0.666	
			0.000		
Pan	Medial	**>**	MLCentral	=	Lateral
		0.000		0.257	
			0.000		
Gorilla	Medial	**>**	Lateral	=	MLCentral
		0.000		0.758	
			0.103		
Pongo	Medial	=	MLCentral	=	Lateral
		0.335		0.841	
			0.026		
Papio	MLCentral	=	Medial	=	Lateral
		0.337		0.380	

Tibia					
Sc.Mean Houns			0.623		
Homo	Anterior	=	Posterior	=	APCentral
		0.984		0.720	
			0.000		
Pan	Anterior	=	Posterior	**>**	APCentral
		0.997		**0.000**	
			0.000		
Gorilla	Posterior	=	Anterior	**>**	APCentral
		0.394		**0.000**	
			0.000		
Pongo	Anterior	**>**	Posterior	**>**	APCentral
		0.001		**0.002**	
			0.000		
Papio	Posterior	=	Anterior	**>**	APCentral
		0.443		**0.000**	

(b) Talus

Talus					
Sc.Mean Houns			**0.001**		
Homo	Medial	**>**	Lateral	=	MLCentral
		0.056		0.488	
			0.000		
Pan	Lateral	=	Medial	**>**	MLCentral
		1.000		**0.000**	
			0.000		
Gorilla	Medial	**>**	Lateral	**>**	MLCentral
		0.005		**0.006**	
			0.009		
Pongo	Lateral	=	Medial	**>**	MLCentral
		0.982		**0.025**	
			0.000		
Papio	Lateral	**>**	Medial	**>**	MLCentral
		0.000		**0.000**	

Talus					
Sc.Mean Houns			0.648		
Homo	APCentral	=	Posterior	=	Anterior
		0.919		0.857	
			0.142		
Pan	Posterior	=	Anterior	=	APCentral
		0.535		0.773	
			0.171		
Gorilla	APCentral	=	Anterior	=	Posterior
		0.993		0.239	
			0.036		
Pongo	Posterior	=	Anterior	=	APCentral
		0.453		0.352	
			0.000		
Papio	Posterior	**>**	APCentral	=	Anterior
		0.003		0.083	

Table 2. 24: Pairwise regional comparisons of subchondral radiodensity (Sc.MeanHouns) in the (a) distal tibia and (b) talus. Only significant ($p<0.05$) comparisons are shown.

(a) Distal tibia

Homo tibia Sc.MeanHouns		
A1 -	**A2** -	**A3** -
B1 -	**B2** -	**B3** -
C1 -	**C2** -	**C3** -

Papio tibia Sc.MeanHouns		
A1> B1 (p<0.001) B2 (p<0.001) B3 (p<0.001)	**A2>** B1 (p<0.001) B2 (p<0.001) B3 (p<0.001)	**A3>** B1 (p<0.001) B2 (p<0.001) B3 (p<0.001)
B1	**B2**	**B3**
C1> B1 (p<0.001) B2 (p<0.001) B3 (p<0.001)	**C2>** A1 (p<0.001) A2 (p=0.048) A3 (p=0.034) B1 (p<0.001) B2 (p<0.001) B3 (p<0.001) C1 (p<0.001) C3 (p=0.004)	**C3>** B1 (p<0.001) B2 (p<0.001) B3 (p<0.001)

P an tibia Sc.MeanHouns		
A1> B2 (p=0.002)	**A2>** B2 (p=0.001)	**A3>** A1 (p<0.001) A2 (p<0.001) B1 (p<0.001) B2 (p<0.001) B3 (p<0.001) C1 (p<0.001)
B1	**B2**	**B3**
C1	**C2>** B1 (p<0.001) B2 (p<0.001) C1 (p=0.002)	**C3>** A1 (p<0.001) A2 (p=0.001) B1 (p<0.001) B2 (p<0.001) B3 (p=0.001) C1 (p<0.001)

Gorilla tibiaSc.MeanHouns		
A1> B1 (p=0.026) B2 (p=0.001)	**A2**	**A3>** B1 (p<0.001) B2 (p<0.001)
B1	**B2**	**B3>** B1 (p=0.017) B2 (p=0.001)
C1> B2 (p=0.004)	**C2>** B1 (p=0.012) B2 (p<0.001)	**C3>** A1 (p=0.015) A2 (p<0.001) B1 (p<0.001) B2 (p<0.001) B3 (p=0.024) C1 (p=0.005) C2 (p=0.033)

Pongo tibia Sc.MeanHouns		
A1> B1 (p<0.001) B2 (p<0.001) B3 (p=0.036) C1 (p<0.001)	**A2>** B1 (p<0.001) B2 (p<0.001) C1 (p=0.001)	**A3>** B1 (p<0.001) B2 (p<0.001) C1 (p=0.008)
B1	**B2**	**B3>** B2 (p=0.042)
C1	**C2>** B1 (p=0.022) B2 (p=0.002)	**C3>** B1 (p=0.005) B2 (p<0.001)

(b) Talus

Homo talus Sc.MeanHouns		
A1 -	**A2** -	**A3** -
B1 -	**B2** -	**B3** -
C1 -	**C2** -	**C3** -

Pan talus Sc.MeanHouns		
A1> A2 (p<0.001) B2 (p<0.001) C2 (p=0.040)	**A2** -	**A3>** A2 (p<0.001) B2 (p<0.001)
B1> A2 (p<0.001) B2 (p<0.001)	**B2** -	**B3>** A2 (p=0.012) B2 (p=0.032)
C1> A2 (p=0.011) B2 (p=0.028)	**C2** -	**C3>** A2 (p<0.001) B2 (p<0.001) B3 (p=0.013) C1 (p=0.015) C2 (p=0.002)

Gorilla talus Sc.MeanHouns		
A1	**A2**	**A3>** A2 (p=0.014) B2 (p=0.007) C1 (p=0.005) C2 (p=0.005)
B1> B2 (p=0.028) C1 (p=0.023) C2 (p=0.020)	**B2**	**B3>** A2 (p=0.012) B2 (p=0.006) C1 (p=0.005) C2 (p=0.004)
C1	**C2**	**C3>** A2 (p=0.012) B2 (p=0.005) C1 (p=0.004) C2 (p=0.004)

Papio talus Sc.MeanHouns		
A1> A2 (p<0.001) A3 (p<0.001) B2 (p<0.001) C2 (p=0.001)	**A2**	**A3>** A2 (p<0.001) B2 (p<0.001)
B1> A2 (p<0.001) A3 (p<0.001) B2 (p<0.001) C2 (p<0.001)	**B2**	**B3>** A2 (p<0.001) A3 (p=0.007) B2 (p<0.001)
C1> A2 (p<0.001) A3 (p<0.001) B2 (p<0.001) B3 (p=0.001) C2 (p=0.001)	**C2>** A2 (p<0.001) B2 (p<0.001)	**C3>** A2 (p<0.001) A3 (p<0.001) B2 (p<0.001) C2 (p<0.001)

Pongo talus Sc.MeanHouns		
A1> A2 (p<0.001) A3 (p=0.002) B2 (p<0.001) B3 (p=0.016) C1 (p=0.001)	**A2**	**A3**
B1> B2 (p=0.020)	**B2**	**B3**
C1	**C2>** B2 (p=0.031)	**C3>** A2 (p<0.001) A3 (p<0.001) B2 (p<0.001) B3 (p=0.002) C1 (p<0.001)

Table 2. 25: Pairwise comparisons of Sc.Th in regions along the mediolateral axis (left) and the anteroposterior axis (right) in the (a) distal tibia and (b) talus.

(a) Distal tibia

Tibia						
Sc.Th			**0.000**			
Homo	Medial	**>**	MLCentral	=	Lateral	
		0.001		0.417		
			0.000			
Pan	Medial	**>**	MLCentral	=	Lateral	
		0.005		0.268		
			0.113			
Gorilla	Medial	=	MLCentral	=	Lateral	
		0.455		0.854		
			0.265			
Pongo	Lateral	=	MLCentral	=	Medial	
		0.955		0.467		
			0.000			
Papio	Lateral	=	MLCentral	**>**	Medial	
		0.659		**0.013**		

Tibia						
Sc.Th			0.206			
Homo	Posterior	=	APCentral	=	Anterior	
		0.287		0.929		
			0.016			
Pan	Posterior	=	Anterior	=	APCentral	
		0.165		0.635		
			0.006			
Gorilla	Posterior	=	Anterior	=	APCentral	
		0.106		0.515		
			0.000			
Pongo	Anterior	=	Posterior	**>**	APCentral	
		0.166		**0.012**		
			0.023			
Papio	Posterior	=	APCentral	=	Anterior	
		0.688		0.165		

(b) Talus

Talus						
Sc.Th			**0.000**			
Homo	Medial	**>**	MLCentral	**>**	Lateral	
		0.006		**0.058**		
			0.001			
Pan	Medial	=	Lateral	=	MLCentral	
		0.711		0.073		
			0.003			
Gorilla	Medial	**>**	Lateral	=	MLCentral	
		0.007		0.958		
			0.027			
Pongo	Medial	=	Lateral	=	MLCentral	
		0.379		0.469		
			0.027			
Papio	Medial	=	Lateral	=	MLCentral	
		0.797		0.104		

Talus						
Sc.Th			**0.000**			
Homo	APCentral	**>**	Anterior	=	Posterior	
		0.047		0.129		
			0.173			
Pan	APCentral	=	Anterior	=	Posterior	
		0.988		0.224		
			0.000			
Gorilla	Anterior	=	APCentral	**>**	Posterior	
		0.999		**0.001**		
			0.002			
Pongo	Anterior	**>**	APCentral	=	Posterior	
		0.009		0.952		
			0.000			
Papio	APCentral	**>**	Posterior	=	Anterior	
		0.000		0.221		

Table 2. 26: Pairwise regional comparisons of subchondral thickness (Sc.Th) in the (a) distal tibia and (b) talus. Only significant ($p<0.05$) comparisons are shown.

(a) Distal tibia

***Homo* tibia Sc.Th**		
A1	**A2**	**A3>** A1 (p=0.006) A2 (p=0.005) B1 (p=0.030)
B1	**B2**	**B3**
C1	**C2**	**C3>** A1 (p=0.006) A2 (p=0.005) B1 (p=0.030)

***Papio* tibia Sc.Th**		
A1	**A2**	**A3**
B1	**B2**	**B3**
C1	**C2>** A2 (p=0.006) A3 (p=0.009) B3 (p=0.023) C3 (p=0.018)	**C3**

***P an* tibia Sc.Th**		
A1	**A2**	**A3>** A1 (p=0.007) A2 (p<0.001) B1 (p<0.001) B2 (p=0.003) C1 (p<0.001)
B1	**B2**	**B3**
C1	**C2>** A1 (p=0.014) A2 (p<0.001) B1 (p=0.001) B2 (p=0.007) C1 (p<0.001)	**C3>** A2 (p<0.001) B1 (p=0.008) C1 (p=0.001)

***Gorilla* tibiaSc.Th**		
A1	**A2**	**A3**
B1	**B2**	**B3**
C1	**C2>** A2 (p=0.002) B1 (p=0.020) B2 (p=0.032)	**C3**

***Pongo* tibia Sc.Th**		
A1> B2 (p<0.001) B3 (p<0.001) C1 (p=0.011)	**A2>** B2 (p=0.014)	**A3**
B1	**B2**	**B3**
C1	**C2>** B2 (p=0.002) B3 (p=0.009)	**C3**

(b) Talus

Homo talus Sc.Th		
A1	**A2**	**A3>** A1 (p=0.035) C1 (p<0.001)
B1	**B2>** C1 (p=0.009)	**B3>** A1 (p<0.001) A2 (p=0.007) B1 (p=0.018) C1 (p<0.001) C2 (p<0.001) C3 (p=0.026)
C1	**C2**	**C3**

Papio talus Sc.Th		
A1> A2 (p=0.002)	**A2**	**A3**
B1> A1 (p=0.022) A2 (p<0.001) A3 (p<0.001) C1 (p<0.001) C2 (p=0.005) C3 (p=0.015)	**B2>** A2 (p<0.001) C1 (p=0.017)	**B3>** A1 (p=0.003) A2 (p<0.001) A3 (p<0.001) C1 (p<0.001) C2 (p=0.001) C3 (p=0.002)
C1	**C2>** A2 (p=0.009)	**C3>** A2 (p=0.003)

Pan talus Sc.Th		
A1> C1 (p=0.008)	**A2**	**A3>** A2 (p<0.001) B3 (p=0.029) C1 (p<0.001)
B1> A2 (p<0.001) B2 (p=0.006) B3 (p=0.003) C1 (p<0.001) C2 (p=0.012)	**B2**	**B3**
C1	**C2**	**C3>** A2 (p=0.021)

Gorilla talus Sc.Th		
A1> C1 (p=0.001)	**A2>** C1 (p=0.035)	**A3>** A2 (p=0.046) C1 (p<0.001) C2 (p=0.001)
B1> C1 (p<0.001) C2 (p=0.034)	**B2>** C1 (p=0.006)	**B3>** C1 (p<0.001)
C1	**C2**	**C3>** C1 (p<0.001)

Pongo talus Sc.Th		
A1> B2 (p=0.006) C1 (p<0.001)	**A2**	**A3>** B2 (p=0.003) C1 (p<0.001)
B1> B2 (p=0.046) C1 (p=0.002)	**B2**	**B3**
C1	**C2**	**C3>** B2 (p=0.033) C1 (p=0.002)

Table 2. 27: Consistency of ranked values in the distal tibia.

The value within each cell of a 3x3 grid is the mean rank value of that variable in that region. A ranked value of 1 is attained if that region consistently had the lowest value in all specimens; a ranked value of 9 is attained if that region consistently had the highest value in all specimens. Kendall's W expresses the level of consistency among specimens. W=0 denotes no consistency (random), W=1 denotes that all specimens had identical patterns of ranked data.

Homo

BV/TV			Tb.Th			Tb.N		
4.6	6.5	1.9	4.9	7.7	3.6	5.4	4.6	2.2
5.7	5.9	3.4	6.6	6.3	4.5	4.5	4.5	2.6
4.2	6.4	6.4	3.8	4.9	2.7	5.9	6.9	8.4
Kendall's W	0.338		Kendall's W	0.341		Kendall's W	0.508	

Tb.DA			Tb.I			Tb.E		
4.2	3.2	5.6	5.8	6.8	4.4	5.7	2.6	4.2
7.4	5.5	6.5	2.6	4.5	3.5	6.6	6.9	7.1
4.2	3.3	5.1	5.8	6.7	4.9	4.5	3.9	3.4
Kendall's W	0.265		Kendall's W	0.265		Kendall's W	0.357	

Sc.%HighDensity			Sc.MeanHouns			Sc.Th		
5.6	4.7	7.2	5.3	4.4	7.2	2.7	2.8	7.1
3.9	1.5	5.0	4.7	2.1	5.4	3.9	4.3	6.4
6.4	4.9	5.8	5.4	4.8	5.7	4.3	5.9	7.5
Kendall's W	0.361		Kendall's W	0.247		Kendall's W	0.433	

Pan

Tb.BV/TV			Tb.Th			Tb.N		
7.4	6.7	4.4	6.7	8.3	4.0	5.8	4.5	4.3
3.3	2.5	1.1	4.2	3.0	1.4	3.9	5.4	3.0
5.9	8.0	5.7	4.8	7.1	5.4	5.7	6.4	6.0
Kendall's W	0.720		Kendall's W	0.614		Kendall's W	0.174	

Tb.DA			Tb.I			Tb.E		
4.3	3.5	4.9	5.7	6.5	5.1	4.0	3.7	4.5
7.0	4.7	6.9	3.0	5.3	3.1	8.0	5.3	7.0
6.7	3.1	3.8	3.3	6.9	6.2	6.0	3.2	3.1
Kendall's W	0.301		Kendall's W	0.301		Kendall's W	0.401	

Sc.%HighDensity			Sc.MeanHouns			Sc.Th		
5.5	5.9	7.5	4.7	5.1	8.3	4.4	2.5	7.4
1.9	1.3	5.6	2.4	1.8	4.9	3.8	4.3	4.6
4.2	5.7	7.3	3.7	6.4	7.7	3.6	7.4	7.0
Kendall's W	0.621		Kendall's W	0.652		Kendall's W	0.437	

Gorilla

Tb.BV/TV			Tb.Th			Tb.N		
7.5	6.5	6.2	7.4	6.2	6.9	4.5	6.9	4.4
3.4	2.9	1.2	4.0	3.2	2.5	3.5	5.9	2.5
5.9	7.8	3.8	5.1	6.2	3.6	3.9	8.3	5.1
Kendall's W	0.693		Kendall's W	0.416		Kendall's W	0.431	

Tb.DA			Tb.I			Tb.E		
4.6	5.2	4.3	5.4	4.8	5.7	5.2	4.6	2.8
6.1	5.4	5.3	3.9	4.6	4.7	7.6	4.8	6.6
5.2	3.6	5.3	4.8	6.4	4.7	4.8	4.1	4.4
Kendall's W	0.066		Kendall's W	0.066		Kendall's W	0.266	

Sc.%HighDensity			Sc.MeanHouns			Sc.Th		
5.8	5.3	6.1	5.3	4.0	6.9	5.2	2.9	6.2
2.4	1.2	6.4	2.5	1.8	5.8	3.6	3.9	4.2
5.8	4.4	7.7	5.1	5.7	8.1	4.5	7.9	6.4
Kendall's W	0.567		Kendall's W	0.532		Kendall's W	0.338	

Pongo

Tb.BV/TV			Tb.Th			Tb.N		
8.4	7.6	3.9	7.1	8.2	4.1	5.2	4.9	4.7
3.7	2.4	1.0	4.2	3.7	1.5	4.8	2.9	1.9
5.2	6.9	5.8	4.1	6.4	5.6	6.9	7.5	6.2
Kendall's W	0.803		Kendall's W	0.560		Kendall's W	0.418	

Tb.DA			Tb.I			Tb.E		
3.5	6.6	5.4	6.5	3.4	4.6	3.8	3.1	6.0
4.7	1.9	5.6	5.3	8.1	4.4	6.4	2.9	6.1
6.0	5.4	5.9	4.0	4.6	4.1	7.0	5.0	4.7
Kendall's W	0.278		Kendall's W	0.278		Kendall's W	0.296	

Sc.%HighDensity			Sc.MeanHouns			Sc.Th		
7.4	5.9	7.9	7.4	7.0	6.8	7.7	6.4	5.5
1.9	1.7	6.6	2.4	1.9	4.6	4.3	2.1	2.6
3.6	4.3	5.7	3.1	5.6	6.4	4.1	7.4	5.0
Kendall's W	0.679		Kendall's W	0.600		Kendall's W	0.512	

Papio

Tb.BV/TV			Tb.Th			Tb.N		
7.2	6.7	3.6	5.2	7.6	5.8	6.4	3.9	2.4
4.4	7.4	1.1	2.3	8.2	4.2	7.2	2.8	2.7
5.7	6.1	2.9	2.9	4.9	3.7	8.8	5.6	5.2
Kendall's W	0.620		Kendall's W	0.533		Kendall's W	0.666	

Tb.DA			Tb.I			Tb.E		
3.8	3.4	5.9	6.2	6.6	4.1	2.8	2.9	6.5
5.4	2.4	5.8	4.6	7.6	4.2	7.5	3.4	6.3
7.7	3.5	7.1	2.3	6.5	2.9	6.4	3.2	6.1
Kendall's W	0.438		Kendall's W	0.438		Kendall's W	0.476	

Sc.%HighDensity			Sc.MeanHouns			Sc.Th		
7.4	7.2	6.7	5.6	6.8	6.5	5.5	2.8	2.9
2.3	1.1	3.2	1.9	2.2	2.1	7.3	5.6	3.0
5.2	6.4	5.5	5.3	8.5	6.2	6.6	8.3	3.0
Kendall's W	0.684		Kendall's W	0.756		Kendall's W	0.616	

Legend

A1	A2	A3
B1	B2	B3
B4	B5	B6

Table 2. 28: Consistency of ranked values in the talus.

The value within each cell of a 3x3 grid is the mean rank value of that variable in that region. A ranked value of 1 is attained if that region consistently had the lowest value in all specimens; a ranked value of 9 is attained if that region consistently had the highest value in all specimens. Kendall's W expresses the level of consistency among specimens. W=0 denotes no consistency (random), W=1 denotes that all specimens had identical patterns of ranked data.

Homo

Tb.BV/TV		
6.1	3.3	6.3
7.2	4.0	6.8
3.2	3.2	4.8

Kendall's W 0.360

Tb.Th		
6.0	6.4	8.1
5.0	4.3	5.9
2.9	3.5	2.8

Kendall's W 0.425

Tb.N		
5.8	1.8	3.8
7.6	4.9	6.1
4.4	5.1	5.5

Kendall's W 0.350

Tb.DA		
6.2	7.6	1.9
6.5	5.5	4.4
3.9	5.8	3.2

Kendall's W 0.427

Tb.I		
3.8	2.4	8.1
3.5	4.5	5.6
6.1	4.2	6.8

Kendall's W 0.427

Tb.E		
7.3	3.8	5.8
6.7	3.7	3.2
8.1	4.4	1.9

Kendall's W 0.576

Sc.%HighDensity		
4.9	2.0	7.6
5.9	1.3	8.4
5.9	2.6	6.1

Kendall's W 0.828

Sc.MeanHouns		
3.7	2.4	7.1
5.5	2.5	8.4
4.4	3.6	7.3

Kendall's W 0.644

Sc.Th		
3.2	4.8	6.6
5.4	5.8	8.4
1.6	3.9	5.5

Kendall's W 0.514

Pan

Tb.BV/TV		
8.8	3.5	5.0
7.8	1.6	4.6
4.8	3.4	5.7

Kendall's W 0.665

Tb.Th		
7.8	6.9	7.7
6.8	3.0	5.2
2.6	2.3	3.0

Kendall's W 0.719

Tb.N		
4.7	1.7	1.8
4.9	4.6	5.1
7.9	7.6	6.9

Kendall's W 0.676

Tb.DA		
5.3	6.5	3.5
6.1	4.1	6.1
4.0	4.1	5.5

Kendall's W 0.167

Tb.I		
4.8	3.5	6.5
3.9	6.0	3.9
6.1	5.9	4.6

Kendall's W 0.167

Tb.E		
4.0	4.4	3.6
4.8	6.6	5.2
4.1	6.8	5.8

Kendall's W 0.174

Sc.%HighDensity		
7.0	3.0	6.2
6.7	2.0	5.1
5.4	3.3	6.5

Kendall's W 0.439

Sc.MeanHouns		
6.8	2.2	6.1
7.2	2.3	4.6
4.5	4.2	7.4

Kendall's W 0.510

Sc.Th		
5.8	2.5	7.6
7.9	4.2	3.7
2.8	4.3	6.5

Kendall's W 0.529

Gorilla

Tb.BV/TV		
8.6	4.9	5.9
7.9	3.4	5.1
3.6	1.5	4.1

Kendall's W 0.668

Tb.Th		
7.4	6.9	7.9
6.1	3.9	5.4
3.1	1.7	2.6

Kendall's W 0.667

Tb.N		
5.6	2.4	1.5
7.1	4.9	4.9
7.1	5.1	6.5

Kendall's W 0.509

Tb.DA		
6.5	4.1	3.0
5.4	6.0	5.6
3.6	6.4	4.4

Kendall's W 0.211

Tb.I		
3.5	5.9	7.0
4.6	4.0	4.4
6.4	3.6	5.6

Kendall's W 0.211

Tb.E		
3.6	3.1	2.9
4.5	7.1	6.2
5.1	7.1	5.4

Kendall's W 0.344

Sc.%HighDensity		
6.5	3.6	7.4
7.3	1.9	5.8
5.0	2.5	5.1

Kendall's W 0.541

Sc.MeanHouns		
6.2	3.4	6.9
6.4	2.6	6.7
2.8	3.0	6.9

Kendall's W 0.509

Sc.Th		
5.6	4.1	7.6
7.1	4.7	6.0
1.3	2.9	5.7

Kendall's W 0.531

Pongo

Tb.BV/TV		
9.0	3.5	4.5
7.5	1.5	5.3
4.9	2.5	6.2

Kendall's W 0.746

Tb.Th		
8.3	6.2	5.7
5.7	1.8	5.8
2.8	3.3	5.3

Kendall's W 0.536

Tb.N		
6.3	1.7	2.3
7.7	4.3	6.2
7.6	3.0	5.8

Kendall's W 0.678

Tb.DA		
3.9	6.7	6.0
4.4	6.5	4.9
5.2	4.5	2.8

Kendall's W 0.217

Tb.I		
6.1	3.3	4.0
5.6	3.5	5.1
4.8	5.5	7.2

Kendall's W 0.217

Tb.E		
4.6	5.5	6.2
5.4	6.0	2.9
5.7	5.0	3.6

Kendall's W 0.164

Sc.%HighDensity		
7.7	4.7	3.2
6.0	2.2	4.4
4.7	4.4	7.8

Kendall's W 0.474

Sc.MeanHouns		
8.2	3.3	4.1
5.8	2.2	4.5
3.2	5.5	8.2

Kendall's W 0.599

Sc.Th		
7.4	5.3	7.9
6.4	2.4	3.5
1.5	4.1	6.5

Kendall's W 0.683

Papio

Tb.BV/TV		
8.4	1.7	5.1
4.9	1.4	6.3
4.4	5.6	7.3

Kendall's W 0.716

Tb.Th		
6.7	4.2	7.2
6.9	2.2	6.7
3.0	5.9	2.3

Kendall's W 0.586

Tb.N		
2.1	5.1	2.8
6.1	6.6	4.6
8.8	5.6	3.3

Kendall's W 0.589

Tb.DA		
3.7	3.8	5.7
5.2	5.9	8.0
2.3	3.0	7.4

Kendall's W 0.504

Tb.I		
6.3	6.2	4.3
4.8	4.1	2.0
7.7	7.0	2.6

Kendall's W 0.504

Tb.E		
4.0	5.3	3.7
6.4	7.3	3.8
4.7	4.6	5.3

Kendall's W 0.199

Sc.%HighDensity		
6.4	1.1	4.1
6.7	1.9	4.7
8.3	5.6	6.2

Kendall's W 0.711

Sc.MeanHouns		
6.6	1.0	3.4
7.1	2.0	5.6
8.2	4.2	6.9

Kendall's W 0.820

Sc.Th		
5.6	1.6	3.8
7.7	5.6	8.3
2.7	4.7	5.1

Kendall's W 0.629

Legend

A1	A2	A3
B1	B2	B3
C1	C2	C3

Table 2. 29: Mean eigenvalues and orientation of the primary eigenvector in each region of the distal tibia.

		Lateral (1)						MLMid (2)						Medial (3)					
	A1	Eigenvalue			Primary Eigenvector (°)			A2	Eigenvalue			Primary Eigenvector (°)			A3	Eigenvalue			Primary Eigenvector (°)		
		1	2	3	Trend	Incline	Variance		1	2	3	Trend	Incline	Variance		1	2	3	Trend	Incline	Variance
	Homo	0.609	0.229	0.162	349	70	0.06	*Homo*	0.519	0.309	0.172	290	47	0.24	*Homo*	0.594	0.276	0.130	295	44	0.09
Anterior	*Pan*	0.524	0.298	0.178	5	78	0.10	*Pan*	0.513	0.296	0.191	112	17	0.44	*Pan*	0.544	0.289	0.168	281	51	0.05
(A)	*Gorilla*	0.561	0.285	0.154	322	84	0.05	*Gorilla*	0.557	0.291	0.152	270	81	0.12	*Gorilla*	0.525	0.321	0.154	276	66	0.15
	Pongo	0.509	0.314	0.178	236	72	0.20	*Pongo*	0.523	0.354	0.123	243	73	0.02	*Pongo*	0.558	0.291	0.150	235	68	0.06
	Papio	0.445	0.342	0.213	14	71	0.29	*Papio*	0.438	0.344	0.218	253	64	0.29	*Papio*	0.523	0.292	0.185	281	25	0.03
	B1	Eigenvalue			Primary Eigenvector (°)			B2	Eigenvalue			Primary Eigenvector (°)			B3	Eigenvalue			Primary Eigenvector (°)		
		1	2	3	Trend	Incline	Variance		1	2	3	Trend	Incline	Variance		1	2	3	Trend	Incline	Variance
	Homo	0.687	0.217	0.097	316	85	0.01	*Homo*	0.669	0.197	0.135	156	85	0.05	*Homo*	0.692	0.187	0.121	101	84	0.00
APMid	*Pan*	0.644	0.206	0.150	280	81	0.01	*Pan*	0.565	0.268	0.167	184	86	0.14	*Pan*	0.622	0.226	0.152	170	80	0.01
(B)	*Gorilla*	0.638	0.207	0.155	272	81	0.01	*Gorilla*	0.568	0.281	0.151	235	84	0.01	*Gorilla*	0.590	0.245	0.165	194	75	0.04
	Pongo	0.581	0.239	0.181	257	73	0.03	*Pongo*	0.466	0.313	0.220	272	83	0.21	*Pongo*	0.566	0.284	0.150	206	74	0.02
	Papio	0.549	0.253	0.197	255	72	0.02	*Papio*	0.431	0.327	0.242	32	87	0.28	*Papio*	0.527	0.286	0.186	201	86	0.01
	C1	Eigenvalue			Primary Eigenvector (°)			C2	Eigenvalue			Primary Eigenvector (°)			C3	Eigenvalue			Primary Eigenvector (°)		
		1	2	3	Trend	Incline	Variance		1	2	3	Trend	Incline	Variance		1	2	3	Trend	Incline	Variance
	Homo	0.591	0.249	0.160	169	69	0.02	*Homo*	0.554	0.273	0.173	166	81	0.08	*Homo*	0.586	0.292	0.122	112	81	0.09
Posterior	*Pan*	0.595	0.261	0.144	208	77	0.01	*Pan*	0.490	0.312	0.198	200	81	0.27	*Pan*	0.512	0.311	0.178	225	78	0.24
(C)	*Gorilla*	0.566	0.282	0.152	226	80	0.03	*Gorilla*	0.525	0.299	0.176	218	74	0.07	*Gorilla*	0.555	0.292	0.154	229	67	0.02
	Pongo	0.588	0.263	0.149	201	79	0.02	*Pongo*	0.548	0.305	0.147	252	71	0.01	*Pongo*	0.544	0.312	0.145	239	67	0.09
	Papio	0.557	0.305	0.138	210	76	0.02	*Papio*	0.446	0.335	0.219	84	55	0.37	*Papio*	0.532	0.320	0.148	237	57	0.13

Table 2. 30: Mean eigenvalues and orientation of the primary eigenvector in each region of the talus.

		Lateral (1)						MLMid (2)						Medial (3)					
	A1	Eigenvalue			Primary Eigenvector (°)			A2	Eigenvalue			Primary Eigenvector (°)			A3	Eigenvalue			Primary Eigenvector (°)		
		1	2	3	Trend	Incline	Variance		1	2	3	Trend	Incline	Variance		1	2	3	Trend	Incline	Variance
	Homo	0.671	0.249	0.081	32	55	0.02	*Homo*	0.589	0.361	0.050	209	68	0.09	*Homo*	0.555	0.271	0.174	171	47	0.04
Anterior	*Pan*	0.470	0.354	0.176	23	54	0.20	*Pan*	0.488	0.355	0.157	272	55	0.22	*Pan*	0.453	0.343	0.204	300	66	0.25
(A)	*Gorilla*	0.496	0.354	0.150	24	55	0.17	*Gorilla*	0.473	0.352	0.175	278	65	0.26	*Gorilla*	0.451	0.348	0.201	307	74	0.13
	Pongo	0.435	0.325	0.240	54	48	0.42	*Pongo*	0.474	0.327	0.199	28	46	0.22	*Pongo*	0.476	0.311	0.213	357	52	0.27
	Papio	0.436	0.336	0.228	34	67	0.20	*Papio*	0.445	0.322	0.233	311	63	0.10	*Papio*	0.455	0.353	0.192	330	58	0.28
	B1	Eigenvalue			Primary Eigenvector (°)			B2	Eigenvalue			Primary Eigenvector (°)			B3	Eigenvalue			Primary Eigenvector (°)		
		1	2	3	Trend	Incline	Variance		1	2	3	Trend	Incline	Variance		1	2	3	Trend	Incline	Variance
	Homo	0.653	0.265	0.082	51	59	0.01	*Homo*	0.570	0.347	0.082	113	85	0.05	*Homo*	0.547	0.350	0.103	211	62	0.07
APMid	*Pan*	0.487	0.343	0.170	67	55	0.12	*Pan*	0.492	0.300	0.208	290	77	0.04	*Pan*	0.492	0.341	0.168	232	65	0.06
(B)	*Gorilla*	0.491	0.342	0.167	60	60	0.04	*Gorilla*	0.530	0.298	0.172	312	85	0.02	*Gorilla*	0.514	0.317	0.169	257	75	0.06
	Pongo	0.451	0.318	0.231	77	63	0.05	*Pongo*	0.477	0.327	0.196	5	82	0.14	*Pongo*	0.425	0.359	0.216	301	79	0.19
	Papio	0.477	0.308	0.215	79	72	0.02	*Papio*	0.495	0.298	0.208	324	81	0.06	*Papio*	0.479	0.377	0.144	241	68	0.23
	C1	Eigenvalue			Primary Eigenvector (°)			C2	Eigenvalue			Primary Eigenvector (°)			C3	Eigenvalue			Primary Eigenvector (°)		
		1	2	3	Trend	Incline	Variance		1	2	3	Trend	Incline	Variance		1	2	3	Trend	Incline	Variance
	Homo	0.650	0.218	0.132	27	73	0.01	*Homo*	0.581	0.337	0.082	54	70	0.04	*Homo*	0.503	0.366	0.131	45	86	0.30
Posterior	*Pan*	0.459	0.337	0.204	74	67	0.40	*Pan*	0.494	0.298	0.208	118	75	0.03	*Pan*	0.491	0.324	0.186	212	43	0.11
(C)	*Gorilla*	0.482	0.318	0.200	101	59	0.10	*Gorilla*	0.530	0.315	0.156	95	79	0.02	*Gorilla*	0.488	0.327	0.185	208	67	0.17
	Pongo	0.466	0.323	0.211	108	58	0.11	*Pongo*	0.450	0.328	0.222	51	77	0.16	*Pongo*	0.409	0.337	0.255	181	79	0.29
	Papio	0.428	0.317	0.254	202	79	0.09	*Papio*	0.433	0.321	0.246	140	80	0.13	*Papio*	0.489	0.342	0.169	310	71	0.23

Figures

(a) Distal tibia

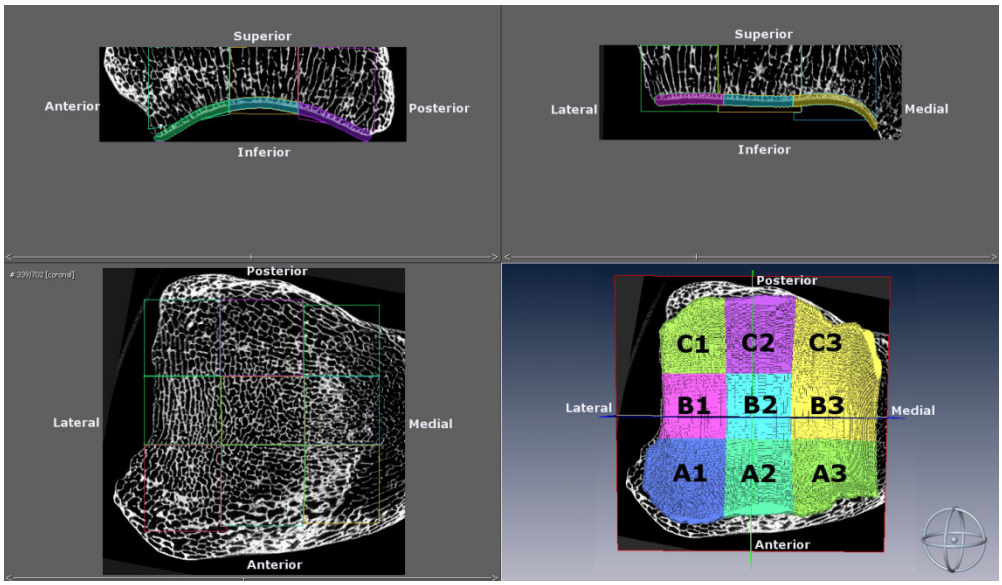

(b) Talus

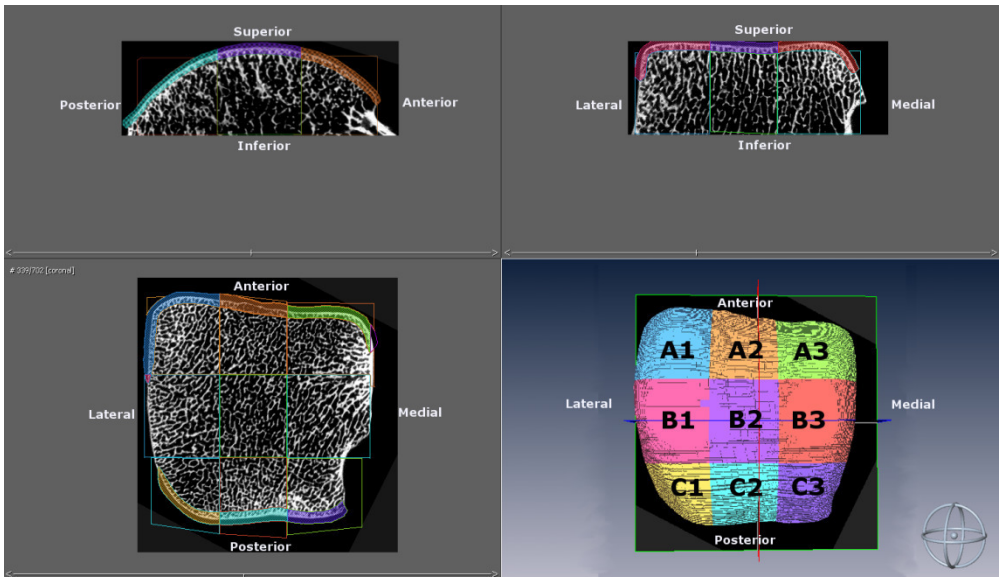

Figure 2. 1: Orientation of (a) distal tibia and (b) talus, and segmentation of the subchondral bone plate and underlying trabecular bone volume into nine regions of interest.
The subchondral bone plate extended slightly onto the malleolar articular surface of the distal tibia and onto both medial and lateral articular facets of the talus.

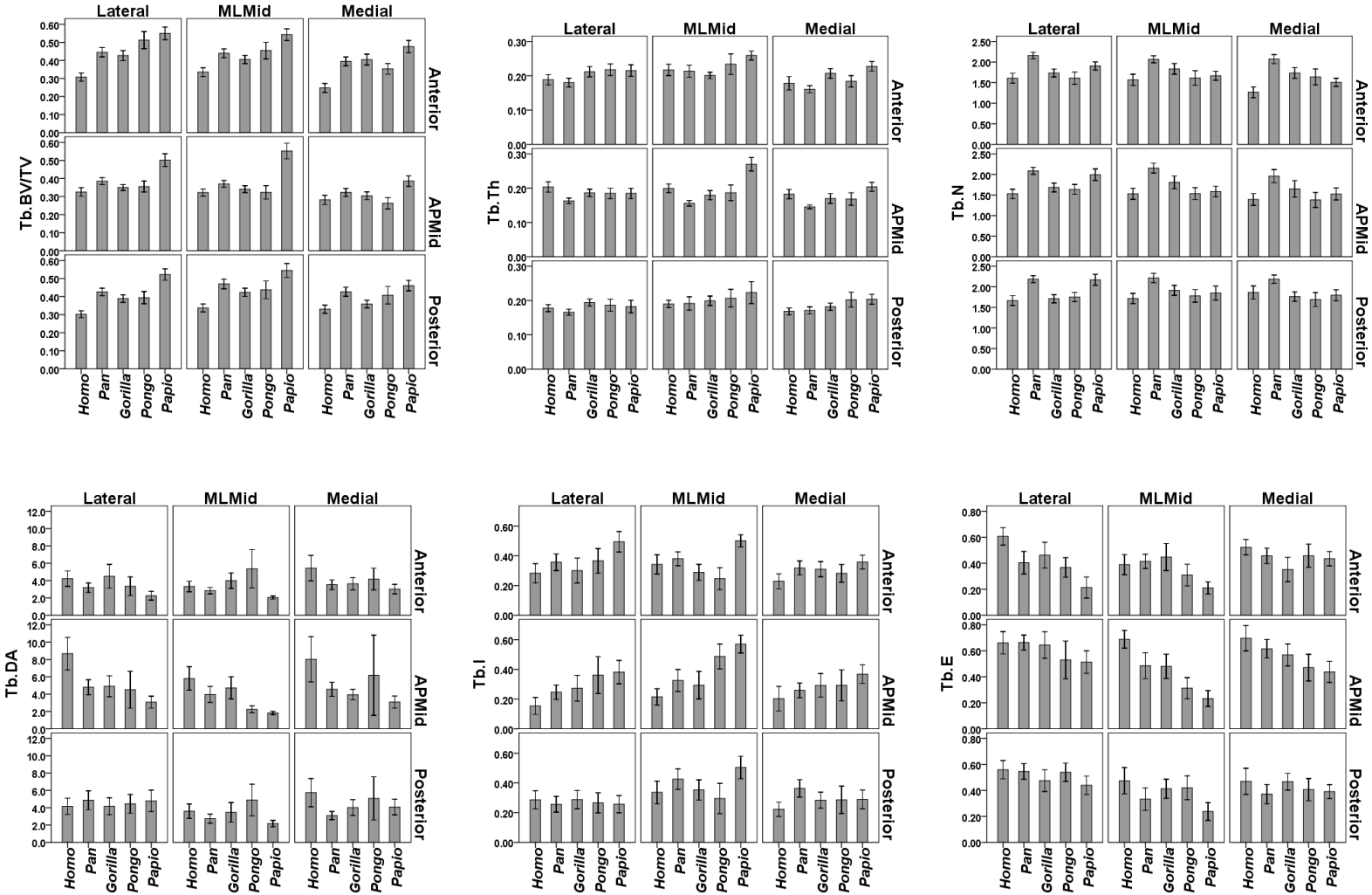
Lateral
MLMid
Medial
Anterior
APMid
Posterior
Tb.BV/TV
Tb.Th
Tb.N
Tb.DA
Tb.I
Tb.E
Homo
Pan
Gorilla
Pongo
Papio

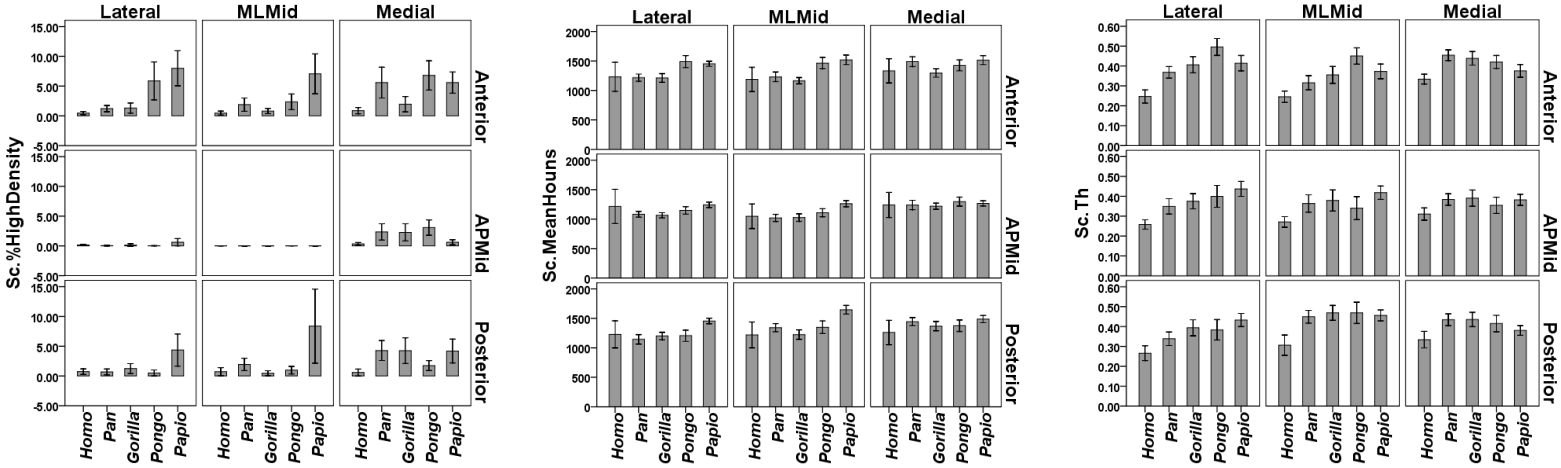

Figure 2. 2: The mean values and 95% confidence interval for each trabecular and subchondral bone scalar variable in the distal tibia, comparing the five species within each of the nine regions.

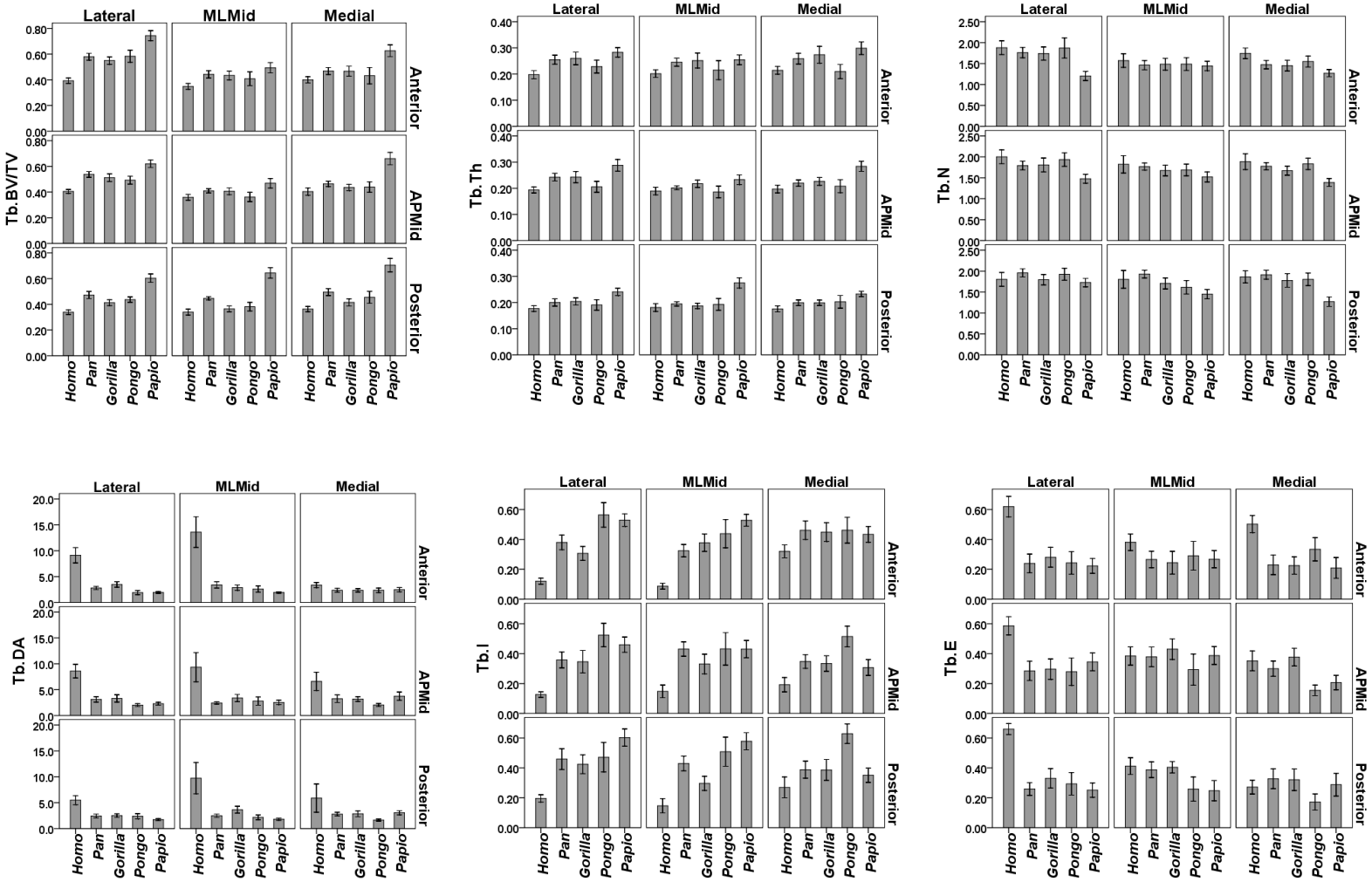
Lateral
MLMid
Medial
Anterior
APMid
Posterior
Tb.BV/TV
Tb.Th
Tb.N
Tb.DA
Tb.I
Tb.E
Homo
Pan
Gorilla
Pongo
Papio

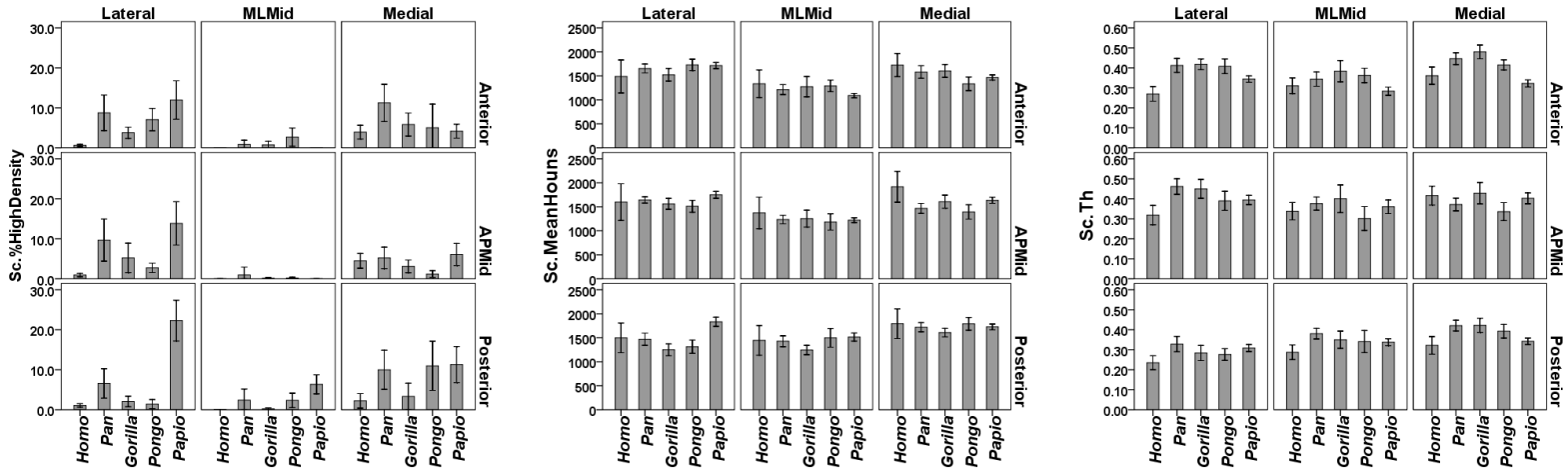

Figure 2. 3: The mean values and 95% confidence interval for each trabecular and subchondral bone scalar variable in the talus, comparing the five species within each of the nine regions.

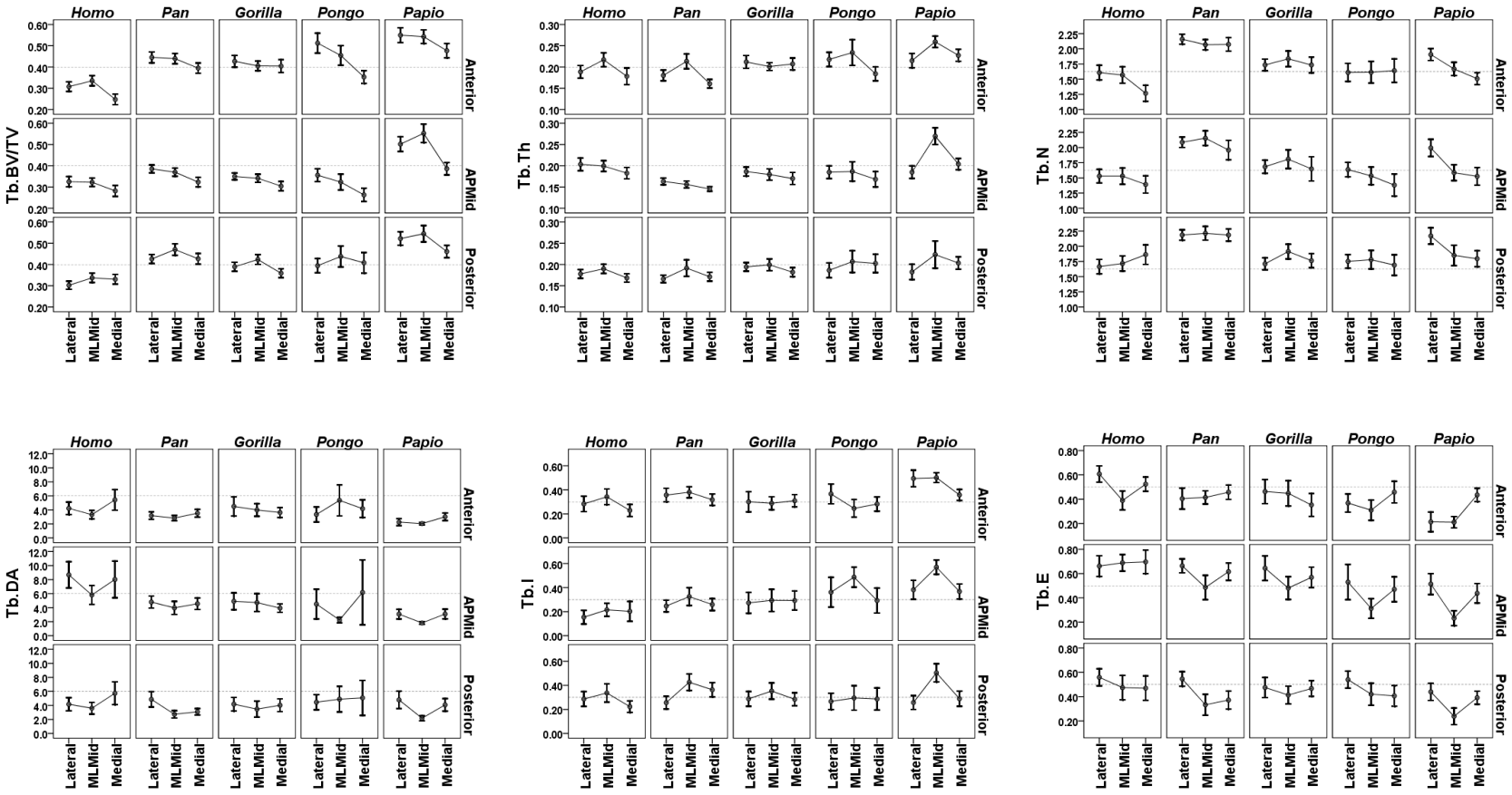
Homo
Pan
Gorilla
Pongo
Papio
Anterior
APMid
Posterior
Lateral
MLMid
Medial
Tb.BV/TV
Tb.Th
Tb.N
Tb.DA
Tb.I
Tb.E

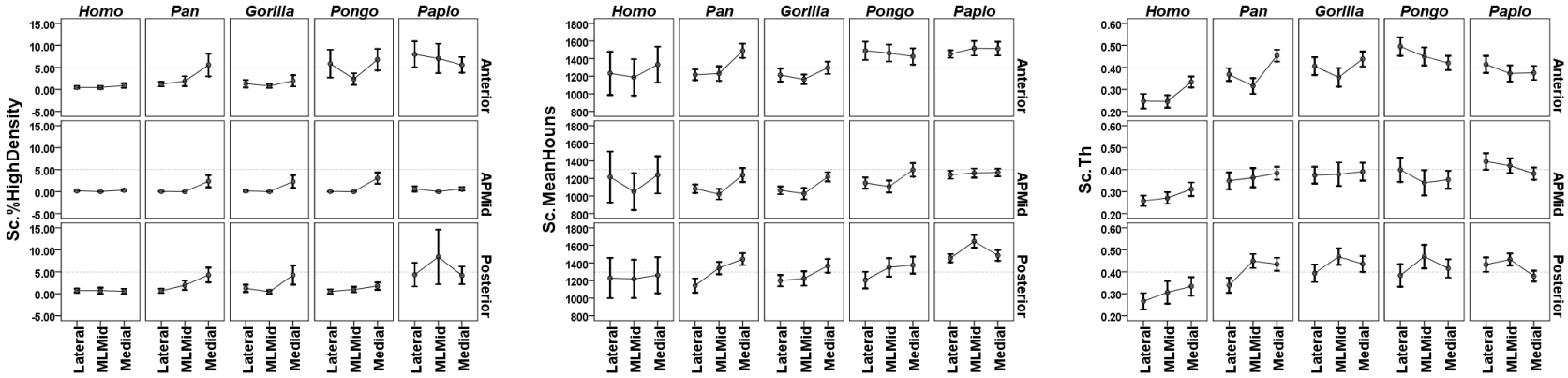

Figure 2. 4: The mean values and 95% confidence interval for each trabecular and subchondral bone scalar variable in the tibia, showing the patterns of distribution of the nine regions for the five species.

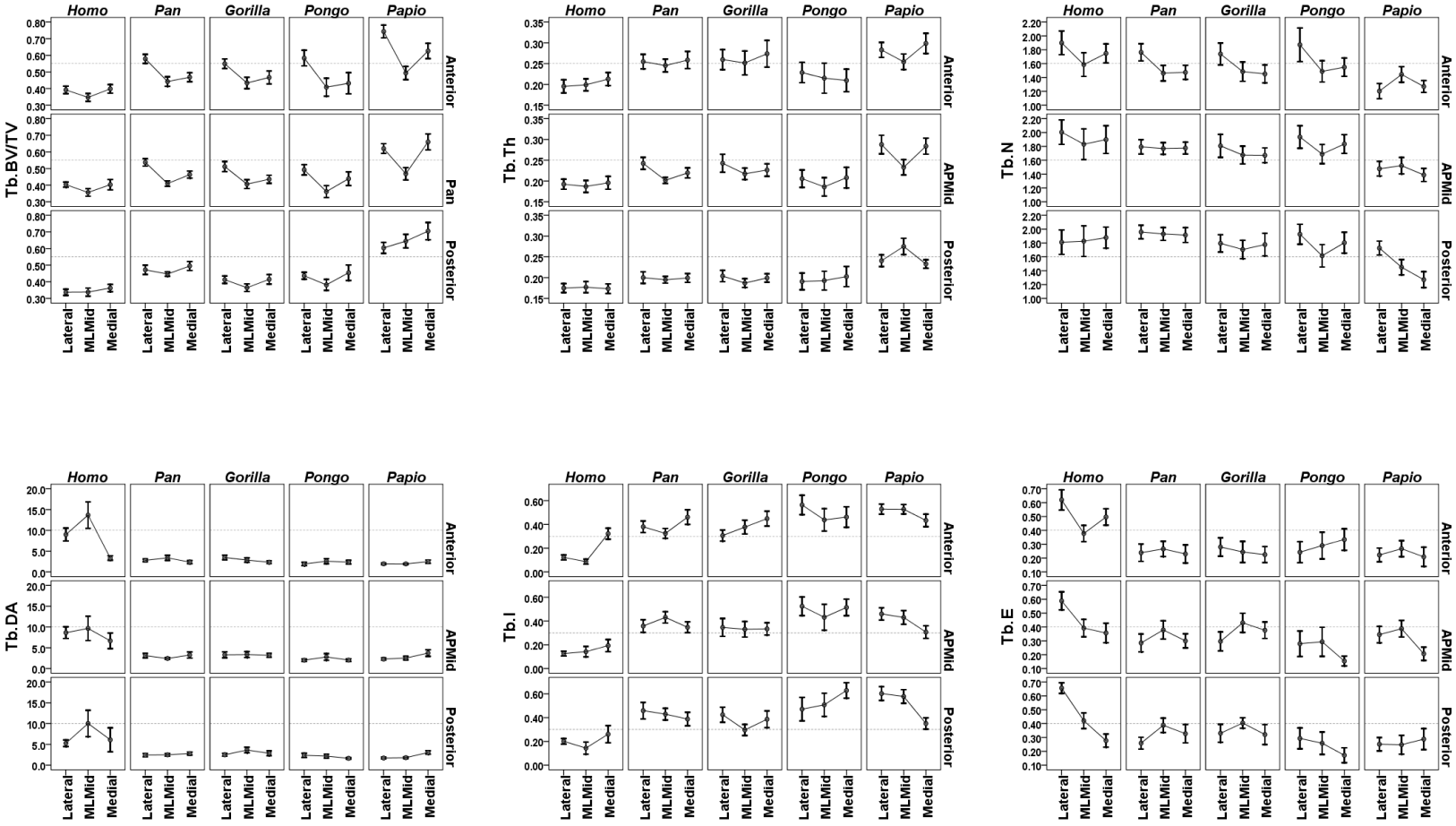
Homo
Pan
Gorilla
Pongo
Papio
Anterior
APMid
Posterior
Lateral
MLMid
Medial
Tb.BV/TV
Tb.Th
Tb.N
Tb.DA
Tb.I
Tb.E

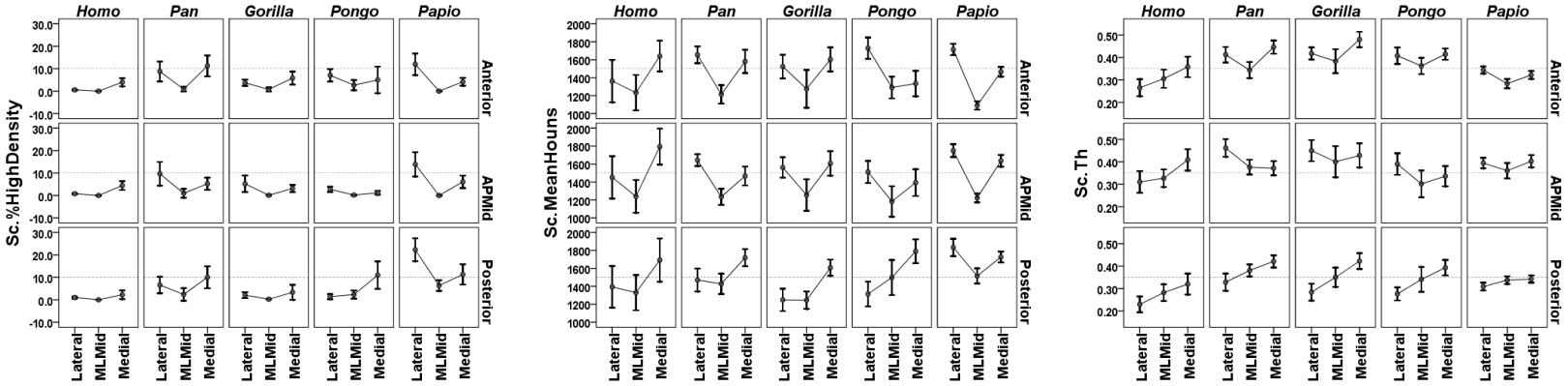

Figure 2. 5: The mean values and 95% confidence interval for each trabecular and subchondral bone scalar variable in the talus, showing the patterns of distribution of the nine regions for the five species.

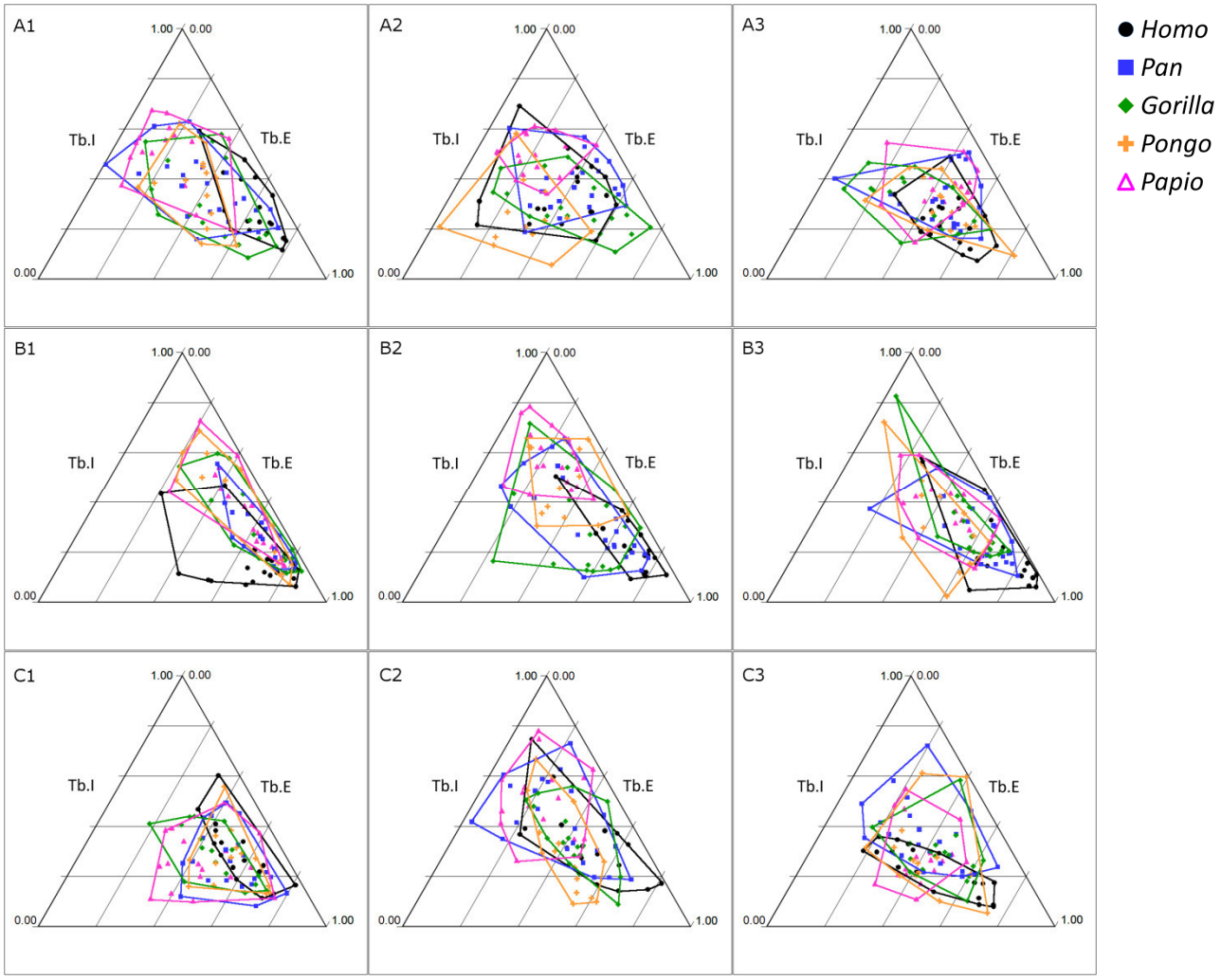

Figure 2. 6: Distribution of trabecular shape indices in the distal tibia.
Within each region, each point plots the Tb.I (τ_3/τ_1) and Tb.E ($1-(\tau_2/\tau_1)$) value; lines were drawn to enclose the distribution of each species for comparative visualization. Points towards the top apex indicate more isotropic trabeculae; points towards the bottom indicate more anisotropic trabeculae. Points towards the bottom left apex indicate more plate-shaped trabeculae; points towards the bottom right apex indicate more rod-shaped trabeculae.

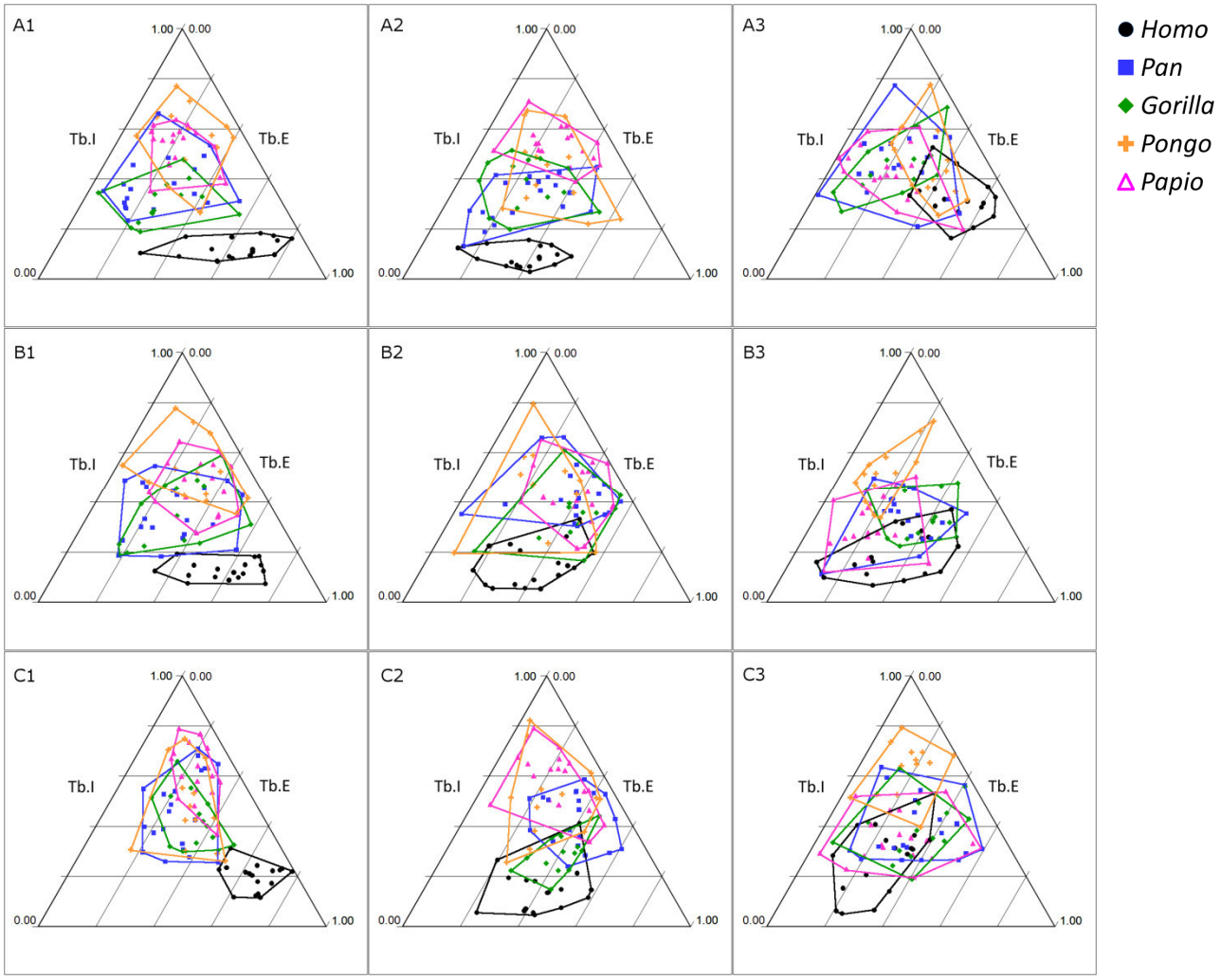

Figure 2. 7: Distribution of trabecular shape indices in the talus.
Within each region, each point plots the Tb.I (τ_3/τ_1) and Tb.E ($1-(\tau_2/\tau_1)$) value; lines were drawn to enclose the distribution of each species for comparative visualization. Points towards the top apex indicate more isotropic trabeculae; points towards the bottom indicate more anisotropic trabeculae. Points towards the bottom left apex indicate more plate-shaped trabeculae; points towards the bottom right apex indicate more rod-shaped trabeculae.

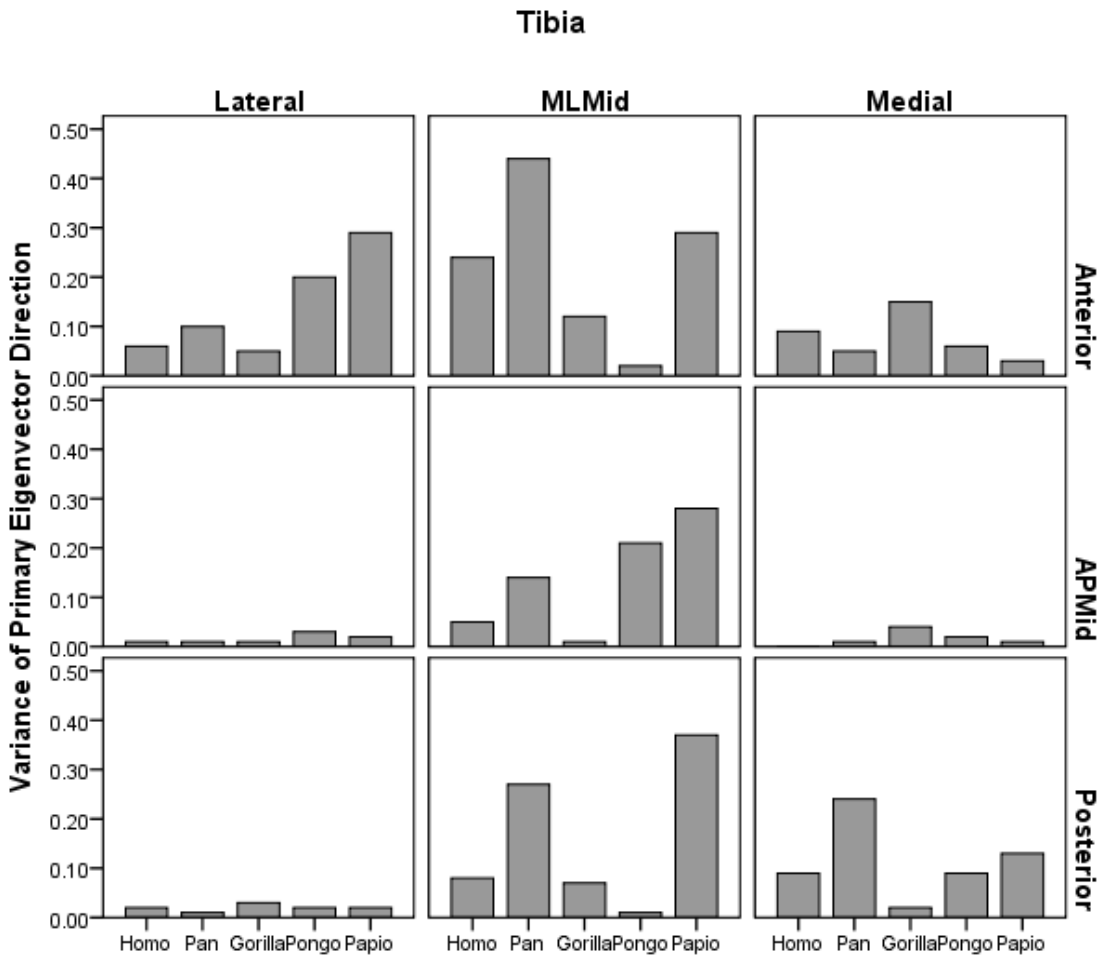

Figure 2. 8: Species comparison of the relative spherical variance in regions of the distal tibia.

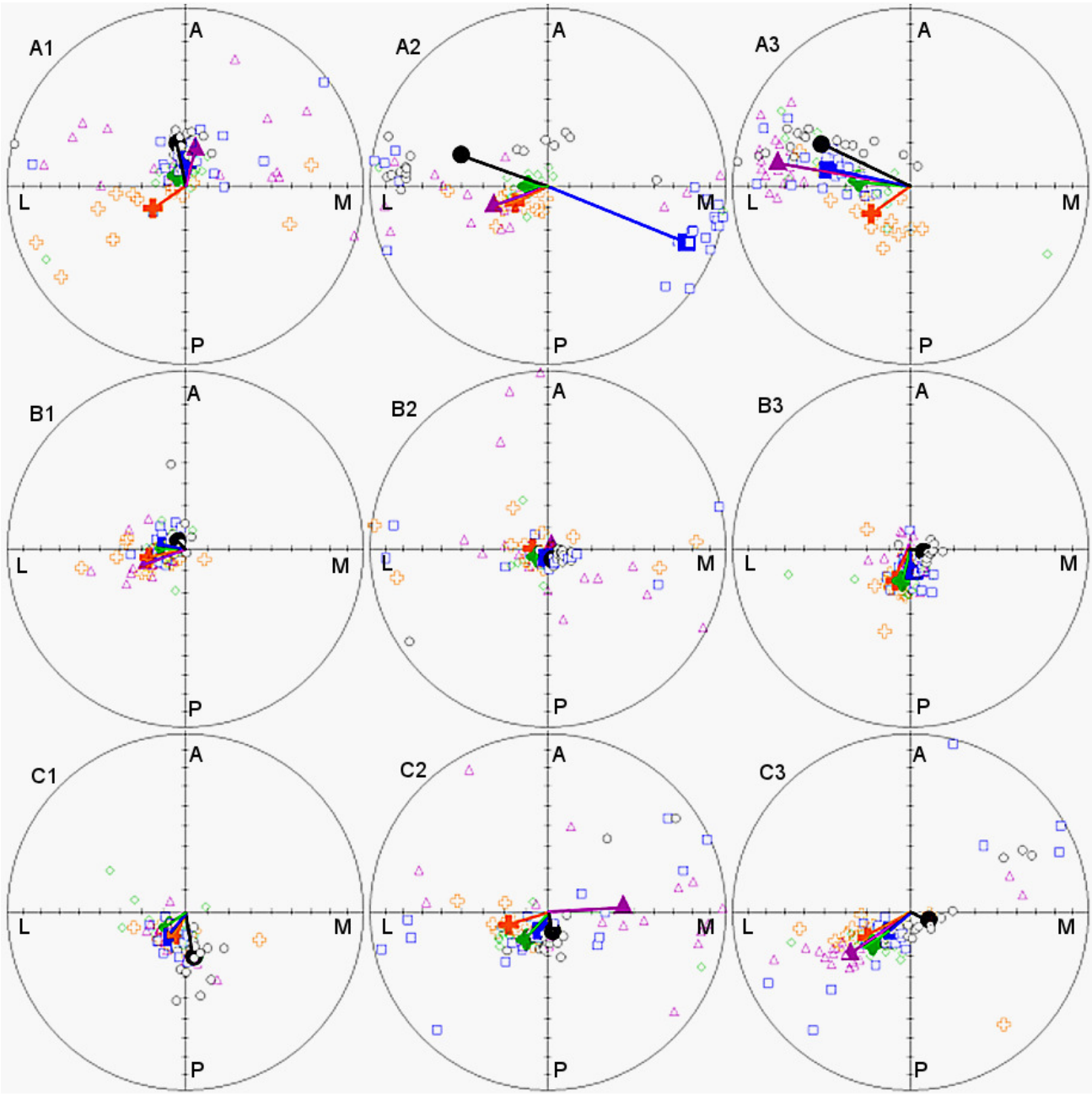

Figure 2. 9: Distribution of the primary trabecular eigenvector direction in each region of the distal tibia.
Each region is represented by a top-down view of a sphere, with each eigenvector depicted with its origin at the center of the sphere and tip on the outer surface of the sphere. Each small point represents one individual. Each large point and line from the center represents the species mean trabecular orientation. Points located towards the center of the circle represent more vertically-oriented trabeculae; points located towards the periphery represent more transversely-oriented trabeculae.

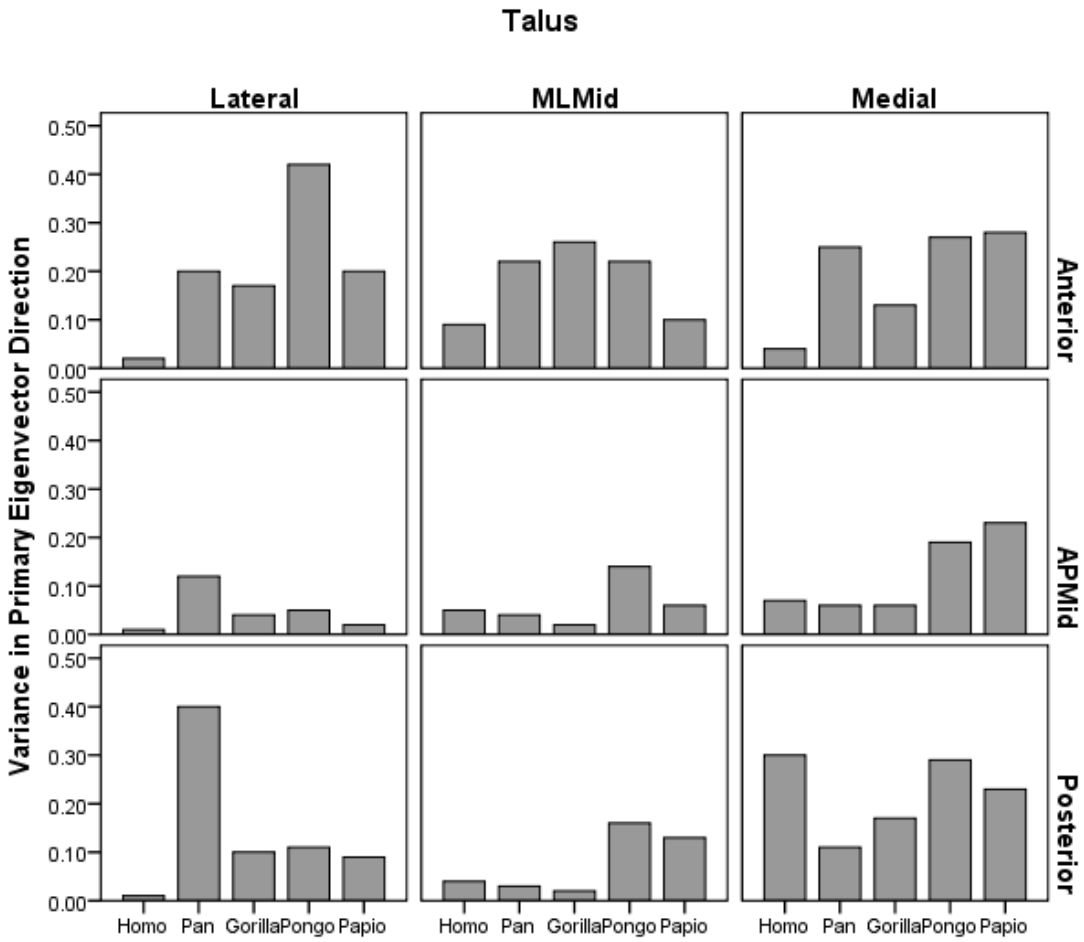

Figure 2. 10: Species comparison of the relative spherical variance in regions of the talus.

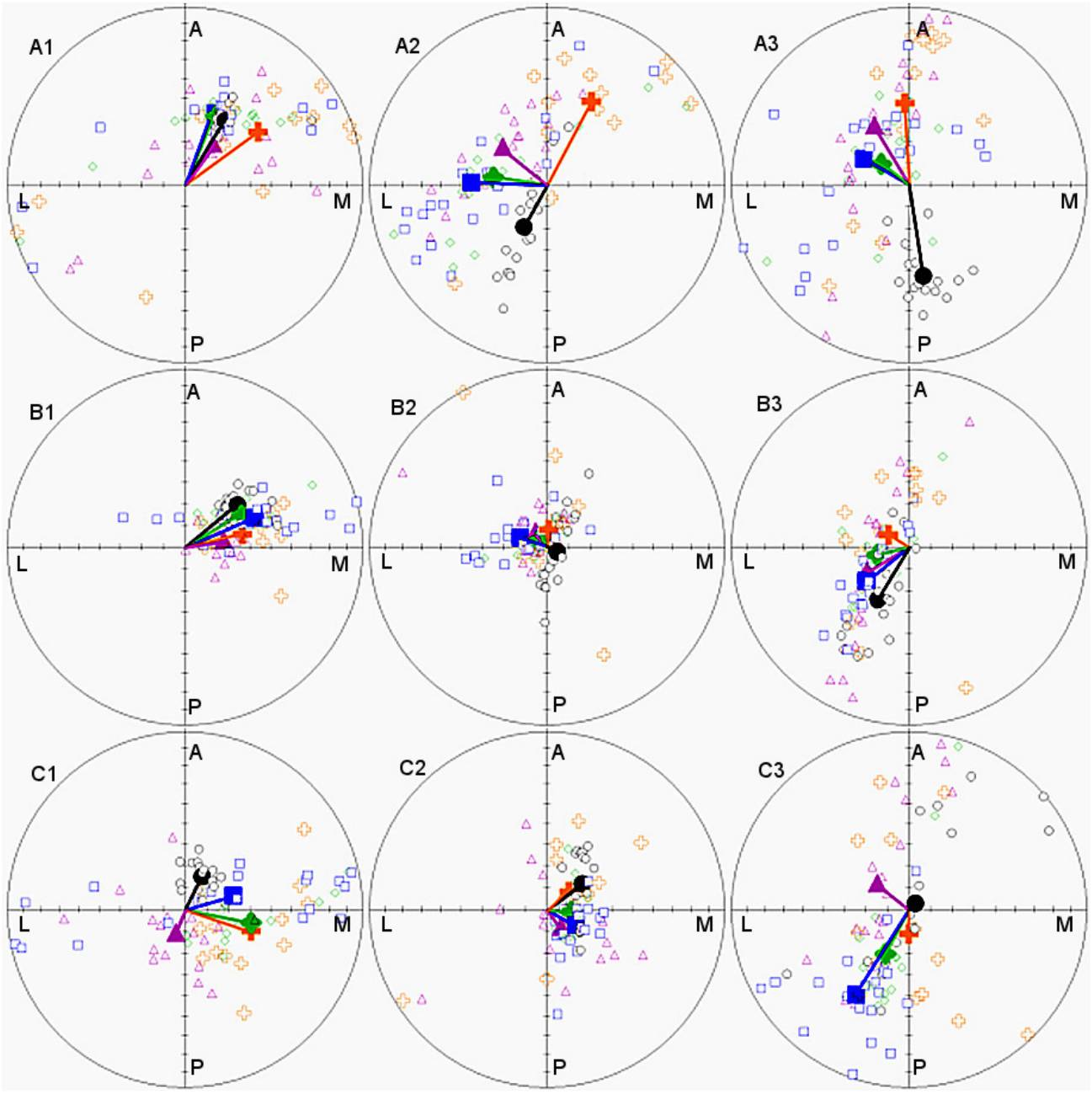

Figure 2. 11: Distribution of the primary trabecular eigenvector direction in each region of the talus.
Each region is represented by a top-down view of a sphere, with each eigenvector depicted with its origin at the center of the sphere and tip on the outer surface of the sphere. Each small point represents one individual. Each large point and line from the center represents the species mean trabecular orientation. Points located towards the center of the circle represent more vertically-oriented trabeculae; points located towards the periphery represent more transversely-oriented trabeculae.

3 Chapter 3: Analysis of the microarchitecture of the KNM-ER 1464 talus

3.1 Introduction

In human evolutionary studies, changes in the morphology of the foot bones hold much significance in the understanding of the transition to obligate bipedality (see review by Harcourt-Smith and Aiello 2004). In particular, the external morphology of the talus bone has long been studied in relation to the habitual posture and locomotion in hominids (Day and Wood 1968; DeSilva 2009; Gebo and Schwartz 2006; Kidd and Oxnard 2002; Lisowski et al. 1974). The talus is the "keystone" of the medial longitudinal arch of the foot, serving to transmit the entire weight of the individual and to align the weight-bearing foot with the substrate during locomotion. Thus it is well positioned to demonstrate the adaptive morphology that led from an ancestral arboreal quadrupedal ape to a terrestrial bipedal human. The talus is also somewhat more frequently and completely preserved in the primate fossil record than other bony elements, further bolstering its potential utility in elucidating the habitual posture of a fossil animal (DeSilva 2008; Gebo and Schwartz 2006; Latimer et al. 1987; e.g., Lisowski et al. 1974).

Comparative studies of the external morphology of the talus demonstrate differences that separate humans from apes (Day and Wood 1968; Kidd et al. 1996; Kidd and Oxnard 2002; Latimer et al. 1987; Lisowski et al. 1974). The angle that the talar neck makes with the talar body is narrower in humans, thought to re-align the hallux with the rest of the foot, making the hallux less mobile for grasping but more stable for propulsion. The angle of talar head torsion is increased in humans, reducing the range of motion of the transverse tarsal joint which also serves to stabilize the human foot into a more efficient propulsive lever. The angle of inclination of the talar neck is increased in humans, associated with the presence of a medial longitudinal arch. The medial border of the talar trochlea is higher in humans than in chimpanzees, which is said to be related to the more vertically oriented tibia in humans due to the valgus knee position.

However, while external traits have been identified that separate humans from the great apes, morphometric studies of some important fossil talus bones reveal unique mosaics of human-like and ape-like features that complicate locomotor reconstruction of these extinct hominins.

The KNM-ER 1464 talus is one such enigmatic talus. The KNM-ER 1464 talus was found on the east side of Lake Turkana in northern Kenya, in Area 6A at Ileret, Koobi Fora (Leakey 1973). Found in the same level, dated to 1.56-1.60 Ma (Wood and Constantino 2007), was a robust right mandibular corpus KNM-ER 801 with a small I_2 and large M_2 and M_3, as well as other isolated teeth, which show the distinctive crown morphology of *Paranthropus boisei* (Leakey 1972). Therefore, it has been assumed that the talus belongs to this robust

australopithecine although its external morphology was demonstrated to have mixed human-like and ape-like characters (Day 1976). In an extensive morphometric analysis of fossil hominin tali, (Gebo and Schwartz 2006) found that KNM-ER 1464 and other robust australopithecines (e.g., TM 1517) share a grooved trochlea, a laterally-projecting fibular facet, a wide head, and a curved medial border of the trochlea. But it was also found to share features with early *Homo* (e.g., KNM-ER 813), such as its large size and short head and neck relative to the trochlea.

Because there is as yet no well-authenticated *P. boisei* skeleton, and both *P. boisei* and early members of *Homo*, *Homo habilis* and *Homo ergaster*/*erectus* are contemporaneously found at localities in East Africa (Spoor et al. 2007), the question persists of how to sort out ownership of unassociated postcranial fossils (Wood and Constantino 2007). Indeed, there is a long-standing debate of the ownership of another fossil talus and foot, OH 8 (Day and Napier 1964; Day and Wood 1968, 1969; Kidd et al. 1996; Oxnard 1972) and a tibia and fibula OH 35 (McHenry 1994; Stern and Susman 1983), from Bed I and Bed II at Olduvai Gorge, Tanzania.

Recently, a series of hominin footprints have been found at Ileret, dated to 1.51-1.53 Ma, and are interpreted to have been made by an essentially modern human foot with a modern human toe-off mechanism, evidenced by an instep reflective of a medial longitudinal arch and well-defined ball beneath the first and second metatarsal heads (Bennett et al. 2009). However, the authors note that the angle of hallucal abduction is intermediate between that found at Laetoli, Tanzania, dated to 3.5 Ma and attributed to *Australopithecus afarensis*, and that of modern humans. The hallux is significantly less abducted (14° relative to the long axis of the foot) compared to the Laetoli footprints (27°), but is still significantly more abducted than that of modern humans (8°). From the stride length and size of the footprints, the authors estimate a relatively large hominid (average height 1.76 +/- 0.26 m), and thus attribute the footprints to the contemporaneous larger-bodied *Homo ergaster*/*erectus* rather than the smaller-bodied *H. habilis* or *P. boisei*.

The possibility arises then, that the relatively large KNM-ER 1464 talus belongs neither to *P. boisei* nor *H. habilis*, but rather to *H. ergaster*/*erectus*. If this is the case, and if *H. ergaster*/*erectus* displayed a modern human gait pattern, then it would be expected that the bony morphology of KNM-ER 1464 would be similar to that of modern humans. Gebo and Schwartz (2006) found some support for this in the examination of the external bony morphology. It is the goal of this study to test this hypothesis from the internal trabecular bone morphology. While a comparison to the internal morphology of other fossil hominid tali is as yet unavailable, this study will use extant hominoids as a comparative functional sample.

If KNM-ER 1464 belonged to a hominid with a modern-human-like foot fully adapted to an energy-efficient striding style of terrestrial gait rather than retaining arboreal abilities, then it is predicted that (1) the regional distribution of trabecular bone morphology and (2) the regional pattern of orientation of trabeculae within the talus should be more similar to modern humans than to non-human hominoids.

3.1.1 Specific predictions

It has been demonstrated by this dissertation that the overall trabecular bone architecture in the talus differs among hominoid species – humans have lower bone volume and greater anisotropy than all other groups, while chimpanzees had greater trabecular number and lower trabecular thickness than all other groups. Thus it is predicted that KNM-ER 1464 would display a level of overall bone volume and anisotropy that is more similar to that of humans than the other species.

The patterns of trabecular bone distribution also differed among species. Relatively greater trabecular bone volume was found equally in the lateral and medial region in humans but more focused in the lateral regions of the non-humans hominoids, presumably related to differences in joint posture during habitual locomotion. Thus it is predicted that KNM-ER 1464 would show patterns of trabecular bone volume and/or thickness that is more similar to that of humans than the other species.

Humans also differed from the other species in that the orientation of trabeculae in the posterolateral and anteromedial regions of the talus were directed toward the posterior calcaneal facet and talar head, respectively, while that of other species tended to be normal to the trochlear surface. It is predicted that KNM-ER 1464 would display primary trabecular orientation similar to that in humans.

3.2 Methods

3.2.1 Study sample

The extant comparative taxa used in this study were modern human (*Homo sapiens sapiens*), gorilla (*Gorilla gorilla gorilla*), chimpanzee (*Pan troglodytes troglodytes*), orangutan (*Pongo pygmaeus*), and baboon (*Papio hamadryas sp*.) (Table 3.1). Adult females of each hominoid species were selected for study in an effort to minimize the potential effects of body size on both locomotor behavior and bone morphology. Male baboons were selected for comparison to similarly minimize effects of body size. Museum records of the female human specimens' mass at death ranged from 44.0-68.0 kg (mean 53.9 kg), which represent a range that is similar to the body mass of female chimpanzees (~ 45 kg) and female gorillas (~71 kg) (Fleagle 1999). Adult status was assessed by epiphyseal fusion on all long bones of each skeleton. Specimens were rejected for analysis if there was evidence of traumatic injury to the limbs or systemic abnormalities such as osteoporosis.

3.2.2 Data collection

The KNM-ER 1464 talus was scanned in July 2008 at the National Museums of Kenya (Nairobi) by Masato Nakatsukasa and Ian Wallace using a Norland-Stratec XCT-Research SA+ pQCT scanner. Each extant talus was scanned individually using the General Electric eXplore Locus SP, (GE Healthcare Pre-Clinical Imaging, London, ON, Canada) housed within the

Department of Biomedical Engineering at the Cleveland Clinic Foundation (see Chapter 2). Both of these systems are designed to image small laboratory animals *in vivo*, where the specimen bed remains stationary while the x-ray source and detector rotate around it.

Care was taken to position and secure each bone in a standard, consistent position on the scanner bed. Both the fossil and extant tali were oriented in the standard basal talar plane (Lisowski et al. 1974) where the posterior and lateral tubercles and the most inferior point of the head rested naturally on the horizontal bed; the anterior edge of the trochlea was oriented perpendicular to the long axis of the scanner.

The fossil specimen was scanned at a voxel resolution of 64 μm, and the extant specimens were scanned at a resolution setting of 45 μm. These resolutions were in the range small enough to produce morphometric results similar to histologic methods (Müller et al. 1996). However, stereological measurements of trabeculae from micro-CT images are sensitive to the image resolution as well as the particular settings on the acquisition system (Kim et al. 2004; Sode et al. 2008). Therefore, a comparison of absolutely measured bone properties would not have been valid. However, any differences caused by the imaging systems was assumed to affect the entire bone uniformly. So the comparison among species of the relative pattern of distribution of values across the talar dome was considered legitimate.

Using GE Microview software (GE Healthcare, http://microview.sourceforge.net), the 3D volumes were digitally reoriented to reproducible, standardized positions that are functionally intuitive based on the horizontal supratalar plane of the ankle joint (Latimer et al. 1987). The talus was oriented relative to the trochlear surface such that in sagittal plane view, the base of the neck and the most posterior point of the trochlear surface were on the same horizontal plane, and in the coronal and transverse planes, the superiormost points of the medial and lateral trochlear rims were level (Figure 3.1). The reoriented volumes were then exported as a stack of 16-bit DICOM format image files. The DICOM image stack of each specimen was imported into *Amira Visualization Software* (Visage Imaging, San Diego CA) for further analysis.

3.2.3 Analysis of subchondral bone

3.2.3.1 Segmentation into slab

The subchondral plate of bone was semi-manually isolated from each joint surface using the brush segmentation tool (Figure 3.1). In approximately every tenth image (0.45 mm) in the volume series, the boundary between air and the articular surface of bone was visually determined and outlined using the brush tool. Care was taken to include only subchondral articular bone but not the surrounding non-articular cortical bone. The manually-selected air-bone boundary was then interpolated between the slices, with subsequent visual verification of accuracy. The thickness of the segmented subchondral slab was standardized to 18 voxels (~0.81 mm), which was visually-approximated to be thick enough to fully encompass the cortical plate while minimizing the inclusion of underlying trabeculae. The set of voxels within the

segmented area was isolated from the rest of the specimen volume (i.e., the trabecular bone and non-articular cortical bone) using the *Amira* arithmetic tool, and saved as a separate volume.

3.2.3.2 Division into anatomical regions

The subchondral bone volume was segmented into a 3x3 grid of nine anatomically-aligned regions (Figures 3.1 and 3.2). The linear mediolateral and anteroposterior dimensions of the isolated subchondral plate were digitally measured and divided into thirds using the *Amira* measurement tool. Each region was thus defined with dimensions of 1/3 of the maximum mediolateral length and 1/3 of the maximum anteroposterior length. The curved trochlear surface required a different, angular approach, whereby the arc between the posteriormost and anteriormost points of the articular surface was measured in degrees and then divided into thirds. The set of voxels within each region was isolated using the *Amira* arithmetic tool, saved as a separate volume, and exported as a stack of 16-bit TIFF format image files.

3.2.3.3 Quantification of thickness

The thickness of the subchondral cortical shell of each articular surface was quantified using *Quant3D* software (Ketcham 2005; Ketcham and Ryan 2004). *Quant3D* was developed for the purpose of quantifying the structure of 3D fabrics and was used primarily in this study to quantify trabecular bone. However, its algorithms were also used here as a subjective method of calculating subchondral thickness by in essence treating the thin subchondral plate of bone as if it were an isolated trabecular plate as follows.

The 16-bit TIFF image stack of each isolated region of the subchondral plate was converted to 8-bit TIFF images using *ImageJ* software (Rasband 1997-2007), then imported into *Quant3D*. The volume containing the thin plate was binarized into bone/non-bone using an adaptive, iterative threshold technique (Ridler and Calvard 1978; Ryan and Ketcham 2002), and the structure analyzed using the star volume distribution (SVD) algorithm (Cruz-Orive et al. 1992; Ketcham and Ryan 2004). In this algorithm, for a given point within the bone structure, intercept lengths (straight-line lengths between bone-air boundaries) are calculated for 513 random angular orientations. The thickness of bone at a given point is defined as the shortest intercept length. Using 2000 random points within the bone volume, calculations were made of the mean thickness of the subchondral bone plate (Sc.Th) within each of the 9 regions.

3.2.4 Analysis of trabecular bone

3.2.4.1 Division into anatomical regions

The trabecular bone volume was segmented into a 3x3 grid of nine roughly cubic, anatomically-aligned regions (Figures 3.1 and 3.2) directly corresponding to the overlying subchondral bone regions defined above. The set of voxels within each region was isolated

using the *Amira* arithmetic tool, saved as a separate volume, and exported as a stack of 16-bit TIFF format image files.

3.2.4.2 Thresholding/Quant3D options

The structure and orientation of the trabecular bone within each region was quantified using *Quant3D* software (Ketcham 2005; Ketcham and Ryan 2004). The 16-bit TIFF image stack of each trabecular region was smoothed from noise using a Gaussian filter and converted to 8-bit TIFF images using *ImageJ* software (Rasband 1997-2007), then imported into *Quant3D.* Anatomical orientation axes were applied, denoting anterior, medial, and superior directions. For each of the nine regions of trabecular bone, a volume of interest (VOI) was defined as being the largest centered sphere that fit completely within each region, without including unwanted cortical bone. Because of natural irregularities in bone shape, the nine VOIs within a given specimen were not exactly the same size. For example, the posterior dimension of the talar trochlea is narrower than the anterior dimension, resulting in posterior VOIs that were consistently smaller than anterior VOIs.

The trabecular bone in the VOI was binarized into bone/non-bone using an adaptive, iterative threshold technique (Ridler and Calvard 1978; Ryan and Ketcham 2002), and the structure analyzed using the star volume distribution (SVD) algorithm (Cruz-Orive et al. 1992; Ketcham and Ryan 2004).

3.2.4.3 Quantification of trabecular architecture and orientation

A fabric tensor describing the orientation of trabeculae within each VOI was calculated using the star volume distribution (SVD) method of *Quant3D* (Ryan and Ketcham 2002). The SVD method of quantifying architectural anisotropy (fabric) has been shown to be the best predictor of mechanical anisotropy (Odgaard et al. 1997). The SVD method is based on the measured length of the longest uninterrupted line from a point lying within trabecular bone to the boundary between bone and air, repeated for a series of uniformly distributed orientations and multiple random points (Cruz-Orive et al. 1992). From these data, a fabric tensor is derived which describes how the moment of inertia of bone varies with orientation (Ketcham 2005). Three eigenvectors, μ_1, μ_2, μ_3, and three eigenvalues, τ_1, τ_2, τ_3, describing the distribution of bone are derived from the fabric tensor (Benn 1994; Ryan and Ketcham 2002). The eigenvectors represent the orientation in 3D space of the primary, secondary, and tertiary material axes. The corresponding eigenvalues, defined such that $(\tau_1 + \tau_2 + \tau_3) = 1$ and $\tau_1 > \tau_2 > \tau_3$, represent the relative magnitudes of each of the three material axes. The first eigenvector is defined to be parallel to the axis of maximum clustering in the data. The specimen is *orthotropic* if the three eigenvalues are distinct in value, *transversely isotropic* if there are two similarly-valued eigenvalues, and *isotropic* if all eigenvalues are approximately equal (a sphere). The degree of anisotropy (DA), defined as the ratio of the highest eigenvalue to the lowest eigenvalue (τ_1/τ_3), is the commonly used ratio to summarize the relative magnitudes. However this value is often

difficult to evaluate and compare because there is no upper bound. Other ratios between the eigenvalues also give an indication of the shape of the trabeculae – whether plate-like or rod-like. If the first eigenvalue is high and the second and third are equally low, then the data indicates a rod-like shape; if the first two eigenvalues are equally high and the third is low, then the data indicates a plate-like shape (Benn 1994). Ding et al. (2002a) demonstrated that plate-like trabeculae are indicative of a high-stress environment while rod-like trabeculae indicate regions of low stress.

The output variables computed by *Quant3D* and used in this analysis are:

- *Relative trabecular bone volume (BV/TV)*: Also known as "bone volume fraction", it is the dimensionless ratio of the number of bone voxels present in the VOI to the total number of voxels in the VOI (Goulet et al. 1994).
- *Trabecular strut thickness (Tb.Th)*: The average trabecular strut thickness (mm) in the VOI, based on the intersections between a superimposed grid of lines and bone voxels (Hildebrand and Ruegsegger 1997).
- *Trabecular number (Tb.N)*: The estimated number of trabecular struts in the VOI, based on the number of intersections between a superimposed grid of lines and bone voxels (Hildebrand and Ruegsegger 1997).
- *Trabecular degree of anisotropy (Tb.DA)*: (τ_1/τ_3). The primary eigenvalue divided by the tertiary eigenvalue. Values closer to 1 denote perfect isotropy; increasingly greater values indicate trabecular struts which are increasingly narrowed onto a single plane (Harrigan and Mann 1984).
- *Trabecular isotropy index (Tb.I)*: (τ_3/τ_1). The inverse of Tb.DA, this property is more intuitive to evaluate trabecular shape because values are bounded between 0 and 1. Values closer to 0 denote trabecular struts that are confined to a single plane (either plate-shaped or rod-shaped); a value of 1 denotes perfect isotropy (sphere-shaped) (Benn 1994).
- *Trabecular elongation index (Tb.E)*: $1-(\tau_2/\tau_1)$. Distinguishes between rod-shaped and plate-shaped trabeculae by indicating the extent of preferred orientation of trabeculae in the major plane defined by eigenvectors 1 and 2. If Tb.I is close to 0, concurrent values of Tb.E closer to 0 denote more plate-shaped trabecular struts; values of Tb.E closer to 1 denote more rod-shaped struts. (Benn 1994).
- *Direction of eigenvectors*: Orientation of the primary and secondary eigenvectors as defined by angle-angle coordinates relative to the center of the VOI.

Thus, the two indices Tb.I and Tb.E used together uniquely define the architecture of the trabecular bone mesh. A trabecular fabric composed of elongated rod-shaped trabeculae will have low Tb.I and high Tb.E. A fabric of flat disc-shaped trabeculae will have low Tb.I and low Tb.E. A completely isotropic fabric with no preferred trabecular orientation will have high Tb.I and low Tb.E.

3.2.5 Statistical analyses

3.2.5.1 Statistical analysis of scalar variables

All comparative analyses were performed using data that was uncorrected for body size. Though certainly the individual animals varied in body size, this variation was deemed to be an important parameter to include because it likely has an effect on morphology both biomechanically and behaviorally (Biewener 2005).

Descriptive statistics were calculated for all variables to investigate their variation across individuals and across regions within the talus. Data exploration revealed approximately normal distributions for all variables within a given talar region (Shapiro-Wilk $p<0.05$).

Multivariate analyses of variance with post-hoc pairwise comparison tests (Games-Howell) was performed (1) among species overall to compare the overall trabecular differences among species, (2) among species within each region to pinpoint whether certain regions are more diagnostic than others, then (3) among regions within each species to characterize the distribution of bone properties across the talar trochlea.

All analyses involving scalar bone architecture variables were performed using SPSS 16.0 software. The significance level of all tests was set at $p < 0.05$.

3.2.5.2 Statistical analysis of orientation vector data

The distribution of trabecular shape indices was visualized using Tri-plot software (www.lboro.ac.uk/research/phys-geog/tri-plot/index.html).

The mean eigenvector and spherical variance was computed using GEOrient software (www.holcombe.net.au/software/rodh_software_georient.htm). The mean eigenvector is the mean resultant of the unit vectors of each sample (Mardia 1972), presented in terms of two values, trend (T_m) and incline (I_m). The trend of a vector is the direction of its projection on a transverse plane, with 0/360 degrees directed anteriorly, 90 degrees directed medially, and 270 degrees directed laterally. The incline of a vector is its superiorly-directed angle from the transverse plane. The spherical variance (s) is a measure (0-1) of the variability of the data as reflected by the resultant (Mardia 1972). A low variance indicates strong vector clustering, while a high variance indicates greater vector dispersion.

3.3 Results

The pQCT images of KNM-ER 1464 showed clear definition of trabecular struts throughout the talus. Some regions appeared to have some high radiodensity deposits that were ambiguous as to whether they represented bone or post-mortem mineral deposits (Figure A10).

3.3.1 Trabecular and subchondral bone

Table 3.2 lists the species mean values, standard deviations and coefficients of variation for each variable overall in the talus and Table 3.3 lists these values in each of the nine regions.

Figure 3.3 compares the value of each metric of bone morphology for KNM-ER 1464 with the means and 95% confidence intervals for each extant species group.

Contrary to predictions, the overall trabecular bone architecture in KNM-ER 1464 was more similar to that of great apes than of humans. Overall, KNM-ER 1464 joined the great apes in having significantly greater Tb.BV/TV than humans ($p<0.001$), but significantly less than baboons ($p=0.002$). The Tb.DA of KNM-ER 1464 was significantly lower than that of humans ($p<0.001$), but was not significantly different from that of the non-human groups. More similarly to humans, however, was that the variation of Tb.DA among regions in KNM-ER 1464 was relatively large (CV = 0.61), indicating that some regions were much more anisotropic than others. KNM-ER 1464 joined the African apes in having greater Tb.I than humans ($p=0.06$) but lower Tb.I than orangutans and baboons ($p<0.001$). KNM-ER 1464 showed a similar level of Tb.E as the non-human groups, which was significantly lower than that of humans. KNM-ER 1464 had significantly greater Tb.Th and Sc.Th than all extant hominoid groups ($p<0.01$), and significantly lower Tb.N than humans, chimpanzees, and orangutans ($p<0.01$).

In the comparison of bone properties of KNM-ER 1464 to the other species within each region, particular regions were notable (Figure 3.3). The anteromedial (A3) and centromedial (B3) regions had greater Tb.BV/TV than the non-human hominoids, and the centrolateral (B1), centromedial (B3), and anterocentral (A2) regions had much greater Tb.Th than in all other species. The lowest Tb.N was most pronounced in the centrolateral (B1) and centromedial (B3) regions. KNM-ER 1464 had the greatest Tb.DA (and lowest Tb.I) among species in the posteromedial (C3) region. The Sc.Th of KNM-ER 1464 was much greater than the other species mostly in the lateral (A1, B1, C3) regions of the talus.

In agreement with predictions, KNM-ER 1464 was similar to humans in that Tb.BV/TV was greatest in the anteromedial (A3) region (Figure 3.4). The pattern of distribution of Tb.E was also similar between humans and KNM-ER 1464 in that greater values of Tb.E were located along the lateral talar margin. But the highest Tb.DA was in the posteromedial (C3) and posterocentral (C2) regions in KNM-ER 1464 while in humans, the highest Tb.DA was found in the anterocentral (A2) region. KNM-ER 1464 showed similar patterns of Tb.Th as most other species, with the thinnest trabeculae in the center of the talus and thickest trabeculae in the anteromedial (A3) region. The pattern of Tb.N in KNM-ER 1464 seems most similar to that of baboons with higher Tb.N in the mid-sagittal regions compared with the lateral and medial talar rims. KNM-ER 1464 was more similar to the non-human groups than the humans in having greater Sc.Th along the lateral margin.

3.3.2 Trabecular shape and orientation

Table 3.4 lists the mean primary, secondary and tertiary eigenvalues and the direction (trend and incline) and variance of the primary eigenvector for each species by ROI. Figure 3.5 depicts the variation in mean shape of the trabecular struts in each region of the talus, respectively. Within each region, Tb.I and Tb.E are plotted in a ternary diagram, where data points towards the top apex indicate more isotropic trabeculae and data points towards the

bottom indicate more anisotropic trabeculae. Data points towards the bottom left apex indicate more plate-shaped trabeculae and data points towards the bottom right apex indicate more rod-shaped trabeculae. Figure 3.6 depicts stereoplots of the principal eigenvector for each specimen by region.

In the anterior and mid-coronal regions of the KNM-ER 1464 talus, the shape of the trabeculae was moderately isotropic resembling that of the great apes rather than the highly anisotropic trabeculae found in humans (Figure 3.5). However, the primary direction of orientation in these regions was most similar to humans (Figure 3.6).

The trabeculae in the posterocentral and posteromedial regions were highly anisotropic and elongated, even more so than in humans. However, unlike in humans and more like the non-human groups, these trabeculae extended inwardly in an orientation that was approximately normal to the articular surface. They were thus directed from posterosuperiorly to anteroinferiorly, but also in a near parasagittal plane, most similar to the primary trabecular orientation found in some chimpanzees (Figure 3.6).

3.4 Discussion

The aim of this study was to compare the internal bone morphology of a fossil hominid talus KNM-ER 1464 with that of extant hominoids to gain insight into the habitual locomotor loads that it may have endured in life. In common with previous comparative studies of the external morphology of this specimen (Day et al. 1976; Gebo and Schwartz 2006; Grausz et al.), the trabecular bone and subchondral bone morphology was found here to have a unique mosaic of human-like, ape-like, and baboon-like features.

The overall trabecular bone volume in KNM-ER 1464 was generally comparable to that of the great ape groups. However, the fossil talus displayed significantly fewer, but significantly thicker, trabeculae than almost all other groups. Only baboons were found to have as few trabeculae per millimeter and almost as thick trabeculae as KNM-ER 1464. The close approximation of the morphology to that of baboons suggests that the locomotor behavior of KNM-ER 1464 may have been somewhat similar. Thicker trabeculae have been shown in rats subjected to endurance treadmill running versus sedentary control rats (Bourrin et al. 1995; Joo et al. 2003), further supporting the suggestion that this fossil individual may have been relatively more active than modern humans or great apes. Indeed, the hypothesis that the morphology of KNM-ER 1464 is consistent with that of Old World monkeys has been raised before in regards to its highly grooved trochlear surface, which guides parasagittal ankle rotation while providing stability from mediolateral movements (Gebo and Schwartz, 2006).

However, one important limitation of this study that cautions comparison of absolute thicknesses across species was that the fossil talus was scanned using different CT systems than was used for the extant tali. Moreover, the fossil talus was scanned at a lower resolution (64 μm) using a pQCT system while the extant tali were scanned at a higher resolution (45 μm) using a micro-CT system. This difference alone may account for the absolutely greater bone thickness displayed by the fossil talus (Kothari et al. 1998; Laib and Ruegsegger 1999; Tabor 2004).

Further evidence of this effect was that the subchondral bone thickness measured in the fossil bone was also much greater than that in the extant bone.

Another effect that must be considered is that the greater mineralization of the fossil talus may influence the resulting thickness measurements. Fossilized bone may potentially be physically thicker due to diagenic processes of mineral deposition into microcracks in the bone (Golder and Christian 2002). Additionally, the difference in source energy used to image the fossil vs. extant bone may have resulted in the appearance of thicker bone in the fossil due to partial volume effects (Zonneveld 2002).

While comparisons of absolute measures of bone volume and thickness may be problematic, comparisons of the *relative* regional patterns of thickness are more likely to be legitimate. The distribution of trabecular bone volume in KNM-ER 1464 was more similar to the pattern in humans than the great apes in that bone volume was more evenly distributed along both lateral and medial rims. The distribution of trabecular elongation in the fossil talus was also more similar to humans in that the regions with relatively the most elongated trabeculae are located along the lateral talar margin. These elongated, rod-shaped trabeculae likely indicate regions of the talus that are subject to relatively low loads, while the more isotropic trabeculae in the central and medial aspect of the joint indicate stronger bone.

The trabeculae in the posterior regions of the fossil talus was found to be extremely plate-like in shape, a feature also shared with the human talus. These anteroposteriorly-oriented plates extended vertically from the trochlear surface to the posterior calcaneal facet, facilitating load-transfer evenly throughout the arc of the movement of the tibia over the talus during gait (Pal and Routal 1998). Trabecular plates have been found to contribute to the compressive strength of bone samples to a much greater degree than do rods (Liu et al. 2009; Liu et al. 2008; Liu et al. 2006). Thus, the presence of these plates implies that the posterior regions of the fossil and human tali may have withstood high compressive forces in life.

Besides the scalar measures of trabecular morphology, the direction of the primary trabecular orientation also differed among regions of the KNM-ER 1464 talus in a mosaic manner. In the anterocentral and anteromedial regions, the primary orientation of trabeculae in the fossil was very similar to that of humans, and decidedly different from the non-human groups. In both the fossil and modern hominid, the primary trabecular orientation was directed anteroinferiorly towards the anterior calcaneal facet and talar neck. In humans, this pattern of trabecular orientation along the anteromedial talar margin is likely a reflection of the human medial longitudinal arch, where the weight of the body from above must be transmitted anteriorly through the calcaneus and navicular bones to the forefoot and posteriorly through the calcaneus. This arched pattern has been described (Athavale et al. 2008; Pal and Routal 1998) but the present study is the first to quantitatively assess this morphology.

The posterior regions of the fossil talus, however, showed primary orientations that were more similar to those of the non-human hominoids in being oriented more or less normal to the articular surface. This configuration suggests a generalized morphology in which habitual loads may have been variable or distributed evenly across the joint. This is in contrast with the

primary orientation in humans which was not oriented surface-normal but was directed more posteroinferiorly towards the posterior calcaneal facet, suggesting that humans may habitually load the joint in a very consistent, narrowly-defined orientation.

The patterns found in the KNM-ER 1464 talus more broadly address the question of how the hominid foot evolved from that of an arboreal quadruped to that of a terrestrial biped. There has been debate on which region of the foot evolved first, the medial (Lewis 1980) or the lateral (Kidd 1999). The results presented here infer that the lateral region of the ankle joint in KNM-ER 1464 was somewhat more human-like while the posterior regions reflect trabecular strength characteristics similar to arboreal primates. The more elongated trabeculae in the lateral talus of humans versus the great apes may be related to decreased and/or more predictable loadbearing that would occur as the tibia is positioned more directly above the talus. In contrast to the great apes that transfer substantial load to the lateral aspect of the talus via the fibulae, the modern human fibula is not thought to generate a compressive load onto the lateral talar trochlea. Rather, the talocrural joint load in humans is borne relatively more medially, being between only the distal tibia and talar trochlea.

Taking all evidence together, the internal morphology of the KNM-ER 1464 talus supports the hypothesis that it belonged to a hominid well-adapted to terrestrial bipedal gait. In this sense, the morphology of this fossil suggests an individual who would have been capable of producing the Ileret footprints.

The analysis of the trabecular morphology of the KNM-ER 1464 fossil talus demonstrates the ability to detect subtle differences in the internal morphology of fossil bones that can aid in the interpretation of the habitual loads experienced during life. It was interesting that some aspects of the trabecular morphology were consistent with interpretations based on the external morphology, such as indicators of a parasagittal type of locomotion. However other aspects were unexpected, such as differences in the primary direction of orientation. The future analysis of other fossil tali will be necessary to place these results in context and to help resolve whether all fossil hominids in this time in East Africa have similar functional morphology or if there are some differences in habitual locomotor behavior.

3.5 Conclusion

The KNM-ER 1464 talus displays internal morphology that in some ways is similar to that of baboons and apes and in other ways is similar to modern humans. The lateral regions of the fossil talus were similar to those of modern humans and support the assumption that it belonged to a bipedal hominid. The primary orientation of trabeculae was similar to that of modern humans in the anterior regions of the talus, suggesting that transfer of body weight from the tibia, through the talus, to the forefoot was important. But the orientation of trabeculae that was found elsewhere in the talus to be generally normal to the articular surface was more similar to that in the non-human groups, perhaps indicating a more generalized level of bone strength able to withstand variations in loading direction.

Tables

Table 3. 1: Comparative study sample.

	Sex	N Talus	Collections	Locomotor behavior
Homo sapiens	F	18	CMNH	Terrestrial plantigrade bipedalism
Pan troglodytes	F	20	CMNH, AMNH, NMNH	Semi-arboreal plantigrade quadrupedalism
Gorilla gorilla	F	15	CMNH, AMNH, NMNH	
Pongo pygmaeus	F	13	NMNH	Arboreal, quadrumanous
Papio hamadryas	M	18	Bramblett (UT Austin)	Terrestrial semi-digitigrade quadrupedalism

AMNH = American Museum of Natural History, CMNH = Cleveland Museum of Natural History, NMNH = Smithsonian National Museum of Natural History.

Table 3. 2: Species means and variation for all study variables in the talus.

	Homo			*Pan*			*Gorilla*			*Papio*			*Pongo*			*KNM-ER 1464*		
	Mean	Std. Dev.	CV	Mean	Std. Dev.	CV	Mean	Std. Dev.	CV	Mean	Std. Dev.	CV	Mean	Std. Dev.	CV	Mean	Std. Dev.	CV
Tb.BV/TV	0.37	0.05	0.13	0.48	0.07	0.15	0.44	0.07	0.16	0.44	0.09	0.21	0.62	0.12	0.19	0.51	0.06	0.11
Tb.DA	7.97	4.96	0.62	2.79	1.02	0.37	3.06	1.02	0.33	2.21	0.83	0.38	2.39	0.98	0.41	4.33	2.63	0.61
Tb.I	0.18	0.10	0.59	0.40	0.12	0.30	0.36	0.11	0.31	0.50	0.15	0.30	0.47	0.14	0.29	0.30	0.14	0.46
Tb.E	0.46	0.17	0.36	0.30	0.13	0.45	0.32	0.13	0.39	0.26	0.14	0.54	0.27	0.13	0.49	0.29	0.10	0.35
Tb.Th	0.19	0.03	0.15	0.22	0.04	0.17	0.23	0.04	0.19	0.20	0.04	0.21	0.27	0.04	0.17	0.31	0.06	0.18
Tb.N	1.82	0.35	0.19	1.76	0.27	0.16	1.68	0.26	0.16	1.75	0.30	0.17	1.42	0.26	0.18	1.42	0.14	0.10
Sc.Th	0.32	0.09	0.29	0.39	0.08	0.21	0.40	0.09	0.24	0.36	0.08	0.23	0.34	0.06	0.16	0.53	0.09	0.17

Table 3. 3: Species means and variation of all variables in the talus by region.
Row A= anterior, Row C = posterior, Column 1 = lateral, Column 3 = medial.

A1

	Homo			*Pan*			*Gorilla*			*Pongo*			*Papio*			*KNM-ER*
	Mean	SD	CV	Mean	SD	CV	Mean	SD	CV	Mean	SD	CV	Mean	SD	CV	*1464*
Tb.BV/TV	0.39	0.04	0.11	0.58	0.06	0.10	0.55	0.05	0.09	0.58	0.08	0.13	0.74	0.08	0.10	0.53
Tb.DA	9.12	2.87	0.31	2.80	0.68	0.24	3.48	0.93	0.27	1.91	0.66	0.35	1.95	0.37	0.19	2.97
Tb.I	0.12	0.04	0.32	0.38	0.10	0.27	0.31	0.08	0.26	0.56	0.14	0.24	0.53	0.08	0.16	0.34
Tb.E	0.62	0.13	0.21	0.24	0.13	0.56	0.28	0.11	0.41	0.24	0.13	0.52	0.22	0.10	0.45	0.37
Tb.Th	0.20	0.03	0.15	0.25	0.04	0.15	0.26	0.04	0.16	0.23	0.04	0.18	0.28	0.04	0.13	0.31
Tb.N	1.88	0.32	0.17	1.76	0.26	0.15	1.74	0.27	0.16	1.87	0.40	0.21	1.20	0.22	0.18	1.45
Sc.Th	0.27	0.07	0.26	0.41	0.07	0.18	0.42	0.05	0.11	0.41	0.06	0.15	0.34	0.03	0.09	0.60

B1

	Homo			*Pan*			*Gorilla*			*Pongo*			*Papio*			*KNM-ER*
	Mean	SD	CV	Mean	SD	CV	Mean	SD	CV	Mean	SD	CV	Mean	SD	CV	*1464*
Tb.BV/TV	0.41	0.03	0.07	0.54	0.05	0.09	0.51	0.05	0.10	0.49	0.05	0.10	0.62	0.06	0.10	0.56
Tb.DA	8.58	2.55	0.30	3.12	1.12	0.36	3.30	1.23	0.37	2.01	0.46	0.23	2.29	0.55	0.24	5.16
Tb.I	0.13	0.04	0.29	0.36	0.11	0.32	0.35	0.13	0.38	0.52	0.13	0.25	0.46	0.10	0.22	0.19
Tb.E	0.59	0.12	0.20	0.28	0.14	0.49	0.30	0.12	0.40	0.28	0.15	0.55	0.34	0.12	0.35	0.43
Tb.Th	0.19	0.02	0.12	0.24	0.03	0.13	0.24	0.04	0.15	0.21	0.03	0.17	0.29	0.04	0.16	0.38
Tb.N	2.00	0.32	0.16	1.79	0.22	0.12	1.81	0.29	0.16	1.94	0.27	0.14	1.48	0.21	0.14	1.25
Sc.Th	0.32	0.09	0.30	0.46	0.08	0.18	0.45	0.08	0.18	0.39	0.08	0.20	0.39	0.05	0.12	0.72

C1

	Homo			*Pan*			*Gorilla*			*Pongo*			*Papio*			*KNM-ER*
	Mean	SD	CV	Mean	SD	CV	Mean	SD	CV	Mean	SD	CV	Mean	SD	CV	*1464*
Tb.BV/TV	0.34	0.03	0.10	0.47	0.06	0.13	0.41	0.04	0.09	0.44	0.03	0.08	0.60	0.07	0.11	0.51
Tb.DA	5.48	1.68	0.31	2.43	0.82	0.34	2.50	0.60	0.24	2.38	0.83	0.35	1.73	0.39	0.22	2.37
Tb.I	0.20	0.05	0.24	0.46	0.15	0.32	0.42	0.11	0.26	0.47	0.16	0.35	0.60	0.12	0.19	0.42
Tb.E	0.66	0.07	0.11	0.26	0.09	0.35	0.33	0.11	0.34	0.29	0.12	0.43	0.25	0.10	0.39	0.35
Tb.Th	0.18	0.02	0.12	0.20	0.03	0.15	0.20	0.02	0.12	0.19	0.03	0.17	0.24	0.03	0.12	0.29
Tb.N	1.80	0.32	0.18	1.96	0.21	0.11	1.79	0.22	0.12	1.93	0.24	0.12	1.73	0.20	0.12	1.37
Sc.Th	0.24	0.07	0.29	0.33	0.08	0.25	0.28	0.07	0.23	0.28	0.05	0.17	0.31	0.04	0.11	0.59

Table 3.3: Species means and variation of all variables in the talus by region.
Row A= anterior, Row C = posterior, Column 1 = lateral, Column 3 = medial.

A2

	Homo			*Pan*			*Gorilla*			*Pongo*			*Papio*			*KNM-ER*
	Mean	SD	CV	Mean	SD	CV	Mean	SD	CV	Mean	SD	CV	Mean	SD	CV	*1464*
Tb.BV/TV	0.35	0.04	0.12	0.44	0.06	0.14	0.43	0.06	0.14	0.41	0.09	0.22	0.49	0.08	0.16	0.51
Tb.DA	13.60	5.79	0.43	3.40	1.30	0.38	2.87	0.92	0.32	2.60	1.01	0.39	1.94	0.31	0.16	3.17
Tb.I	0.09	0.04	0.44	0.32	0.09	0.27	0.38	0.10	0.27	0.44	0.16	0.36	0.53	0.08	0.15	0.32
Tb.E	0.38	0.11	0.28	0.27	0.12	0.44	0.24	0.13	0.54	0.29	0.16	0.55	0.27	0.12	0.43	0.31
Tb.Th	0.20	0.03	0.14	0.25	0.03	0.13	0.25	0.05	0.20	0.21	0.06	0.28	0.25	0.04	0.15	0.31
Tb.N	1.57	0.32	0.20	1.46	0.24	0.16	1.48	0.24	0.16	1.49	0.25	0.17	1.44	0.23	0.16	1.68
Sc.Th	0.31	0.08	0.25	0.34	0.08	0.22	0.38	0.09	0.24	0.36	0.06	0.16	0.28	0.04	0.15	0.47

B2

	Homo			*Pan*			*Gorilla*			*Pongo*			*Papio*			*KNM-ER*
	Mean	SD	CV	Mean	SD	CV	Mean	SD	CV	Mean	SD	CV	Mean	SD	CV	*1464*
Tb.BV/TV	0.36	0.04	0.12	0.41	0.04	0.09	0.41	0.05	0.11	0.36	0.06	0.16	0.47	0.07	0.16	0.48
Tb.DA	9.34	5.47	0.59	2.43	0.50	0.21	3.38	1.21	0.36	2.79	1.32	0.47	2.53	0.85	0.33	2.58
Tb.I	0.15	0.08	0.56	0.43	0.10	0.24	0.33	0.11	0.34	0.43	0.18	0.42	0.43	0.12	0.27	0.39
Tb.E	0.38	0.12	0.31	0.38	0.14	0.37	0.43	0.12	0.28	0.29	0.17	0.59	0.39	0.12	0.31	0.26
Tb.Th	0.19	0.03	0.15	0.20	0.02	0.08	0.22	0.02	0.11	0.19	0.04	0.20	0.23	0.04	0.16	0.31
Tb.N	1.82	0.40	0.22	1.77	0.18	0.10	1.67	0.22	0.13	1.69	0.23	0.14	1.52	0.24	0.16	1.39
Sc.Th	0.34	0.08	0.25	0.38	0.07	0.19	0.40	0.12	0.30	0.30	0.10	0.33	0.36	0.07	0.19	0.55

C2

	Homo			*Pan*			*Gorilla*			*Pongo*			*Papio*			*KNM-ER*
	Mean	SD	CV	Mean	SD	CV	Mean	SD	CV	Mean	SD	CV	Mean	SD	CV	*1464*
Tb.BV/TV	0.34	0.05	0.13	0.45	0.03	0.06	0.36	0.04	0.11	0.38	0.06	0.14	0.64	0.08	0.13	0.40
Tb.DA	9.74	5.89	0.61	2.49	0.69	0.28	3.65	1.14	0.31	2.17	0.76	0.35	1.80	0.42	0.23	7.71
Tb.I	0.15	0.09	0.64	0.43	0.11	0.25	0.30	0.08	0.28	0.51	0.16	0.32	0.58	0.12	0.20	0.13
Tb.E	0.41	0.11	0.27	0.39	0.11	0.29	0.40	0.07	0.16	0.26	0.13	0.52	0.25	0.14	0.55	0.11
Tb.Th	0.18	0.03	0.16	0.19	0.02	0.09	0.19	0.02	0.10	0.19	0.04	0.19	0.28	0.04	0.14	0.23
Tb.N	1.80	0.41	0.23	1.93	0.20	0.10	1.71	0.23	0.13	1.61	0.27	0.17	1.45	0.22	0.15	1.53
Sc.Th	0.29	0.07	0.25	0.38	0.06	0.15	0.35	0.07	0.21	0.34	0.09	0.27	0.34	0.03	0.10	0.46

Table 3.3: Species means and variation of all variables in the talus by region.
Row A= anterior, Row C = posterior, Column 1 = lateral, Column 3 = medial.

A3

	Homo			*Pan*			*Gorilla*			*Pongo*			*Papio*			*KNM-ER*
	Mean	SD	CV	Mean	SD	CV	Mean	SD	CV	Mean	SD	CV	Mean	SD	CV	*1464*
Tb.BV/TV	0.40	0.05	0.12	0.47	0.06	0.12	0.47	0.07	0.14	0.43	0.11	0.24	0.63	0.09	0.15	0.59
Tb.DA	3.36	0.98	0.29	2.37	0.82	0.35	2.35	0.57	0.24	2.36	0.72	0.30	2.48	0.82	0.33	1.91
Tb.I	0.32	0.08	0.27	0.46	0.13	0.28	0.45	0.11	0.24	0.46	0.14	0.31	0.43	0.11	0.25	0.52
Tb.E	0.50	0.11	0.22	0.23	0.14	0.61	0.23	0.10	0.44	0.33	0.13	0.39	0.21	0.14	0.67	0.34
Tb.Th	0.21	0.03	0.14	0.26	0.04	0.17	0.27	0.06	0.20	0.21	0.05	0.21	0.30	0.05	0.16	0.40
Tb.N	1.74	0.25	0.14	1.47	0.22	0.15	1.45	0.22	0.15	1.55	0.22	0.14	1.27	0.17	0.14	1.27
Sc.Th	0.36	0.08	0.23	0.45	0.06	0.14	0.48	0.06	0.12	0.41	0.04	0.10	0.32	0.04	0.11	0.48

B3

	Homo			*Pan*			*Gorilla*			*Pongo*			*Papio*			*KNM-ER*
	Mean	SD	CV	Mean	SD	CV	Mean	SD	CV	Mean	SD	CV	Mean	SD	CV	*1464*
Tb.BV/TV	0.40	0.06	0.14	0.46	0.04	0.10	0.44	0.04	0.10	0.44	0.07	0.15	0.66	0.10	0.15	0.54
Tb.DA	6.61	3.43	0.52	3.25	1.57	0.48	3.19	0.79	0.25	2.04	0.49	0.24	3.73	1.60	0.43	3.58
Tb.I	0.19	0.09	0.48	0.35	0.10	0.28	0.33	0.09	0.27	0.51	0.12	0.22	0.31	0.11	0.35	0.28
Tb.E	0.35	0.13	0.37	0.30	0.11	0.36	0.38	0.10	0.27	0.15	0.06	0.38	0.21	0.10	0.47	0.19
Tb.Th	0.20	0.03	0.15	0.22	0.03	0.12	0.23	0.03	0.11	0.21	0.04	0.20	0.28	0.04	0.14	0.35
Tb.N	1.89	0.37	0.19	1.78	0.18	0.10	1.67	0.18	0.11	1.83	0.22	0.12	1.39	0.19	0.14	1.29
Sc.Th	0.42	0.09	0.22	0.37	0.07	0.18	0.43	0.09	0.22	0.34	0.07	0.22	0.40	0.05	0.14	0.48

C3

	Homo			*Pan*			*Gorilla*			*Pongo*			*Papio*			*KNM-ER*
	Mean	SD	CV	Mean	SD	CV	Mean	SD	CV	Mean	SD	CV	Mean	SD	CV	*1464*
Tb.BV/TV	0.36	0.04	0.11	0.49	0.06	0.12	0.41	0.05	0.12	0.45	0.08	0.17	0.70	0.10	0.15	0.46
Tb.DA	5.89	5.32	0.90	2.80	0.76	0.27	2.86	0.99	0.35	1.64	0.34	0.21	3.05	0.83	0.27	9.49
Tb.I	0.27	0.14	0.50	0.39	0.12	0.31	0.39	0.12	0.32	0.63	0.11	0.17	0.35	0.10	0.27	0.11
Tb.E	0.27	0.09	0.33	0.33	0.14	0.43	0.32	0.12	0.39	0.17	0.09	0.52	0.29	0.15	0.53	0.22
Tb.Th	0.18	0.02	0.13	0.20	0.02	0.11	0.20	0.02	0.09	0.20	0.04	0.20	0.23	0.02	0.09	0.25
Tb.N	1.86	0.28	0.15	1.91	0.23	0.12	1.78	0.28	0.16	1.80	0.25	0.14	1.27	0.23	0.18	1.50
Sc.Th	0.32	0.09	0.27	0.42	0.06	0.14	0.42	0.06	0.15	0.39	0.06	0.15	0.34	0.03	0.10	0.44

Table 3. 4: Mean eigenvalues and orientation of the primary eigenvector in each region of the talus

	Lateral (1)							MLMid (2)							Medial (3)						
	A1	Eigenvalue			Primary Eigenvector (°)			A2	Eigenvalue			Primary Eigenvector (°)			A3	Eigenvalue			Primary Eigenvector (°)		
		1	2	3	Trend	Incline	Variance		1	2	3	Trend	Incline	Variance		1	2	3	Trend	Incline	Variance
	Homo	0.671	0.249	0.081	32	55	0.02	***Homo***	0.589	0.361	0.050	209	68	0.09	***Homo***	0.555	0.271	0.174	171	47	0.04
Anterior	***Pan***	0.470	0.354	0.176	23	54	0.20	***Pan***	0.488	0.355	0.157	272	55	0.22	***Pan***	0.453	0.343	0.204	300	66	0.25
(A)	***Gorilla***	0.496	0.354	0.150	24	55	0.17	***Gorilla***	0.473	0.352	0.175	278	65	0.26	***Gorilla***	0.451	0.348	0.201	307	74	0.13
	Pongo	0.435	0.325	0.240	54	48	0.42	***Pongo***	0.474	0.327	0.199	28	46	0.22	***Pongo***	0.476	0.311	0.213	357	52	0.27
	Papio	0.436	0.336	0.228	34	67	0.20	***Papio***	0.445	0.322	0.233	311	63	0.10	***Papio***	0.455	0.353	0.192	330	58	0.28
	KNM-ER 1464	0.508	0.321	0.171	20	59	*NA*	***KNM-ER 1464***	0.499	0.343	0.158	186	58	*NA*	***KNM-ER 1464***	0.457	0.304	0.239	177	50	*NA*
	B1	**Eigenvalue**			**Primary Eigenvector (°)**			**B2**	**Eigenvalue**			**Primary Eigenvector (°)**			**B3**	**Eigenvalue**			**Primary Eigenvector (°)**		
		1	**2**	**3**	**Trend**	**Incline**	**Variance**		**1**	**2**	**3**	**Trend**	**Incline**	**Variance**		**1**	**2**	**3**	**Trend**	**Incline**	**Variance**
	Homo	0.653	0.265	0.082	51	59	0.01	***Homo***	0.570	0.347	0.082	113	85	0.05	***Homo***	0.547	0.350	0.103	211	62	0.07
APMid	***Pan***	0.487	0.343	0.170	67	55	0.12	***Pan***	0.492	0.300	0.208	290	77	0.04	***Pan***	0.492	0.341	0.168	232	65	0.06
(B)	***Gorilla***	0.491	0.342	0.167	60	60	0.04	***Gorilla***	0.530	0.298	0.172	312	85	0.02	***Gorilla***	0.514	0.317	0.169	257	75	0.06
	Pongo	0.451	0.318	0.231	77	63	0.05	***Pongo***	0.477	0.327	0.196	5	82	0.14	***Pongo***	0.425	0.359	0.216	301	79	0.19
	Papio	0.477	0.308	0.215	79	72	0.02	***Papio***	0.495	0.298	0.208	324	81	0.06	***Papio***	0.479	0.377	0.144	241	68	0.23
	KNM-ER 1464	0.568	0.322	0.110	70	70	*NA*	***KNM-ER 1464***	0.471	0.347	0.182	119	80	*NA*	***KNM-ER 1464***	0.479	0.388	0.134	198	56	*NA*
	C1	**Eigenvalue**			**Primary Eigenvector (°)**			**C2**	**Eigenvalue**			**Primary Eigenvector (°)**			**C3**	**Eigenvalue**			**Primary Eigenvector (°)**		
		1	**2**	**3**	**Trend**	**Incline**	**Variance**		**1**	**2**	**3**	**Trend**	**Incline**	**Variance**		**1**	**2**	**3**	**Trend**	**Incline**	**Variance**
	Homo	0.650	0.218	0.132	27	73	0.01	***Homo***	0.581	0.337	0.082	54	70	0.04	***Homo***	0.503	0.366	0.131	45	86	0.30
Posterior	***Pan***	0.459	0.337	0.204	74	67	0.40	***Pan***	0.494	0.298	0.208	118	75	0.03	***Pan***	0.491	0.324	0.186	212	43	0.11
(C)	***Gorilla***	0.482	0.318	0.200	101	59	0.10	***Gorilla***	0.530	0.315	0.156	95	79	0.02	***Gorilla***	0.488	0.327	0.185	208	67	0.17
	Pongo	0.466	0.323	0.211	108	58	0.11	***Pongo***	0.450	0.328	0.222	51	77	0.16	***Pongo***	0.409	0.337	0.255	181	79	0.29
	Papio	0.428	0.317	0.254	202	79	0.09	***Papio***	0.433	0.321	0.246	140	80	0.13	***Papio***	0.489	0.342	0.169	310	71	0.23
	KNM-ER 1464	0.482	0.315	0.204	219	68	*NA*	***KNM-ER 1464***	0.495	0.441	0.064	161	68	*NA*	***KNM-ER 1464***	0.530	0.414	0.056	187	30	*NA*

Figures

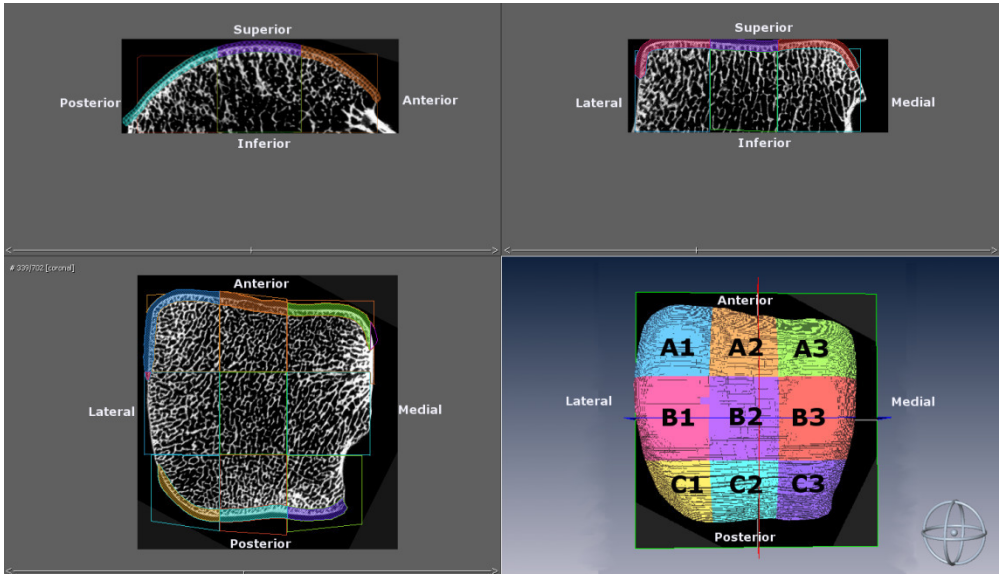

Figure 3. 1: Orientation of the talus, and segmentation of the subchondral bone plate and underlying trabecular bone volume into nine regions of interest.
The subchondral bone plate extended slightly onto both medial and lateral articular facets of the talus.

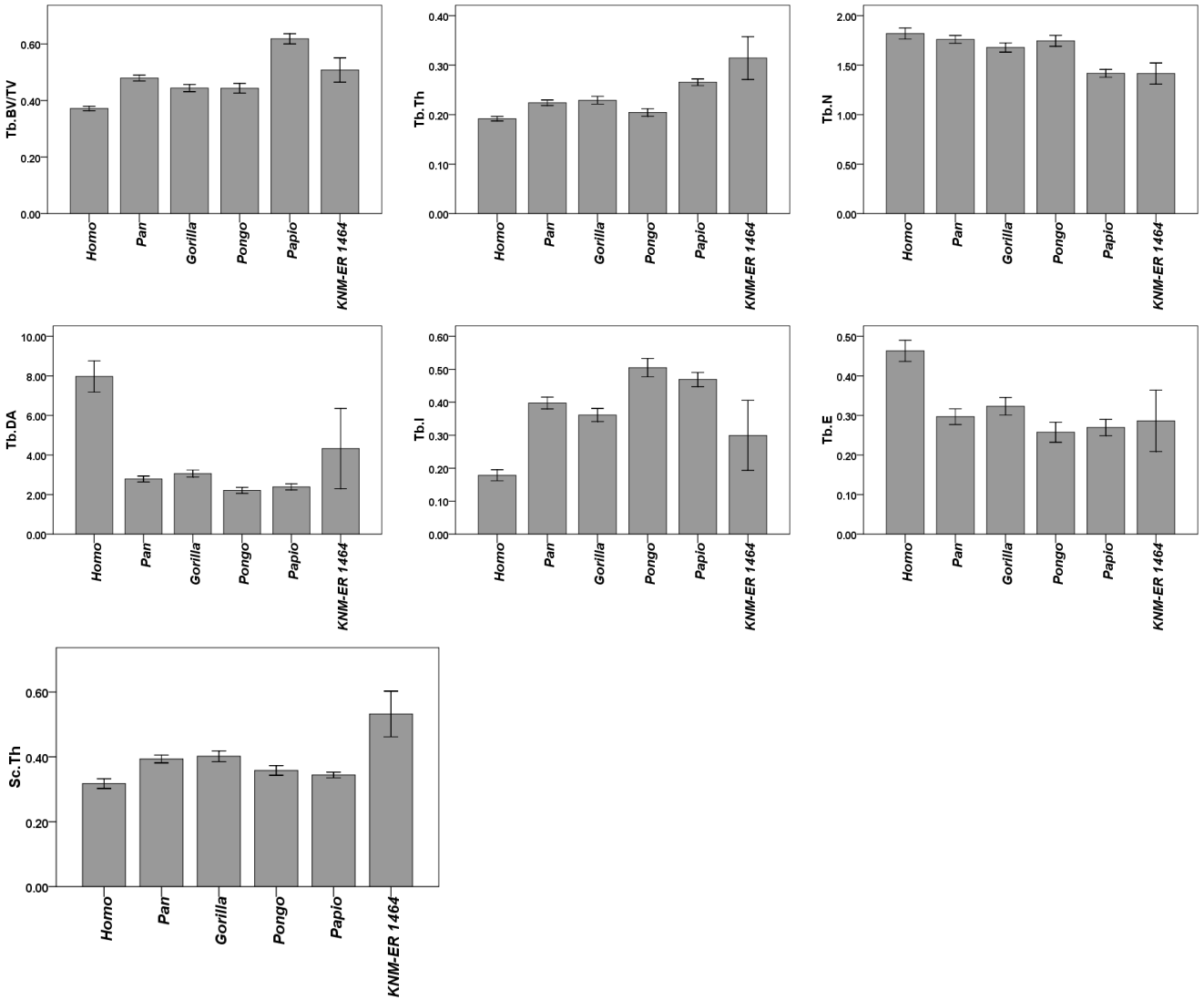

Figure 3. 2: The mean values and 95% confidence intervals for whole talus.

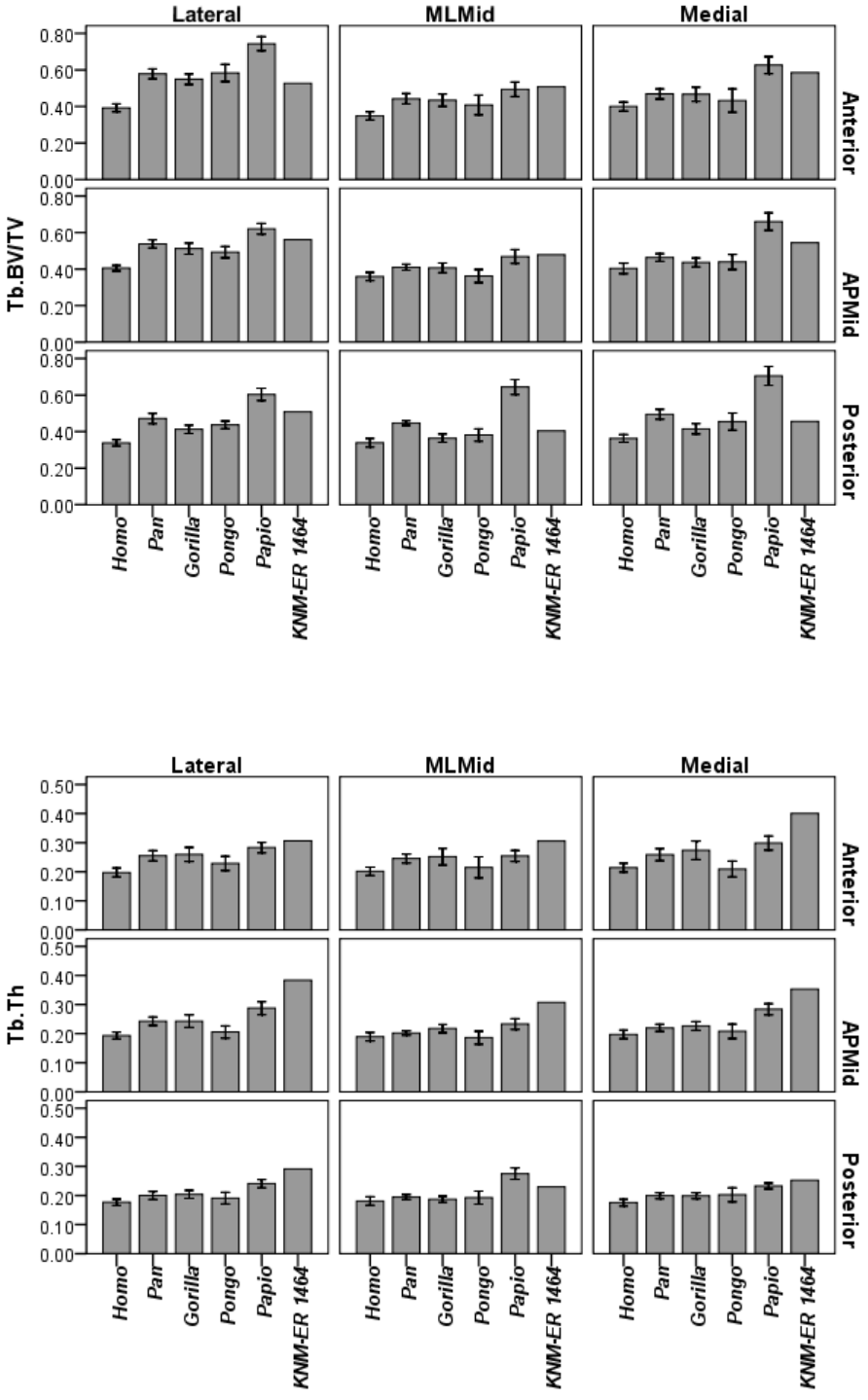

Figure 3. 3: Comparison of KNM-ER 1464 to extant groups by region.

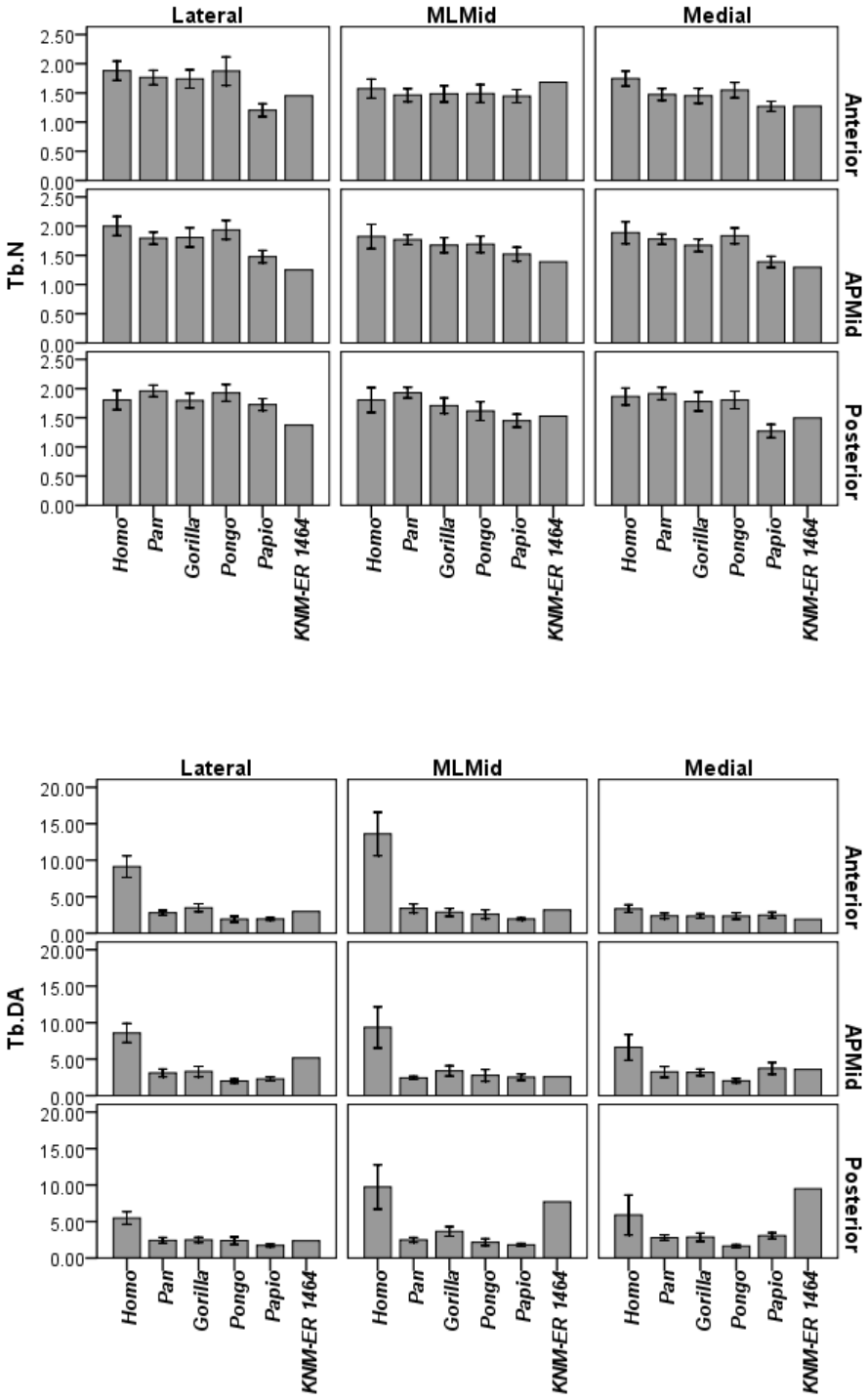

Figure 3.3: Comparison of KNM-ER 1464 to extant groups by region.

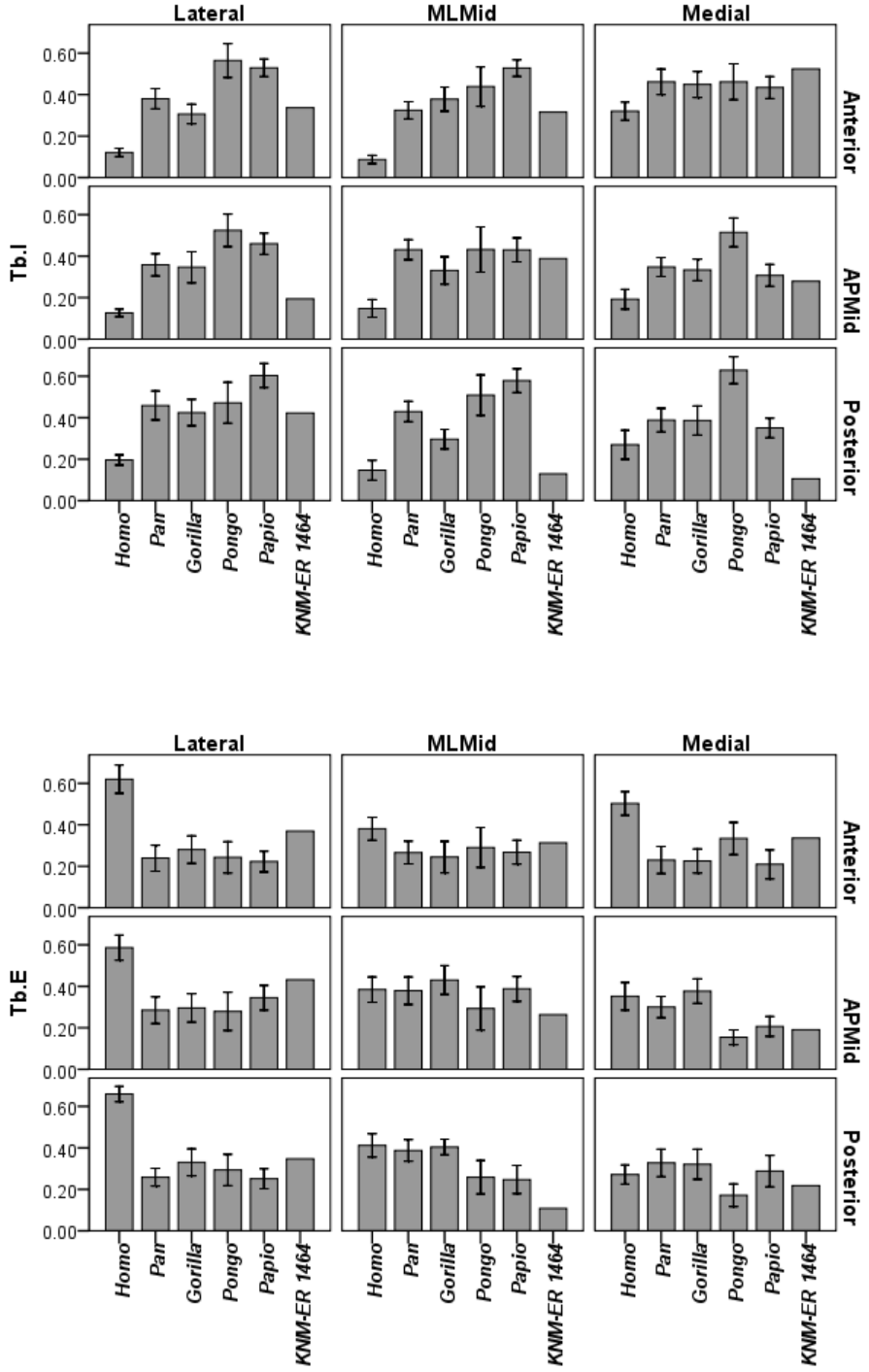

Figure 3.3: Comparison of KNM-ER 1464 to extant groups by region.

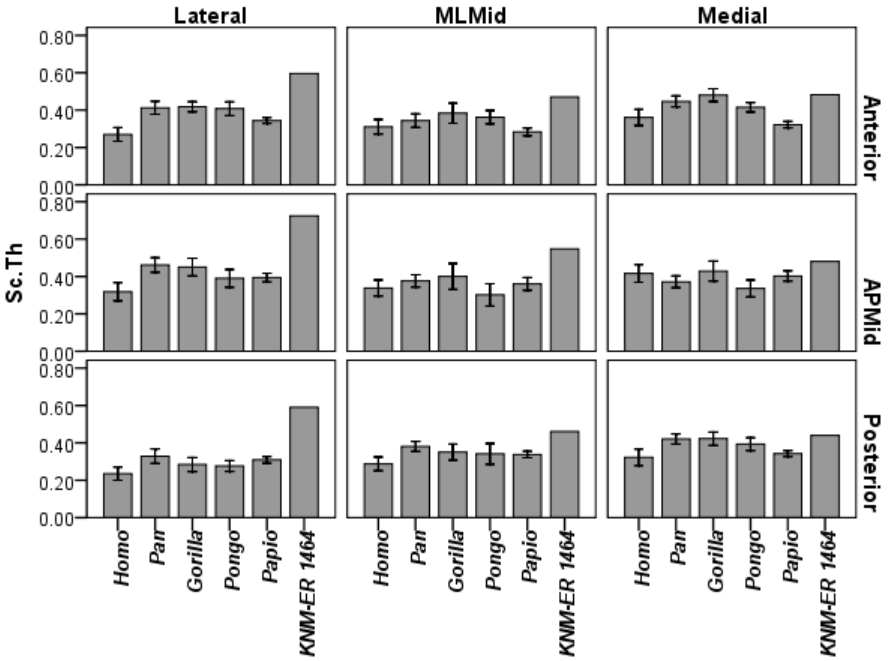

Figure 3.3: Comparison of KNM-ER 1464 to extant groups by region.

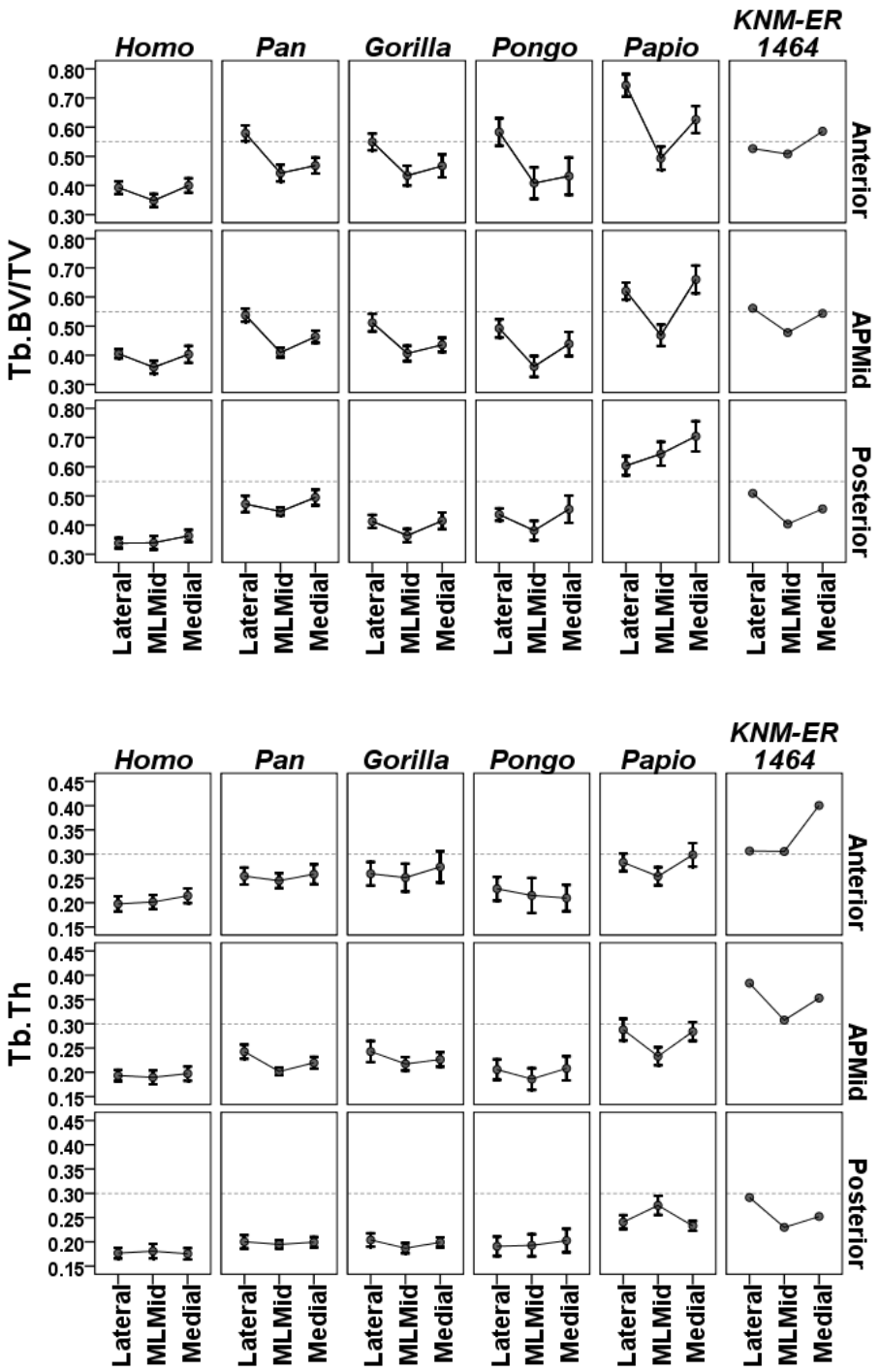

Figure 3. 4: Patterns of distribution within each species.

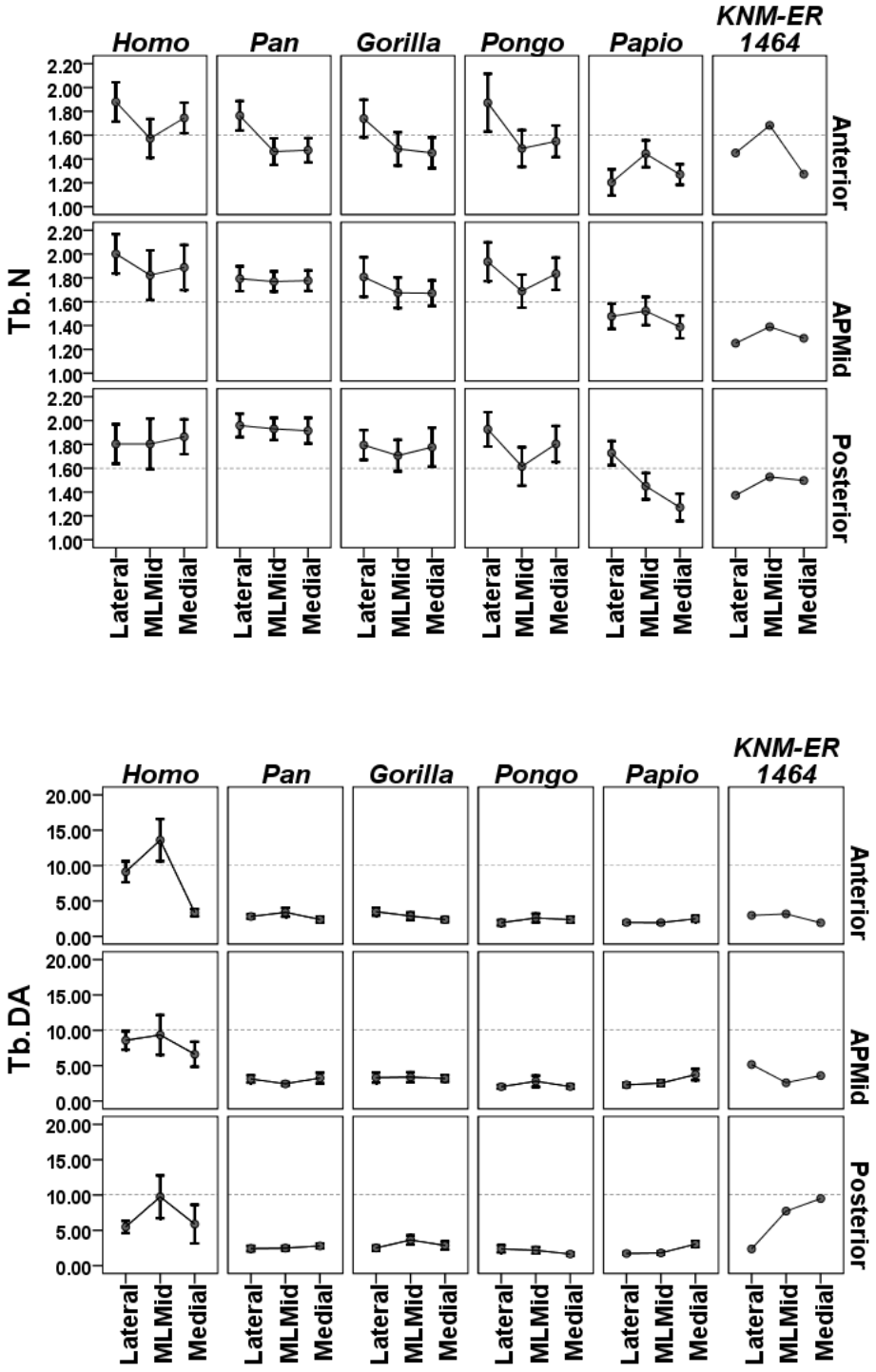

Figure 3.4: Patterns of distribution within each species.

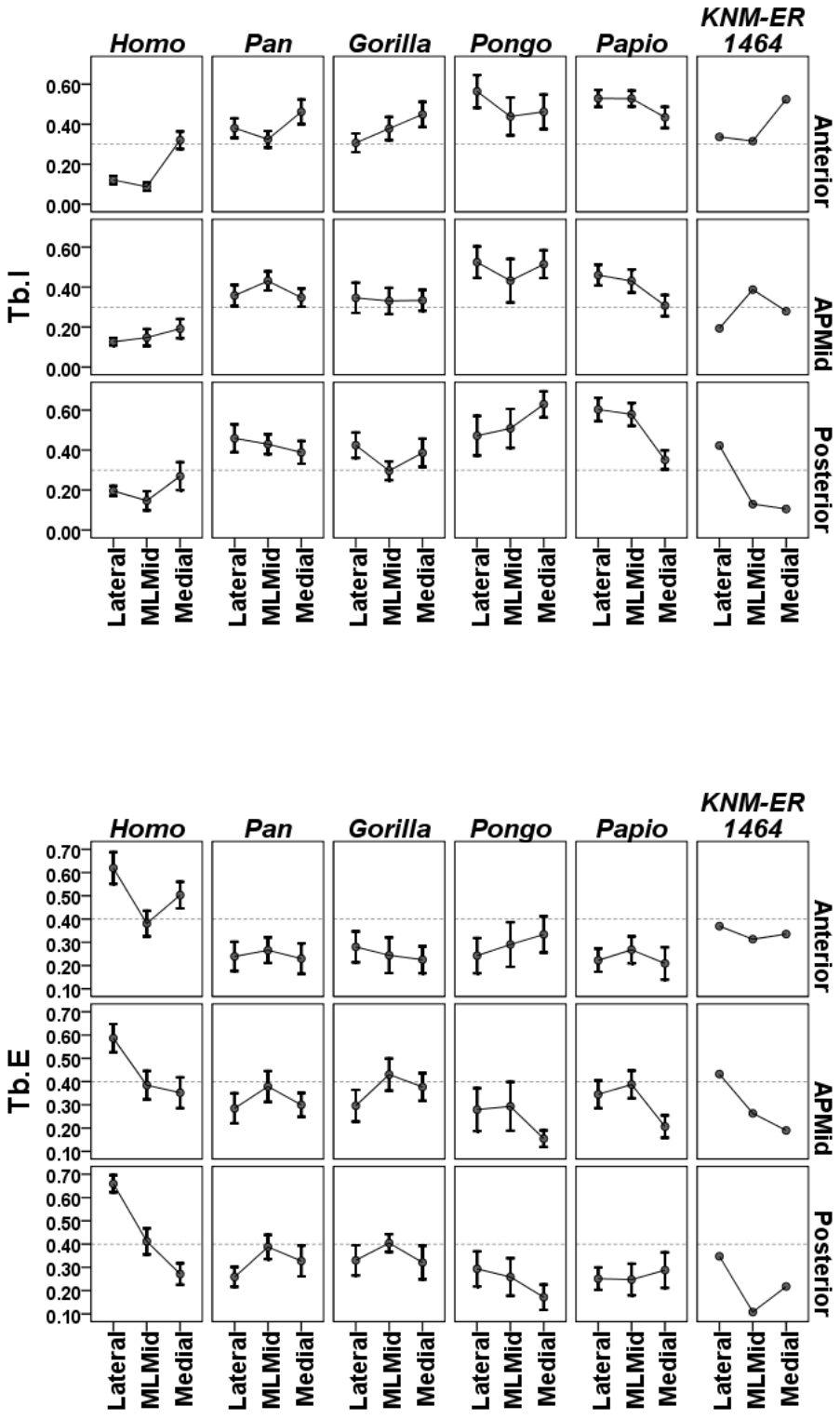

Figure 3.4: Patterns of distribution within each species.

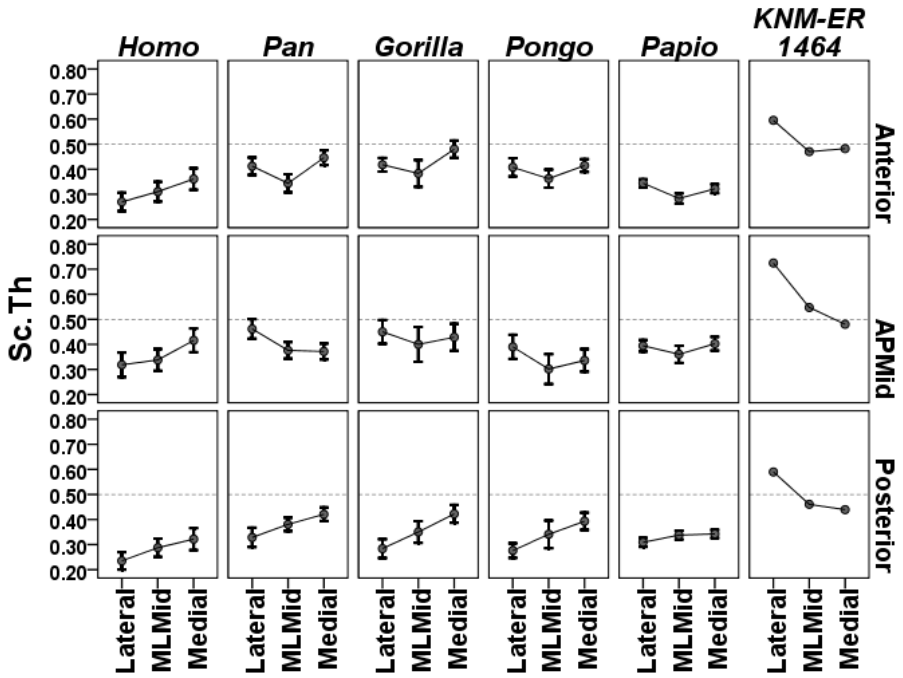

Figure 3.4: Patterns of distribution within each species.

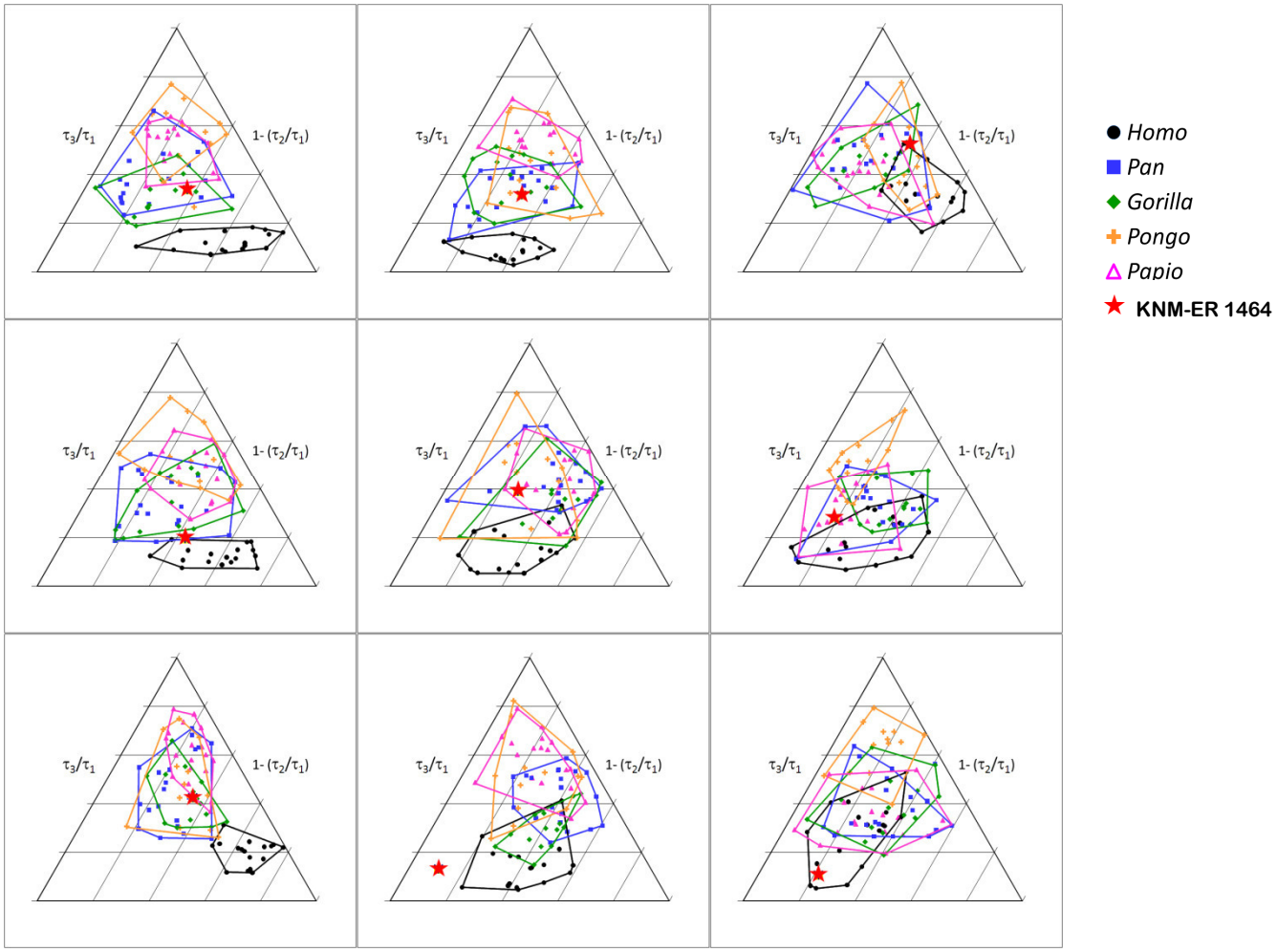

Figure 3. 5: Distribution of trabecular shape indices.
Within each region, each point plots the Tb.I (τ_3/τ_1) and Tb.E ($1-(\tau_2/\tau_1)$) value; lines were drawn to enclose the distribution of each species for comparative visualization. Points towards the top apex indicate more isotropic trabeculae; points towards the bottom indicate more anisotropic trabeculae. Points towards the bottom left apex indicate more plate-shaped trabeculae; points towards the bottom right apex indicate more rod-shaped trabeculae.

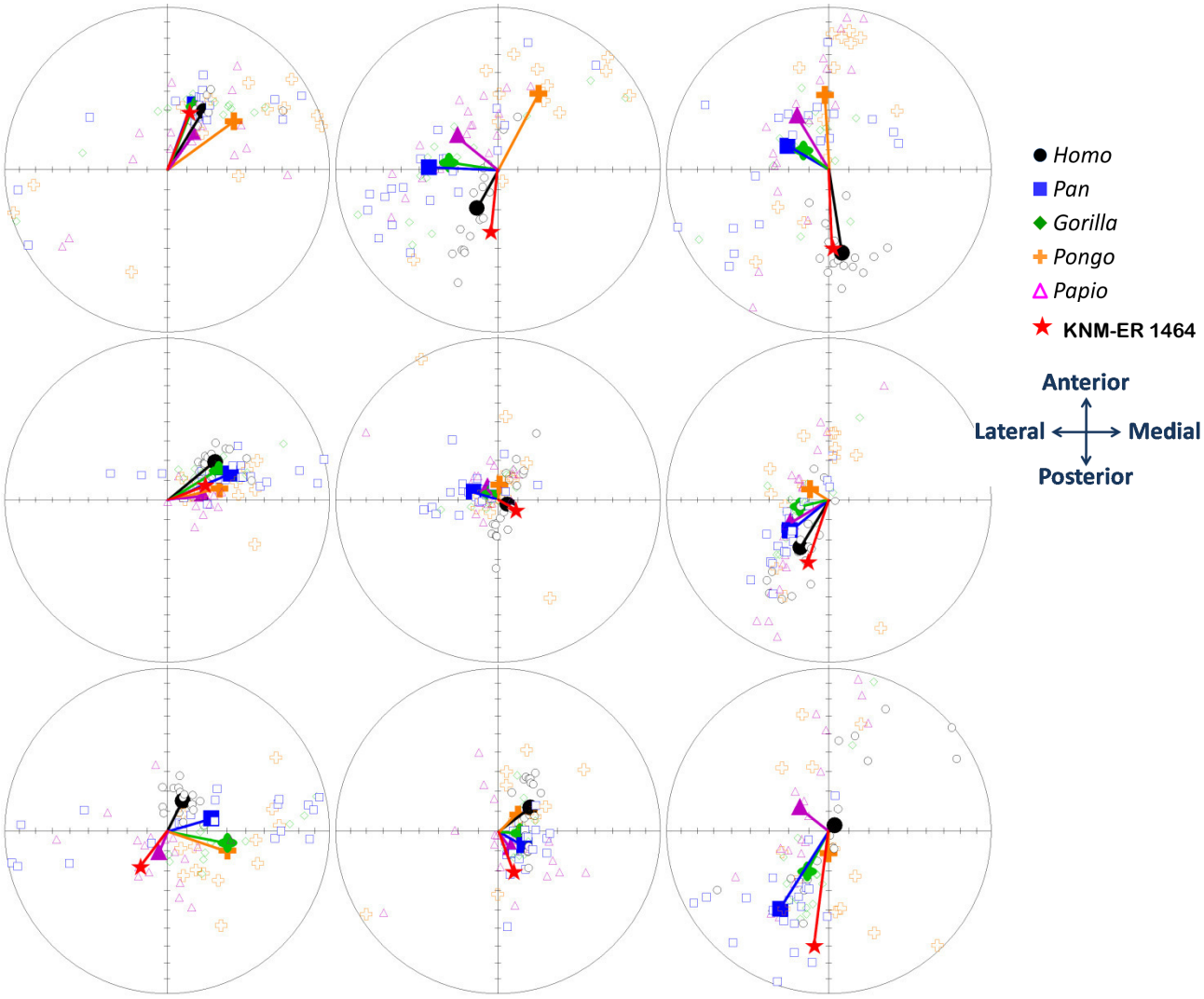

Figure 3. 6: Distribution of the primary trabecular eigenvector direction in each region of the talus.
Each region is represented by a top-down view of a sphere, with each eigenvector depicted with its origin at the center of the sphere and tip on the outer surface of the sphere. Each small point represents one individual. Each large point and line from the center represents the species mean trabecular orientation. The KNM-ER 1464 fossil is represented by a star. Points located towards the center of the circle represent more vertically-oriented trabeculae; points located towards the periphery represent more transversely-oriented trabeculae.

1

Dissertation Conclusion

This dissertation sought to gain a better understanding of whether subchondral bone and trabecular bone morphology in the tibiotalar joint hold useful information about habitual loads that may help in the interpretation of behavior of fossil hominids. Previous studies of comparative functional morphology have independently examined the patterns of subchondral and trabecular bone variables as indicators of habitual load, but this study is the first to examine both lines of evidence simultaneously within both articulating components of a joint. Additionally, this study is the first to describe bone microstructure in the hominoid talocrural joint and thus provides comparative data for both clinical and theoretical biomedical studies of bone morphology and biomechanics, as well as for studies in paleoanthropology.

The method of using micro-computed tomography to quantify the relative radiodensity of subchondral bone produced results that agreed with previous studies that used conventional radiographs; that is, the most radiodense subchondral bone was located in the medial regions of both the human distal tibial plafond and talar trochlea (Muhlhofer et al. 2009; Müller-Gerbl 2001; Müller-Gerbl and Putz 1995). These regions were furthermore consistent with kinetic and kinematic studies of the human ankle which show greater joint load medially during normal walking.

The trabecular bone volume was more evenly distributed across the anterior and posterior aspects of the tibia and lateral and medial aspects of the talus. If it is presumed that the internal morphology reflects a lifetime average of joint loads, the morphology that was found in this study implies that in modern humans the average habitual loads are focused on the anterior and posterior tibial rims and on the lateral and medial talar rims.

The quantitative results of the shape and primary orientation of trabeculae agreed with previous qualitative studies in showing primarily vertically-directed rod-shaped trabecular struts in the tibia, but mostly anteroposteriorly-directed plate-shaped trabeculae in the talar body.

The comparative study identified significant differences among species in overall subchondral and trabecular bone morphology. Humans were distinguished by overall thinner subchondral bone, lower trabecular bone volume and greater trabecular anisotropy than the great apes. Baboons had overall more radiodense subchondral bone, greater trabecular bone volume and trabecular thickness, but fewer trabecular number and lower trabecular anisotropy than the other groups. Chimpanzees were distinguished by greater trabecular number and lower trabecular thickness in the distal tibia than all other groups. The relatively decreased trabecular bone volume in humans versus the apes has been shown previously for other skeletal regions and implies that human trabecular bone is mechanically weaker. This more gracile trabecular morphology is perhaps an epigenetic adaptive response to relatively low or predictable joint

loads, or may be a genetic characteristic of modern humans that is related to the overall skeletal gracilization of modern humans (Ruff et al. 1993; Trinkaus 1997). Conversely, baboons showed overall greater subchondral and trabecular bone strength, implying habitual exposure to relatively greater or less predictable joint loads.

Surprisingly, the distribution of subchondral bone radiodensity and trabecular quantity in the distal tibia and talus was generally less consistent within the human sample than within any of the other species, which contradicts the stereotype of human posture and locomotion as relatively more repetitive and predictable versus that of the other hominoids. Only the distribution of subchondral bone radiodensity in the talus was as predicted, with patterns in the more terrestrial humans and baboons more consistent than those in the more arboreal great apes.

Species differed in the patterns of distribution of subchondral and trabecular bone properties across the tibiotalar joint. Compared to humans, greater subchondral bone radiodensity was found more strongly in the medial regions of the distal tibia in the African apes, but in the anterolateral region of the orangutan distal tibia and the posterocentral region of the baboon distal tibia. Applying the interpretation from the human data, this result implies that these regions of greater subchondral bone radiodensity may be indicative of regions of the distal tibia under habitual loading. This interpretation is consistent with behavioral observations of a varus ankle posture in the African apes during both terrestrial quadrupedalism and vertical climbing, with a highly dorsiflexed and somewhat adducted ankle in the orangutan, and with the semi-digitigrade baboon ankle.

The distribution of subchondral bone radiodensity in the talus mirrored that in the distal tibia, supporting the hypothesis that this feature reflects common intra-articular load. In the African apes, the lateral region of the talus also displayed high radiodensity, presumably reflecting shared contact load from the distal fibula.

The distribution of trabecular bone in the distal tibia of the great apes was largely similar to that in humans, with increased bone volume along the anterior and posterior regions. In sharp contrast, in baboons the greatest trabecular bone volume and thickness was found in the central region of the distal tibia, implying that high magnitude loads were borne more directly in the center. Whether this is a feature related to the more high-speed nature of baboon locomotion is to be determined.

In the analysis of trabecular bone shape and primary orientation, a diagnostic locomotor signal was not found in the distal tibia that would be of help in interpreting locomotor behavior beyond features measureable in the external morphology. Trabecular shape indices quantified in the distal tibia did not distinguish among hominoid species, again implying that habitual loads through the distal tibia are largely similar in these species despite differences in locomotor behaviors. Humans, chimpanzees, and gorillas all show more plate-shaped trabeculae in the anterocentral and posterocentral regions which imply these regions withstood greater habitual loads in life. Both orangutans and baboons display more plate-shaped trabeculae in the central region, implying a different distribution of habitual load. The primary orientation of trabeculae

in the distal tibia also was largely similar among species, although there were slight differences that agree with postural differences such as the more varus ankle of African apes.

In the talus, humans showed the greatest overall consistency in trabecular orientation, supporting the stereotype that humans are much less variable in the direction of habitual joint load within the ankle. Orangutans showed the greatest overall variance in trabecular orientation, supporting the stereotype that the joint loads in orangutan locomotion are more variable. The primary orientation of trabeculae in the talus differs among species in ways that were predicted from behavioral observations. Humans differed from the non-human groups in that the orientation of trabeculae in the posterolateral and anteromedial regions were directed toward the posterior calcaneal facet and talar head, respectively, while that of other groups tended to be normal to the trochlear surface.

These distinct differences among species in trabecular orientation in the talus were used to interpret habitual locomotor behaviors from an isolated fossil talar bone, KNM-ER 1464. The KNM-ER 1464 talus displays internal morphology that in some ways is similar to that of baboons and apes and in other ways is similar to modern humans. The lateral regions of the fossil talus were similar to those of modern humans and support the assumption that it belonged to a bipedal hominid. Many features were found to be shared with baboons, such as thicker trabeculae overall and the regional distribution of trabecular number and anisotropy, which raise the possibility that the fossil hominid engaged in behavioral activities involving relatively prolonged high magnitude loads at the ankle. The primary orientation of trabeculae was similar to that of modern humans in the anterior regions of the talus, suggesting that transfer of body weight from the tibia, through the talus, to the forefoot was important. But the orientation of trabeculae that was found elsewhere in the talus to be generally normal to the articular surface was more similar to that in the non-human groups, perhaps indicating a more generalized level of bone strength able to withstand variations in loading direction.

Future directions

The findings of this dissertation raise additional questions related to the hypothesis that trabecular bone and subchondral bone properties reflect habitual load. Future studies will examine other human populations to determine to what extent the morphology shown here is specific to the post-industrial urban human female versus universal to all modern human bipeds. For example, analysis of the internal ankle morphology of an archeological population such as the late Woodland Libben Population curated at Kent State University, Ohio (Lovejoy et al. 1977) may help elucidate how morphology differs between sexes, with activity level and between shod and unshod individuals. Furthermore, an ontogenetic series would help to understand both when the unique human characteristics emerge in childhood, and how bones change with age. Comparatively, future studies will be expanded to include other models of arboreal versus terrestrial behavior to further clarify the extent to which morphology reflects locomotion versus genetics.

It has been the assumption in these studies that greater subchondral bone radiodensity and thickness, and greater trabecular bone volume and isotropy indicate mechanically stronger bone. This can be tested using finite element analyses constructed from the same micro-ct images to help further validate the patterns of morphology against applied joint load.

The analysis of additional fossil specimens would help put the morphology of the ankle bones into temporal context and may provide additional clues in how the modern human ankle evolved.

Literature cited

Abel, R., & Macho, G. A. (2011). Ontogenetic changes in the internal and external morphology of the ilium in modern humans. *Journal of Anatomy, 218*(3), 324-335.

Adam, C., Eckstein, F., Milz, S., & Putz, R. (1998). The distribution of cartilage thickness within the joints of the lower limb of elderly individuals. *Journal of Anatomy, 193*, 203-214.

Ahluwalia, K. (2000). *Knee joint load as determined by tibial subchondral bone density: its relationship to gross morphology and locomotor behavior in catarrhines.* Ph.D. Thesis, Stony Brook University, Stony Brook, NY.

Aiello, L., & Dean, C. (2002). *An Introduction to Human Evolutionary Anatomy*. London: Elsevier.

Anderson, D. D., Goldsworthy, J. K., Li, W., Rudert, M. J., Tochigi, Y., & Brown, T. D. (2007). Physical validation of a patient-specific contact finite element model of the ankle. *Journal of Biomechanics, 40*(8), 1662-1669.

Anderson, F. C., & Pandy, M. G. (2003). Individual muscle contributions to support in normal walking. *Gait & Posture, 17*(2), 159-169.

Athavale, S. A., Joshi, S. D., & Joshi, S. S. (2008). Internal architecture of the talus. *Foot & Ankle International, 29*(1), 82-86.

Benn, D. I. (1994). Fabric shape and the interpretation of sedimentary fabric data. *Journal of Sedimentary Research Section a-Sedimentary Petrology and Processes, 64*(4), 910-915.

Bennett, M. R., Harris, J. W. K., Richmond, B. G., Braun, D. R., Mbua, E., Kiura, P., et al. (2009). Early hominin foot morphology based on 1.5-million-year-old footprints from Ileret, Kenya. *Science, 323*(5918), 1197-1201.

Biewener, A. A. (1983). Allometry of quadrupedal locomotion - the scaling of duty factor, bone curvature and limb orientation to body size. *Journal of Experimental Biology, 105*(Jul), 147-171.

Biewener, A. A. (2005). Biomechanical consequences of scaling. *Journal of Experimental Biology, 208*(9), 1665-1676.

Biewener, A. A., Fazzalari, N. L., Konieczynski, D. D., & Baudinette, R. V. (1996). Adaptive changes in trabecular architecture in relation to functional strain patterns and disuse. *Bone, 19*(1), 1-8.

Bourrin, S., Palle, S., Pupier, R., Vico, L., & Alexandre, C. (1995). Effects of physical training on bone adaptation in 3 zones of the rat tibia. *Journal of Bone and Mineral Research, 10*(11), 1745-1752.

Bryant, R. J., Wastney, M. E., Martin, B. R., Wood, O., McCabe, G. P., Morshidi, M., et al. (2003). Racial differences in bone turnover and calcium metabolism in adolescent females. *Journal of Clinical Endocrinology & Metabolism, 88*(3), 1043-1047.

Calhoun, J. H., Eng, M., Li, F., Ledbetter, B. R., & Viegas, S. F. (1994). A Comprehensive study of pressure distribution in the ankle joint with inversion and eversion. *Foot & Ankle International, 15*(3), 125-133.

Carlson, K. J., Lublinsky, S., & Judex, S. (2008). Do different locomotor modes during growth modulate trabecular architecture in the murine hind limb? *Integrative and Comparative Biology, 48*(3)*,* 385-393.

Carlson, K. J., & Patel, B. A. (2006). Habitual use of the primate forelimb is reflected in the material properties of subchondral bone in the distal radius. *Journal of Anatomy, 208*(6), 659-670.

Clarke, R. J. (2002). Newly revealed information on the Sterkfontein Member 2 *Australopithecus* skeleton. *South African Journal of Science, 98*(11-12), 523-526.

Clarke, R. J., & Tobias, P. V. (1995). Sterkfontein Member 2 foot bones of the oldest South African hominid. *Science, 269*(5223), 521-524.

Cotter, M. M., Simpson, S. W., Latimer, B. M., & Hernandez, C. J. (2009). Trabecular microarchitecture of hominoid thoracic vertebrae. *Anatomical Record-Advances in Integrative Anatomy and Evolutionary Biology, 292*(8), 1098-1106.

Cowin, S. C. (2001). The false premise in Wolff's Law. In S. C. Cowin (Ed.), *Bone biomechanics handbook* (2nd ed., pp. 30-35). Boca Raton: CRC Press.

Cruz-Orive, L. M., Karlsson, L. M., Larsen, S. E., & Wainschtein, F. (1992). Characterizing anisotropy: a new concept. *Micron Microscopica Acta, 23*, 75-76.

Cunningham, C. A., & Black, S. M. (2009a). Anticipating bipedalism: trabecular organization in the newborn ilium. *Journal of Anatomy, 214*(6), 817-829.

Cunningham, C. A., & Black, S. M. (2009b). Development of the fetal ilium - challenging concepts of bipedality. *Journal of Anatomy, 214*(1), 91-99.

D'Août, K., Vereecke, E., Schoonaert, K., De Clercq, D., Van Elsacker, L., & Aerts, P. (2004). Locomotion in bonobos (*Pan paniscus*): differences and similarities between bipedal and

quadrupedal terrestrial walking, and a comparison with other locomotor modes. *Journal of Anatomy, 204*(5), 353-361.

Day, M. H., Leakey, R. E. F., Walker, A. C., & Wood, B. A. (1976). New hominids from East Turkana, Kenya. *American Journal of Physical Anthropology, 45*(3), 369-435.

Day, M. H., & Napier, J. R. (1964). Fossil foot bones. *Nature, 201*(492), 969.

Day, M. H., & Wood, B. A. (1968). Functional affinities of the Olduvai Hominid 8 talus. *Man, 3*(3), 440-455.

Day, M. H., & Wood, B. A. (1969). Hominoid tali from East Africa. *Nature, 222*(5193), 591.

de Asla, R. J., Wan, L., Rubash, H. E., & Li, G. (2006). Six DOF *in vivo* kinematics of the ankle joint complex: Application of a combined dual-orthogonal fluoroscopic and magnetic resonance imaging technique. *Journal of Orthopaedic Research, 24*(5), 1019-1027.

DeSilva, J. M. (2008). *Vertical climbing adaptations in the anthropoid ankle and midfoot: implications for locomotion in Miocene catarrhines and Plio-Pleistocene hominins.* Ph.D. Thesis, University of Michigan, Ann Arbor, MI.

DeSilva, J. M. (2009). Functional morphology of the ankle and the likelihood of climbing in early hominins. *Proceedings of the National Academy of Sciences of the United States of America, 106*(16), 6567-6572.

DeSilva, J. M., & Throckmorton, Z. J. (2010). Lucy's flat feet: The relationship between the ankle and rearfoot arching in early hominins. *Plos One, 5*(12).

Ding, M., Odgaard, A., Danielsen, C. C., & Hvid, I. (2002a). Mutual associations among microstructural, physical and mechanical properties of human cancellous bone. *Journal of Bone and Joint Surgery-British Volume, 84B*(6), 900-907.

Ding, M., Odgaard, A., Linde, F., & Hvid, I. (2002b). Age-related variations in the microstructure of human tibial cancellous bone. *Journal of Orthopaedic Research, 20*(3), 615-621.

Doran, D. M. (1993). Comparative locomotor behavior of chimpanzees and bonobos - the influence of morphology on locomotion. *American Journal of Physical Anthropology, 91*(1), 83-98.

Doube, M., Kłosowski, M. M., Wiktorowicz-Conroy, A. M., Hutchinson, J. R., & Shefelbine, S. J. (2011). Trabecular bone scales allometrically in mammals and birds. *Proceedings of the Royal Society B*, in press.

Eckstein, F., Hudelmaier, M., Cahue, S., Marshall, M., & Sharma, L. (2009). Medial-to-lateral ratio of tibiofemoral subchondral bone area is adapted to alignment and mechanical load. *Calcified Tissue International, 84*(3), 186-194.

Eckstein, F., Merz, B., Schon, M., Jacobs, C. R., & Putz, R. (1999). Tension and bending, but not compression alone determine the functional adaptation of subchondral bone in incongruous joints. *Anatomy and Embryology, 199*(1), 85-97.

Eckstein, F., Müller-Gerbl, M., Steinlechner, M., Kierse, R., & Putz, R. (1995). Subchondral bone density in the human elbow assessed by computed tomography osteoabsorptiometry - a reflection of the loading history of the joint surfaces. *Journal of Orthopaedic Research, 13*(2), 268-278.

Fajardo, R. J. (2004). *Comparative micro-CT analysis of anthropoid trabecular architecture.* Ph.D. Thesis, Stony Brook University, Stony Brook, NY.

Fajardo, R. J., & Müller, R. (2001). Three-dimensional analysis of nonhuman primate trabecular architecture using micro-computed tomography. *American Journal of Physical Anthropology, 115*(4), 327-336.

Fleagle, J. G. (1999). *Primate Adaptation and Evolution*. San Diego: Academic Press.

Frost, H. M. (1999). An approach to estimating bone and joint loads and muscle strength in living subjects and skeletal remains. *American Journal of Human Biology, 11*(4), 437-455.

GE Healthcare. (2006). *eXplore Locus User Guide, Direction 2394683, Revision 2*.

Gebo, D. L. (1986). Anthropoid origins - the foot evidence. *Journal of Human Evolution, 15*(6), 421-430.

Gebo, D. L. (1992). Plantigrady and foot adaptation in African apes - implications for hominid origins. *American Journal of Physical Anthropology, 89*(1), 29-58.

Gebo, D. L., & Schwartz, G. T. (2006). Foot bones from Omo: Implications for hominid evolution. *American Journal of Physical Anthropology, 129*(4), 499-511.

Golder, W., & Christian, A. (2002). Quantitative CT of dinosaur bones. *Journal of Computer Assisted Tomography, 26*(5), 821-824.

Goulet, R. W., Goldstein, S. A., Ciarelli, M. J., Kuhn, J. L., Brown, M. B., & Feldkamp, L. A. (1994). The relationship between the structural and orthogonal compressive properties of trabecular bone. *Journal of Biomechanics, 27*(4), 375-389.

Graham, D. J., & Midgley, N. G. (2000). Graphical representation of particle shape using triangular diagrams: An Excel spreadsheet method. *Earth Surface Processes and Landforms, 25*(13), 1473-1477.

Grausz, H. M., Leakey, R. E., Walker, A. C., & Ward, C. V. (2007) Associated cranial and postcranial bones of *Australopithecus boisei.* In F. E. Grine (Ed.), *Evolutionary History of the "Robust" Australopithecines* (pp. 127-132). New York: Aldine de Gruyter.

Grote, H. J., Amling, M., Vogel, M., Hahn, M., Posl, M., & Delling, G. (1995). Intervertebral variation in trabecular microarchitecture throughout the normal spine in relation to age. *Bone, 16*(3), 301-308.

Haraguchi, N., Armiger, R. S., Myerson, M. S., Campbell, J. T., & Chao, E. Y. S. (2009). Prediction of three-dimensional contact stress and ligament tension in the ankle during stance determined from computational modeling. *Foot & Ankle International, 30*(2), 177-185.

Harcourt-Smith, W. E. H. (2002). *Form and Function in the Hominoid Tarsal Skeleton*: Ph.D. Thesis, University College London.

Harcourt-Smith, W. E. H., & Aiello, L. C. (2004). Fossils, feet and the evolution of human bipedal locomotion. *Journal of Anatomy, 204*(5), 403-416.

Harrigan, T. P., & Mann, R. W. (1984). Characterization of microstructural anisotropy in orthotropic materials using a 2nd rank tensor. *Journal of Materials Science, 19*(3), 761-767.

Harrison, T. (1989). New postcranial remains of *Victoriapithecus* from the Middle Miocene of Kenya. *Journal of Human Evolution, 18*(1), 3-54.

Hernandez-Molina, G., Neogi, T., Hunter, D. J., Niu, J., Guermazi, A., Reichenbach, S., et al. (2008). The association of bone attrition with knee pain and other MRI features of osteoarthritis. *Annals of the Rheumatic Diseases, 67*(1), 43-47.

Hildebrand, T., & Ruegsegger, P. (1997). A new method for the model-independent assessment of thickness in three-dimensional images. *Journal of Microscopy-Oxford, 185*, 67-75.

Howard, C. B., & Benson, M. K. D. (1992). The ossific nuclei and the cartilage anlage of the talus and calcaneum. *Journal of Bone and Joint Surgery-British Volume, 74*(4), 620-623.

Hubbard, A. M., Meyer, J. S., Davidson, R. S., Mahboubi, S., & Harty, M. P. (1993). Relationship between the ossification center and cartilaginous anlage in the normal hindfoot in children - study with MR-imaging. *American Journal of Roentgenology, 161*(4), 849-853.

Huiskes, R. (2000). If bone is the answer, then what is the question? *Journal of Anatomy, 197*, 145-156.

Hunt, A. E., Smith, R. M., Torode, M., & Keenan, A. M. (2001). Inter-segment foot motion and ground reaction forces over the stance phase of walking. *Clinical Biomechanics (Bristol, Avon), 16*(7), 592-600.

Hunt, K. D. (1991). Positional behavior in the Hominoidea. *International Journal of Primatology, 12*(2), 95-118.

Hunt, K. D. (2004). The special demands of great ape locomotion and posture. In A. E. Russon & D. R. Begun (Eds.), *The Evolution of Thought.* (pp. 172-189). Cambridge: Cambridge University Press.

Hunt, K. D., Cant, J. G. H., Gebo, D. L., Rose, M. D., Walker, S. E., & Youlatos, D. (1996). Standardized descriptions of primate locomotor and postural modes. *Primates, 37*(4), 363-387.

Hvid, I., Rasmussen, O., Jensen, N. C., & Nielsen, S. (1985). Trabecular bone strength profiles at the ankle joint. *Clinical Orthopaedics and Related Research* (199), 306-312.

Johanson, D. C., Lovejoy, C. O., Kimbel, W. H., White, T. D., Ward, S. C., Bush, M. E., et al. (1982). Morphology of the Pliocene partial hominid skeleton (AL 288-1) from the Hadar Formation, Ethiopia. *American Journal of Physical Anthropology, 57*(4), 403-451.

Johnston, J. D., Kontulainen, S. A., Masri, B. A., & Wilson, D. R. (2010). A comparison of conventional maximum intensity projection with a new depth-specific topographic mapping technique in the CT analysis of proximal tibial subchondral bone density. *Skeletal Radiology, 39*(9), 867-876.

Johnston, J. D., Masri, B. A., & Wilson, D. R. (2009). Computed tomography topographic mapping of subchondral density (CT-TOMASD) in osteoarthritic and normal knees: methodological development and preliminary findings. *Osteoarthritis and Cartilage, 17*(10), 1319-1326.

Joo, Y. I., Sone, T., Fukunaga, M., Lim, S. G., & Onodera, S. (2003). Effects of endurance on three-dimensional trabecular bone microarchitecture in young growing rats. *Bone, 33*(4), 485-493.

Jungers, W. L., Harcourt-Smith, W. E. H., Larson, S. G., Morwood, M. J., & Djubiantono, T. (2008). Hobbit bipedalism: functional anatomy of the foot of *Homo floresiensis*. *American Journal of Physical Anthropology*, *46*, 127.

Kabel, J., van Rietbergen, B., Odgaard, A., & Huiskes, R. (1999). Constitutive relationships of fabric, density, and elastic properties in cancellous bone architecture. *Bone, 25*(4), 481-486.

Kanamoto, S., Ogihara, N., & Nakatsukasa, M. (2011). Three-dimensional orientations of talar articular surfaces in humans and great apes. *Primates, 52*(1), 61-68.

Kawcak, C. E., McIlwraith, C. W., Norrdin, R. W., Park, R. D., & James, S. P. (2001). The role of subchondral bone in joint disease: a review. *Equine Veterinary Journal, 33*(2), 120-126.

Ketcham, R. A. (2005). Three-dimensional grain fabric measurements using high-resolution X-ray computed tomography. *Journal of Structural Geology, 27*(7), 1217-1228.

Ketcham, R. A., & Ryan, T. M. (2004). Quantification and visualization of anisotropy in trabecular bone. *Journal of Microscopy-Oxford, 213*, 158-171.

Kidd, R. (1999). Evolution of the rearfoot - A model of adaptation with evidence from the fossil record. *Journal of the American Podiatric Medical Association, 89*(1), 2-17.

Kidd, R., & Oxnard, C. (2005). Little foot and big thoughts - a re-evaluation of the Stw573 foot from Sterkfontein, South Africa. *Homo-Journal of Comparative Human Biology, 55*(3), 189-212.

Kidd, R. S., O'Higgins, P., & Oxnard, C. E. (1996). The OH8 foot: A reappraisal of the functional morphology of the hindfoot utilizing a multivariate analysis. *Journal of Human Evolution, 31*(3), 269-291.

Kidd, R. S., & Oxnard, C. E. (2002). Patterns of morphological discrimination in selected human tarsal elements. *American Journal of Physical Anthropology, 117*(2), 169-181.

Kim, D. G., Christopherson, G. T., Dong, X. N., Fyhrie, D. P., & Yeni, Y. N. (2004). The effect of microcomputed tomography scanning and reconstruction voxel size on the accuracy of stereological measurements in human cancellous bone. *Bone, 35*(6), 1375-1382.

Kothari, M., Keaveny, T. M., Lin, J. C., Newitt, D. C., Genant, H. K., & Majumdar, S. (1998). Impact of spatial resolution on the prediction of trabecular architecture parameters. *Bone, 22*(5), 437-443.

Lai, Y. M., Qin, L., Hung, V. W. Y., Choy, W. Y., Chan, S. T., Chan, L. W. C., et al. (2006). Trabecular bone status in ultradistal tibia under habitual gait loading: A pQCT study in postmenopausal women. *Journal of Clinical Densitometry, 9*(2), 175-183.

Lai, Y. M., Qin, L., Yeung, H. Y., Lee, K. K. H., & Chan, K. M. (2005). Regional differences in trabecular BMD and micro-architecture of weight-bearing bone under habitual gait loading - A pQCT and microCT study in human cadavers. *Bone, 37*(2), 274-282.

Laib, A., & Ruegsegger, P. (1999). Calibration of trabecular bone structure measurements of *in vivo* three-dimensional peripheral quantitative computed tomography with 28-µm-resolution microcomputed tomography. *Bone, 24*(1), 35-39.

Latimer, B., & Lovejoy, C. O. (1989). The calcaneus of *Australopithecus afarensis* and its implications for the evolution of bipedality. *American Journal of Physical Anthropology, 78*(3), 369-386.

Latimer, B., Ohman, J. C., & Lovejoy, C. O. (1987). Talocrural joint in African hominoids - Implications for *Australopithecus afarensis*. *American Journal of Physical Anthropology, 74*(2), 155-175.

Leakey, L. S. B., Tobias, P. V., & Napier, J. R. (1964). A new species of genus *Homo* from Olduvai Gorge. *Nature, 202*, 7-9.

Leakey, R. E. F. (1972). Further evidence of lower Pleistocene hominids from East Rudolf, North Kenya, 1971. *Nature, 237*(5353), 264-&.

Leakey, R. E. F. (1973). Further evidence of lower Pleistocene hominids from East Rudolf, North Kenya, 1972. *Nature, 242*(5394), 170-173.

Leardini, A., Benedetti, M. G., Berti, L., Bettinelli, D., Nativo, R., & Giannini, S. (2007). Rear-foot, mid-foot and fore-foot motion during the stance phase of gait. *Gait & Posture, 25*(3), 453-462.

Lewis, O. J. (1980). The joints of the evolving foot . 1. the ankle joint. *Journal of Anatomy, 130*(May), 527-543.

Lieberman, D. E., Devlin, M. J., & Pearson, O. M. (2001). Articular area responses to mechanical loading: Effects of exercise, age, and skeletal location. *American Journal of Physical Anthropology, 116*(4), 266-277.

Lisowski, F. P., Albrecht, G. H., & Oxnard, C. E. (1974). Form of talus in some higher primates - a multivariate study. *American Journal of Physical Anthropology, 41*(2), 191-215.

Lisowski, F. P., Albrecht, G. H., & Oxnard, C. E. (1976). African fossil tali - Further multivariate morphometric studies. *American Journal of Physical Anthropology, 45*(1), 5-18.

Liu, X. S., Bevill, G., Keaveny, T. M., Sajda, P., & Guo, X. E. (2009). Micromechanical analyses of vertebral trabecular bone based on individual trabeculae segmentation of plates and rods. *Journal of Biomechanics, 42*(3), 249-256.

Liu, X. S., Sajda, P., Saha, P. K., Wehrli, F. W., Bevill, G., Keaveny, T. M., et al. (2008). Complete volumetric decomposition of individual trabecular plates and rods and its morphological correlations with anisotropic elastic moduli in human trabecular bone. *Journal of Bone and Mineral Research, 23*(2), 223-235.

Liu, X. W. S., Sajda, P., Saha, P. K., Wehrli, F. W., & Guo, X. E. (2006). Quantification of the roles of trabecular microarchitecture and trabecular type in determining the elastic modulus of human trabecular bone. *Journal of Bone and Mineral Research, 21*(10), 1608-1617.

Lovejoy, C. O., Latimer, B., Suwa, G., Asfaw, B., & White, T. D. (2009). Combining prehension and propulsion: The foot of *Ardipithecus ramidus*. *Science, 326*(5949), 8.

Lovejoy, C. O., McCollum, M. A., Reno, P. L., & Rosenman, B. A. (2003). Developmental biology and human evolution. *Annual Review of Anthropology, 32*, 85-109.

Lovejoy, C. O., Meindl, R. S., Mensforth, R. P., & Barton, T. J. (1985). Multifactorial determination of skeletal age at death - a method and blind tests of its accuracy. *American Journal of Physical Anthropology, 68*(1), 1-14.

Lovejoy, C. O., Meindl, R. S., Ohman, J. C., Heiple, K. G., & White, T. D. (2002). The Maka femur and its bearing on the antiquity of human walking: Applying contemporary concepts of morphogenesis to the human fossil record. *American Journal of Physical Anthropology, 119*(2), 97-133.

Lovejoy, C. O., Meindl, R. S., Pryzbeck, T. R., Barton, T. S., Heiple, K. G., & Kotting, D. (1977). Paleodemography of Libben Site, Ottawa County, Ohio. *Science, 198*(4314), 291-293.

Lundgren, P., Nester, C., Liu, A., Arndt, A., Jones, R., Stacoff, A., et al. (2008). Invasive *in vivo* measurement of rear-, mid- and forefoot motion during walking. *Gait & Posture, 28*(1), 93-100.

MacLatchy, L., & Müller, R. (2002). A comparison of the femoral head and neck trabecular architecture of *Galago* and *Perodicticus* using micro-computed tomography (μCT). *Journal of Human Evolution, 43*(1), 89-105.

Madry, H., van Dijk, C. N., & Müller-Gerbl, M. (2010). The basic science of the subchondral bone. *Knee Surg Sports Traumatol Arthrosc, 18*(4), 419-433.

Maga, M., Kappelman, J., Ryan, T. M., & Ketcham, R. A. (2006). Preliminary observations on the calcaneal trabecular microarchitecture of extant large-bodied hominoids. *American Journal of Physical Anthropology, 129*(3), 410-417.

Marchi, D. (2007). Relative strength of the tibia and fibula and locomotor behavior in hominoids. *Journal of Human Evolution, 53*(6), 647-655.

Mardia, K. V. (1972). *Statistics of Directional Data*. New York: Academic Press.

Matricali, G. A., Bartels, W., Labey, L., Dereymaeker, G. P. E., Luyten, F. P., & Sloten, J. V. (2009). High inter-specimen variability of baseline data for the tibio-talar contact area. *Clinical Biomechanics, 24*(1), 117-120.

Mazurier, A., Volpato, V., & Macchiarelli, R. (2006). Improved noninvasive microstructural analysis of fossil tissues by means of SR-microtomography. *Applied Physics a-Materials Science & Processing, 83*(2), 229-233.

McHenry, H. M. (1994). Early hominid postcrania. In R. S. Corruccini & R. L. Ciochon (Eds.), *Integrative Paths to the Past* (pp. 251-268). Englewood Cliffs, NJ: Prentice Hall.

McKay, H., Liu, D. M., Egeli, D., Boyd, S., & Burrows, M. (2011). Physical activity positively predicts bone architecture and bone strength in adolescent males and females. *Acta Paediatrica, 100*(1), 97-101.

Meindl, R. S., Russell, K. F., & Lovejoy, C. O. (1990). Reliability of age at death in the Hamann-Todd Collection - Validity of subselection procedures used in blind tests of the Summary Age Technique. *American Journal of Physical Anthropology, 83*(3), 349-357.

Meldrum, D. J. (1989). *Terrestrial adaptations in the feet of African cercopithecines.* Ph.D. Thesis, Stony Brook University, Stony Brook, NY.

Meldrum, D. J. (1991). Kinematics of the Cercopithecine foot on arboreal and terrestrial substrates with implications for the interpretation of hominid terrestrial adaptations. *American Journal of Physical Anthropology, 84*(3), 273-289.

Menetrey, J., Unno-Veith, F., Madry, H., & Van Breuseghem, I. (2010). Epidemiology and imaging of the subchondral bone in articular cartilage repair. *Knee Surgery Sports Traumatology Arthroscopy, 18*(4), 463-471.

Milz, S., Eckstein, F., & Putz, R. (1997). Thickness distribution of the subchondral mineralization zone of the trochlear notch and its correlation with the cartilage thickness: An expression of functional adaptation to mechanical stress acting on the humeroulnar joint? *Anatomical Record, 248*(2), 189-197.

Milz, S., & Putz, R. (1994). Quantitative morphology of the subchondral plate of the tibial plateau. *Journal of Anatomy, 185*, 103-110.

Mittra, E., Rubin, C., & Qin, Y. X. (2005). Interrelationship of trabecular mechanical and microstructural properties in sheep trabecular bone. *Journal of Biomechanics, 38*(6), 1229-1237.

Morton, D. J. (1922). Evolution of the human foot. I. *American Journal of Physical Anthropology, 5*(4), 305-336.

Muhlhofer, H., Ercan, Y., Drews, S., Matsuura, M., Meissner, J., Linsenmaier, U., et al. (2009). Mineralisation and mechanical strength of the subchondral bone plate of the inferior tibial facies. *Surgical and Radiologic Anatomy, 31*(4), 237-243.

Müller-Gerbl, M. (2001). Anatomy and biomechanics of the ankle joint. *Orthopade, 30*(1), 3-11.

Müller-Gerbl, M., & Putz, R. (1995). Functional anatomy of the ankle joint. In U. F. A. Heim (Ed.), *The Pilon Tibial Fracture* (pp. 2-25). Philadelphia: W.B. Saunders Company.

Müller-Gerbl, M., Putz, R., Hodapp, N., Schulte, E., & Wimmer, B. (1989). Computed tomography-osteoabsorptiometry for assessing the density distribution of subchondral bone as a measure of long-term mechanical adaptation in individual joints. *Skeletal Radiology, 18*(7), 507-512.

Müller-Gerbl, M., Putz, R., Kenn, R., & Kierse, R. (1993). People in different age-groups show different hip joint morphology. *Clinical Biomechanics, 8*(2), 66-72.

Müller, R., Hahn, M., Vogel, M., Delling, G., & Ruegsegger, P. (1996). Morphometric analysis of noninvasively assessed bone biopsies: Comparison of high-resolution computed tomography and histologic sections. *Bone, 18*(3), 215-220.

Murray, R. C., Vedi, S., Birch, H. L., Lakhani, K. H., & Goodship, A. E. (2001). Subchondral bone thickness, hardness and remodelling are influenced by short-term exercise in a site-specific manner. *Journal of Orthopaedic Research, 19*(6), 1035-1042.

Neogi, T., Nevitt, M., Niu, J. B., Sharma, L., Roemer, F., Guermazi, A., et al. (2010). Subchondral bone attrition may be a reflection of compartment-specific mechanical load: the MOST Study. *Annals of the Rheumatic Diseases, 69*(5), 841-844.

Neumann, D. A. (2010). Ankle and Foot. In D. A. Neumann (Ed.), *Kinesiology of the Musculoskeletal System: Foundations for Rehabilitation* (2nd ed., pp. 573-626). St. Louis: Mosby Elsevier.

Noble, J., & Alexander, K. (1985). Studies of tibial subchondral bone density and its significance. *Journal of Bone and Joint Surgery-American Volume, 67A*(2), 295-302.

Nowak, M. G., Carlson, K. J., & Patel, B. A. (2010). Apparent density of the primate calcaneo-cuboid joint and its association with locomotor mode, foot posture, and the "midtarsal break". *American Journal of Physical Anthropology, 142*(2), 180-193.

Odgaard, A., Kabel, J., van Rietbergen, B., Dalstra, M., & Huiskes, R. (1997). Fabric and elastic principal directions of cancellous bone are closely related. *Journal of Biomechanics, 30*(5), 487-495.

Oxnard, C. E. (1972). Some African fossil foot bones - Note on interpolation of fossils into a matrix of extant species. *American Journal of Physical Anthropology, 37*(1), 3-&.

Pal, G. P., & Routal, R. V. (1998). Architecture of the cancellous bone of the human talus. *Anatomical Record, 252*(2), 185-193.

Patel, B. A. (2009). Not so fast: Speed effects on forelimb kinematics in Cercopithecine monkeys and implications for digitigrade postures in primates. *American Journal of Physical Anthropology, 140*(1), 92-112.

Patel, B. A. (2010). The interplay between speed, kinetics, and hand postures during primate terrestrial locomotion. *American Journal of Physical Anthropology, 141*(2), 222-234.

Patel, B. A., & Carlson, K. J. (2006). Subchondral bone mineral density in the distal radius reflects habitual use of the forelimb in sloths and anteaters (Order Xenarthra). *Integrative and Comparative Biology, 45*(6), 1176-1176.

Patel, B. A., & Carlson, K. J. (2007). Bone density spatial patterns in the distal radius reflect habitual hand postures adopted by quadrupedal primates. *Journal of Human Evolution, 52*(2), 130-141.

Patel, B. A., & Carlson, K. J. (2008). Apparent density patterns in subchondral bone of the sloth and anteater forelimb. *Biology Letters, 4*(5), 486-489.

Pauwels, F. (1980). *Biomechanics of the Locomotor Apparatus. (Translated by P. Maquet and R. Furlong)*. Berlin: Springer-Verlag.

Pearson, O. M. (2000). Activity, climate, and postcranial robusticity - Implications for modern human origins and scenarios of adaptive change. *Current Anthropology, 41*(4), 569-607.

Polk, J. D. (2002). Adaptive and phylogenetic influences on musculoskeletal design in cercopithecine primates. *Journal of Experimental Biology, 205*(21), 3399-3412.

Polk, J. D. (2004). Influences of limb proportions and body size on locomotor kinematics in terrestrial primates and fossil hominins. *Journal of Human Evolution, 47*(4), 237-252.

Polk, J. D., Blumenfeld, J., & Ahluwalia, D. (2008). Knee posture predicted from subchondral apparent density in the distal femur: An experimental validation. *Anatomical Record-Advances in Integrative Anatomy and Evolutionary Biology, 291*(3), 293-302.

Polk, J. D., Williams, S. A., Peterson, J. V., Roseman, C. C., & Godfrey, L. R. (2010). Subchondral bone apparent density and locomotor behavior in extant primates and subfossil lemurs *Hadropithecus* and *Pachylemur*. *International Journal of Primatology, 31*(2), 275-299.

Pontzer, H., Lieberman, D. E., Momin, E., Devlin, M. J., Polk, J. D., Hallgrimsson, B., et al. (2006). Trabecular bone in the bird knee responds with high sensitivity to changes in load orientation. *Journal of Experimental Biology, 209*(1), 57-65.

Radin, E. L., Martin, R. B., Burr, D. B., Caterson, B., Boyd, R. D., & Goodwin, C. (1984). Effects of mechanical loading on the tissues of the rabbit knee. *Journal of Orthopaedic Research, 2*, 221-234.

Rafferty, K. L., & Ruff, C. B. (1994). Articular structure and function in *Hylobates*, *Colobus*, and *Papio*. *American Journal of Physical Anthropology, 94*(3), 395-408.

Rasband, W. S. (1997-2007). *ImageJ*: U. S. National Institutes of Health, Bethesda, Maryland, USA, http://rsb.info.nih.gov/ij/.

Ridler, T. W., & Calvard, S. (1978). Picture thresholding using an iterative selection method. *Ieee Transactions on Systems Man and Cybernetics, 8*(8), 630-632.

Roemer, F. W., Neogi, T., Nevitt, M. C., Felson, D. T., Zhu, Y., Zhang, Y., et al. (2010). Subchondral bone marrow lesions are highly associated with, and predict subchondral bone attrition longitudinally: the MOST study. *Osteoarthritis and Cartilage, 18*(1), 47-53.

Roesler, H. (1981). Some historical remarks on the theory of cancellous bone structure (Wolff's Law). In S. C. Cowin (Ed.), *Mechanical properties of bone* (pp. 27-42). New York: ASME-AMD.

Roesler, H. (1987). The history of some fundamental concepts in bone biomechanics. *Journal of Biomechanics, 20*(11-12), 1025-1034.

Rose, M. D. (1977). Positional behaviour of olive baboons (*Papio anubis*) and its relationship to maintenance and social activities. *Primates, 18*, 59-116.

Rubin, C., Turner, A. S., Mallinckrodt, C., Jerome, C., McLeod, K., & Bain, S. (2002). Mechanical strain, induced noninvasively in the high-frequency domain, is anabolic to cancellous bone, but not cortical bone. *Bone, 30*(3), 445-452.

Ruff, C. B. (2006). Gracilization of the modern human skeleton - The latent strength in our slender bones teaches lessons about human lives, current and past. *American Scientist, 94*(6), 508-514.

Ruff, C. B., & Leo, F. P. (1986). Use of computed tomography in skeletal structure research. *Yearbook of Physical Anthropology, 29*, 181-196.

Ruff, C. B., Trinkaus, E., Walker, A., & Larsen, C. S. (1993). Postcranial robusticity in *Homo:* 1. Temporal trends and mechanical interpretation. *American Journal of Physical Anthropology, 91*(1), 21-53.

Ryan, T. M. (2001). *The structure and function of trabecular bone in the femoral head of strepsirhine primates.* Ph.D. Thesis. University of Texas, Austin, TX.

Ryan, T. M., & Ketcham, R. A. (2002). The three-dimensional structure of trabecular bone in the femoral head of strepsirrhine primates. *Journal of Human Evolution, 43*(1), 1-26.

Ryan, T. M., & Ketcham, R. A. (2005). Angular orientation of trabecular bone in the femoral head and its relationship to hip joint loads in leaping primates. *Journal of Morphology, 265*(3), 249-263.

Ryan, T. M., & Krovitz, G. E. (2006). Trabecular bone ontogeny in the human proximal femur. *Journal of Human Evolution, 51*(6), 591-602.

Ryan, T. M., & van Rietbergen, B. (2005). Mechanical significance of femoral head trabecular bone structure in *Loris* and *Galago* evaluated using micromechanical finite element models. *American Journal of Physical Anthropology, 126*(1), 82-96.

Saparin, P., Scherf, H., Hublin, J., Fratzl, P., & Weinkamer, R. (2009). The trabecular bone architecture in proximal femora of primates with different locomotor preferences indicates different adaptation mechanisms. *Bone, 44*, 219.

Scherf, H., & Hublin, J. J. (2010). Morphological differences in humeral cancellous bone of Neanderthals and extant hominids. *American Journal of Physical Anthropology*, *50*, 207.

Scherf, H., Tilgner, R., & Hublin, J. J. (2009). Effects of locomotion - Morphological differences in humeral cancellous bone of hominids and their relation to habitual loading conditions of the shoulder joint. *American Journal of Physical Anthropology*, 229-229.

Schmitt, D. (2003). Insights into the evolution of human bipedalism from experimental studies of humans and other primates. *Journal of Experimental Biology, 206*(9), 1437-1448.

Schmitt, D., & Larson, S. G. (1995). Heel contact as a function of substrate type and speed in primates. *American Journal of Physical Anthropology, 96*(1), 39-50.

Segal, N. A., Anderson, D. D., Iyer, K. S., Baker, J., Torner, J. C., Lynch, J. A., et al. (2009). Baseline articular contact stress levels predict incident symptomatic knee osteoarthritis development in the MOST cohort. *Journal of Orthopaedic Research, 27*(12), 1562-1568.

Simkin, P. A., Heston, T. F., Downey, D. J., Benedict, R. S., & Choi, H. S. (1991). Subchondral architecture in bones of the canine shoulder. *Journal of Anatomy, 175*, 213-227.

Smit, T. H., Odgaard, A., & Schneider, E. (1997). Structure and function of vertebral trabecular bone. *Spine, 22*(24), 2823-2833.

Smith, R. J., & Jungers, W. L. (1997). Body mass in comparative primatology. *Journal of Human Evolution, 32*(6), 523-559.

Sode, M., Burghardt, A. J., Kazakia, G. J., Link, T. M., & Majumdar, S. (2010). Regional variations of gender-specific and age-related differences in trabecular bone structure of the distal radius and tibia. *Bone, 46*(6), 1652-1660.

Sode, M., Burghardt, A. J., Nissenson, R. A., & Majumdar, S. (2008). Resolution dependence of the non-metric trabecular structure indices. *Bone, 42*(4), 728-736.

Spoor, F., Leakey, M. G., Gathogo, P. N., Brown, F. H., Anton, S. C., McDougall, I., et al. (2007). Implications of new early *Homo* fossils from Ileret, east of Lake Turkana, Kenya. *Nature, 448*(7154), 688-691.

Stern, J. T., & Susman, R. L. (1983). The locomotor anatomy of *Australopithecus afarensis*. *American Journal of Physical Anthropology, 60*(3), 279-317.

Stock, J. T. (2006). Hunter-gatherer postcranial robusticity relative to patterns of mobility, climatic adaptation, and selection for tissue economy. *American Journal of Physical Anthropology, 131*(2), 194-204.

Susman, R. L., & Stern, J. T. (1982). Functional morphology of *Homo habilis*. *Science, 217*(4563), 931-934.

Swartz, S. M., Parker, A., & Huo, C. (1998). Theoretical and empirical scaling patterns and topological homology in bone trabeculae. *Journal of Experimental Biology, 201*(4), 573-590.

Tabor, Z. (2004). Analysis of the influence of image resolution on the discriminating power of trabecular bone architectural parameters. *Bone, 34*(1), 170-179.

Takechi, H., Ito, S., Takada, T., & Nakayama, H. (1982). Trabecular architecture of the ankle joint. *Anatomia Clinica, 4*(3), 227-233.

Tanck, E., Homminga, J., Van Lenthe, G. H., & Huiskes, R. (2001). Increase in bone volume fraction precedes architectural adaptation in growing bone. *Bone, 28*(6), 650-654.

Thomsen, J. S., Ebbesen, E. N., & Mosekilde, L. (2002). Predicting human vertebral bone strength by vertebral static histomorphometry. *Bone, 30*(3), 502-508.

Thorpe, S. K. S., & Crompton, R. H. (2006). Orangutan positional behavior and the nature of arboreal locomotion in Hominoidea. *American Journal of Physical Anthropology, 131*(3), 384-401.

Tochigi, Y., Rudert, M. J., Saltzman, C. L., Amendola, A., & Brown, T. D. (2006). Contribution of articular surface geometry to ankle stabilization. *Journal of Bone and Joint Surgery-American Volume, 88A*(12), 2704-2713.

Tommasini, S. M., Morgan, T. G., van der Meulen, M. C. H., & Jepsen, K. J. (2005). Genetic variation in structure-function relationships for the inbred mouse lumbar vertebral body. *Journal of Bone and Mineral Research, 20*(5), 817-827.

Trinkaus, E. (1997). Appendicular robusticity and the paleobiology of modern human emergence. *Proceedings of the National Academy of Sciences of the United States of America, 94*(24), 13367-13373.

Trinkaus, E. (2005). Anatomical evidence for the antiquity of human footwear use. *Journal of Archaeological Science, 32*(10), 1515-1526.

Turner, C. H. (1998). Three rules for bone adaptation to mechanical stimuli. *Bone, 23*(5), 399-407.

Ulrich, D., Van Rietbergen, B., Laib, A., & Ruegsegger, P. (1999). The ability of three-dimensional structural indices to reflect mechanical aspects of trabecular bone. *Bone, 25*(1), 55-60.

Vereecke, E., D'Aout, K., De Clercq, D., Van Elsacker, L., & Aerts, P. (2003). Dynamic plantar pressure distribution during terrestrial locomotion of bonobos (*Pan paniscus*). *American Journal of Physical Anthropology, 120*(4), 373-383.

Vesterby, A., Mosekilde, L., Gundersen, H. J. G., Melsen, F., Holme, K., & Sorensen, S. (1991). Biologically meaningful determinants of the *in vitro* strength of lumbar vertebrae. *Bone, 12*(3), 219-224.

von Eisenhart, R., Adam, C., Steinlechner, M., Müller-Gerbl, M., & Eckstein, F. (1999). Quantitative determination of joint incongruity and pressure distribution during simulated gait and cartilage thickness in the human hip joint. *Journal of Orthopaedic Research, 17*(4), 532-539.

Wang, C. L., Cheng, C. K., Chen, C. W., Lu, C. M., Hang, Y. S., & Liu, T. K. (1995). Contact areas and pressure distributions in the subtalar joint. *Journal of Biomechanics, 28*(3), 269-279.

Ward, C. V. (2002). Interpreting the posture and locomotion of *Australopithecus afarensis*: Where do we stand? *Yearbook of Physical Anthropology, 45*, 185-215.

Ward, K., Alsop, C., Caulton, J., Rubin, C., Adams, J., & Mughal, Z. (2004). Low magnitude mechanical loading is osteogenic in children with disabling conditions. *Journal of Bone and Mineral Research, 19*(3), 360-369.

Witte, H., Preuschoft, H., & Recknagel, S. (1991). Human body proportions explained on the basis of biomechanical principles. *Z. Morph. Anthropol., 78*, 407-423.

Wolff, J. (1892). *Das Gesetz der Transformation der Knochen*. Berlin: A Hirschwald.

Wood, B., & Constantino, P. (2007). *Paranthropus boisei*: Fifty years of evidence and analysis. In *Yearbook of Physical Anthropology* (Vol. 50, pp. 106-132). New York: Wiley-Liss, Inc.

Wood, B. A. (1974). Evidence on locomotor pattern of *Homo* from Early Pleistocene of Kenya. *Nature, 251*(5471), 135-136.

Wunderlich, R. (1999). *Pedal form and plantar pressure distribution in Anthropoid primates*, Ph.D. Thesis. Stony Brook University, Stony Brook, NY.

Zonneveld, F. W. (2002). Applications and pitfalls of CT-based 3-D imaging of hominid fossils In B. Mafart & H. Delingette (Eds.), *Three-dimensional imaging in paleoanthropology and prehistoric archaeology* (pp. 5-9). Oxford: British Archaeological Report International Series 1049

Appendix

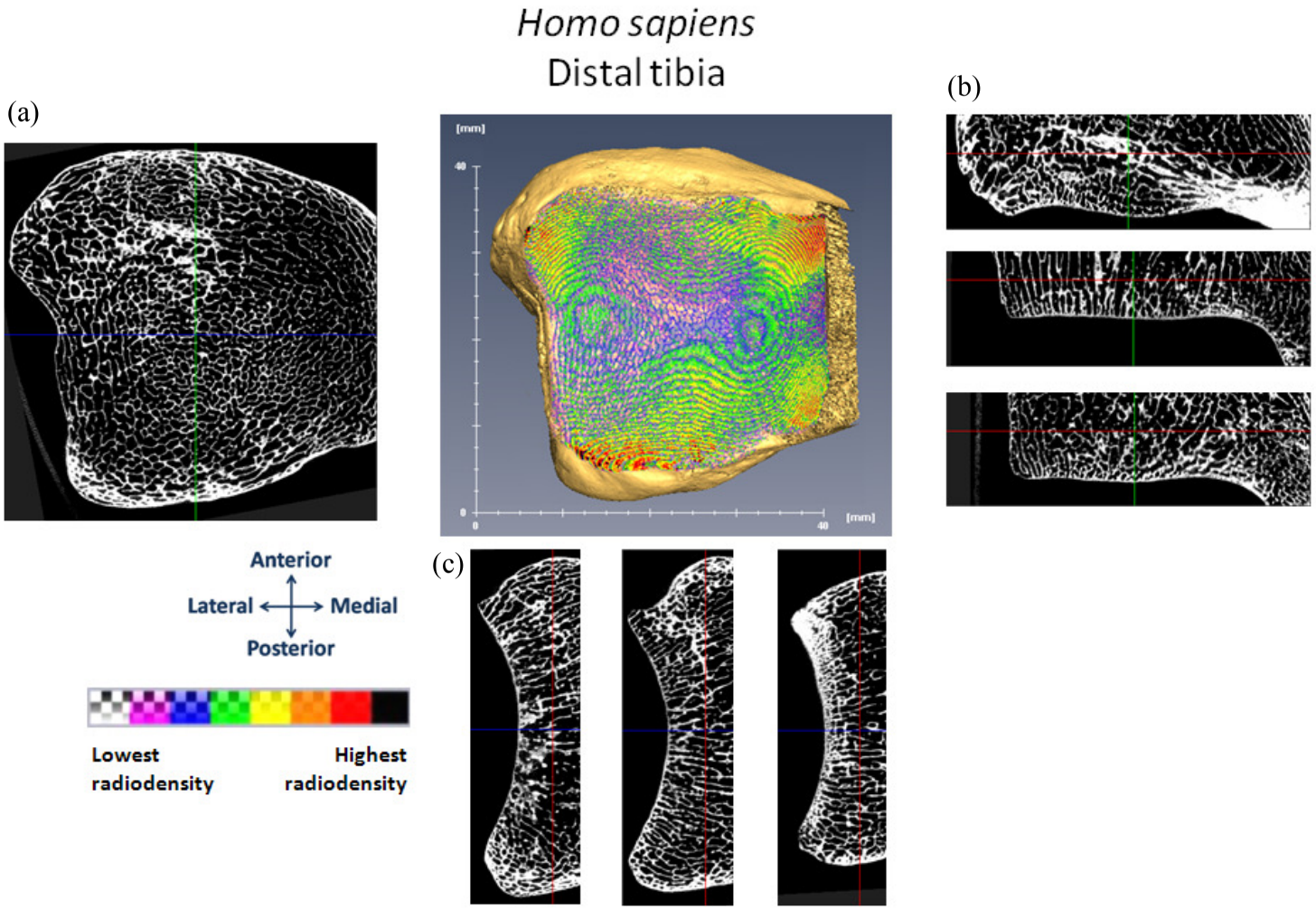

Figure A. 1: Representative micro-CT images of a *Homo sapiens* distal tibia.
The false-color map represents the relative intensity of subchondral bone radiodensity. Shown are representative images of the trabecular bone structure in the transverse plane (a), and in each third of the bone along the coronal axis (b) and along the sagittal axis (c).

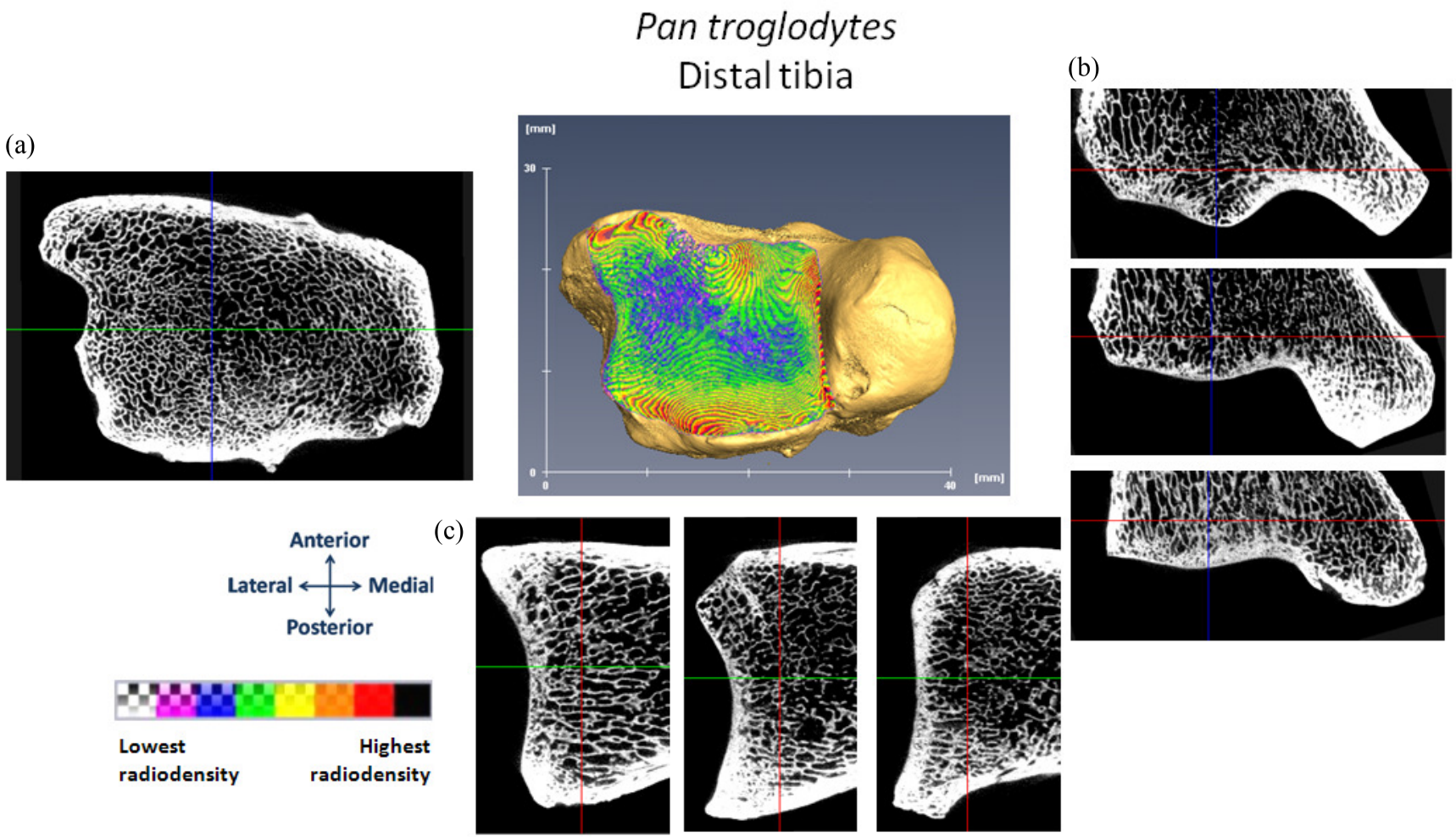

Figure A. 2: Representative micro-CT images of a *Pan troglodytes* distal tibia.
The false-color map represents the relative intensity of subchondral bone radiodensity. Shown are representative images of the trabecular bone structure in the transverse plane (a), and in each third of the bone along the coronal axis (b) and along the sagittal axis (c).

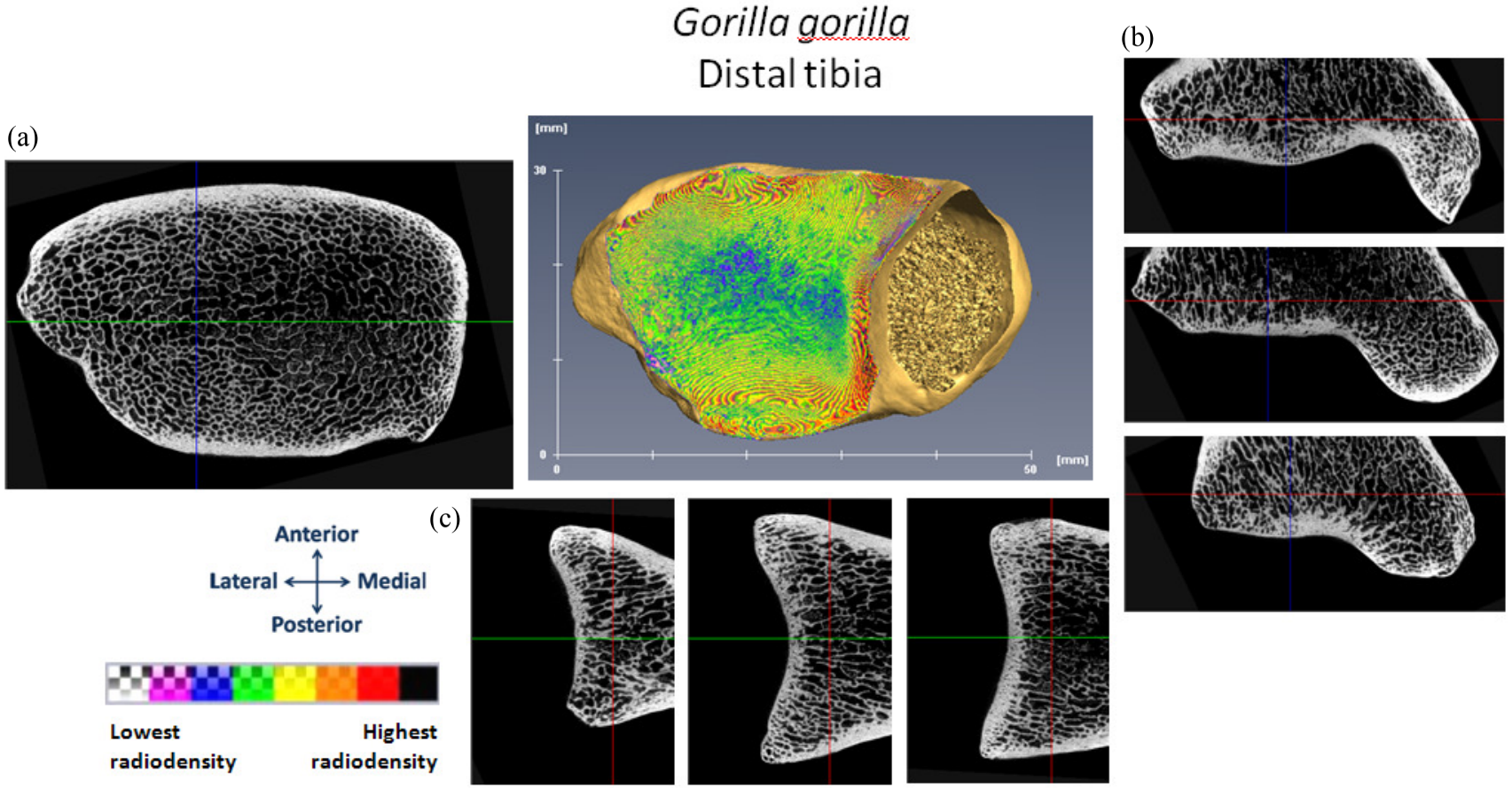

Figure A. 3: Representative micro-CT images of a *Gorilla gorilla* distal tibia.
The false-color map represents the relative intensity of subchondral bone radiodensity. Shown are representative images of the trabecular bone structure in the transverse plane (a), and in each third of the bone along the coronal axis (b) and along the sagittal axis (c).

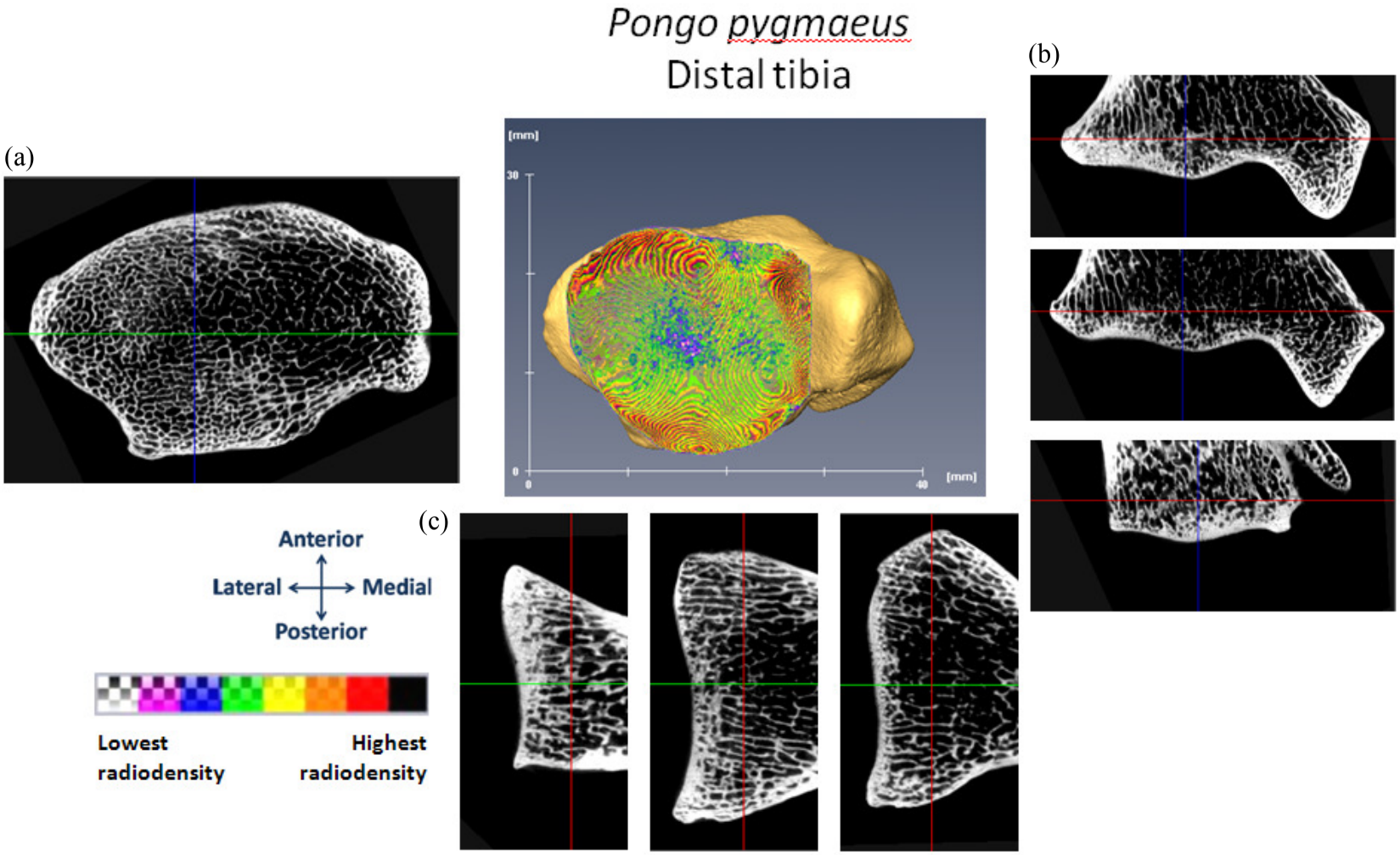

Figure A. 4: Representative micro-CT images of a *Pongo pygmaeus* distal tibia.
The false-color map represents the relative intensity of subchondral bone radiodensity. Shown are representative images of the trabecular bone structure in the transverse plane (a), and in each third of the bone along the coronal axis (b) and along the sagittal axis (c).

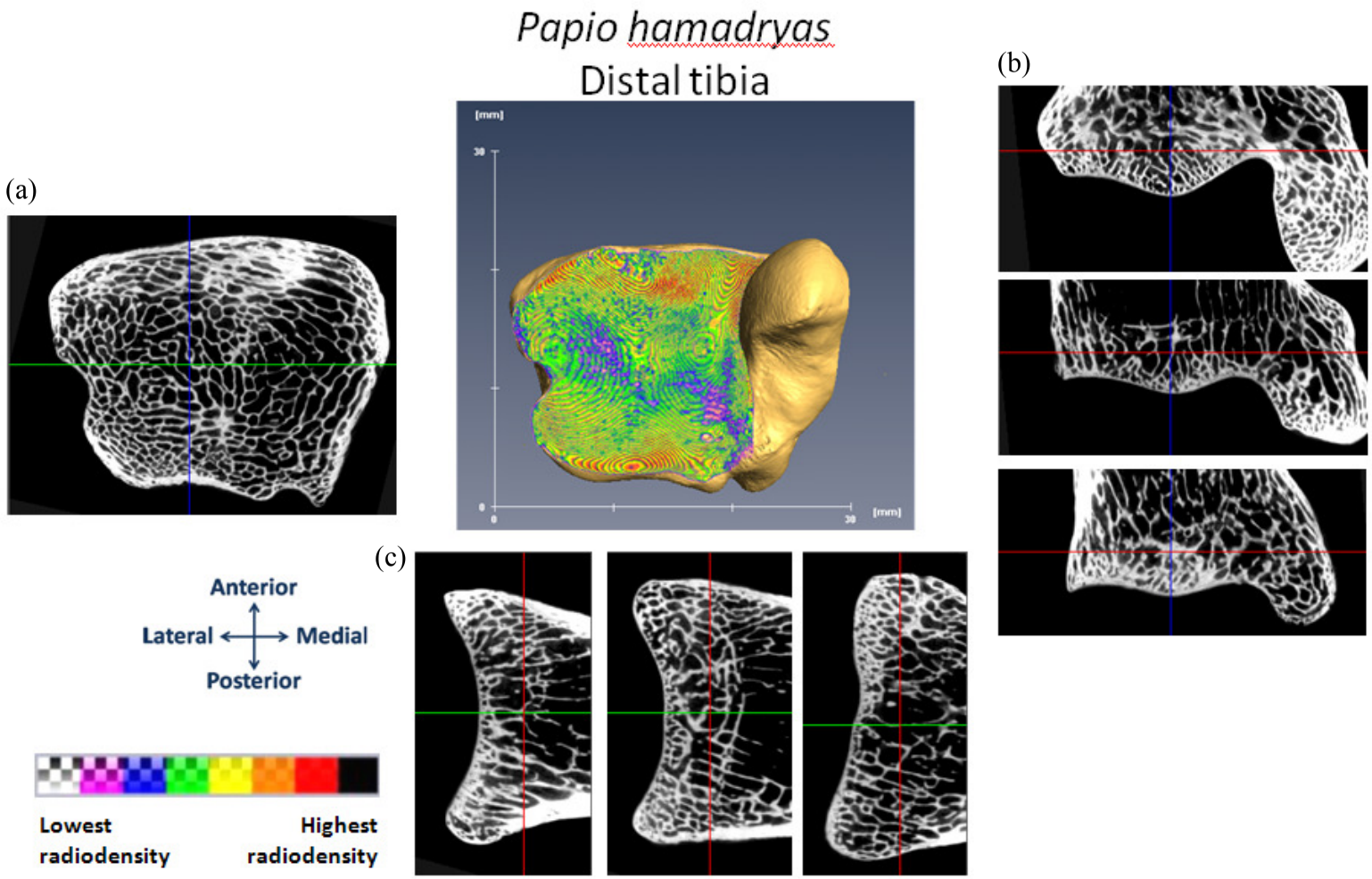

Figure A. 5: Representative micro-CT images of a *Papio hamadryas* distal tibia.
The false-color map represents the relative intensity of subchondral bone radiodensity. Shown are representative images of the trabecular bone structure in the transverse plane (a), and in each third of the bone along the coronal axis (b) and along the sagittal axis (c).

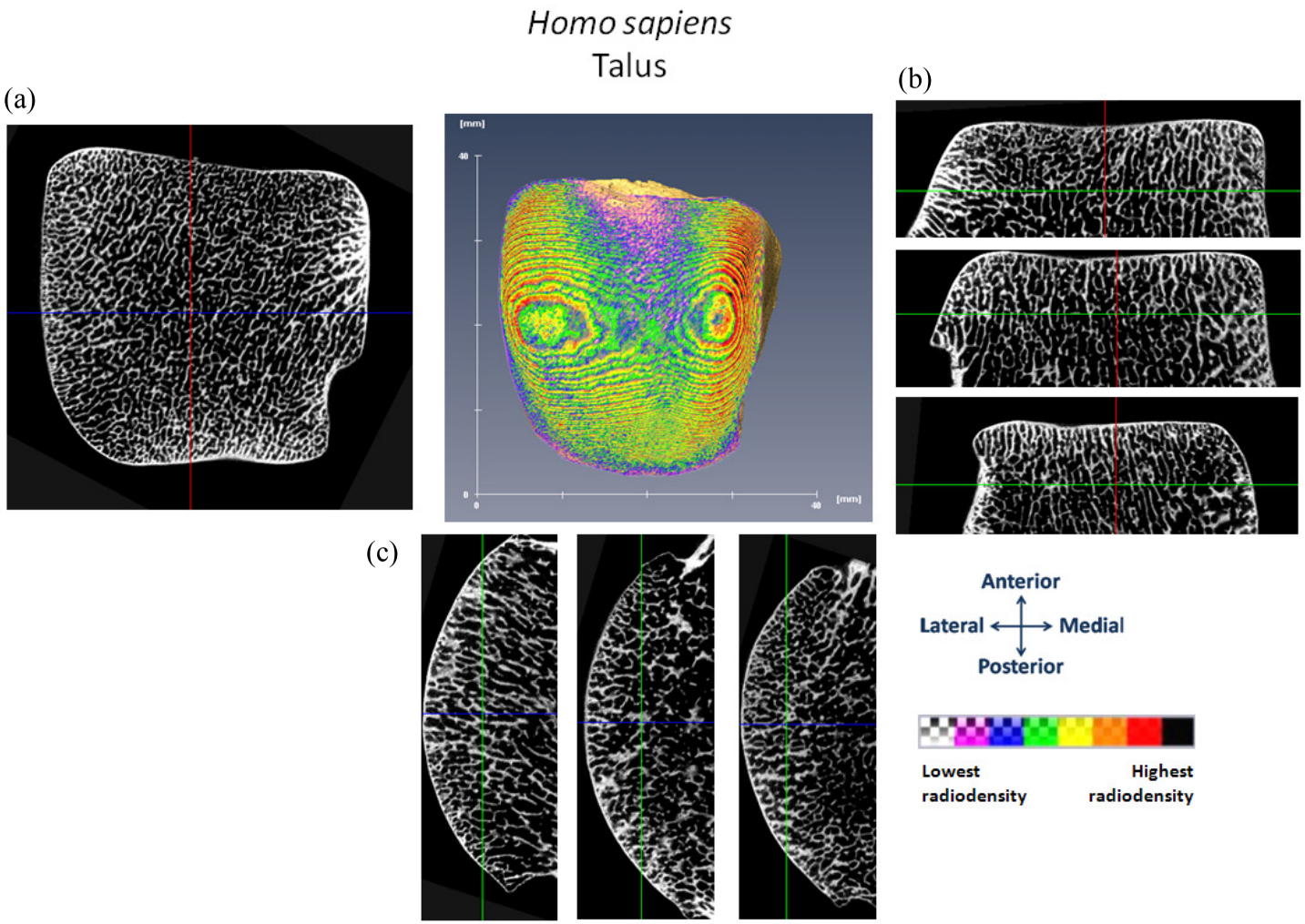

Figure A. 6: Representative micro-CT images of a *Homo sapiens* talus.
The false-color map represents the relative intensity of subchondral bone radiodensity. Shown are representative images of the trabecular bone structure in the transverse plane (a), and in each third of the bone along the coronal axis (b) and along the sagittal axis (c).

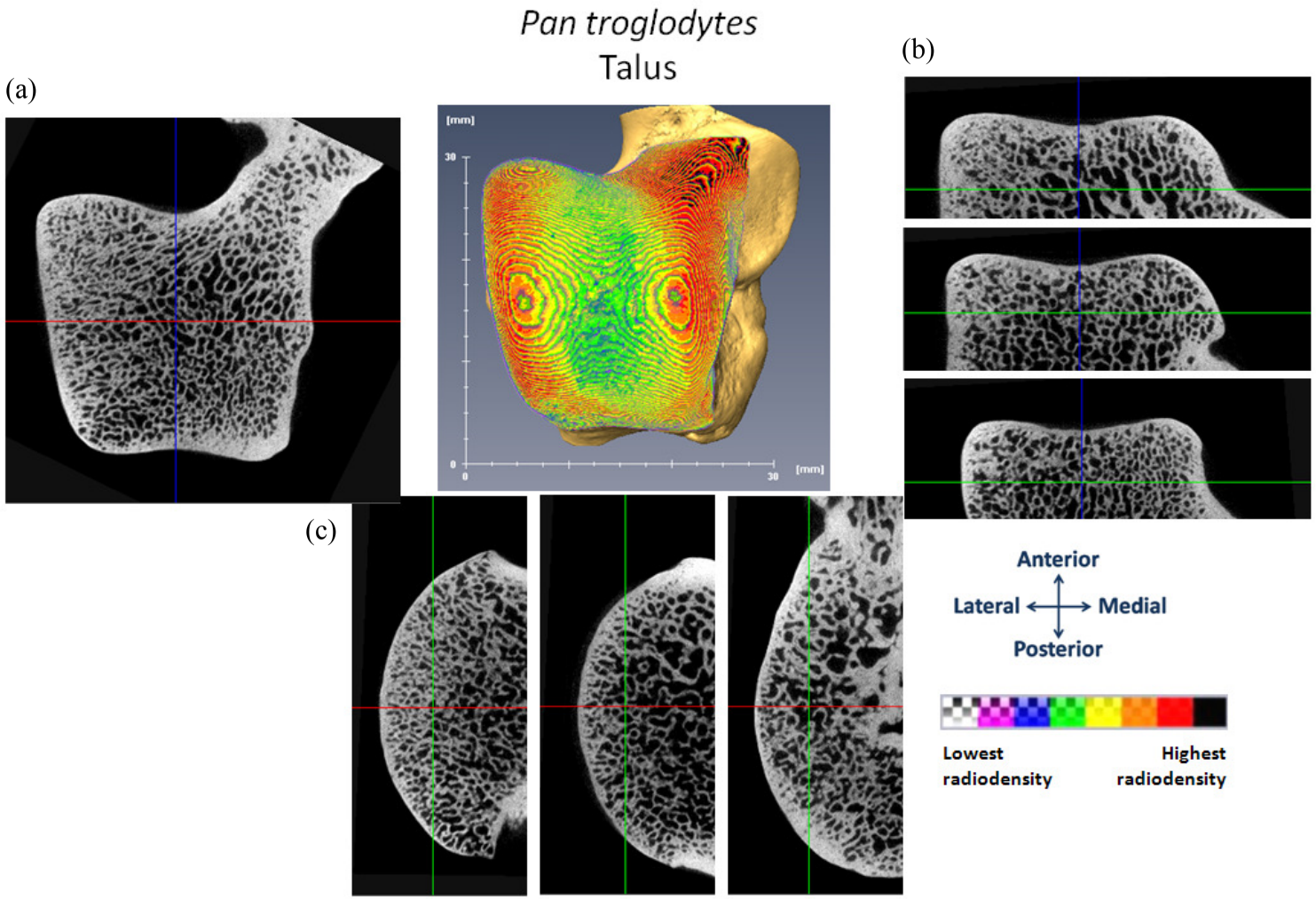

Figure A. 7: Representative micro-CT images of a *Pan troglodytes* talus.
The false-color map represents the relative intensity of subchondral bone radiodensity. Shown are representative images of the trabecular bone structure in the transverse plane (a), and in each third of the bone along the coronal axis (b) and along the sagittal axis (c).

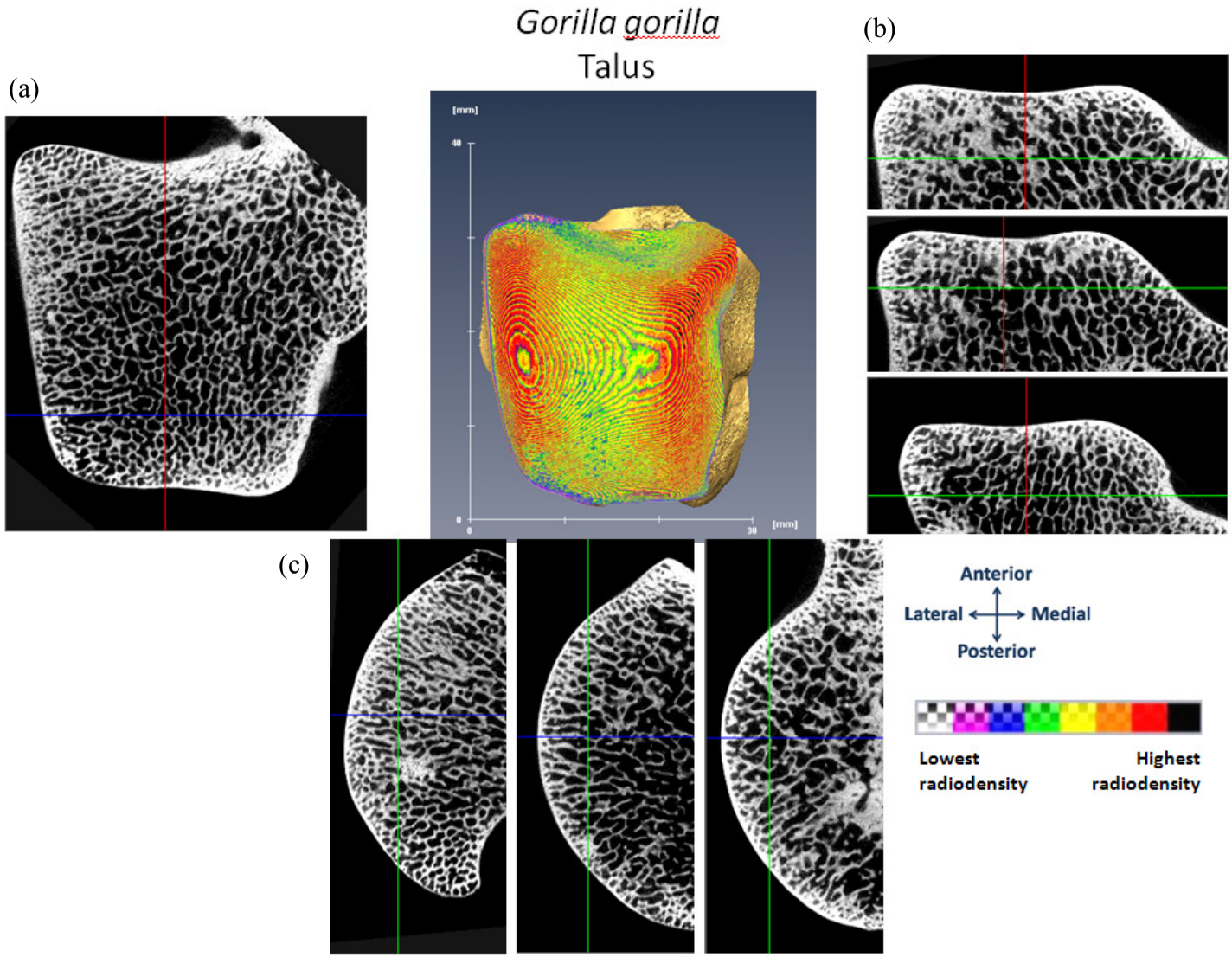

Figure A. 8: Representative micro-CT images of a *Gorilla gorilla* talus.
The false-color map represents the relative intensity of subchondral bone radiodensity. Shown are representative images of the trabecular bone structure in the transverse plane (a), and in each third of the bone along the coronal axis (b) and along the sagittal axis (c).

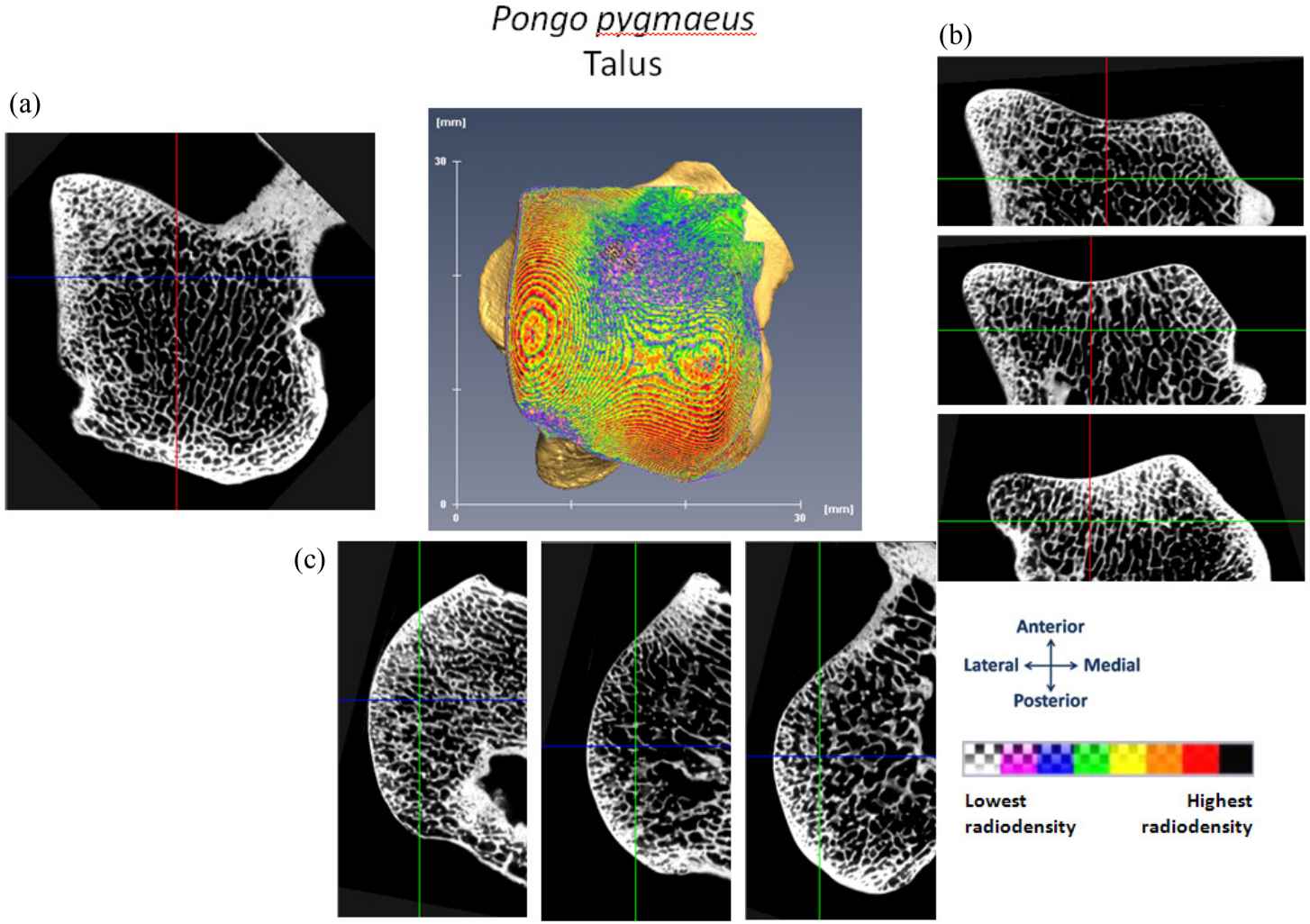

Figure A. 9: Representative micro-CT images of a *Pongo pygmaeus* talus.
The false-color map represents the relative intensity of subchondral bone radiodensity. Shown are representative images of the trabecular bone structure in the transverse plane (a), and in each third of the bone along the coronal axis (b) and along the sagittal axis (c).

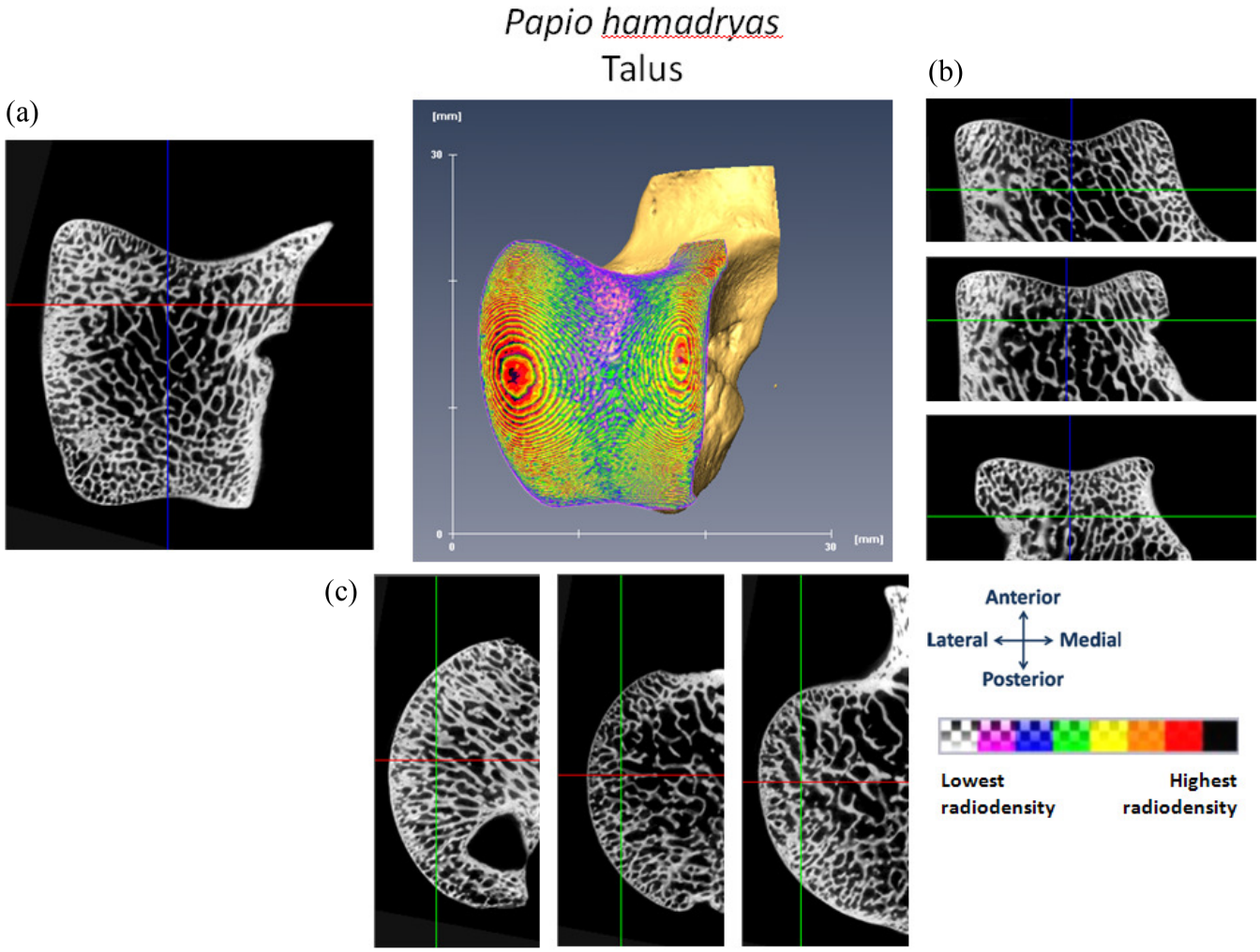

Figure A. 10: **Representative micro-CT images of a *Papio hamadryas* talus.**
The false-color map represents the relative intensity of subchondral bone radiodensity. Shown are representative images of the trabecular bone structure in the transverse plane (a), and in each third of the bone along the coronal axis (b) and along the sagittal axis (c).

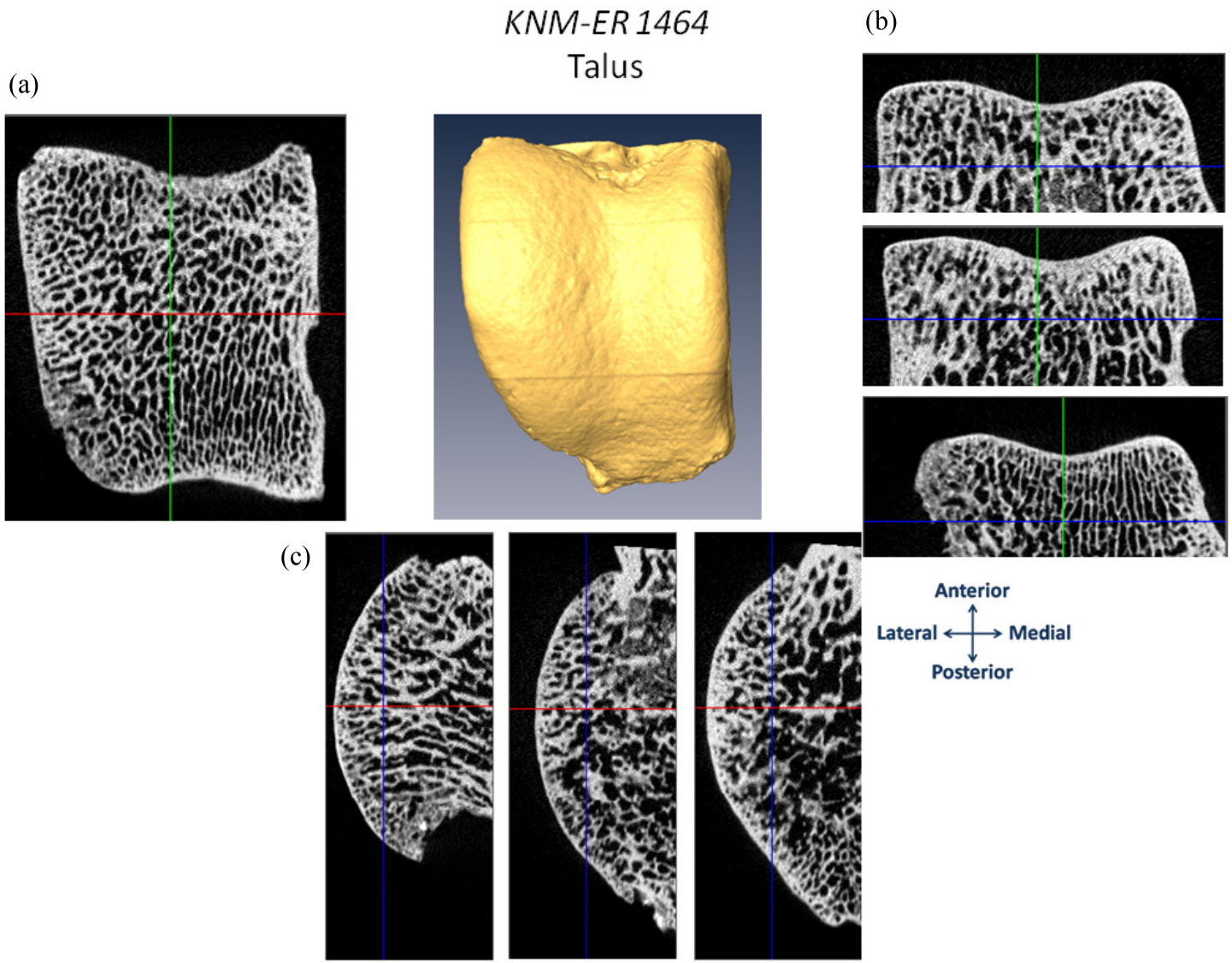

Figure A. 11: Micro-CT images of the KNM-ER 1464 talus.
Shown are images of the trabecular bone structure in the transverse plane (a), and in each third of the bone along the coronal axis (b) and along the sagittal axis (c).